STOCHASTIC FEASIBILITY ASSESSMENTS OF ORBITAL PROPELLANT DEPOT AND COMMERCIAL LAUNCH ENABLED SPACE EXPLORATION ARCHITECTURES

A Thesis
Presented to
The Academic Faculty

by

Patrick R. Chai

In Partial Fulfillment
of the Requirements for the Degree
Doctor of Philosophy in the
School of Aerospace Engineering

Georgia Institute of Technology
December 2014

STOCHASTIC FEASIBILITY ASSESSMENTS OF ORBITAL PROPELLANT DEPOT AND COMMERCIAL LAUNCH ENABLED SPACE EXPLORATION ARCHITECTURES

Approved by:

Dr. Alan W. Wilhite, Advisor
School of Aerospace Engineering
Georgia Institute of Technology

Dr. Brian J. German
School of Aerospace Engineering
Georgia Institute of Technology

Dr. Mitchell L.R. Walker
School of Aerospace Engineering
Georgia Institute of Technology

Dr. Carlee A. Bishop
Georgia Tech Research Institute
Georgia Institute of Technology

Dr. David J. Chato
Propulsion and Propellants Branch
NASA Glenn Research Center

Date Approved: October 31, 2014

ACKNOWLEDGEMENTS

First and foremost, I would like to thank my advisor, Dr. Alan Wilhite, for his support through my entire graduate career. There have been many times during the past six years when I doubted whether or not I would ever complete the degree, but he always provided enough motivation to keep me going. This dissertation would not have been possible without his continued support and his unwavering belief in me.

I would like to acknowledge my colleagues and friends for their support in my academic work. To Dr. Erik Axdhal, Dr. Dale Arney, Christopher Jones, Dr. Rafael Lugo, Dr. Ashley Korzun, and Dr. Brad Steinfeldt - thank you so much for all of your help getting my proposal, dissertation, and defense in order. I couldn't have done it without you. To my dearest friends Phyllis Petronello, Brent Rivard, Alex Rivard, Mannfred Slotnick, and Dana Notestine - thanks for believing in me. Additionally, I would like to thank Dr. Doug Stanley and the entire Graduate Education staff at the National Institute of Aerospace for their support.

Finally, I would like to thank my family for providing me with every opportunity to be successful in life. I am truly blessed to have their support and their love. They say good things in life are worth waiting, sorry it took so long.

TABLE OF CONTENTS

LIST OF TABLES

LIST OF FIGURES

NOMENCLATURE

Acronyms

GH_2	Gaseous Hydrogen
LH_2	Liquid Hydrogen
LO_2	Liquid Oxygen
AFRL	Air Force Research Laboratory
CDF	Cumulative Distribution Function
CER	Cost Estimating Relationship
COP	Coefficient of Performance
CPS	Cryogenic Propulsion Stage
CTV	Crew Transfer Vehicle
DSH	Deep Space Habitat
EDS	Earth Departure Stage
EOR	Earth Orbit Rendezvous
EPM	Electric Propulsion Module
ESAS	Exploration Systems Architecture Study
ETO	Earth-to-Orbit
FY	Fiscal Year
G-M	Gifford-McMahon

HEFT	Human Exploration Framework Team
HLLV	Heavy Lift Launch Vehicle
IR	Infrared
ISCPD	In-Space Cryogenic Propellant Depot
ISS	International Space Station
J-T	Joule-Thompson
KS	Kick Stage
LEO	Low Earth Orbit
LOR	Lunar Orbit Rendezvous
LSAM	Lunar Surface Access Module
MER	Mass Estimating Relationship
MHTB	Multipurpose Hydrogen Test Bed
MLI	Multi-Layer Insulation
MMSEV	Multi-Mission Space Exploration Vehicle
mT	Metric Ton = 1,000 kg
NEA	Near Earth Asteroid
NEO	Near Earth Object
NMF	Net Mass (Dry Mass less Engine Mass)
OF	Oxidizer-to-Fuel
RD^3	Research & Development Degrees of Difficulty

ROI	Return on Investment	
RTG	Radioisotope Thermoelectric Generator	
SEET	Space Environment and Effects Tool	
SEP	Solar Electric Propulsion Stage	
SOFI	Spray On Foam Insulation	
TELOS	Technology, Economic, Legal, Operation, Schedule	
TFU	Theoretical First Unit	
TLI	Trans-Lunar Injection	
TNV	Technology Need Value	
TRL	Technology Readiness Level	
ULA	United Launch Alliance	
VSE	Vision for Space Exploration	
ZBO	Zero Boil-Off	

Symbols

α	Surface Absorptivity	
α_c	Accommodation Coefficient	
$\bar{N}$	Multi-Layer Insulation Density	$[layers/cm]$
$\bar{X}$	Sample Mean	
χ	Uncertainty Correction Factor	
ΔV	Change in Velocity	$[km/s]$

$\dot{q}$	Heat Rate	$[W/s]$
ϵ	Surface Emissivity	
η	Cryocooler Efficiency as Fraction of Carnot Efficiency	
γ	Ratio of Specific Heat	
γ_m	Area Density of Multilayer Insulation Sheets	$[kg/m^2]$
γ_s	Area Density of Multilayer Insulation Spacer Material	$[kg/m^2]$
λ	MLI Performance Coefficient Exponent	
$\chi_{\mathrm{F_{CS/BC}}}$	χ for Crew System / Ballistic Capsule Unit Cost	
$\chi_{\mathrm{F_{EL}}}$	χ for Liquid Propellant Rocket Engines Unit Cost	
$\chi_{\mathrm{F_{EV}}}$	χ for Expendable Vehicles Unit Cost	
$\chi_{\mathrm{H_{BC}}}$	χ for Ballistic Capsule Development Cost	
$\chi_{\mathrm{H_{CS}}}$	χ for In Space Crew System Development Cost	
$\chi_{\mathrm{H_{EL}}}$	χ for Liquid Propellant Rocket Engines Development Cost	
$\chi_{\mathrm{H_{EV}}}$	χ for Expendable Vehicles Development Cost	
$\chi_{\mathrm{M_{20K}}}$	χ for 20K Cryocooler Thermal Mechanical Unit Mass	
$\chi_{\mathrm{M_{80K}}}$	χ for 80K Cryocooler Thermal Mechanical Unit Mass	
$\chi_{\mathrm{M_{\gamma_m}}}$	χ for Insulation Sheet Specific Mass	
$\chi_{\mathrm{M_{\gamma_s}}}$	χ for Insulation Spacer Specific Mass	
$\chi_{\mathrm{M_{CPI}}}$	χ for Cold Plumbing & Insulation Subsystem	
$\chi_{\mathrm{M_{Engine}}}$	χ for Engine Mass	

$\chi_{\mathrm{M_{H2Tank}}}$	χ for Hydrogen Tank Mass	
$\chi_{\mathrm{M_{Misc}}}$	χ for Cables & Miscellaneous Subsystem	
$\chi_{\mathrm{M_{O2Tank}}}$	χ for Oxygen Tank Mass	
$\chi_{\mathrm{M_{Rad}}}$	χ for Radiator Subsystem	
$\chi_{\mathrm{M_{SHT}}}$	χ for Structure & Heat Transport Subsystem	
$\chi_{\mathrm{M_{Skirts}}}$	χ for Intertank & Skirt Mass	
σ_{B}	Stefan-Boltzmann Constant	$[W/m^2\text{-}K^4]$
A_{o}	Total Radiating Surface Area	$[m^2]$
C_2	Propellant Mixer Duty Cycle	
f_{eclipse}	Eclipse Factor for the Cryocooler	
H_{vap}	Latent Heat of Vaporization	[J/kg]
M_{tank}	Mass of Propellant Tank	[kg]
P_{in}	Cryocooler Electrical Input Power	$[W]$
Q_{er}	Earth Reflected Albedo Heat Load	$[W/m^2]$
Q_{IR}	Earth Infrared Radiation Heat Load	$[W/m^2]$
Q_{i}	Internal Instrument Heat Load	$[W/m^2]$
Q_{m}	Heat Load Through Propellant Mixer	[W]
Q_{para}	Parasitic Heat Load	[W]
Q_{p}	Penetration Heat Load	[W]
Q_{sun}	Solar Direct Thermal Radiation Heat Load	$[W/m^2]$

Q_s	Structural Heat Load	[W]
V_{tank}	Volume of Propellant Tank	$[m^3]$
μ	Population Mean	
σ	Population Standard Deviation	
A_t	Propellant Tank Surface Area	$[m^2]$
b	Number of Bernoulli trials	
C_1	Gas Conduction Constant	$[m/s\text{-}K]$
C_r	MLI Performance Coefficient for Radiation	
C_s	MLI Performance Coefficient for Conduction	
f_1	Development Standard Factor	
f_2	Technical Quality Factor	
f_3	Team Experience Factor	
$F_{CS/BC}$	Unit Cost for Crew System and Ballistic Capsule	[Wk-Yr]
F_{EL}	Unit Cost for Liquid Propellant Rocket Engines	[Wk-Yr]
F_{EV}	Unit Cost for Expendable Vehicles	[Wk-Yr]
H_a	Alternate Hypothesis	
H_o	Null Hypothesis	
H_{BC}	Development Cost for Ballistic Capsule	[Wk-Yr]
H_{CS}	Development Cost for In Space Crew System	[Wk-Yr]
H_{EL}	Development Cost for Liquid Propellant Rocket Engines	[Wk-Yr]

H_{EV}	Development Cost for Expendable Vehicles	[Wk-Yr]
k_{NMF}	Net Mass Fraction	
M_{dry}	Dry Mass of Vehicle	[kg]
M_{engine}	Engine Mass	[kg]
M_{prop}	Propellant Mass	[kg]
M_{ref}	Reference Mass for Cost Estimating Relationship	[kg]
N	Number of Multi-Layer Insulation	
n	Sample Size	
N_Q	Number of Qualification Test Fire for Rocket Engine Development	
p	Individual Event Probability	
Q_C	Cryocooler Cooling Capacity	$[W]$
Q_{net}	Net Heat Load	[J]
t_m	Thickness of Multilayer Insulation Sheets	$[m]$
t_s	Thickness of Multilayer Insulation Spacer Material	$[m]$
z	z-Hypothesis Test Statistic	
k	Material Thermal Conductivity	$[W/m\text{-}K]$
M	Molecular Weight of Gas	$[kg/mol]$
P	Pressure	[Pa]
R	Gas Constant	$[kJ/mol\text{-}K]$
R^2	Coefficient of Determination	

Superscripts and Subscripts

C	Cold Surface
H	Warm Surface

SUMMARY

The 2010 National Space Policy of the United State of America introduced by President Obama directed NASA to set far reaching exploration milestones that included a crewed mission to a Near Earth Asteroid by 2025 and a crewed mission to Martian orbit by the mid-2030s. The policy was directly influenced by the recommendations of the 2009 Review of United States Human Space Flight Plans Committee, which called for an evolutionary approach to human space exploration and emphasized the criticality of budgetary, programmatic, and program sustainability. One potential method of improving the sustainability of exploration architectures is the utilization of orbital propellant depots with commercial launch services.

In any exploration architecture, upwards of seventy percent of the mass required in orbit is propellant. A propellant depot based architecture allows propellant to be delivered in small increments using existing commercial launch vehicles, but will require three to five times the number of launches as compared to the using the NASA planned 70 to 130 metric ton heavy lift launch system. Past studies have shown that the utilization of propellant depots in exploration architectures have the potential of providing the sustainability that the Review of United States Human Space Flight Plans Committee emphasized. However, there is a lack of comprehensive analysis to determine the feasibility of propellant depots within the framework of human space exploration.

The objective of this research is to measure the feasibility of a propellant depot and commercial launch based exploration architecture by stochastic assessment of technical, reliability, and economic risks. A propellant depot thermal model was

developed to analyze the effectiveness of various thermal management systems, determine their optimal configuration, quantify the uncertainties in the system models, and stochastically compute the performance feasibility of the propellant depot system. Probabilistic cost analysis captured the uncertainty in the development cost of propellant depots and the fluctuation of commercial launch prices, and, along with the cost of launch failures, provided a metric for determining economic feasibility. Probabilistic reliability assessments using the launch schedule, launch reliability, and architecture requirements of each phase of the mission established launch success feasibility. Finally, an integrated stochastic optimization was performed to determine the feasibility of the exploration architecture.

The final product of this research is an evaluation of propellant depots and commercial launch services as a practical method to achieving economic sustainability for human space exploration. A method for architecture feasibility assessment is demonstrated using stochastic system metrics and applied in the evaluation of technical, economic, and reliability feasibility of orbital propellant depots and commercial launch based exploration architectures. The results of the analysis showed the propellant depots based architectures to be technically feasible using current commercial launch vehicles, economically feasible for having a program budget less than $4 billion per year, and have launch reliability approaching the best single launch vehicle, Delta IV, with the use of redundant vehicles. These results serve to provide recommendations on the use of propellant depots in exploration architectures to the Moon, Near Earth Objects, Mars, and beyond.

CHAPTER I

INTRODUCTION

The purpose of this research is to measure the overall feasibility of propellant depot and commercial launch based exploration architectures by stochastic assessment of technical, reliability, and economic metrics. The research will focus on three subtopics: the detailed system modeling of the orbital propellant depot thermal system to enable technology requirements definition and optimization, the economic benefits of commercially launched and fueled propellant depot as determined by stochastic cost analysis of all of the relevant systems, and demonstration of improvement in launch reliability of an orbital propellant based exploration architecture compared to existing exploration plans.

1.1 Motivation

In 2009 the Review of United States Human Space Flight Plans Committee, also known as the Augustine Committee, was charged by the Office of Science and Technology Policy to review the multitude of options for human spaceflight and human exploration after the planned retirement of the Space Shuttle Program. The result of the six month review was a 150 page report documenting various recommendations for the future of United States space policy [1]. The committee's primary finding was to achieve the goal of human space exploration to other planetary bodies would require budgetary, programmatic, and program sustainability. The committee judged the nine year old Constellation Program [2] to be so far behind schedule and underfunded that meeting any of its objectives would be impossible. In response to the review, President Obama canceled the Constellation Program and enacted the 2010 National Space Policy of the United States of America [3].

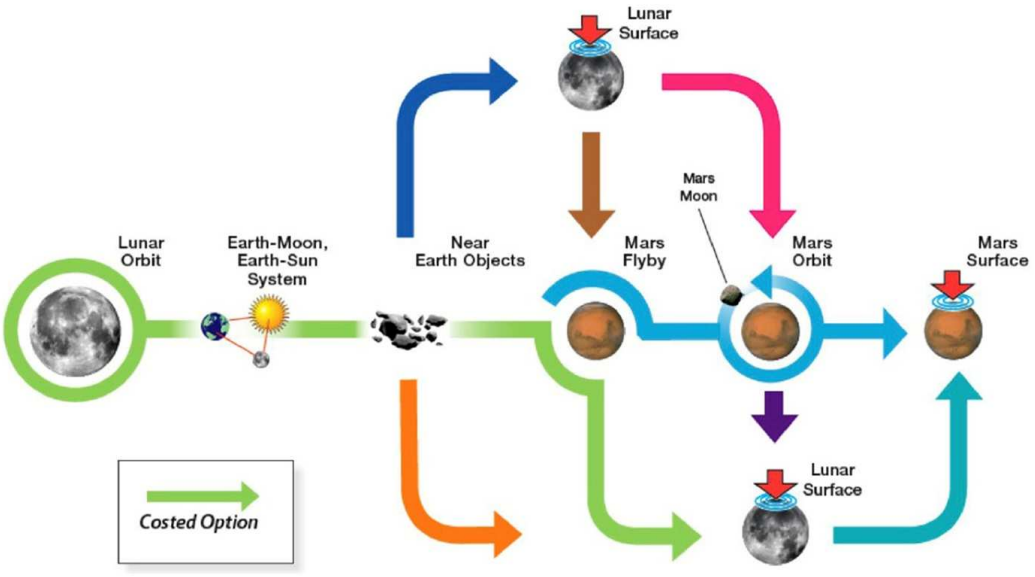

Figure 1: Augustine Commissions Options for Exploration within Flexible Path Strategy [1]

The National Space Policy set forth new and far-reaching exploration milestones that include a crewed mission to a near Earth object (NEO) by 2025 and a crewed mission to Martian orbit by the mid-2030s. The exploration milestones was inspired by the "Flexible Path to Mars" strategy outlined by the Augustine committee [1]. The goal of the flexible path strategy is to take incremental steps towards Mars, allowing astronauts to learn, live, and work in free space under similar conditions to those found on the way to Mars. Following the flexible path strategy allows humanity to gain ever-increasing operational experience in space, growing in duration from a few weeks to several years in length, and moving from close proximity to the Earth to as far away as Martian orbit. These incremental steps involve several intermediate destinations to explore before reaching the Martian surface. Figure 1, reproduced from the Augustine committee's report [1], shows a notional representation of the flexible path option to Mars.

Following these recommendations, NASA assembled a Human Exploration Framework Team (HEFT) to begin defining new exploration plans for NASA. The primary

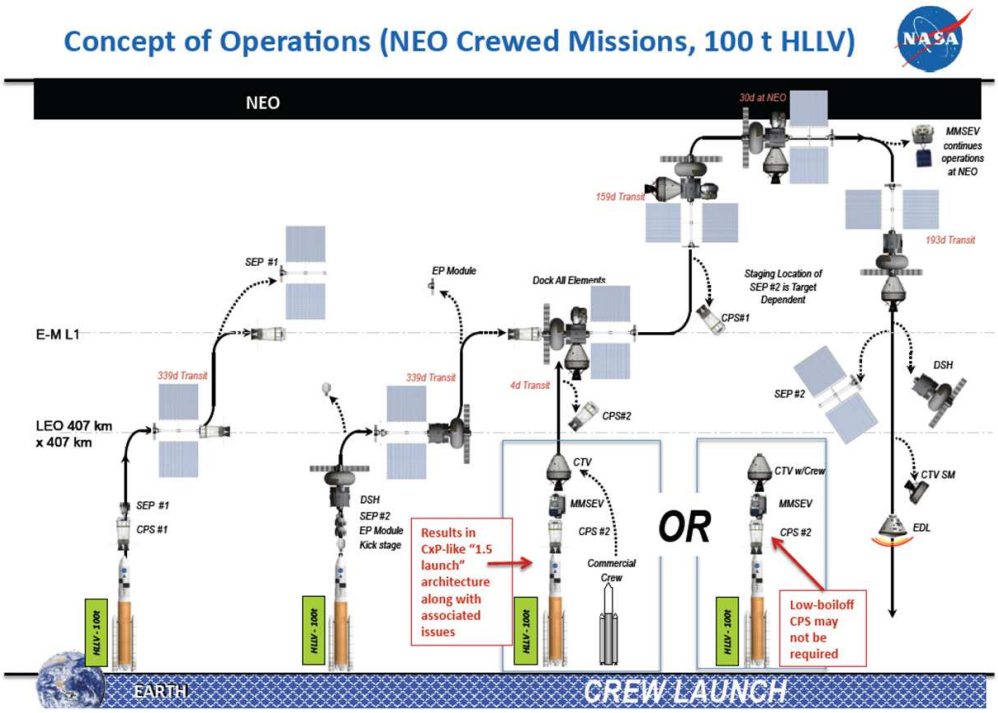

Figure 2: Human Exploration Framework Team Concept of Operation for Crewed Mission to Near Earth Object [4]

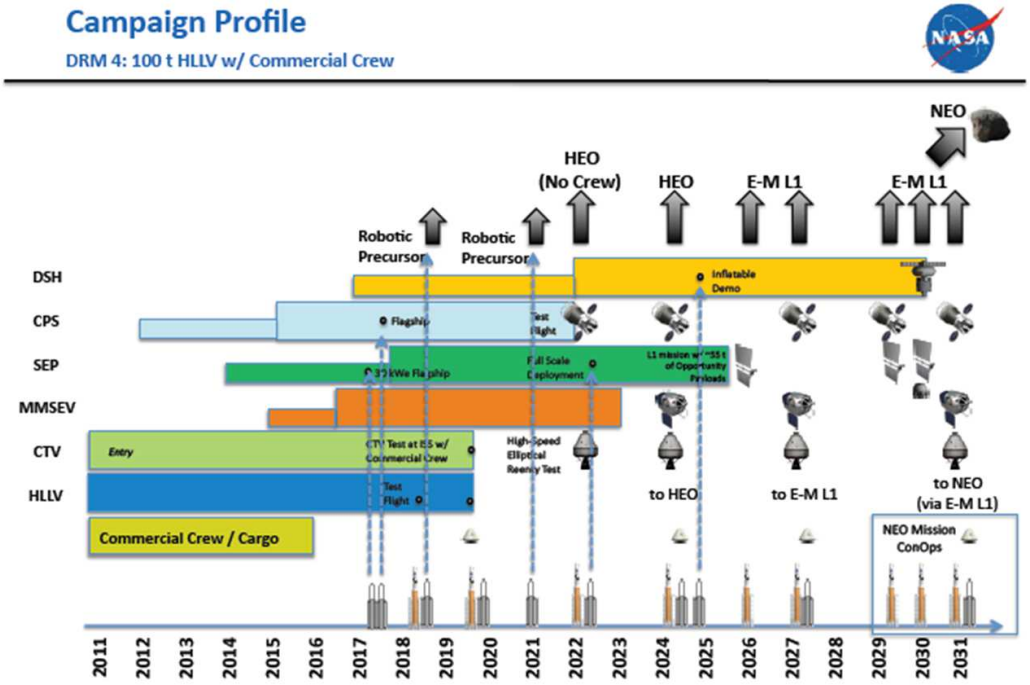

Figure 3: Human Exploration Framework Team Campaign Profile for Crewed Mission to Near Earth Object [4]

challenge for the exploration framework team was to define an exploration plan that satisfies the exploration science goals, while also meeting budget constraints and be able to weather any changes in the political climate. The current baseline HEFT architecture is a manned mission to a Near Earth Object (NEO) shown in Figure 2 [4] with a campaign profile and schedule shown in Figure 3. The baseline exploration architecture calls for the development of a Space Shuttle derived Heavy Lift Launch Vehicle (HLLV), as well as seven additional unique in-space exploration elements: a Solar Electric Propulsion stage (SEP), a Multi-Mission Space Exploration Vehicle (MMSEV), a Deep Space Habitat (DSH), a Crew Transfer Vehicle (CTV), a Cryogenic Propulsion Stage (CPS), an Electric Propulsion Module (EPM), and a Kick Stage (KS).

The development of these unique systems has a tremendous impact on the overall cost and schedule for the mission. HEFT's analysis estimates that the NEO baseline mission would require a 20 year development and integration program with a total architecture cost of roughly $144 billion (FY11) [4] with yearly costs between $5.5 billion and $8.5 billion. This two-decade exploration program would culminate in a single manned mission to a near Earth asteroid (NEA) in 2031. At first glance, this plan does little to address the sustainability requirement laid out in the Augustine Commission's report because it is essentially the same architecture as the cancelled Constellation program but to a different destination.

HEFT cost estimate, summarized in Table 1, shows the most costly elements are the Space Shuttle derived heavy lift launch system and the supporting ground operation and infrastructure. HEFT estimates the total cost of the heavy lift launch system development program to be $54 billion (FY11) over the next 20 years [4] which would include six test flights (increasing payload capability from 70 metric ton (mT) to 130 mT) and the first three operational flights of the 100 mT version of the HLLV to deliver hardware for the 2031 NEA mission. The launch cost of the HLLV,

Table 1: Human Exploration Framework Team Program Total Cost Estimate in FY11 $million [4] for 2030 Near Earth Asteroid Mission

Heavy Lift Launch Vehicle	$53,921 m	*37.47%*
Ground Operation & Infrastructure	$16,801 m	*11.68%*
Crew Transfer Vehicle-E Prime	$15,153 m	*10.53%*
Solar Electric Propulsion	$14,875 m	*10.34%*
Deep Space Habitat	$9,617 m	*6.68%*
Program Integration	$9,187 m	*6.38%*
Multi-Mission Space Exploration Vehicle	$6,315 m	*4.39%*
Cryogenic Propulsion Stage	$4,813 m	*3.34%*
Commercial Crew Development	$4,453 m	*3.09%*
Commercial	$3,883 m	*2.70%*
Mission Operation	$3,175 m	*2.21%*
Robotic Precursor	$1,703 m	*1.18%*
Total	**$143,896 m**	

estimated by summing the development and operation cost over the entire program and dividing by the total number of flights, is close to $8 billion per flight. As a point of comparison, the Apollo's Saturn V rocket and the Space Shuttle were both estimated to cost $3.7 and $1.6 billion per flight over the course of their respective programs [5].

For all human exploration beyond low Earth orbit, HLLVs have played an integral part in delivering the crew and mission elements into orbit [6–8]. In all of these architectures, the development and operation of these heavy-lift vehicles are major cost drivers. The Apollo program was able to overcome the high cost of heavy-lift launch vehicles because of the enormous budget it had in the mid to late 1960s. Figure 4 plots NASA's budget as a percentage of the United States' Federal Spending from 1958 to present. NASA's budget peaked in 1966 at 4.4% of the all federal spending [9] and has steadily decreased since then. After the first few moon landings, the Apollo program felt the impact of federal budget restrictions and eventually was cancelled because it was unsustainable under the reduced budget.

With the average yearly cost of the HEFT program at greater than $7 billion and

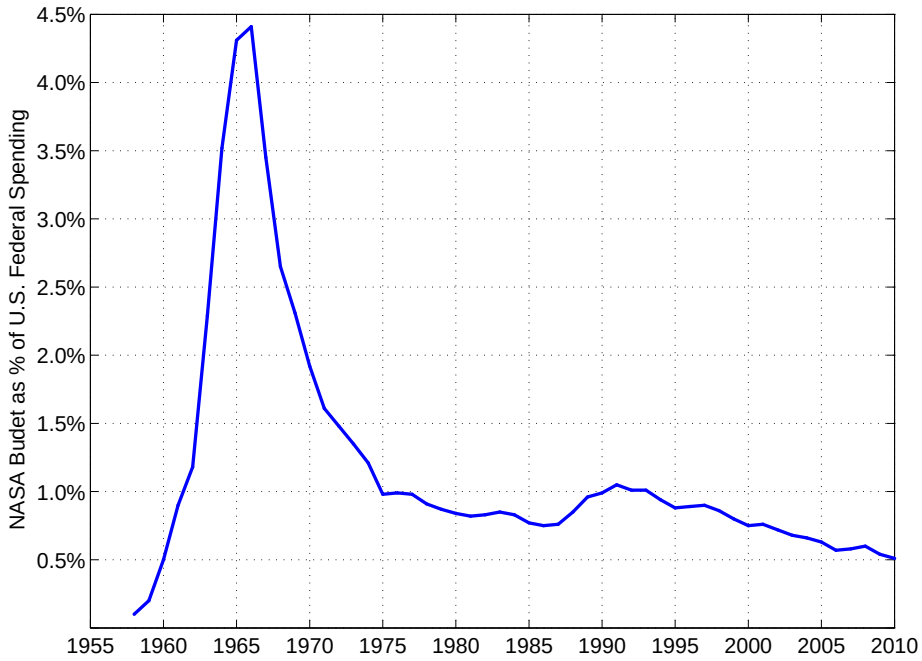

Figure 4: NASA's Budget as Percentage of U.S. Federal Spending from 1958 to 2010 [9]

the current exploration system budget of $3.5 billion per year, the architecture does not seem to be economically feasible. In order to achieve sustainable human space exploration, a radical change is needed to create an innovative architecture that does not rely solely on large HLLVs that account for more than 50% of the projected program budget. The Augustine committee recognized this, and identifies several technology areas that are critical for sustainable exploration [1]. One of the identified technologies is "Propellant Storage and Transfer in Space." Numerous studies in the past decade have examined using this technology in exploration architectures especially in tandem with commercially available launch vehicles that are operated by private companies. A comprehensive literature review of these studies is given in Chapter 2. Some studies have shown the potential of dramatically reducing the cost and improving the flexibility of the architecture [5, 10–12], other studies argue that the technology required is too risky [13] and that the depot based architecture

cannot replace the need for HLLV [14]. The purpose of this dissertation is to provide a comprehensive evaluation of the utilization of the orbital propellant depot and propellant transfer technologies in space to improve the current beyond low Earth orbit (LEO) exploration architectures.

1.2 Research Goals

The objective of the research is to systematically assess the feasibility of propellant depots and commercial launch based space exploration architectures. The research will present a method for comprehensive examination of feasibility assessment for space system architectures and application of the method to measure feasibility for propellant depot and commercial launch based architectures. The methodology must extend beyond traditional feasibility assessment and be able to capture the uncertainties that are inherent in the analysis of different exploration architectures. In order to achieve this, the following research question is posed that will serve as the foundation of the research.

Research Question: How can feasibility of propellant depot based space exploration architectures be comprehensively measured without bias?

Hypothesis: Feasibility can be measured objectively with definition of constraints and systematic assessment of all areas of the architecture that may violate the constraints. Stochastic system metrics can be used to determine the sensitivity of architecture feasibility to both uncertainties in metric evaluation as well comparison between multiple design options. This definition of feasibility will be discussed in Chapter 3.

To answer this research question and evaluate the hypothesis, this dissertation will accomplish several research goals. They are as follows:

1. **Develop models for evaluating technical performance metrics for the available design options.**

To analyze the technical performance, system level models are created to evaluate the various design option that are available. The models need to have the flexibility to evaluate large number of design options for multiple areas of interest. Performance metrics are used to determine if the propellant depot based architecture satisfies the basic mission requirements and architecture feasibility.

2. **Determine a method to incorporate constraints and requirements into system analysis to establish feasibility.**

Defining feasibility requires proper definition of constraints in each of the areas of interest. These constraints must be derived from physical properties of the architecture and requires extensive literature review to establish realistic constraints. The design options will be evaluated to determine constraint satisfaction for the entire feasibility topic of interest and the elimination of non-feasible designs.

3. **Investigate the sensitivity of performance metrics to design options.**

Feasibility of the architecture performance is extended to include the sensitivity of the performance of the system design option within the design space. Ideally, the most feasible architecture will have design options that have high performance in all categories of interest and are relatively insensitive to design changes. The sensitivity of constraint violation to the design options will serve as a major decision driver for design feasibility.

4. **Determine the impact of uncertainties in system level modeling on the feasibility assessments and identify the high risk elements of the architecture.**

With any models, there are uncertainties inherent in the estimation of various performance metrics. These uncertainties can have significant impact on design feasibility as well as the satisfaction of constraint. The uncertainties in the evaluation of all performance metrics must be quantified, and their impact on the overall architecture performance must be analyzed in detail. The understanding of the impact of uncertainties on the architecture performance is paramount to the evaluation of architecture feasibility.

1.3 Dissertation Outline

This chapter introduced the purpose of this research and presented the motivation for the research and provided context for the discussion of human space exploration. The primary research question and the research objectives are presented to set the basis for objective feasibility assessment.

Chapter 2 presents a discussion on the background and history of the propellant depot based exploration architecture. An extensive literature review of recent exploration architectures provides context for the discussion of the multitude of design options within the exploration design space. This chapter also presents a detailed discussion on the technology required to enable propellant depot exploration architecture, and defines the necessary subsystems for further evaluation. Finally, the chapter presents a review of the challenges to a propellant depot based architecture that will serve as a basis for feasibility evaluation.

Chapter 3 presents the definition of feasibility and a literature review of feasibility studies to establish a method for feasibility assessment. The literature review shows a lack of clear definition of feasibility with no standard method to evaluate feasibility of a concept. The chapter presents the development of the feasibility assessment method used for this dissertation that is based on the stochastic evaluation of system metrics and the application of constraints to assess feasibility in a probabilistic manner. The

chapter finishes with an example of the probabilistic feasibility assessment.

Chapter 4 features the first feasibility assessment topic. The chapter begins with a definition of the exploration architecture and describes the necessary analysis to evaluate the propellant depot architecture. The thermal system model is developed in the chapter because of its unique system integration, and the system mass estimation method is presented. These models are used for the evaluation of system requirements for the all of the feasibility assessments in the dissertation. The performance metrics are evaluated for the various thermal system design options. System level trade studies are conducted to determine the optimal thermal system option for long term cryogenic fluid storage. System level mass estimations provide the context for feasibility assessment in other areas of interest. The uncertainties of the thermal system performance and the system mass estimation are presented, and the performance feasibility is assessed using commercial launch vehicle payload as a constraint.

Chapter 5 discusses the propellant aggregation mission feasibility with the utilization of commercial launch vehicles. This chapter presents a method to estimate the reliability of launch vehicles based on launch records with Bayesian probability. The problems with utilization of newly development launch vehicles is described, and the analysis to evaluate the probability of propellant aggregation success with different launch vehicles is presented. This chapter ends with discussion of the impact of redundancy on the propellant aggregation mission.

Chapter 6 investigates the economic feasibility of the propellant depot exploration architecture. A system level cost method is presented to evaluate the cost of the unique elements in the alternate architecture. The cost of these elements is incorporated into the baseline architecture with the common elements, and the overall architecture cost is presented as a comparison to the baseline. An analysis of NASA's budget history provides an estimate of the cost constraint for the exploration architecture.

Chapter 7 integrates the three feasibility topics of interest into an integrated assessment of the propellant depot exploration architecture. Various design option's impact on system level feasibility metrics is discussed in a series of pairwise feasibility comparisons. The chapter summarizes these feasibility assessments and presents the overall architecture feasibility and a comparison to the baseline architecture.

Finally, Chapter 8 provides conclusions of the overall feasibility of propellant depot based space exploration architecture. Discussion of the challenges to the depot architecture is revisited, and the stochastic feasibility assessment to address each of the challenges is summarized. The chapter finishes the dissertation with remarks on the contribution of the dissertation to the field of engineering system studies and brief discussion of suggestion future work.

CHAPTER II

BACKGROUND

As discussed in Chapter 1, the current NASA human exploration architecture [4] with its reliance on HLLVs is unlikely to be sustainable due to the present fiscally restrictive environment. In order to meet the recommendations of the Augustine committee [1] and achieve sustainability for human space exploration, an alternate architecture is needed. Before establishing an alternate architecture, the deficiencies of the current architecture must be identified.

For all human exploration beyond LEO, both flown missions and conceptual designs, at least one heavy lift class launch vehicle, with payload capability of 70 mT or more, is required to accomplish the mission objectives [6–8, 15]. During the Apollo program, the mission was not possible without the development of the Saturn V rocket, which to this day is still the largest rocket ever built. During the 1990's, several studies and architectures were developed for sending human expeditions to Mars, and these design reference architectures all rely on development of a Space Shuttle derived HLLV, which has a payload capacity of roughly 85 mT [16].

The Constellation Program [2], which is the result of then President Bush's Vision for Space Exploration [17] and NASA's supporting Exploration System Architecture Study (ESAS) [7], calls for the simultaneous development of a Space Shuttle derived Ares I launch vehicle for the crew and a heavy lift Ares V launch vehicle for in-space systems and transportation. Finally, the most recent iteration of the architecture design cycle, as a result from President Obama's National Space Policy [3], calls for the incremental development of the 70 mT, 100 mT, and 130 mT Space Launch System [4]. Despite the fact that the destination, mission objective, and mission

requirements are different for all of these studies, the use of heavy lift class launch vehicles is always assumed.

The challenge with the utilization of the heavy lift class launch vehicle is that they are a major cost driver for the architectures [18]. Examining the cost breakdown for the HEFT program (Table 1), one can see the development and implementation of the Space Launch System, which along with its ground support, accounts for more than 50% of the entire program's projected budget. Similarity, the cost overrun associated with the development of the Ares I and Ares V were the primary contributing factors for the cancellation of the Constellation Program [1]. Thus, there is a dire need to investigate alternate architectures that do not require the use of HLLVs.

2.1 Propellant Depot Background

Without a heavy lift class launch vehicle, the mass required in orbit must be delivered incrementally in smaller segments with present or projected commercial launch vehicles. This can be accomplished with the implementation of on orbit propellant storage and transfer technologies, as recommended by the Augustine commission [1]. An orbital propellant depot is defined as a system that enables the aggregation of propellant and refueling of spacecraft elements in orbit. A propellant depot can serve two primary purposes: it can be used to service satellites [19] that have reached end-of-life by consuming all of its orbital maneuvering fuel, or it can be used to store propellants for exploration missions that require large amounts of propellant. For typical exploration missions beyond LEO, regardless of the destination, the propellant mass can account for 70% or more of the total assembled mass in orbit [20]. Table 2 shows the breakdown of the assembled mass in orbit of the four major exploration missions and mission concepts in human history. Each of the mission's assembled mass in LEO consists of large quantities of propellant that are required for the mission. Typically, the large quantity of propellant is justification for the HLLV requirement. The use

Table 2: Breakdown of Assembled Mass in Orbit for Various Human Exploration Missions [4, 6–8, 16]

	Apollo Program	Constellation Program	NASA Design Reference Mission	HEFT	
Destination	*Lunar*	*Lunar*	*Mars*	*Asteroid*	
Mass in LEO	135	168	486	254	mT
Propellant	103	126	348	192	mT
% Propellant	77%	75%	72%	76%	

of a propellant depot allows the architecture to decouple a large percentage of the required mass from the mission critical path and eliminate the HLLV requirement.

The origin of the propellant depot concept can be traced back to the Apollo program. During the architectural selection process, a concept called Earth Orbit Rendezvous (EOR) was considered [6,15], as shown in Figure 5. The concept included two launches of a smaller launch vehicle (as compared to the Saturn V) to deliver the manned spacecraft and the propellant separately. Liquid oxygen would have been transferred from the tanker to the manned spacecraft in Low Earth Orbit (LEO) before the trans-lunar injection maneuver. The single launch Lunar Orbit Rendezvous (LOR) option was ultimately selected despite the high cost associated with the Saturn V vehicle because the EOR option posed higher risk to the mission success due to the two-launch requirement and the tight schedule constraint due to propellant boil-off because of a lack of cryogenic storage technologies in the 1960s.

Propellant transfer remained a major component of architecture design even after being eliminated from the Apollo program due to the potential for drastic increases in capability for long duration exploration missions. However, as the focus of NASA shifted from exploration to LEO operation with the Space Shuttle and the International Space Station (ISS), the value of propellant storage and transfer technology diminished. With the recent retirement of the Space Shuttle program and the renewed interest in beyond LEO exploration, the propellant depot concept has become relevant again. In the past decade, NASA and industry experts have been examining

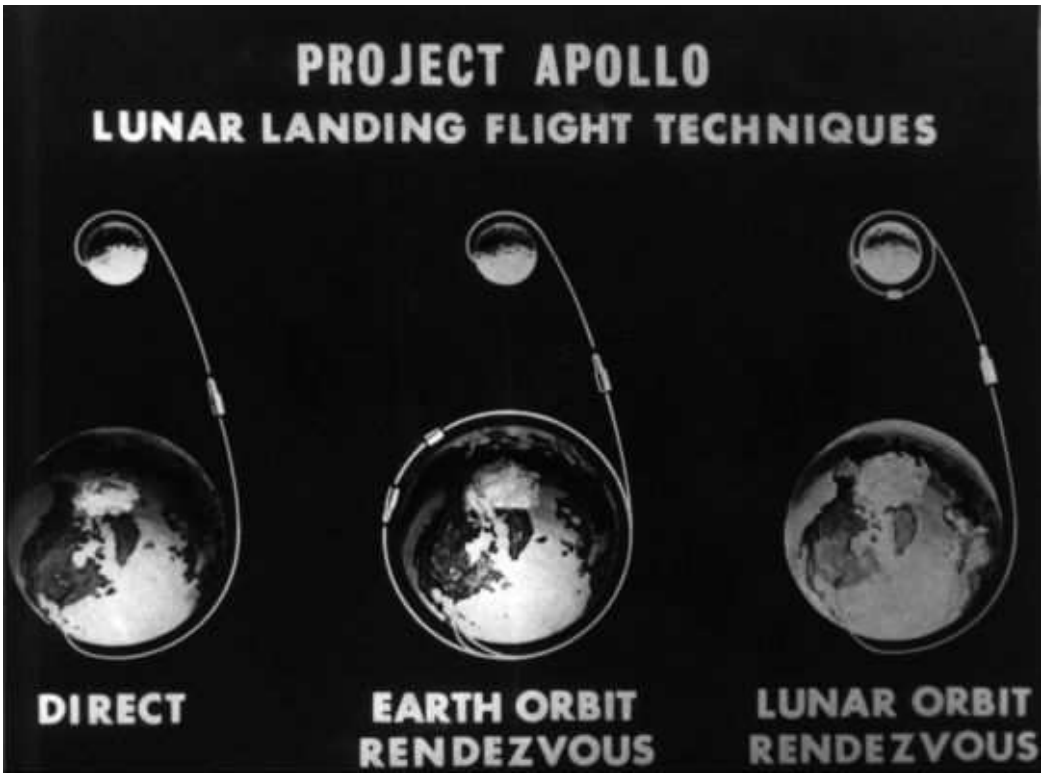

Figure 5: Apollo Program Lunar Mission Mode Comparison [6]

the potential benefits of propellant transfer technologies to the human exploration architecture. Below is a summary of recent literature on the topic of propellant depot research in the context of human space exploration.

2.2 Recent Literature Review

Howell, Mankins, and Fikes' 2005 paper [21] discussed the notional concept of using propellant depots in exploration missions. The paper describes In-Space Cryogenic Propellant Depot (ISCPD) as a "broad class of new concepts of operations with the potential to meet several of the important challenges of enabling affordable pre-positioning of key logistics (including fuel, hardware, and appropriate systems) to points beyond LEO." The paper states that the primary challenge to achieving sustainability in space exploration and space operation beyond LEO is the affordability

of positioning assets and consumables in orbit. The authors identified four key elements to solving this challenge: 1) Lower cost of Earth-to-Orbit (ETO) transport, 2) Highly Autonomous assembly, 3) Affordable pre-positioning of fuel and other materials, and 4) Reusable, high reliable, and high energy space transportation. The paper concludes that the utilization of ISCPD will contribute to all four of the identified key elements, and the technology development for ISCPD requirement is fundamental for establishing robust space exploration infrastructure and is applicable across a wide spectrum of exploration objectives.

Fikes, Howell, and Henley's 2006 paper [22] examined the benefits of refueling elements of the Constellation program in orbit. The paper provided an overview of a broad systems study that examined the potential locations for ISCPD. The study's primary finding is the identification of different technology development needs (which will be addressed in a later section), and the conclusion that "[ISCPD] systems offer significant advantages for NASA space exploration systems." [22].

Similarly, the Boeing Company's 2007 paper [12] by Chandler, Bienhoff, Cronick, and Grayson detailed the company's study on utilizing propellant depot as a means to improve the performance of the Constellation program. The Boeing Company's propellant depot concept is modular [12, 23] as shown in Figure 6. The depot consists of a central truss system with six tank modules that are derived from Delta IV upper stages. The central truss has robotic arms to berth the tank modules and utilizes autonomous rendezvous and docking capabilities demonstrated by Orbital Express [24]. The depot is sized to accommodate the propellant requirements of the lunar reference mission, specifically the descent module, as defined in ESAS. Each tank module has a capacity of 25 mT, yielding a total depot capacity of 150 mT. Each module holds two fluids, storing approximately 21 mT of LO_2 and 4 mT of LH_2. For the Constellation program, a 180% increase in payload landed on the lunar surface is possible with refueling of the ESAS Earth Departure Stage (EDS) and using

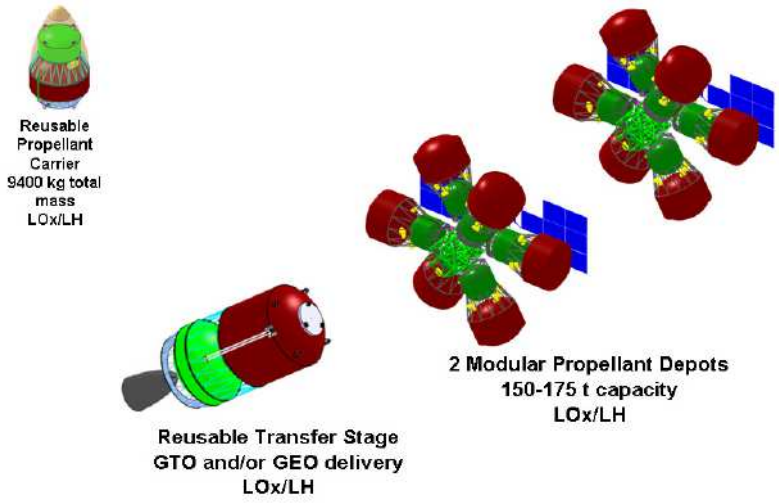

Figure 6: Boeing's Multi-Launch Dual-Fuel Modular Propellant Depot Concept, reproduced from [23]

the full EDS for the trans-Lunar injection (TLI) maneuver. The result of the Boeing study is confirmed by Young's Ph.D. Dissertation in 2009 [25].

Young's dissertation provided an extensive examination of the impact of on-orbit refueling on the Constellation program [25]. The dissertation concludes that significant improvement to the mission capability, in terms of payload delivery, is possible by utilizing a propellant depot and refueling the EDS of the Constellation program. In addition, Young concludes a significant cost saving is possible with the utilization of ISCPD as well as improvements in the extensibility of the architecture. However, these studies are limited to relatively short term propellant storage in space (roughly 90 days), which would not be ideal for longer duration and higher performance required missions like Mars or Asteroids.

Arney and Wilhite's 2009 journal paper [18] and Georgia Tech's graduate team at the 2009 Revolutionary Technical Challenge design competition forum [26] (Figure 7) both provided optimization for propellant depot based lunar exploration architectures. Arney's paper optimized an ESAS-like mission to the lunar surface using commercial launch vehicles and commercial propellant depots. The optimized architecture demonstrates that it is possible to design an exploration architecture without

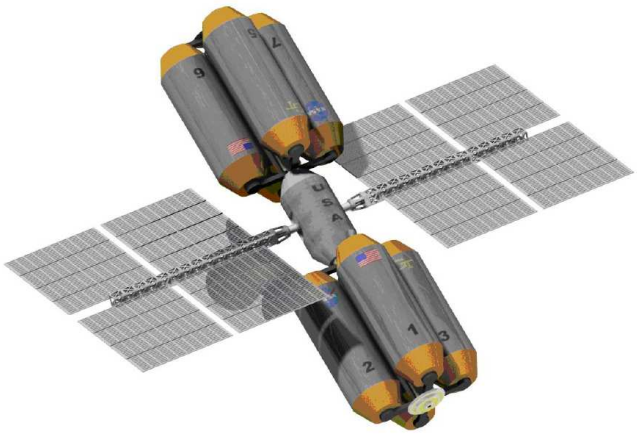

Figure 7: Propellant Depot Concept Art from Georgia Tech Revolutionary Technical Challenge Graduate Research Team, reproduced from [26]

the heavy-lift launch vehicle and provide more payload to the lunar surface than the ESAS architecture. The 2009 competition paper [26] by the Georgia Tech students provided analysis of a more extensive design space, and optimized the architecture based on a combination of five figures of merit; extensibility, heritage, performance, reliability, and cost. The final optimized solution utilizes a heavy lift class launch vehicle in tandem with small commercial launch vehicles and propellant depot. The analysis from these two papers demonstrated the significant advantage of a propellant depot based architecture as compared to a traditional architectures. A depot based architecture provides better performance, extensibility, and lower cost when compared to the baseline non-depot based architecture, and "creating a sustainable space transportation system [18]."

The 2008 paper [27] by United Launch Alliance's Kutter, Zegler, Neil and Pichford detailed the efforts by the company to join the propellant depot market because of their extensive experience with using cryogenic upper stages. Combined with the 2009's survey paper by Goff, Kutter, Zegler, Bienhoff, Chandler and Marchetta [23], the three primary ULA depot designs are presented. The first is a disposable single-use propellant depot, using a Centaur upper stage tank and its residual propellant to

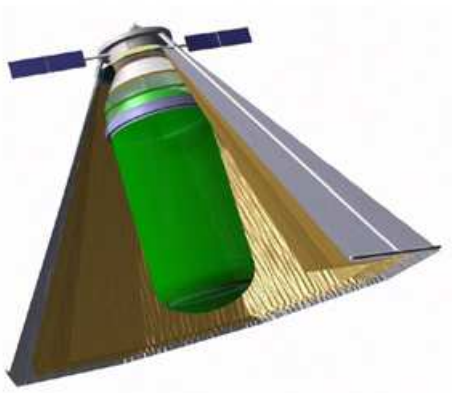

Figure 8: United Launch Alliance's Single-Fluid, Single-Launch Depot Concept, reproduced from [23]

resupply another vehicle. This single-use tanker would have limited storage capability and a very short designed lifetime. It would likely be used at first as a technology demonstrator and later as a tanker spacecraft to refuel other orbital depots. The benefit of this concept is that it requires very little technology advancement. The tanks are derived from existing Centaur tanks and can be launched on existing boosters. Thermal management of the cryogenic fluid is entirely passive utilizing multi-layer insulation as well as minimum structural penetration design and pre-launch pressurization and cooling. The tanks would hold approximately 20 metric tons of liquid oxygen and can develop experience with on-orbit cryogenic propellant handling, storage and transfer.

The second concept is a simple, single-fluid, single-launch concept [23, 27], shown in Figure 8. This concept has longer duration storage capability than the single-use concept and has the ability to be refueled. This concept consists of a 4.57 meter diameter tank with MLI and sun-shield for thermal management. It can be launched on an existing 5 meter diameter payload fairing on an Atlas V, Delta IV, or Arianne 5. It contains only a single fluid, capable of housing 140 mT of LO_2 or 15 mT of LH_2.

The third and final ULA concept is a near-term, single-launch LO_2/LH_2 depot to support manned space flight beyond LEO [23], shown in Figure 9. The LH_2 tank

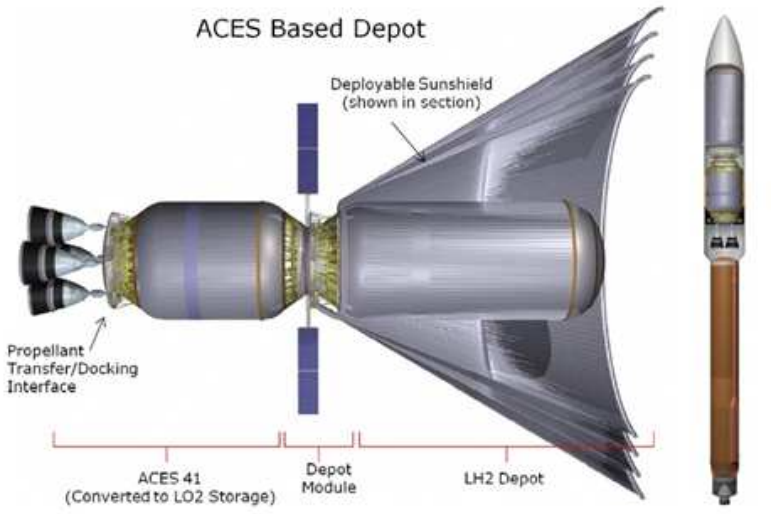

Figure 9: United Launch Alliance's Double-Fluid, Single-Launch Propellant Depot Concept, reproduced from [27]

is similar to the single-fluid reusable concept with a 5 meter diameter fairing. The LO_2 tank is constructed by modifying the launch vehicles existing upper-stage to accommodate the requirements set by the depot. The two tanks are joined in the middle by an equipment deck that holds the attachment points for the sun-shield and the solar panels. The exact size of the depot depends on the modifications to the upper stage. The design, based on the ULA Advanced Common Evolved Stage (ACES), would hold 121 mT of total propellant (106 mT of LO_2 and 15 mT of LH_2).

Bell Aerospace also provided a depot concept derived from a Centaur vehicle [28], shown in Figure 10, which is very similar to ULA's first design concept. The depot stores both LO_2 and LH_2. The LH_2 module is a modified Centaur tank. The LH_2 module tank is launched with ambient temperature helium to reduce the requirement on the skin gauge. The LH_2 module holds 7.6 mT of propellant and utilizes vapor cooling, a composite strut, and GH_2 (gaseous hydrogen) ullage. The LO_2 module uses the Centaur's LH_2 tank to store the LO_2, with a volume of 48 m^3, and a capacity of 53 mT. New valves and plumbing are required to convert the Centaur vehicle to handle different cryogenic fluids.

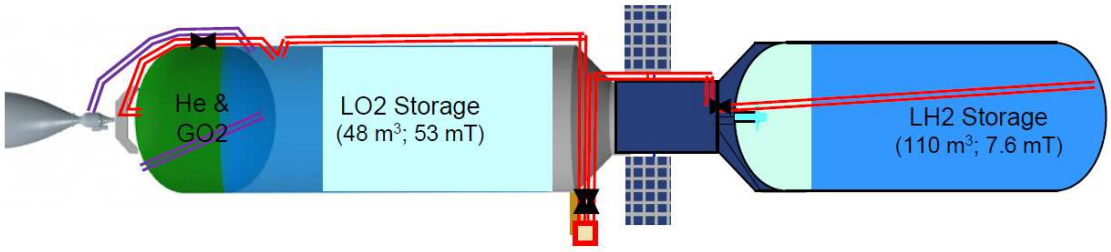

Figure 10: Bell Aerospace's Simple Propellant Depot Concept, reproduced from [28]

Zegler and Kutter's 2010 paper [29] provided an expanded discussion on the utilization of the ULA propellant depot and provided a compelling argument for the need for a propellant depot based architecture. The paper laid out a plan for evolutionary steps to gradually increase the capability of the propellant depot to satisfy the demands of increasing mission difficulty. Zegler and Kutter conclude that the propellant depot technologies are foundational to space exploration and "no serious Lunar or Mars architecture can avoid depots." The reasoning behind this conclusion is their belief that the heavy lift system path is not sustainable because it can only "economically perform the highest-level exploration tasks...due to its size, cost, [and] organizational entanglements." [29] This sentiment is routinely shared among other authors [5, 18, 30] who have examined the benefits of propellant depot based architectures.

Both Goff [23] and Kutter [27] conclude that while significant technology development effort is still required, the ability to refuel propulsion stages in orbit has tremendous potential benefits to the entire space community. Both studies presented near-term options as well as technology needs to provide long-term benefits to more aggressive exploration missions and destinations. Currently, ULA is preparing for a demonstration flight to test many relevant technologies for on-orbit fluid management and transfer. This demonstration flight, the Cryogenic Orbital Testbed (CRYOTE) mission [31] shown in Figure 11, is slated to be one of the first official proof-of-concepts

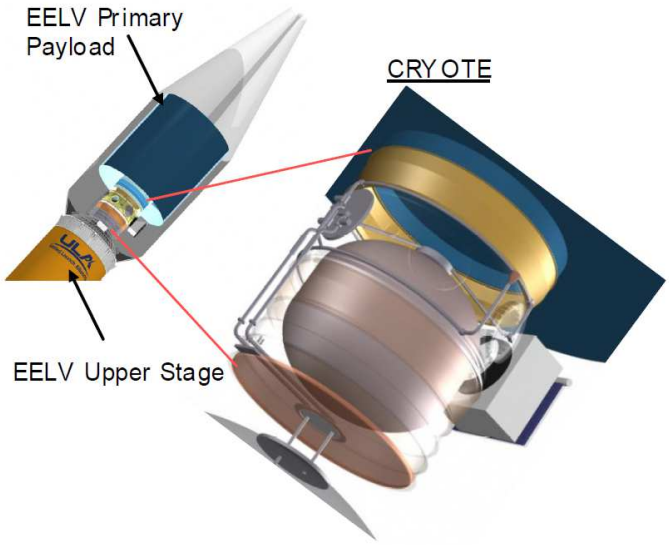

Figure 11: ULA's Cryogenic Orbital Testbed Vehicle on an Atlas V Launch Vehicle, reproduced from [23]

for large volume on-orbit fluid management and transfer of cryogenic fluids. The mission was scheduled to be flown as a secondary payload on an Atlas V mission in 2012; however, funding issues have yet to be resolved and the mission is still pending.

2.3 Propellant Depot Taxonomy

In order to fully understand the technological needs for a propellant depot based exploration architecture, a proper definition of the different components of a propellant depot is necessary. By examining the literature, the propellant depot system can be broken into four primary categories; structural subsystem, electrical power subsystem, propulsion subsystem, and the fluid management subsystem.

The structural subsystem serves as the backbone of the propellant depot system. The primary components are the tanks that serve as storage vessels for the propellant. Storage tanks are fairly common in space architectures because many of the exploration missions require large amounts of propellants. Tanks are generally made of aluminum alloys as a compromise between strength-to-weight ratio of the materials and cryogenic fluid compatibility. Composite materials have been proposed as

a replacement for improved performance [32, 33]; however, testing and large scale demonstration was conducted in 2014, but flight demonstration is still needed. The structural subsystem also includes the inter-tank adapters, the thrust structures that support the engine loads, and all other structural supports that are necessary for the tanks to survive the launch and in-space environments.

The electrical subsystems provide all of the power for the vehicle during its designed lifetime. For vehicles with short designed lifetime, lithium-ion batteries may be sufficient to provide the required power. For the majority of satellites and spacecrafts, power generation from solar arrays that are designed to provide enough power at their end-of-life operation [34]. The subsystem also includes the electrical power distribution to the entire vehicle and conversion systems for regulating the electrical power supply.

The propulsion subsystem provides the maneuvering capability for the propellant depot vehicle. Depending on the design, location, and required function for the depot system, the maneuvering requirements can be drastically different. A simple "dummy" propellant depot may have no propulsion system and rely solely on the rendezvous vehicle to capture the depot for propellant transfer. On the other end of the spectrum, a sophisticated depot system may have the capability to perform sub-orbital burns [25] to obtain orbit after separating from the launch vehicle as well as in-space maneuvers such as station keeping burns, Earth departure burns, and planetary insertion burns. The design for the propulsion system will be dependent of the mission requirements and the complete architecture optimization. A few of the available options include traditional chemical engines using cryogenic fluids, chemical engines using storable propellants, cold gas thrusters, solid propellant motors, high energy electric propulsion systems, and nuclear based propulsion systems [35].

The fluid management subsystem consists of different elements for long-term storage and transfer of the propellant in micro-gravity environment. This subsystem is

the most challenging as it is unique to the propellant depot system and because of the technology development required. Insulation, refrigeration, and other thermal management technologies will need to be employed to ensure the health of the fluids in storage. These thermal system technologies are discussed in detail in the next section. A work breakdown structure of the propellant depot subsystems is shown in Figure 12.

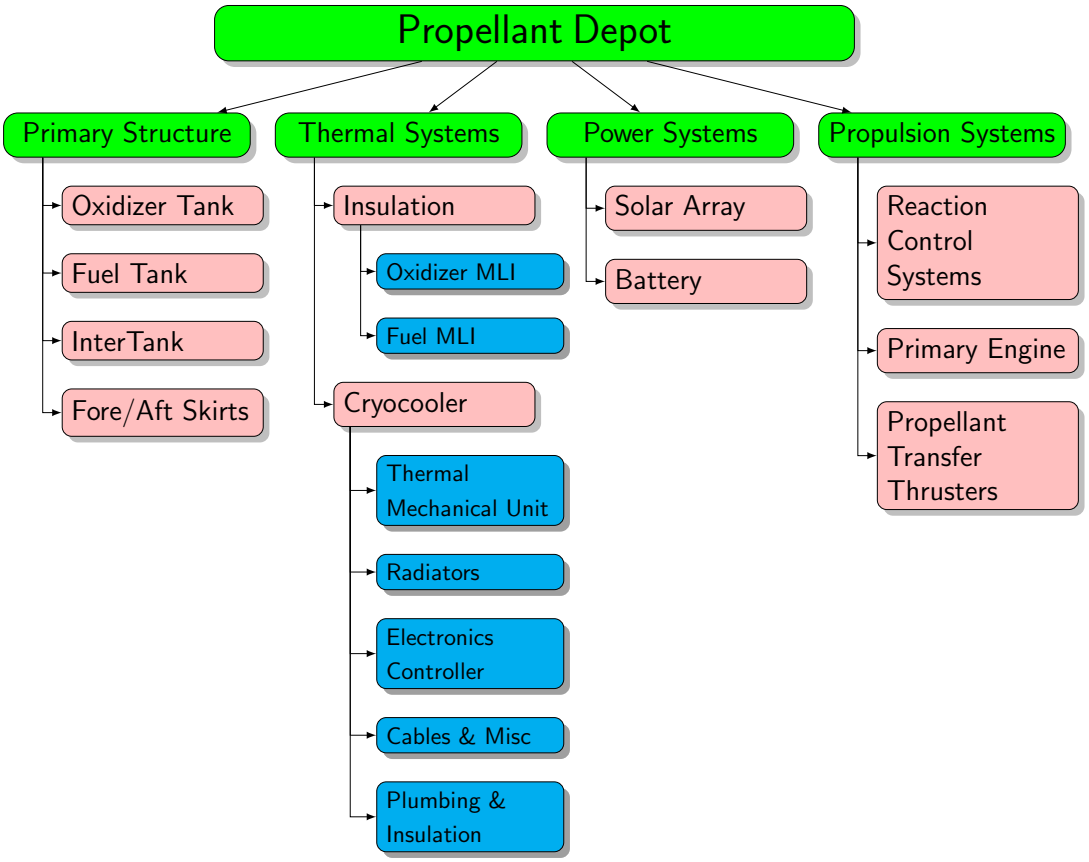

Figure 12: Propellant Depot Work Breakdown Structure

2.4 Propellant Depot Technology

The primary technology required for an on-orbit propellant depot is long-term cryogenic fluid management in a low-gravity environment. Cryogenic fluids have been used in spacecraft since before the Apollo program and are used expensively in propulsion and life support systems due to its high efficiency and superior performance. Thus,

the management of these cryogenic fluids is vital to the mission success. During the Apollo program, cryogenic fluids were used as both propellant for the trans-Lunar injection (TLI) maneuver and fuels for the fuels cells to generate electricity and water for the life support system [36, 37]. However, the thermal management for these fluids was very rudimentary, limiting the mission duration of the lunar missions.

In the harsh environment of space, the management of these fluids at cryogenic temperatures is extremely difficult. Without an active cryogenic cooling system, the temperature of the cryogenic fluids will increase due to heat penetrated through the insulation, causing the fluids to boil and pressure increase inside the storage tanks. In order to maintain proper pressure in the tanks, the excess pressure needs to be vented into space to avoid tank structural failure. This venting of the excess gas reduces the overall useable fluid for the mission, called boil-off loss, and therefore reduces the performance of the overall mission. During the Apollo program, after the spacecraft has achieved orbit, the crew only had six hours to perform the necessary vehicle health checkout before the TLI maneuver. This time constraint is due primarily to the boil-off of the cryogenic propellant in the Saturn V's SIV-B stage, which is used for the TLI maneuver. If the vehicle check out cannot be performed in a timely manner, the mission would be aborted due to the loss of performance of the upper stage vehicle [38].

The boil-off problem is also one of the primary reasons the EOR option was not selected for the Apollo mission. The Earth Orbit Rendezvous (EOR) mission requires the launch of two smaller launch vehicles, with a rendezvous in LEO where propellant and supplies is transferred from one to another, before the second vehicle depart for the moon. At the time, the technology for fluid management is limited to only a few hours on orbit, thus it would require an unreasonably strict launch schedule for the two launch vehicles. The risk associated with the launch schedule was deemed too high, and thus the EOR option was not selected [6].

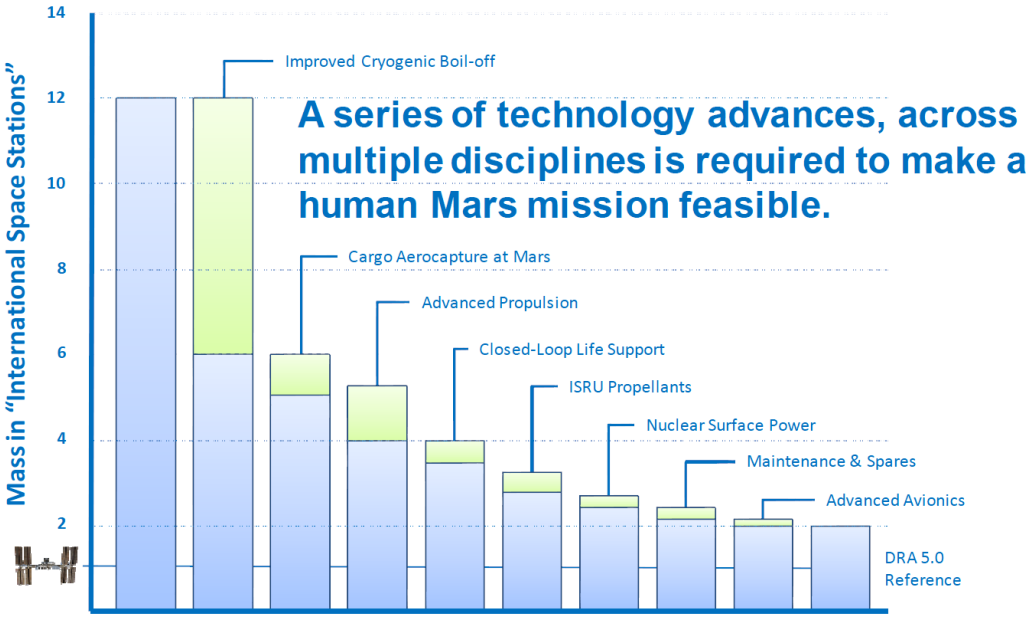

Figure 13: NASA Office of the Chief Technologist Mars Mission Mass Saving Potential due to Technology Investment [39]

Similarly, the cryogenic fluid boil-off problem is observed in the ESAS architecture and the Constellation program. The Constellation program adopted the EOR strategy, launching an unmanned Earth Departure Stage (EDS) with the Lunar Surface Access Module (LSAM) before a separate crew launch to rendezvous with the EDS [7]. But similar to the Apollo EOR concept, the cryogenic fluid boil-off imposed a schedule constraint on the two launches. Analysis of the then state-of-the-art in cryogenic fluid management resulted in a maximum 90 day loiter time for the EDS/LSAM stack in LEO before the crew is launched and the TLI burn. Failure for the crew launch to meet this schedule resulted in a loss of mission, as the performance of the EDS would be insufficient to perform the TLI maneuver due to boil-off losses.

For longer duration missions, the problem of cryogenic boil-off is even more profound. Combined with the enormous amount of cryogenic propellant that is required for high performance exploration missions, to Mars and beyond, makes in-space cryogenic fluid management a critical technology. In fact, NASA's Design Reference Architectures for human Mars mission requires zero boil-off (ZBO) technology for all

of its mission modes to be successful [8, 16]. NASA's Office of the Chief Technologist identifies cryogenic thermal management as the biggest game changing technology development for the reduction of mass required in orbit, as shown in Figure 13 [39]. Advancement in long-term cryogenic thermal management can significantly reduce the cost of an exploration architecture. An orbital propellant depot will benefit from the development of long-term thermal management. As the literature review showed, reduction in cost and complexity as well as increase in reliability, extensibility and flexibility of an exploration architecture are possible with the utilization of orbital propellant depots.

Dr. David Chato of NASA Glenn Research Center presented an assessment of the current state of technologies required for a cryogenic propellant depot [13]. A summary of this assessment is presented in Table 3 [13]. The Technology Readiness Level (TRL) for each technology element is given along with notable accomplishments performed in ground tests. Also, issues for in-space application and the desirability of a flight test are presented. Note that, to advance to a TRL of 6, the technology must be tested in a relevant environment, which typically involves a flight test. The Cryogenic Propellant Storage and Transfer (CPST) demonstration flight, scheduled for 2018, was unfortunately cancelled due to escalating cost.

2.4.1 Cryogenic Fluid Management

The first three technologies identified by Chato [13] addresses the long term in-space cryogenic fluid management challenge. Passive storage describes different techniques to mitigate the boil-off of the cryogenic fluids without directly interacting with the fluids. Instead, these technologies serve as a barrier between the external heating and the cryogenic fluids. The simplest form of passive storage management technology is insulation materials that can be applied directly to the storage tank wall. Most launch vehicles that employ cryogenic fluids for its propulsion systems have some

Table 3: Assessment of Technologies for a Cryogenic Propellant Depot [13]

Technology	TRL	Past Accomplishments	Low-G Issues
Passive Storage	5	3%/Month loss demonstrated with large scale LH_2 test	Low-G thermal stratification effects unknown
Active Storage	3-4	Sub-scale LN_2 demo (10W, 97K Cryocooler), large scale demo with commercial cryocooler	Low-G thermal stratification effects unknown
Pressure Control	4	Large-scale TVS demo with spray bar, sub-scale TBS demo with axial jet mixer	Low-G heat transfer and fluid dynamics affects mixing, de-stratification and cycle rate
Liquid Acquisition	3	Bubble point testing with LN_2, historical data (1960s)	Low-G heat transfer significantly affects liquid acquisition device performance
Fluid Transfer	3	Sub-scale demo of chill and no-vent fill testing	Transfer operation strongly affected by low-G
Mass Gauging	3	Components testing with simulant fluid (LN_2) and limited LH_2	some concepts strongly affected by low-G heat transfer and fluid behavior

form of spray-on foam insulation (SOFI) to protect the cryogenic fluids from the environmental heat on the launch pads [40, 41].

The most commonly used passive cryogenic thermal management system in space is multi-layer insulation (MLI). MLI is constructed of multiple layers of thin sheets of high reflective materials with thermal spacers between the layers. Its primary purpose is to reduce heat loss rate by thermal radiation and conduction. Currently it is used extensively on spacecrafts [42, 43] and satellites. MLI systems are efficient in the space vacuum environment due to low conduction heat loss and no convection heat loss mechanism. As noted by Chato [13], current state of the art in MLI technology can reduce the boil-off of LH_2 to roughly 3% per month, which can still be substantial in long duration exploration architectures. This improved technology led to the 90 days on orbit constraint for the Constellation program, as compared to 6 hours for the Apollo program in the 1960s.

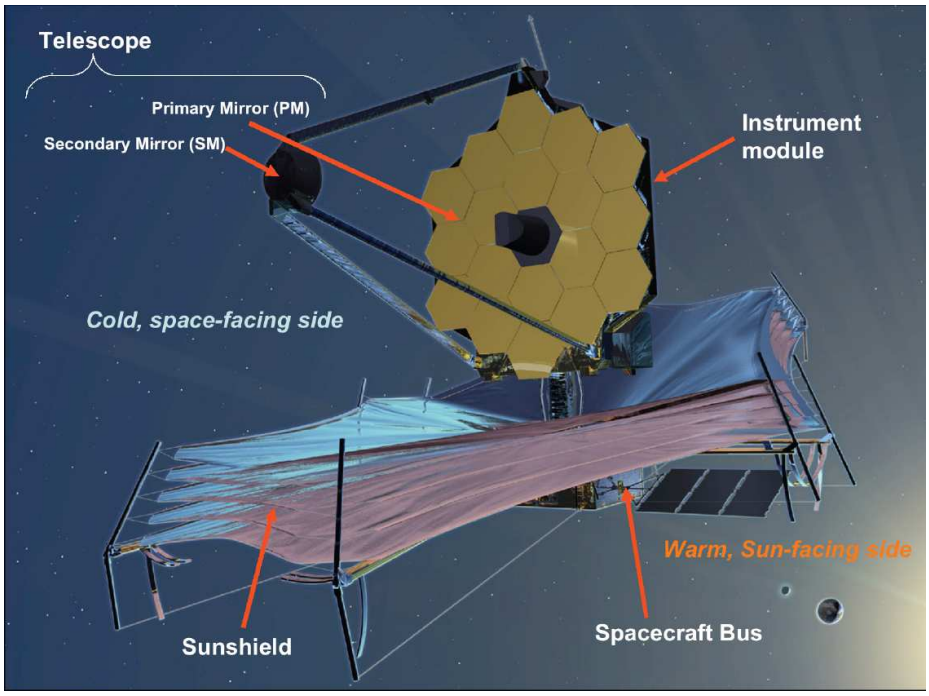

Figure 14: James Webb Space Telescope's Sun Shield, reproduced from [44]

The other primary forms of passive storage technologies are various types of optical shields such as sun-shields [23, 29, 45], which are being employed on the James Webb Space Telescope [44,46] as shown in Figure 14, or vapor cooled shields [47], which can be considered a semi-active storage technology because it uses the vented gas from the storage tank to keep the shields cold. These shields are not directly attached to the storage tanks, but serve as an additional barrier between the environment and the cryogenic fluids. The James Webb Space Telescope uses the sun-shield (Figure 14) to block direct sun light to both improve the imagining capability of the telescope and to keep the receiver mirror at near absolute zero temperature. ULA's propellant depot concept (Figure 9) also utilizes a form of optical sun-shield to improve the performance of the other thermal management system.

It must be noted that regardless of which form of passive storage technology is employed, the inherent nature of the technology is that it can only reduce the heat rate penetration, it cannot completely eliminate it. Thus, boil-off of the cryogenic fluid is

inevitable if only passive storage technologies are employed [30]. For short term missions, the boil-off of the fluid may be manageable, as seen during the Apollo program and the Constellation program; however, for multi-year manned Mars missions, the losses need to be eliminated completely.

The second technology area identified by Dr. Chato [13] is active storage cryocooler which maintain the temperature of cryogenic fluids with refrigeration. Cryocoolers transfer heat from the cryogenic fluids to another working fluid and releases the heat through heat exchangers to maintain the temperature of the cryogenic fluids below its boiling point. Cryocoolers have been used extensively on spacecraft in the past two decades. All of the space-qualified cryocoolers developed to date have been used on small satellites or probes maintaining the small amounts of cryogenic fluid used for cooling instruments [48, 49]. These cryocoolers have a relatively small amount of cooling capacity at the cryogenic temperature required.

ter Brake [50] in 2002 and Radebaugh [51] in 2009 provided two recent surveys on the state-of-the-art in cryocooler technologies. ter Brake cataloged performance data from 235 cryocoolers with cooling capacities below a few tens of watts and operating temperature between 4 and 120 Kelvin (K). The 2002 survey [50] combined the data from several previous surveys, including the 1969 survey by Daunt [52], 1974 survey by Strobridge, the 1984 survey by Smith [53], and the 1999 survey by Bruning [54]. Several papers have examined the use of cryocoolers for propellant depot architectures [30, 55], and many exploration architectures often assume ZBO technology exists [8, 16, 26] in order to make the mission possible. The implication of the ZBO assumption will be addressed in this dissertation.

2.4.2 Propellant Acquisition and Transfer

In addition to the long-term management of cryogenic fluid on orbit, two major areas of technology development are necessary for cryogenic propellant depots. The first is

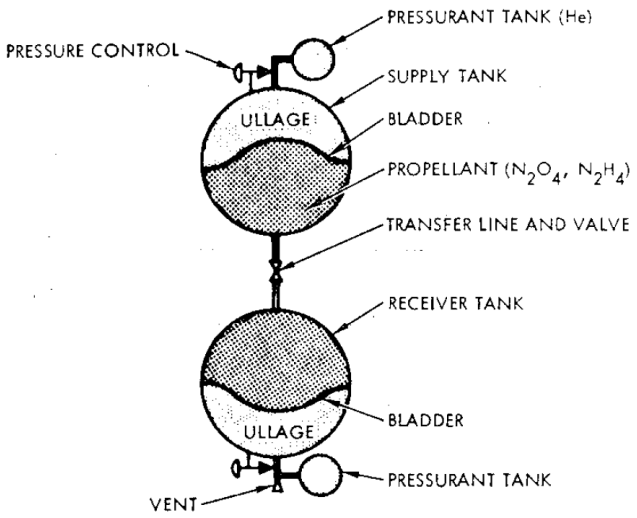

Figure 15: Schematic of a Pressure Fed Propellant Transfer System [59]

acquisition and transfer of the cryogenic fluids in a low-G environment. Transferring propellant from one system to another in orbit is a fairly routine operation today. The Russian Space Agency pioneered the propellant transfer techniques back in the 1970's with numerous mission demonstrations with the Salyut Space Station [56]. Since then, NASA has performed experimental missions such as the Orbital Refueling System in 1984 aboard the Space Shuttle Challenger (STS 41-G) [57], the Super Fluid On-Orbit Transfer demo in 1993 on the Space Shuttle Endeavor (STS-57) [57], and the Orbital Express demonstration mission in 2007 [19]. In addition, both the Russian Space Agency's Progress Vehicle and European Space Agency's Automated Transfer Vehicle have performed numerous propellant resupply missions to the International Space Station [58].

Propellant transfer in orbit is challenging due to the low-gravity environment. The European Automatic Transfer Vehicle uses a secondary tank to provide high pressure gases to force liquid from the transfer tank to the receiver tank on the International Space Station [58]. Figure 15 shows a schematic of this type of transfer [59]. This option provides an efficient way of moving fluids; however, using this system on a large resupply propellant tanker may require larger than acceptable pressurization

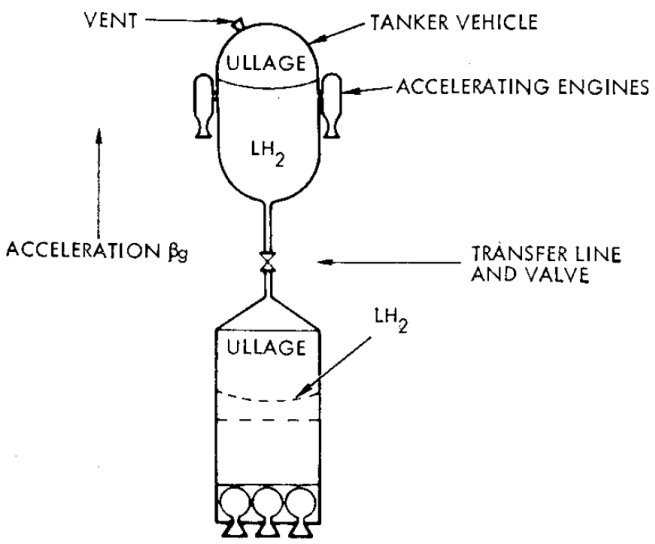

Figure 16: Schematic of a Thrust Fed Propellant Transfer System [59]

tanks. Russian Progress vehicles [57] have used bladders or membranes to transfer storable liquids to resupply the space station. This is a simple method for propellant transfer; however, most bladders are polymer or synthetic rubber based and have not been demonstrated for use with cryogenic fluids. Another method utilizes a transfer pump system, much like the demonstrated Orbital Express mission [19]; however, the system has yet to be utilized to transfer cryogenic fluid.

The most mature concept is propellant settling that leverages on decades of experience with upper stage engines for start-up in orbit. Upper stage engines address fluid transfer with acceleration by firing small solid rocket motors to provide appropriate engine start-up propellant flow rate from the tanks to the combustion chamber [35]. Figure 16 shows a schematic of this type of transfer [59]. For a propellant depot, depending on the required flow rate, the acceleration required can be addressed with small reaction control system thrusters using the excess boil-off, expendable solid rocket motors on the propellant tankers, or centripetal acceleration. The disadvantage of these systems is the need for a propulsion system to provide consistent vehicle acceleration for the duration of the transfer.

Several concepts have been proposed for fluid transfer without using rocket motors to settle the propellants. One of these involves generating rotational acceleration by spinning the storage tanks to settle the propellant in the desired location for the duration of the propellant transfer [57]. One concept envisions using electrodynamic tethers to accomplish the rotation of the propellant depot to settle the propellant [60]. This concept provides propellant settling without using reaction mass or expending propellants, but requires a large rotating structure which presents additional rendezvous and docking challenges. Another concept uses strong permanent magnets or electromagnets to force the liquid within the tanks to assume desired orientations [61–63]. Since LO_2 is paramagnetic and LH_2 are slightly diamagnetic, a strong magnetic field can influence the fluids to behave accordingly. However, the mass of the large magnet can be prohibitive; but it provides accurate control over the position of the fluids.

A completely different set of technologies have been proposed for transferring propellant without settling of the fluids. NASA Glenn has been conducting extensive research in the field of no-vent fill by pressurizing the tanks with boil-off gas of the propellant and then sub-cooling the liquid to return the vapor back to liquid state to minimize the boil-off losses [64–66]. Ground experimental testing has demonstrated the concept with minimal boil-off loss during the transfer; however, a flight demonstration has yet to be completed. Another non-settled transfer concept utilizes capillary flow and surface tension [67–69]. This type of device consists of multiple channels located within close proximity of tank wall. The portion of the channel facing the tank wall is covered with a tightly woven screen, and the screen tension of the propellant trapped in the pores of the screen prevents the flow of vapor into the channel to ensure vapor free fluid flow. A flight demonstration of this type of technology was scheduled for 2018 but has since been cancelled.

2.4.3 Propellant Mass Gauging

The final technology area for a propellant depot concept identified by Dr. Chato is mass gauging. Accurate measurement of the amount of propellant in a storage tank is vital to the success of any mission. Mass gauging in orbit is challenging due to the micro-gravity environment. Traditional methods of performing mass gauging are not directly applicable. Various concepts have been proposed to resolve the problem with low-gravity mass gauging. An optical mass gauge utilizes fiber optics to transmit light particles from the hardware to the tank and back to the receiver [70]. LO_2 has good fluid property for this particular application. In addition, laser based systems have also been proposed and designed to serve this purpose [71]. Compression mass gauge operate operates under the principle of slightly changing the volume of the tank by oscillating a bellow and measuring the resulting pressure change to compute the fluid level; however, the design of the bellow is challenging for cryogenic propellant [72]. Radio frequency mass gauge calls for measuring radio frequency response of the tank at various levels and using the data to compare to measurement in-flight to determine the fill level [73]. Testing of this type of mass gauge has been completed in low gravity aircraft.

2.5 Propellant Depot Concept of Operation

The design space of an exploration architecture based on propellant depots is expansive. However, regardless of the choices, the primary enablers for depot based architectures are the ability to decouple the propellant delivery mass from mission critical path and the use of low-cost commercial launch providers to deliver propellants. As illustrated in Table 2, regardless of destination, roughly three-quarters of the mass required in orbit for any exploration architecture consists of propellant which has little intrinsic value relative to the cost of the in space hardware.

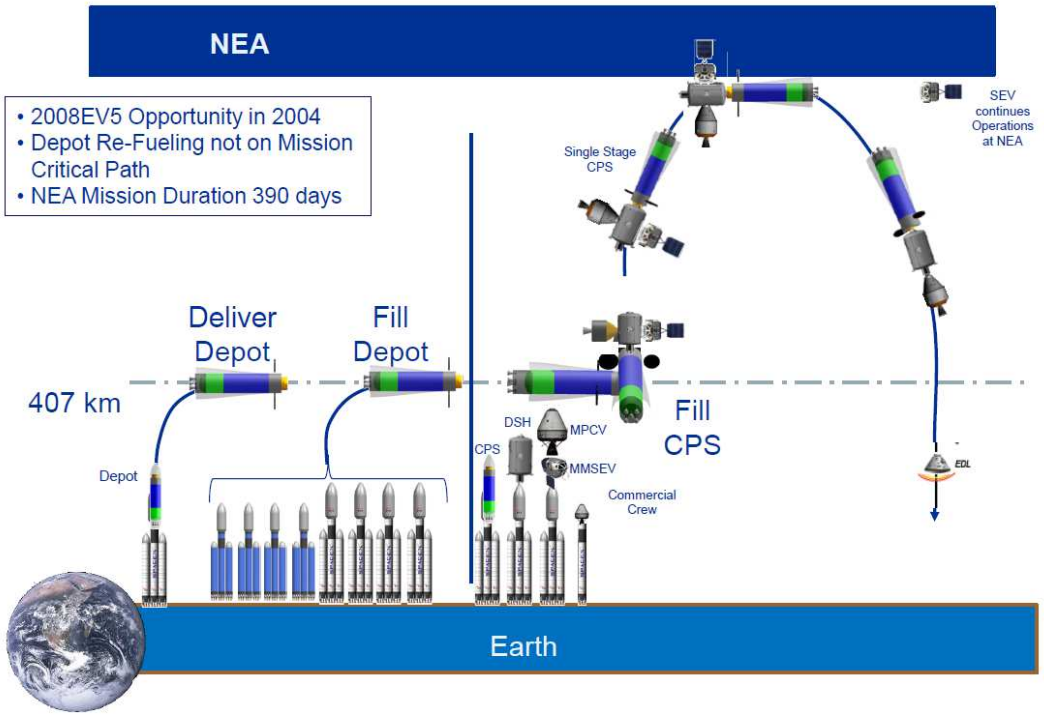

Figure 17: Notional Manned Exploration Architecture to a Near Earth Asteroid utilizing Low-Earth Orbit Propellant Depot, reproduced from [11]

Figure 17 shows a notional exploration architecture for a manned mission to an asteroid using a LEO propellant depot. The exploration architecture is divided into two distinct phases; the propellant aggregation phase and the mission operations phase. During the propellant aggregation phase, an empty or partially filled propellant depot is launched into orbit. Then propellant is aggregated over time with numerous commercial and/or government launch vehicles delivering tankers to rendezvous with the depot. As will be discussed later, there are no critical time constraint to the schedule of the propellant delivery as the mission elements and the crew have yet to be launched. However, there are scenarios in which the buildup must meet certain schedule constraints, such as in the case of a Mars mission, where the performance is highly depended on the planetary phasing. In this case, the utilization of multiple launch providers with multiple launch pads may be more ideal than any single launcher concept. In addition, because the primary payloads for these launches are

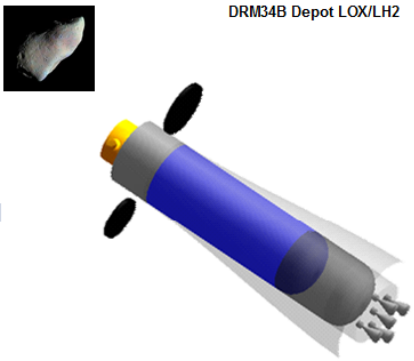

DRM34B Depot LOX/LH2

Propellants	LOX/LH2
Stage Diameter	6 m
Stage Length	28 m
Oxidizer Boiloff	0%/month
Fuel Boiloff	0.5%/month
Sub-orbital T/W	0.72
Orbital T/W	0.20
Power	3736 W
Cryocooler Power	2736 W
Mass Growth, %	30
# Engines / Type	5 RL10 B-2
Engine Isp (100%)	464 sec

	Mass, kg
2. Body Structure	8,835
3. Induced Environmental Protection	485
5. Main Propulsion	1,764
6. Orient Control Separation	193
7. Prime Power	261
8. Power Conversion and Distribution	52
9. Guidance and Navigation	38
10. Instrumention	32
11. Communication	97
12. Thermal Control	2,193
16. Range Safety and Abort	69
16a. Mass Growth Allowance	4,212
19. Ordanance	20
Dry Mass	**18,252**
21. Residual Propellant	4,616
23. Inflight Losses	30
25a. RCS Propellant	5,938
25. Total Propellant inc Boiloff	230,799
IMLEO	**315,208**

Description:

The combined propellant depot and CPS stage is capable of holding enough O2 and H2 (225MT) to perform NEA missions requiring up to 7 km/s of delta-V when used as a CPS stage. Both the Depot and CPS have MLI (SOFI for ground hold and 60 layer MLI), cryocoolers, and sunshield. Power is with Ultraflex solar cells.

Both the Depot and Depot-Derived CPS can be launched from a Falcon Heavy or Delta IV Heavy replacing the second stage of the launch vehicle and using the RL 10 engines to place itself into a 407 km, 28.5 deg inclination circular orbit.

Propellant Burn 1	187,354
Payload Burn 1	55,574
DeltaV Burn 1	4,228
Propellant Burn 2	31,273
Payload Burn 2	55,574
DeltaV 2	1,342
Propellant 3	6,978
Payload 3	48,281
DeltaV 3	395

Figure 18: Propellant Depot Example for a Manned Mission to Asteroid

relatively inexpensive propellants, a common propellant tanker can be used on multiple launch vehicles to reduce cost.

Separate but parallel from the propellant aggregation phase is the mission operations phase. While propellant is being aggregated in orbit, the mission hardware as well as the crew can be prepared simultaneously. As the necessary propellant for the mission has been accumulated, the hardware and the crew can be launched into orbit, rendezvous with the depot to take on the necessary propellant, and perform the mission nominally. In the notional architecture shown in Figure 17, the nominal mission utilizes the same hardware as the current HEFT in-space elements [4], but instead of launching the element on the heavy lift class Space Launch System, the elements are broken down into smaller increments, launched on commercial launch vehicles and assembled in orbit. As will be discussed later, the mass of each of the in-space element is less than the capability of current launch vehicles. A baseline propellant depot vehicle for the notional exploration architecture to an asteroid is shown in Figure 18.

The notional architecture (Figure 17) shows the utilization of propellant depot

Table 4: Potential Propellant Depot Architecture Design Space

Location	**Design**	**Propellant**	**Passive Management**
Low Earth Orbit	Existing Upper Stages	LO_2 Only	SOFI
High Earth Orbit	Dedicated Single Use	LH_2 Only	State-of-Art MLI
Geo-Synch Orbit	Dedicated Multi-Use	LO_2/LH_2	Sun Shield
Earth Moon L1	Modular Design	CH_4 Only	Vapor-Cooled Shield
Earth Moon L2		LO_2/CH_4	Vapor Venting
Low Lunar Orbit		RP-1	
Martian Orbit		LO_2/RP-1	

Transfer	**Mass Gauging**	**Resupply**	**Active Management**
Thrust Settled	Optical Sensors	Earth Only	None
Rotation Settled	Radio Frequency	In-Situ Moon	80K Cryocooler
Pressure Fed	Compression Sensors	In-Situ Mars	20K Cryocooler
Unsettled			Zero-Boil-Off
No-Vent Fill			
Magnetic Field			

Power	**Propulsion**	**Launch Vehicles**
Battery	None	Delta IV Heavy
Fuel Cells	Cold Gas Thruster	Atlas V 551
Solar Array	Solid Motors	Falcon 9
RTG	Chemical Engines	Falcon Heavy
	Electric Propulsion	Ariane 5
	Nuclear Propulsion	Russian Proton/Soyuz/Zenit

in a single architecture, in reality, the design space is quite large. Many studies in literature have mentioned the possibility of placing propellant depots in different near Earth locations to maximize its potential benefits. Zegler and Kutter [29] discussed the possibility of putting propellant depots in the Earth-Moon Lagrangian points to increase the flexibility of the overall architecture. In addition, these locations may provide provided reduced solar heating as compared to LEO [11].

Table 4 shows the potential design space for the utilization of propellant depot in exploration architectures. The design space can be further expanded to consider the different commercial launch operations as well as the different cryogenic fluid

management requirements. The location for the propellant depot will directly impact the environment in which the cryogenic fluids experiences and the payload delivery capability of the launch vehicle resupplying the depot as well as the departure condition of the exploration missions. The design and the propellant capacity of the depot will be dependent on the mission requirements, as well as the desire for flexibility and extensibility of the depot. The type of propellant stored by the propellant depot is also dependent on the mission requirements, as well as the potential for in-situ resources/propellant production. The exploration of the full propellant depot architecture design space is well beyond the scope of this dissertation. However, the methods developed in this thesis are well suited to evaluate the architecture feasibility of the different design options.

2.6 Commercial Launch Industry

Up until late 1970's, all of the launch vehicles delivering payload into orbit (both government and commercial) were owned and operated by government agencies. Much like passenger and cargo airlines in the early days of aviation, every aspect of the operation is highly regulated and restrictive. With a combination of public and private funding, the Arianespace Company created the first commercial Ariane launch vehicles to deliver commercial and government payloads to orbit. The first Ariane launch occurred on December 24, 1979 and delivered a payload into orbit successfully. Since then, Arianespace and five different iterations of the Ariane launch vehicles have had over 200 successful launches. [74]

The United States was not far behind in the commercial launch industry. Once the Space Shuttle became operational, the government turned over existing expendable launch vehicles to the commercial sectors while keeping the Space Shuttle as the primary payload delivery system for the United States. Boeing and Lockheed-Martin operated the Delta, Atlas, and Titan families of launch vehicles and began developing

Table 5: U.S. Commercial Launch Vehicle Payload Capability Summary [75–77]

	Falcon 9	Falcon Heavy*	Delta IV Heavy	Atlas V 551	
Payload	9,900	51,000	23,600	19,000	[kg]
Diameter	4.6	4.6	5.13	4.57	[m]
Length	11.4	11.4	11.7-22.4	10.2-16.3	[m]
Price (FY11)	$53M	$81-127M	$300M	$290M	
$/kg	$5.4k	$1.6k-$2.5k	$12.7k	$15.3k	

them for commercial use; however, it wasn't until the Challenger accident that the importance of these programs became apparent. The United States military, needing flexibility and reliability with delivering its payloads, turned to the commercial expendable launch vehicles. Still, the demand for the vehicles lagged behind supply. Because the Space Shuttle and the expendable launch vehicles were unable to achieve their designed launch rates, the fixed cost associated with the operation and upkeep of the infrastructure of the vehicles kept the prices of launch vehicles relatively high. Thus, the utilization of commercial launch vehicles in an exploration architecture was always seen as undesirable because of the high cost of commercial launch and the fairly low payload capability [14]. Less payload capability results in more required launches which increases the total cost of the overall architecture.

In the past decade, there has been a change in the commercial launch industry landscape. Space Technology Exploration Corporation (SpaceX) entered the market in 2002 and may rewrite the economics of commercial launch market. SpaceX has moved 95% of the design and manufacturing of the launch vehicles and subsystems in house to drastically reduce the launch prices they offer, as shown in Table 5. Much like the disruption of the low cost airlines in the 1970's, SpaceX's entry may fundamentally change how commercial space companies conduct business.

The primary providers for commercial launch vehicles in the United States are United Launch Alliance and SpaceX. The payload capabilities of the current U.S.

*Currently in Development, First Operational Flight Scheduled for 2014-2015 [78]

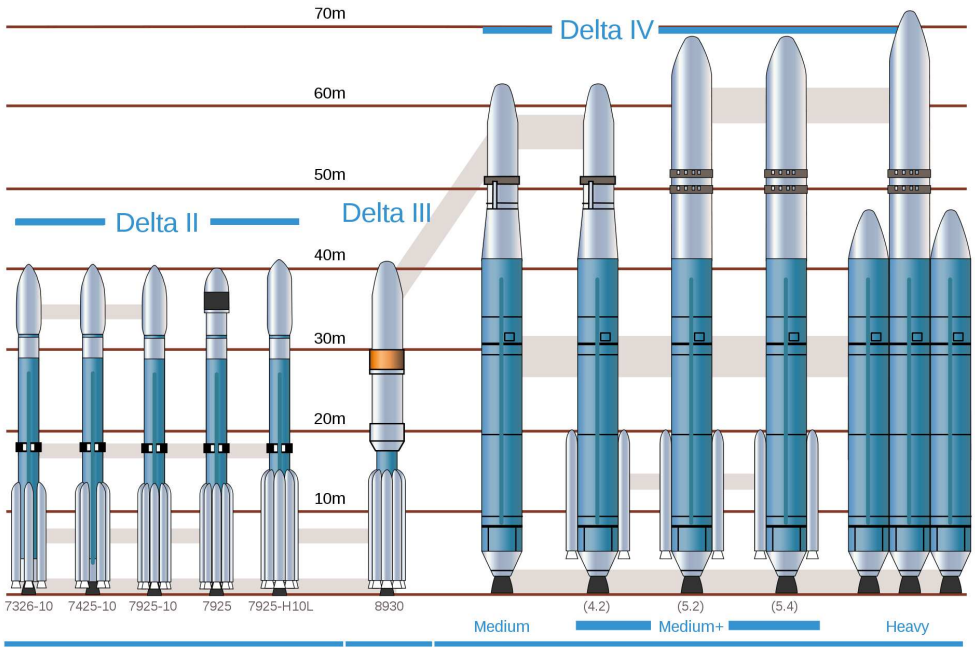

Figure 19: Boeing's Delta Family of Launch Vehicle, reproduced from [79]

commercial launch vehicles can be summarized in Table 5. Boeing's Delta families of launch vehicles were first introduced in the 1960s as modified United States Air Force Thor ballistic missiles. Currently, United Launch Alliance operates two families of Delta vehicles; the Delta II and the Delta IV, shown in Figure 19. The largest in the family is the Delta IV Heavy vehicle, capable of delivering 23,600 to 28,000 kg of payload to LEO, at a FY 11 price of $300 million [76].

Similarly, the original Lockheed Martin's Atlas family of launch vehicles (Figure 20), which began as intercontinental ballistic missiles, was converted to launch payloads into orbit. Currently, only the Atlas V variant is still in operational. The largest of which is the Atlas V 551 vehicle, with a payload capability of 19,000 kg to LEO at a price of $290 million [77]. SpaceX's Falcon 9 is the newest commercial launch vehicle. Since the first flight in 2010, it has had eight successful flights, including sending Dragon capsule to the International Space Station. The Falcon 9 is scheduled to have more than 10 launches in 2014, with increasing number of launches as the demand for the vehicle increases. The Falcon 9 has a payload capability of less than 10,000 kg

Figure 20: Lockheed Martin's Atlas Family of Launch Vehicle, reproduced from [79]

costing $53 million per flight. Comparing to the other two United Launch Alliance launch vehicles, this constitutes a 50 to 70% reduction in the cost of LEO payload delivery. The Falcon Heavy vehicle, currently slated for a 2015 first test flight, will reduce the price of payload delivery even further, as it has a design LEO payload of over 50,000 kg at a targeted price of $130 million.

In terms of launch reliability, both the Delta and the Atlas have impeccable launch records that demonstrate their high reliability. Since its initial launch in 1989, there have been 154 Delta II launches, with only three recorded failures of the vehicle [74]. The Delta IV family has 21 launches since its first flight in 2002, with only one partial failure that caused the payload to be inserted into an incorrect orbit. The Atlas family of vehicle, since 1968, has had 229 launches with only 16 failures [74].

Outside the United States, Japan, China, Russia, and the European Space Agency all have their own launch vehicles that can provide payload delivery to low Earth orbit with varying payload capability and launch prices. One of the primary analyses that this dissertation will examine is the utilization of the emerging launch market to satisfy the high demand of payload delivery by a propellant depot based architecture.

The analysis and discussion will be presented in a later chapter.

2.7 Challenges to Propellant Depot Based Architecture

The potential benefits of a propellant depot enabled exploration architectures were briefly described in Chapter 1. As with any new ideas and concepts, there are numerous challenges to its implementation. The primary challenges to the propellant depot based exploration architecture can be divided into three topics; the technology and performance requirements of the proposed depot system, the reliability and safety of the overall mission with the large number of required flights, and the cost of requiring higher number of launch vehicles. These three challenges were summarized by former NASA administrator Dr. Michael Griffin in his opinion editorial in 2011 titled "Propellant Depots Instead of Heavy Lift?" [14].

The primary challenge to the technology requirement is due to the management of on-orbit boil-offs of the cryogenic fluids, as the "the ability to maintain it in its cryogenic state is critical." [14] Dr. Griffin states that with today's technology, on-orbit fluid management systems can achieve "liquid hydrogen boil-off losses of about 0.35 percent per day, or about 10 percent of the fuel per month." [14] For exploration architectures that require hundreds of metric tons of propellant aggregated in orbit over the course of many months, boil-off loss of up to 10% per month makes the depot based architecture unattractive. Especially because the payload capability of current commercial launch vehicles are relatively low. The technology requirement to achieve zero-boil-off is relatively immature as shown by Dr. Chato's report [13]. Thus the boil-off loss reduces the performance of the overall system to an unacceptable level. However, recent developments in cryogenic fluid management technology have made dramatic impacts on the overall system performance.

Challenge to the overall safety and reliability of the architecture is the fact that by

launching the required mass into orbit using smaller launch vehicles, the overall probability of successful mission is drastically reduced. With each launch vehicle having an independent success probability of 98%, requiring 3 of these launches will result in an overall success probability of roughly 94%. However, if the required number of launches increased to 10 or 15, as in the case of a propellant depot based architecture, the overall mission success probability is reduced to 81% and 74% respectively. Thus, an architecture that requires a large number of launches cannot be seriously considered for human space exploration if employed by this series approach.

Finally, the economic challenge is "that marginal specific cost of payload to orbit is generally lower for larger launch vehicles." [14] This is observed in all other forms of transportation, where larger vehicles generally provide better economics for delivering cargo or people from one location to another. In addition, the economic attractiveness of a depot based architecture is subject to the ever changing economics and payload delivery capability of the of commercial launch market. These three areas of concern give rise to three specific research questions and hypothesis that are addressed in this dissertation.

Research Question 1: What are the major technical and performance challenges for a long term orbital propellant depot, and how do these challenges impact the feasibility of the overall exploration architecture?

Hypothesis: The primary technical challenge resides in the long-term storage and transfer of cryogenic fluids in micro-gravity. Both of these areas can be addressed with current state of the practice technologies with minimal development efforts and will not negatively impact the overall performance of the architecture.

Research Question 2: How does the utilization of propellant depot and commercial launch impact the overall mission reliability, safety, and payload manifesting of

exploration architectures?

Hypothesis: All currently planned mission elements can be broken down into elements that fit on existing commercial launch vehicles. Overall mission reliability can be improved with system reliability growth which benefits from increase launch numbers. Redundant systems can be utilized with depot based architecture which can provide additional reliability improvement.

Research Question 3: What are the economic implications of utilizing commercial launch services with orbital propellant depots on overall feasibility of the exploration architecture?

Hypothesis: A propellant depot with commercial launch based exploration architecture provides significant cost savings compared to the exploration plans utilizing heavy lift launch vehicles. The propellant depot architecture presents program costs that can fit within a more realistic level of budget expectation. The utilization of commercial launch vehicles to deliver propellant to orbit also provides a more stable economic platform for long term space exploration.

These research questions and their corresponding hypothesis will be addressed in this dissertation with extensive literature search, complex modeling and simulation, and detailed analysis of the results in the coming chapters in order to establish the feasibility of a propellant depot based exploration architecture. Research question 1 will be addressed in Chapter 4, question 2 will be addressed in Chapter 5, and question 3 will be addressed in Chapter 6.

CHAPTER III

METHODOLOGY

This chapter presents the methodology used in this dissertation for evaluating exploration architectures for various feasibility metrics. A literature review of the definition and methodology for feasibility assessment is presented and the deficiencies of current methods are discussed. To address these deficiencies, formulation of a stochastic feasibility assessment method is presented. The use of stochastic methods in risk assessment techniques strengthens current feasibility assessment methods and provides a quantitative evaluation of overall feasibility. This chapter concludes with a notional feasibility assessment example. The areas of feasibility challenges identified in Chapter 2 will be addressed in Chapters 4, 5, and 6.

3.1 Feasibility Definition

Feasible*(adj.): capable of being done or carried out <a feasible plan>; capable of being used or dealt with successfully; reasonable; likely.* [80]

The assessment of the feasibility of any concept by definition is subjective. The dictionary definition [80] uses terms like "likely," "reasonable," and "capable," all of which are subjective. Depending on the perspective of the individual or group performing the feasibility assessment, drastically different conclusions can be reached as each individual has their own definition of "reasonable" or "likely". The definition also uses the word "successfully" in the definition, implying that in order to for something to be feasible, it needs to meet some objective or measure of success. In optimization problems, feasibility is defined only in the presence of constraints [81] and is generally a Boolean quantity.

In complex engineering systems, feasibility studies are critical to ensuring the

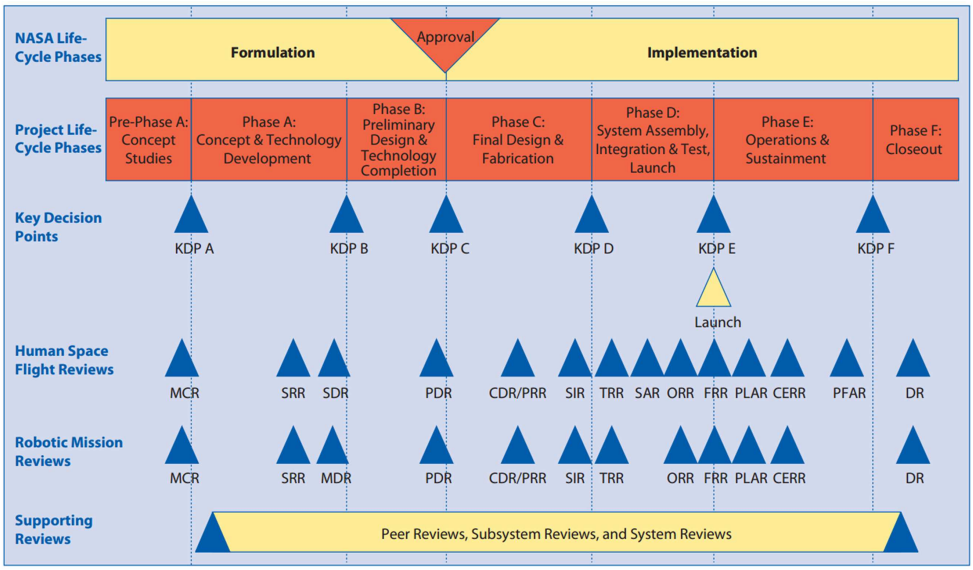

Figure 21: NASA Project Life Cycle, reproduced from [82]

success of a program. NASA's project life cycle as defined by the System Engineering handbook is shown in Figure 21 [82]. The handbook states that the primary purpose of Pre-Phase A stage of the project life cycle is to "devise various feasible concepts from which new projects (programs) can be selected" and that "conceptual designs are often offered to demonstrate feasibility and support programmatic estimates." The emphasis of the Pre-Phase A stage is to establish feasibility and desirability of the concept. In essence, during this stage of a project life cycle, the feasibility of the concepts should be well understood and only feasible concepts will progress to the Phase A stage. However, the handbook does not specifically define the measurement used for feasibility but relies on expert opinions which can be subjective in nature.

Feasibility studies are conducted during early phases of product life cycle where major design decisions are made. These decisions can have dramatic impact on the ultimate characteristics and overall cost of the system. These design decisions are made while the knowledge of the system is very limited and minimal budget and research effort are available to improve the knowledge during this phase. The NASA System Engineering Handbook states that during the Pre-Phase A feasibility study,

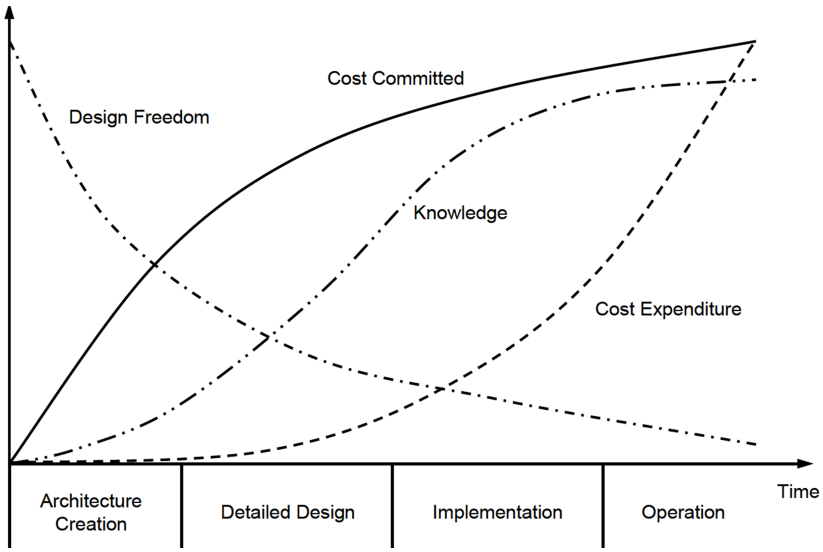

Figure 22: Notional Cost, Freedom, and Knowledge in Program Design Life Cycle [83]

"analysis and designs are accordingly limited in both depth and number of options." [82].

This is illustrated in Figure 22 in a notional representation of the cost, design freedom, and knowledge about a product during the design life cycle [83]. The results of the Pre-Phase A step in the design life cycle significantly impacts the final operational characteristics of the system, thus "it is essential that life-cycle considerations be an inherent aspect of the feasibility analysis activity. [84]" If a conceptual level study can include all life-cycle considerations along with the uncertainties that are inherent in these early design phases, the overall knowledge of the concept can be improved. By increasing the knowledge of the design earlier in the life cycle, more informed decisions can be made to maintain the design freedom during the pre-conceptual level and thereby decreasing the cost committed early in the project.

3.1.1 Literature Review

A search for feasibility studies in the aerospace literature reveals a wide range of use for the term applied to different levels of analysis. Some papers discussed in detail the feasibility of subsystem level components through modeling and simulation [85,86] and

experimental testing [87], and others addressed only with system level analysis [88–90]. A review of a selection of these feasibility studies provides a general overview of what the aerospace community have used as benchmark to determine concept feasibility.

- Deckert and Hickey's paper [91] in 1970 examined the feasibility of vertical and short take-off and landing aircraft. The study provide one of the best examples of utilizing the standard system engineering process of defining the design requirements, providing a system level trade study, and evaluating the concepts through the entire life-cycle consideration. The study provided sound design recommendations for the different types of aircraft concept under consideration; however, the study fails to discuss the actual feasibility of the various concepts.

- Loftus et al.'s feasibility evaluation [87] in 1972 on powder rockets documented a detailed design and testing of ammonium perchlorate/aluminum powder propellant rocket engine. The study details the design and modeling process of estimating the performance of various powders for rocket use and follows with experimental testing results to validate and demonstrate the feasibility of using solid powders as a propellant in rocket engines. The success of the experimental testing was used to validate the concept feasibility.

- Hawke et al.'s feasibility study [88] in 1981 on electromagnetic rail-gun launchers presented detailed technical analysis of the proposed launcher system that includes identification of "limiting factors that influence designs". The design of the rail-gun launcher was such that it satisfied the limiting factors identified. The study concluded that although more research and development is needed in order to extend the launch capability of the rail-gun, there are no physical limitations to the overall feasibility of the concept. These defined physical limitations were used to justify the feasibility of the proposed concept.

- Parlos and Metzger's feasibility study [86] in 1994 on a contained pulsed nuclear propulsion engine utilized detailed modeling of the overall engine and preliminary analysis using off-the-shelf materials to demonstrate a potential for the engine to have thrust-to-weight ratio greater than one. The conclusion of the study states that, after the complete analysis, it is conceivable that the concept can be built and tested without physics and engineering challenges. The requirement for engine thrust-to-weight ratio greater than one is the author's definition of the technical challenges to the concept's overall design was used as the constraint for concept feasibility.

- Heaton and Longuski's feasibility assessment [85] in 2003 on Uranian satellite tour using Galileo style trajectory focuses on the design and analysis of potential trajectories for an example mission to the Uranian satellites. The study provides an example trajectory given a set of guidelines and constraints and demonstrates that the feasibility of the mission by showing feasible solution.

- Takayanagi et al.'s feasibility assessment [89] in 2010 on a nonstop Mars sample return system provided a detailed parametric study of aeroshell designs for a Mars aero-flyby sample collection mission. The conclusion of the assessment was a selection of a candidate aeroshell that is feasible for the mission with emphasis on ease of the manufacturing process. In addition, experimental testing was conducted to demonstrate the accuracy of the computational models. These experiment validations can be related to TRL completions which makes the concept feasible.

- Brophy et al.'s feasibility study [90] in 2011 on an asteroid return mission examined concept of sending a robotic system to retrieve a 10,000 kg asteroid to the ISS. The study identified eight feasibility issues with the concept, ranging from the identification of potential asteroids to trajectory of the asteroid return

and the docking of the asteroid to the ISS. A detailed technical analysis of each of the identified issues was presented and the study concludes that the concept is feasible by the end of this decade (2019) because there were no show stoppers identified.

From the literature review, it is clear that there is a general lack of uniformity when using the term "feasibility study." In many instances, the title of the paper would include the term; however, no discussion of how feasibility is demonstrated exist in the text. The most common use for the term seems to focus on the ability for the concept to satisfy the goals or requirements set forth in the introduction and many of these requirements are limited in scope. Additionally, the subjectivity of the term feasibility is observed as each author uses their own opinion to describe what they think constitutes a feasible solution.

In order to determine the feasibility of a propellant depot in the framework of an exploration architecture, there is a need to quantify feasibility. From the literature study, one can determine the methods required to evaluate feasibility. Deckert and Hickey [91] demonstrated the need for a system level trade study and the evaluation of the concept to help assess the feasibility. Loftus [87] showed how feasibility can be proven with experimental testing of the concept in question. Hawke [88], Parlos [86], and Heaton [85] all showed the need for requirements and constraint definition in the feasibility assessment process. Finally, Takayanagi [89] and Brophy [90] showed the need to present solutions that meet all the necessary requirements to demonstrate the feasibility of the proposed concept. The next section describes in more detail the methods used in literature to analyze a system or concept for feasibility so the deficiencies with current feasibility studies can be identified.

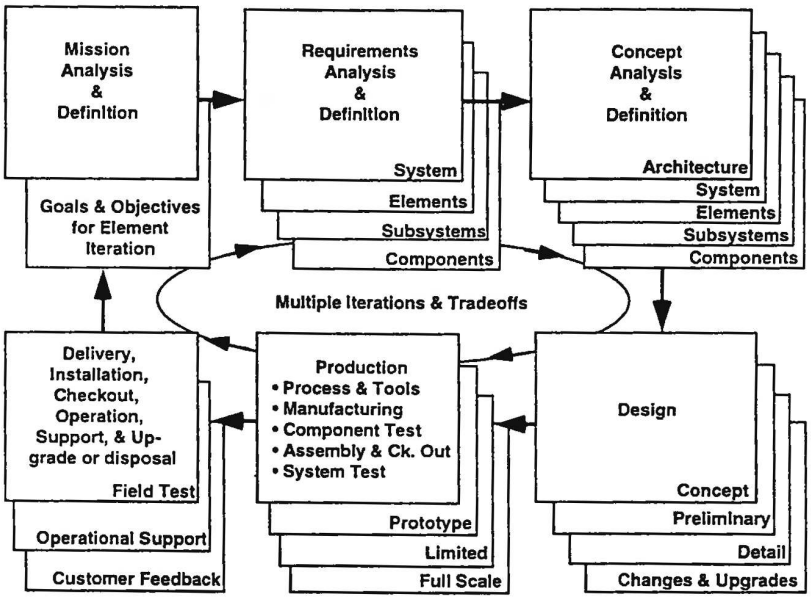

Figure 23: System Engineering Process, reproduced from [92]

3.2 Feasibility Assessment

For a conceptual level study to be feasible, the concept must be capable to be designed and developed successfully, as per the definition [80]. In this sense, the feasibility of a concept can be separated into two components: whether or not the concept can accomplish its objective and satisfy its constraints and whether or not the concept can be developed and built within a time and budget constraint (NASA System Engineering Handbook [82]). These are two separate questions: one addressing the performance of the proposed design and the other addressing the economics and system integration requirement of the concept.

3.2.1 Performance Evaluation

The performance evaluation portion of the feasibility assessment is the most common type of feasibility study conducted in literature. The evaluation process closely follows the first few steps of the system engineering process [92] (Figure 23), from mission and requirement analysis and definition to concept design and evaluation. All of the

examples of feasibility studies presented in the previous section provided this form of feasibility assessment.

The primary goal of the performance evaluation is to investigate whether the concept is capable of meeting the requirements of the study. All of the studies presented in the literature search have specific requirements in mind and the subsequent analyses in the paper were conducted to meet these requirements. For example, Brophy [90] wanted to investigate the possibility of retrieving an asteroid from beyond the cis-lunar space and bring it back to the ISS for examination. The team analyzed potential targets for retrieval, conceptually designed a capture system for the asteroid, simulated low-thrust trajectories for the mission, and provided mass estimates for the spacecraft and subsystems.

Brophy's analysis focused on the technical aspects of the mission design. Can a candidate asteroid be identified? Yes; the paper showed that there should be a plethora of candidate asteroids that fit within the requirement of 10,000 kg mass. Can the asteroid be captured? Yes; the paper demonstrated a concept to retrieve the asteroid using a newly developed system. Can a spacecraft get to the asteroid and back? Yes; using a new solar electric propulsion system, the team designed a trajectory to send the craft to and from the asteroid. Can the spacecraft be launched into orbit? Yes; with mass estimate of each of the components, the spacecraft has low enough mass to be launched on currently available launch vehicles.

All of these performance evaluations demonstrated that for each of the feasibility questions, a technical analysis can be performed to answer the question. Thus, the concept is feasible because there exists a solution that satisfies the requirements set forth by the study. However, even though the analysis showed that the solution exists, very little consideration is given to the actual integration and operation or the overall cost of the proposed concept. The concept proposed the use of several new technologies such as the solar electric propulsion system and the asteroid retrieval

device. The performance of these devices was assumed to be capable of satisfying the requirements. The feasibility claim of the study hinges on the performance assumptions of these new technologies, thus the technology integration must be part of the feasibility analysis. To accomplish this, NASA utilizes different readiness scales to quantify the technology maturation process.

3.2.2 Readiness Levels

The second part of feasibility assessment addresses the technology and system integration requirement for the proposed concepts. With any proposed concept the infusion of new technologies or new systems is inevitable. The performance of these new technologies and systems are captured in the performance evaluation and these evaluations can be crucial to the overall success of the concept. Thus, the belief that these new technologies can be iterated into the concept successfully is pivotal to the determination of overall concept feasibility.

The successful integration of different technologies into a concept is difficult to quantify. There isn't a mathematical equation or analysis that can show whether or not a technology is going to be successful or not. In order to combat this difficulty, prescriptive or soft metrics are needed to make informed decisions. NASA developed a readiness scale to assess the maturity of technologies and to provide a consistent comparison of the level of advancement of the different technologies. NASA's scale defines the maturity of any technology into nine levels and the definition of each of the levels was published by Mankins [93] in a 1995 white paper. The Technology Readiness Level (TRL) scale is summarized in Table 6.

The TRL scale provided a definition of different levels of technology maturity. TRL level 6 is typical level of technology maturity in which the initiation of a development program is appropriate. Using the scale to evaluate technologies that are required for any proposed concept provide a preliminary measure of feasibility of the

Table 6: NASA's Definition of Technology Readiness Levels [93]

Level	Technology Readiness
1	Basic principles observed and reported
2	Technology concept and/or application formulated
3	Analytical and experimental critical function and/or characteristic proof-of-concept
4	Component and/or breadboard validation in laboratory environment
5	Component and/or breadboard validation in relevant environment
6	System/subsystem model or prototype demonstration in a relevant environment (ground or space)
7	System prototype demonstration in a space environment
9	Actual system completed and "flight qualified" through test and demonstration (ground or space)
9	Actual system "flight proven" through successful mission operations

concept that is useful in comparing multiple concepts. For example, if concept A utilizes ten technologies that are all TRL 4 and concept B utilizes ten technologies that are all TRL 7, then it may be said that concept B is more feasible than concept A. However, this type of comparison is flawed on two fronts.

First, while the example provided a somewhat clear winner when it comes to feasibility, in reality, the required technologies are typically scattered across the TRL scales which can make the feasibility claim more challenging. If concept A utilizes two technologies with TRL 4 and two with TRL 7 while concept B utilizes one technology with TRL 2 and three with TRL 9, it would be difficult to determine which of the two concepts is more feasible. Second, while the TRL scale provided a way to systematically evaluate the technologies that are required for any concept, there is no information regarding the advancement difficulty or probability of the technology to advance from one level to another. NASA recognizes this deficiency

Table 7: NASA's Definition of Research & Development Degrees of Difficulty [94]

Level	Research Development Degree of Difficulty
I	A very low degree of difficulty is anticipated in achieving research and development objectives for this technology *Probability of Success in Normal R&D Effort 99%*
II	A moderate degree of difficulty should be anticipated in achieving R&D objectives for this technology *Probability of Success in Normal R&D Effort 90%*
III	A high degree of difficulty anticipated in achieving R&D objectives for this technology *Probability of Success in Normal R&D Effort 80%*
IV	A very high degree of difficulty anticipated in achieving R&D objectives for this technology *Probability of Success in Normal R&D Effort 50%*
V	The degree of difficulty anticipated in achieving R&D objectives for this technology is so high that a fundamental breakthrough is required *Probability of Success in Normal R&D Effort 20%*

and developed a second scale to evaluate the degree of difficulty of the technology maturation process. This scale is published in a second white paper by Mankins [94] in 1998 and the definition is summarized in Table 7.

The Research & Development Degree of Difficulty (RD^3) scale ranks the difficulty of the technology maturation from level one through five. The goal of the development of the RD^3 scale is to work in tandem with the TRL scale to provide a more comprehensive evaluation of the maturity of technologies. However, the same problems experienced with using TRL scales also exist with the RD^3 scale. There is no systematic way to evaluate two concepts if the technologies it uses are across multiple TRLs and RD^3s. There are system engineering techniques that can be employed for selection of the concept based on different weighting scales, such as the Technology Need Value (TNV) [95], but these methods do not fully address the problems with using TRL and RD^3 scales. In general, moving technology from one readiness level to the next requires research and development efforts that can have dramatic impact

on the economics of the concept. This will be discussed in more detail in Chapter 6.

3.2.3 Feasibility Study Deficiencies

The aerospace industry examples demonstrate two distinct areas of deficiencies in a feasibility study. The first area is the incompleteness in the analysis of a concept for feasibility. The examples listed in the previous section demonstrate the narrow focus of typical feasibility studies. For example, while the Uranian satellite tour proposed by Heaton [85] is technically feasibility in the sense that a trajectory can be designed, no considerations were given to whether or not propulsion and guidance systems can achieve the accuracy of the proposed trajectory. In addition, the study was conducted under specific guidelines and constraints; however, no analysis is presented to discuss the impact of these guidelines on the feasibility of the trajectory or any uncertainty involved with the modeling and simulation results. In the asteroid retrieval case [90], the analysis provided a rigorous examination of all of the different technical aspects of the mission, but it gave no considerations to the cost of achieving the objectives or the benefit of such a mission.

To adress this problem, techniques from the corporate and business world can be used as a guide. In the business world, feasibility assessment mainly focuses on the economics of the proposed concept. Rigorous cost-benefit analysis is typical in a business feasibility assessment and formal Return on Investment (ROI) analysis is used as the primary figure of merit to determine feasibility [96]. The ROI provides the assessment of whether or not the proposed concept is "bankable." The ROI analysis is critical in the risk assessment of business proposals to determine the likelihood of the concept being profitable. In addition to economic aspect of feasibility, the business world's feasibility study also addresses other topics such as the schedule, operation, and legal aspects of the concept. These areas of investigation make up the TELOS feasibility acronym (Technology, Economics, Legal, Operation, Schedule)

that is common in the corporate setting [97, 98].

The TELOS feasibility technique outlines the systematic approach to analyze a concept for feasibility. The general question for each area can be summarized as [99]:

Technical:	*How likely is the concept capable of being built?*
Economic:	*How likely is the concept return worth the investment?*
Legal:	*Will the concept violate any laws or create legal problems for the company?*
Operation:	*Will the concept solve the problem that it is created to remedy?*
Schedule:	*Is it likely the concept be built in time to realize the benefit and/or meet constraints?*

By applying the TELOS feasibility approach to aerospace system feasibility studies, one can begin to analyze the concept in a more comprehensive format, thereby increasing the knowledge during the pre-conceptual phase of the project life cycle and mitigating the impact of poor decisions early in the life cycle.

The second area of deficiency is the lack of objective measure for feasibility. The technology and system integration portion of the feasibility assessment may use readiness scales that are defined by NASA and evaluated by subject matter experts. The fundamental problem with these evaluation metrics is that they are qualitative in nature. By using qualitative measures to evaluate concepts, information that may be critical for feasibility assessment may be lost. The two scales, presented in the previous section and other scales available in literature, are only as good as the opinion of the technical experts and their interpretation of the scales. Furthermore, these scales are subject to the opinion and motivation of the evaluators. Adding to the complexity of concept feasibility definition, feasibility studies in literature perform assessments at different stages of system maturation; ranging from the pre-conceptual design phase

to the experimental testing phase. The declaration of concept feasibility across such a wide range of maturation levels creates confusion in the use of feasibility assessments.

In addition, by categorizing the technologies into discrete levels, the information that is used to aid the evaluators in selecting the levels for the different technologies is lost. The information may provide more insight into the specific technologies and, most importantly, the impact of the technology on the overall concept. The readiness scales are not sufficient for systematic evaluation of architecture feasibility due to these deficiencies. From an engineering/scientific standpoint, the feasibility of a concept cannot be demonstrated or proven unless the concept can be manufactured and perform exactly as described. This creates a problem for studies in the conceptual design phase. How can one determine the feasibility of proposed concept when it cannot be proven or demonstrated without significant investment to test the concept to in a relevant environment? Of course, in the business world, the answer to this is the simple ROI analysis. However, ROI would be very difficult to apply to aerospace concepts as the benefit of a scientific mission or space exploration architecture cannot typically be quantified in monetary value. Also, the investment uncertainty and risk is can be very difficult to quantify. Instead, the feasibility of the proposed concept will depend highly on the underlying motivation and the level of risk the decision makers are willing to take.

There is a need to correlate the feasibility of a concept with the level of **risk** that the concepts present. Going back to the definition of feasibility, recall that concepts must be able to carried out successfully. Thus, by correlating risk into the feasibility analysis, the question changes from *Is the concept feasible?* to *How **likely** is it that the concept is feasible?*. Therefore, given a set of requirements and constraints that the concept need to meet, the question becomes *What is the **likelihood** for the concept to meet all of the requirements and constraints?*. And if new technologies or new integration techniques are needed, then the question becomes *What is the **likelihood***

that the system can be built to achieve all of the performance requirements? The assessment of risk, however, is not an easy task as it may be an "imprecise process involving judgment and intuition" [100].

In order to demonstrate feasibility at the conceptual study level and avoid subjectivity in the conclusion of feasibility, metrics that are used to make the conclusion must include all of the uncertainties that exist in the analysis. The analysis must be comprehensive, including all the factors that can threaten the likelihood of concept maturation, and it must provide enough data for the decision makers to make unbiased evaluation. Many conventional engineering designs use deterministic approach and provide mostly single point data for decision makers. Typically, uncertainties in the design are handled with the application of design margins or factors of safety. This is demonstrated in almost all of the example feasibility studies examined in the presented literature search. There is a need for an alternate method to evaluate concepts performance to better capture these uncertainties. The method in this dissertation utilizes stochastic performance evaluation and quantification of the uncertainty in technology and system integration to provide probabilistic evaluation metrics for feasibility assessments.

3.3 Stochastic Feasibility Assessment

The two primary deficiencies of current feasibility assessment methodology are that they are generally limited to technical areas and are subjective in nature. During the conceptual design phase, the system performance prediction is vital to ensure that the system meets its requirements, delivered on schedule, and developed within allocated cost. Early in the design process, these performance predictions are critical to the concept feasibility assessments. Poor predictions during this phase can have devastating impact on the system's performance, cost, and schedule. The previous section discussed these deficiencies in detail and presented the need for feasibility

assessments that is probabilistic in nature [101]. The reasoning behind the need for stochastic based techniques stems from the desire to infuse the technical uncertainties of the proposed concepts in the conceptual design process. Feasibility claims that rely on the author's expertise in the field and determination of the lack of "show stopping" technical issues for the concept is simply not sufficient [102].

To accomplish an objective evaluation of concept feasibility, the requirements and constraints to the concept must be defined and the corresponding system level metrics evaluated through system analysis. In the simplest form, feasibility of the concept can be established with an evaluation that ensures all constraints and requirements are satisfied. However, this method does not account for the technical assumptions and their uncertainties in the computation of the system evaluation metrics. Quantification of these uncertainties and the evaluation of the impact of uncertainty on the feasibility of proposed concepts are crucial to providing an objective evaluation. In addition, sensitivity of the concept feasibility to requirements and constraint changes during the analysis must also be part of the overall evaluation process.

3.3.1 Uncertainty Definition

For any system metric evaluation, two types of uncertainties exists; aleatory uncertainty and epistemic uncertainty [103, 104]. Aleatory uncertainty describes inherent variation in the physical system, typically due to the random nature of input data. It is also called objective uncertainty and irreducible uncertainty because it cannot be reduced by gathering more data. Material properties such as density, emissivity, and absorptivity are good examples of aleatory uncertainty because these attributes can vary from different production batches of the materials. These variations can be captured mathematically with a probabilistic distribution [105] through experimental testing of material samples from different batches. Similarly, environmental parameters such as air pressure and temperature can be considered as aleatory uncertainty

and probability distribution of these parameters can be developed from historical data.

Epistemic uncertainty describes variation due to ignorance, lack of knowledge, or incomplete information of the system under consideration. If knowledge of the system can be improved, then the epistemic uncertainty can be reduced. Thunnissen [106] separates epistemic uncertainty into three categories: model, behavioral, and phenomenological. Model epistemic uncertainty stems from the lack of data about a parameter or value of the system. For example, the generation of mass or cost estimating relationships based on historical data has model epistemic uncertainty. Behavioral epistemic uncertainty is related to actions of an individual or an organization. For example, the uncertainty of projecting the NASA budget for program planning has large behavioral epistemic uncertainty. Finally, phenomenological epistemic uncertainty addresses the "unknown unknowns" of the system when extreme conditions or unimaginable phenomena occur. Theoretically, if perfect knowledge of the system is achieved, epistemic uncertainty is completely eliminated [105].

Ideal feasibility assessment can be conducted only after complete knowledge of the system is available and epistemic uncertainty is eliminated; however this is rarely the case. As stated in previous section, feasibility studies are typically conducted during the Pre-Phase A step of the project life cycle where the knowledge of the system is very low. This lack of knowledge contributes to a high level of uncertainty to the concept under consideration and therefore high levels of risk. Complete knowledge of the system is rarely achievable and is almost impossible during the early phases of the project life cycle. Thus, it is paramount to address uncertainty directly within the feasibility assessment process.

3.3.2 Uncertainty Assessment

The process of uncertainty assessment reveals valuable information about the potential areas of concern for feasibility and provides understanding of the important metrics that impacts the concept feasibility. Uncertainty assessment is critical in order to understand the implication of the lack of knowledge of a design. Uncertainty assessment begins with the collection of data where information of similar systems in the past can provide insight into key metrics that may derail the development of the current system. Historical data is a common source for information in uncertainty assessment. From past concepts, experimental or physical flight data can be collected and assembled into estimating relationships that correlates design variables to the system metrics of interest. These estimating relationships take the average of the existing data, while the uncertainty in this estimation can be drawn directly from the residuals of the data. Probabilistic distribution functions can be assembled from the residuals of the data points to best capture the behavior of the data and can be used in the modeling and simulation step to capture the uncertainty of the estimating relationship.

If no historical data exists for a system, e.g. new technology, the data collection process becomes more complex. The only other source of information is the judgment of experts. This requires the elicitation of beliefs from knowledgeable experts in the area of interest. Any historical information that helps the expert formulate the elicitation values may be used. In this form, experts estimate the probability of a performance metrics given a set of assumptions; and if enough experts are sampled, the expert's opinions can be used to generate the probability distribution function used to construct the model.

Regardless of the method, the data must be synthesized with the performance evaluation of the concept. This process typically involves statistical sampling and

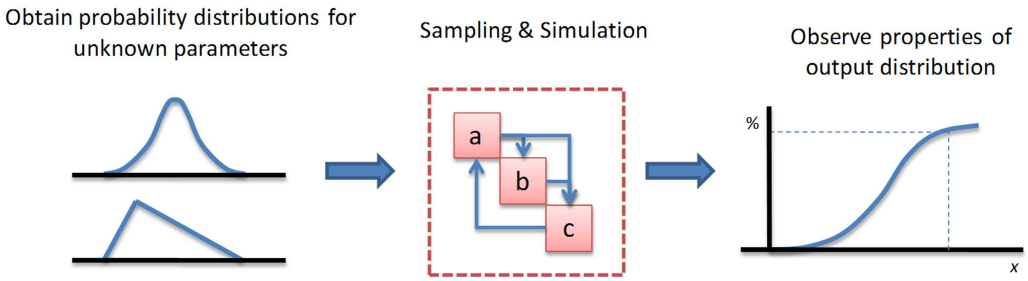

Figure 24: Monte Carlo Simulation Method

simulation to capture the variation in the performance estimation. Monte Carlo simulation [107] is often used in this capacity. A Monte Carlo simulation is a stochastic simulation in which a statistical sampling experiment is performed with a model, as illustrated by Figure 24. The resulting output distribution describes the behavior of the performance metric as a function of the uncertainties of both the system (Epistemic) and the design variables (Aleatory). These behaviors are critical in the evaluation of the concept feasibility, as it directly impacts the requirement and constraint satisfaction.

3.3.3 Requirements & Constraints

The addition of uncertainty analysis to the feasibility assessment process allows for better understanding of the relationship between the system metric of interest and its associated constraints or requirements. Rather than a simple comparison of the system metrics to ensure all constraints are satisfied, uncertainty of the system metrics is quantified to generate probability distributions of the system metrics. The corresponding constraint can be evaluated on this probability distribution to compute the probability of satisfaction of the constraint by the particular system metric, therefore completing a stochastic evaluation of feasibility.

For example, the feasibility of using a new power supply unit on a spacecraft may be constrained to the mass allowance of the unit. Uncertainty in the mass estimation of the power supply unit exists during the preliminary design phase. Historical data

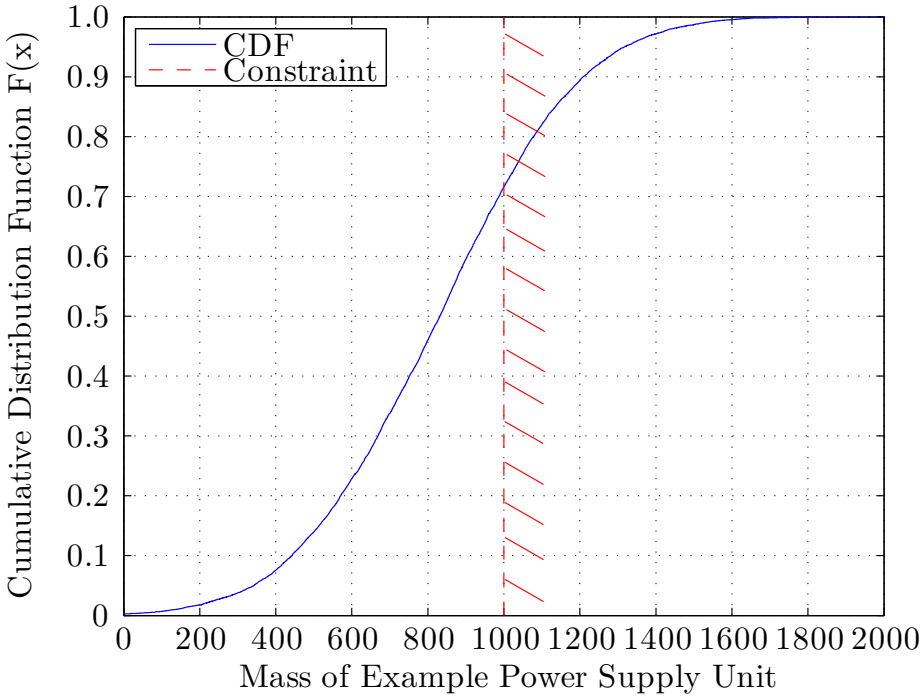

Figure 25: Example Stochastic Feasibility of a Power Supply Unit for a Spacecraft

exists for power supply units of the same class and function, so the uncertainty of the mass estimation can be quantified with Monte Carlo simulation sampling the residuals of the mass estimating relationships. The probability distribution of the power unit's mass and the allocated mass constraint are then used to evaluate the feasibility of using this particular power supply unit on the spacecraft. An example cumulative distribution function of the power supply unit mass and the corresponding sample constraint for the spacecraft is shown in Figure 25. In this particular example, the intersection of the cumulative distribution function and the 1,000 kg mass constraint show that there is a 70% probability that the mass of the power unit will be less than or equal to the constraint. Therefore, if the mass constraint is exactly 1,000 kg, then there is a 70% probability that the power unit mass will meet this particular constraint given the uncertainty in the mass estimation, equating to a 70% probability of being feasible.

By converting feasibility from a Boolean quantity to a probabilistic quantity, information is used to evaluate concept feasibility. In fact, it leaves the decision of feasibility to the decision maker in terms of the levels of risk they are willing to take. For example, one decision maker may decide that a 50% probability of system metric meeting the constraint is enough for a concept to be feasible; another decision maker may have a threshold at 90%. The ability to present the information to the decision makers provides a better understanding of the risk levels in the design.

3.4 Architecture Feasibility

Feasibility of the overall architecture must be comprehensive in nature. The methodology described in this chapter can be implemented for each of the areas presented in Section 2.7 with proper definition of the constraints in each areas and stochastic evaluation of the system metric. Sensitivity of the architecture feasibility to the constraint can be determined with stochastic analysis of system metric and evaluation of the probability of satisfying the constraints. In addition, uncertainty in the constraint itself can be examined with joint probability distribution of the system metric and accompanying constraints. The overall feasibility of the architecture can be quantified with joint probability distributions of the different feasibility areas with properly defined weightings if desired.

The technical and performance feasibility of the depot architecture is dependent on the successful utilization of on orbit cryogenic fluid management technologies. To evaluate this area of feasibility, a system model of the cryogenic fluid management system is necessary. The formulation of this model and the performance evaluation of the various cryogenic fluid management technologies are presented in Chapter 4. The uncertainty in the performance of the cryogenic fluid management technology is integrated with mass estimation uncertainty. The system mass is used as the performance metric, and launch vehicle payload is used as the constraint for evaluation

of system feasibility.

The mission launch reliability feasibility is dependent on the choice of launch vehicle and the vehicle's launch reliability. An examination of historical launch records can provide an initial estimate of launch vehicle reliability; however, this method cannot estimate the reliability of a newly developed system. Detailed probability risk assessments [108, 109] of the launch vehicle's subsystem can be time consuming and is not ideal for conceptual level studies. As defined later in Chapter 5, utilization of Bayesian probability methods allows the use of existing launch records to predict the inherent reliability of the launch vehicle. The overall launch reliability of the propellant depot architecture is evaluated utilizing Monte Carlo sampling of launch reliability distribution derived from Bayesian probability. The formulation of the launch reliability distribution and the evaluation of launch reliability feasibility are presented in Chapter 5.

The economic feasibility of the propellant depot architecture is dependent on both the chosen cryogenic fluid management technology and the chosen launch vehicles. The cost performance evaluation is performed using cost estimating relationships that are derived from historical programs [110]. The uncertainty in the cost estimation is quantified by using probabilistic simulation or the residuals to capture the variability in the cost of the historical programs. The economic feasibility evaluation methods and results are presented in Chapter 6. Finally, the three areas of feasibility is integrated into a cohesive architecture feasibility analysis and presented in Chapter 7.

CHAPTER IV

TECHNICAL AND PERFORMANCE FEASIBILITY ASSESSMENTS

The long term storage of cryogenic fluids in orbit is one of the major technical challenges of an on-orbit propellant depot [14]. The Earth Orbit Rendezvous option during the Apollo program [6] was deemed too risky in 1961 because of the schedule constraint resulting from the boil-off of the cryogenic fluids. The recent Constellation Program [7] attempted to mitigate the effects of boil-off by imposing a 90-day loiter limit between the cargo launch and the crew launch, which placed significant schedule constraints on the program. NASA's human exploration of Mars' design reference architecture [8] assumed zero boil-off of cryogenic fluids with the assumption of advanced thermal management technologies.

To understand the impact of these technologies on the overall feasibility of the propellant depot architecture, a model for the thermal properties of propellant depot was developed. This model analyzes a passive insulation system to mitigate the heat that penetrates to the cryogenic fluids from external sources. In addition, an active system is modeled to remove the excess heating using cryogenic refrigeration system. The primary figures of merit for the system level analysis are the boil-off of the cryogenic fluids when there is excess heat and the additional refrigeration mass that mitigates the boil-off.

4.1 Space Thermal Environment

The primary factor in determining the on-orbit heat load is the space environment. In LEO, factors that contribute to the heat load include the sun's direct radiation,

albedo reflected off the Earth's surface, and the infrared energy emitted from its surface. Direct solar radiation is the greatest source of environmental heating on all orbiting spacecraft. The solar irradiance at the Earth's mean distance from the sun (1 AU) has an average value of 1,367 W/m^2 [34]. Due to Earth's slight elliptical orbit around the sun (eccentricity = 0.017) [111], the intensity varies approximately plus or minus three and a half percent [112], from 1,322 W/m^2 to 1,414 W/m^2 [34, 112].

Earth's albedo, sunlight that is reflected off the surface, experienced by an orbiting spacecraft is dependent on both orbit inclination and altitude. Reflectivity is generally greater over land as compared to the ocean. Ice, snow, and cloud coverage as well as the local solar incident angle can all have direct impact on the overall reflectivity. Energy that is not reflected by Earth is absorbed and eventually emitted as infrared (IR) energy. The amount of IR energy experienced by an orbiting spacecraft is also dependent on the orbit and location, because the local temperature of the Earth's surface changes the amount of energy emitted.

These different heat load sources contribute to the overall system heat load depending on the orientation of the spacecraft. The overall thermal control of a spacecraft in orbit is achieved with energy balance. The radiation emitted by both the Sun and Earth can be either absorbed or reflected by the spacecraft's surface, depending on the material. Conservation of energy for thermal equilibrium requires that the energy absorbed and the energy generated by the spacecraft must equal the energy dissipated.

$$E_{\text{absorbed}} + E_{\text{internal}} = E_{\text{dissipated}} \tag{1}$$

The total thermal energy transferred into and out of the spacecraft is a function of the spacecraft's surface absorptivity, emissivity, surface area, and the geometric orientation with respect to the thermal radiation source. Absorptivity is the material property that describes the percentage of incoming energy that is absorbed by the

material. Emissivity is the material property that describes the percentage of energy emitted relative to an ideal black body at the same temperature. A true black body would have an emissivity value of 1, while any real world object or materials would have an emissivity value between 0 and 1. Absorptivity and emissivity are dimensionless quantities. Figure 26 shows typical values for absorptivity and emissivity of different types of spacecraft and thermal control materials [113].

The solar energy of an orbit is a function of the specific orbit altitude and orientation of the spacecraft. One method to accomplish this is with Analytical Graphic's System Tool Kit software and the built-in Space Environment and Effect Tool (SEET). SEET has the capability to compute the spacecraft's equilibrium temperature based on the spacecraft's orientation and surface properties. SEET treats the spacecraft as a single isothermal node to determine steady state temperature with the user specified surface thermal characteristics. The temperature computation is based on either spherical or planar objects with a specified orientation. With the energy conservation equation and the Stefan-Boltzmann Law, the equilibrium external temperature (T_o) of the spacecraft can be computed in SEET by solving this equation,

$$\sigma_{\mathrm{B}} T_{\mathrm{o}}^4 = \left[\frac{(Q_{\mathrm{sun}} + Q_{\mathrm{er}})\,\beta + Q_{\mathrm{i}}}{\epsilon} + Q_{\mathrm{IR}} \right] \frac{1}{A_o} \tag{2}$$

Where σ_{B} is the Stefan-Boltzmann constant ($5.670373 \times 10^{-8} W/m^2\text{-}K^4$), Q_{sun} is the direct thermal radiation from the Sun, Q_{er} is the Earth reflected albedo, Q_{IR} is the radiant infrared power emitted from the Earth, Q_{i} is the heat produced by the spacecraft's internal systems, β is the surface absorptivity, ϵ is the surface emissivity, and A_{o} is the total radiating surface area. Figure 27 show the contour plots for the average equilibrium temperature for a spherical isothermal node in a 400 km circular orbit at 28.5 degree inclination over the course of a year. This plot can be examined in concert with Figure 26 to determine the average temperature of spacecraft constructed with various materials. The figure shows the average temperature ranges between 200

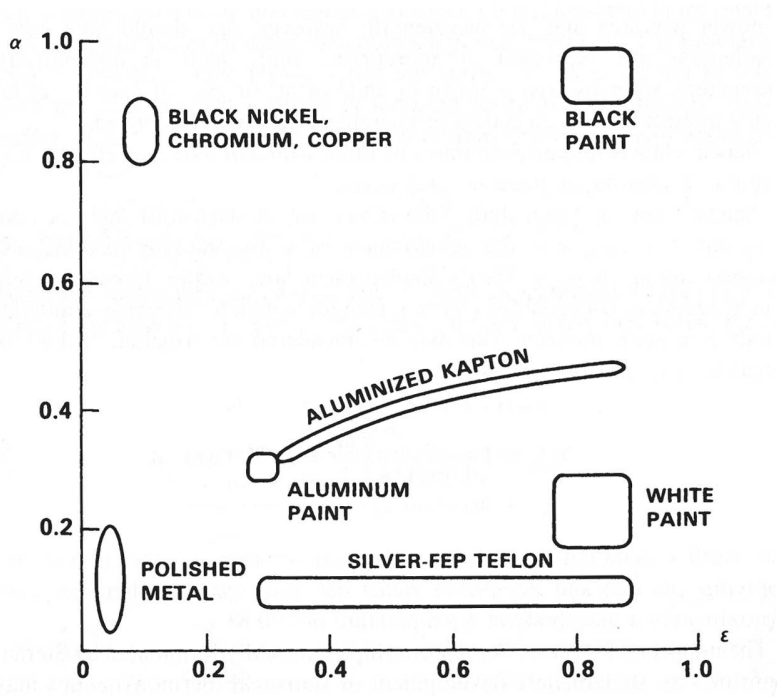

Figure 26: Absorptivity and Emissivity of Typical Thermal Control Materials [113]

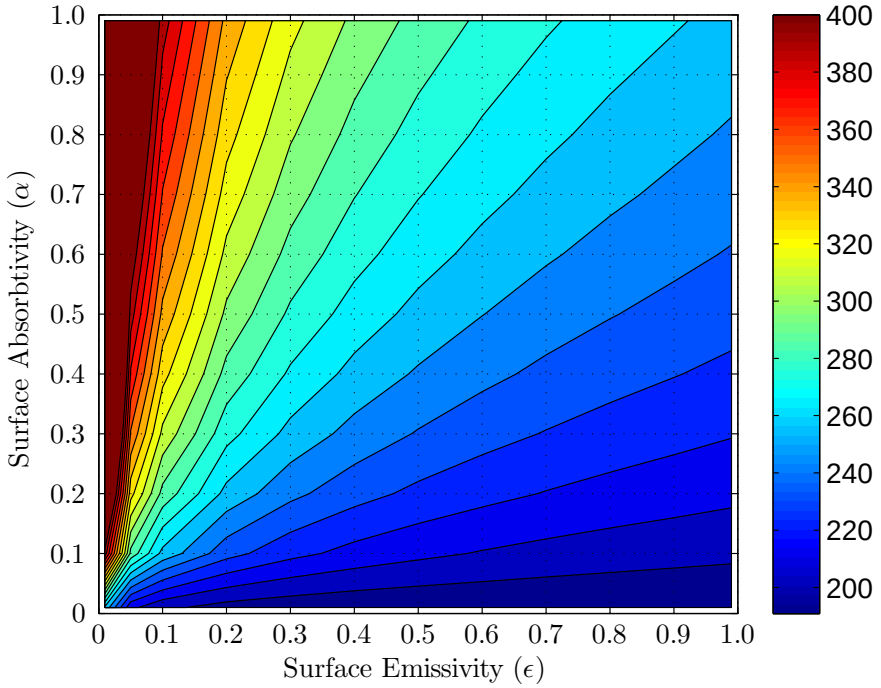

Figure 27: Average Equilibrium Temperature (K) Contours of a Spherical Node in 400 km 28.5^o Inclination Circular Orbit

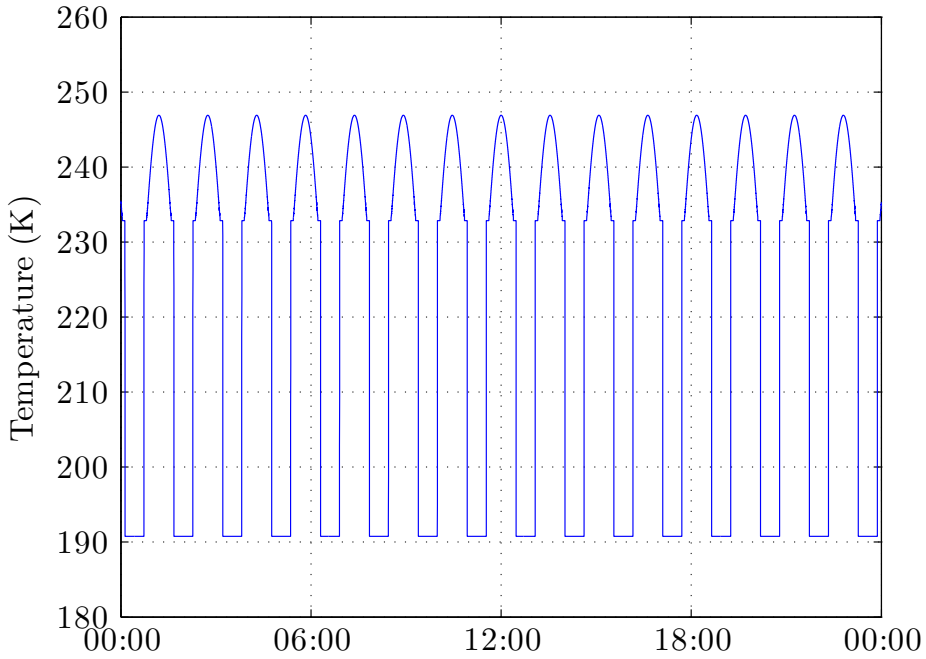

Figure 28: Equilibrium Temperature Profile of Spherical Node with White Paint ($\alpha = 0.22$, $\epsilon = 0.85$) in 400 km 28.5^o Inclination Circular Orbit

K and 400 K.

The temperature of an actual spacecraft will depend highly on the outer surface thermal properties. To minimize the surface temperature, materials with low absorptivity and high emissivity are desired. For white paint, the absorptivity ranges from 0.15 to 0.29 and the emissivity ranges from 0.76 to 0.92, as shown in Figure 26 [113]. The wide range of absorptivity and emissivity can have dramatic impact on the surface temperature, and consequently, the thermal heat load on the cryogenic propellant. Figure 28 shows the equilibrium temperature profile of a spherical node using medium values for the absorptivity and emissivity ($\alpha = 0.22\epsilon = 0.85$) of white paint in a 400 km circular orbit at 28.5 degree inclination. The equilibrium temperature for the day ranges between 190 K and 240 K. Over the course of an entire year, the average temperature for the spherical node is 219 K.

The average temperature for the spacecraft can fluctuate further due to the ranges

Table 8: Yearly Average Temperature Experience by a Spherical Node with White Paint Absorptivity and Emissivity Range in a 400 km 28.5^o Inclination Circular Orbit

α \ ϵ	0.78	0.80	0.82	0.84	0.86	0.88	0.90	0.92	
0.29	227.9	227.3	226.6	226.0	225.4	224.8	224.3	223.7	K
0.27	226.1	225.4	224.8	224.2	223.6	223.1	222.5	222.0	K
0.25	224.1	223.5	222.9	222.4	221.8	221.3	220.8	220.3	K
0.23	222.1	221.5	221.0	220.4	219.9	219.4	218.9	218.4	K
0.21	220.0	219.5	218.9	218.4	217.9	217.4	217.0	216.5	K
0.19	217.9	217.3	216.8	216.3	215.9	215.4	215.0	214.5	K
0.17	215.6	215.1	214.6	214.1	213.7	213.3	212.9	212.5	K
0.15	213.2	212.7	212.3	211.8	211.4	211.0	210.7	210.3	K

of absorptivity and emissivity of the material. Table 8 shows the average yearly temperature for the same spherical node from Figure 28 when the node's absorptivity and emissivity is varied across the range for white paint (Figure 26). Across the entire range, the average temperature can vary from 210 to 228 K. Additionally, the overall temperature that the spacecraft experiences can vary due to the actual geometry of the spacecraft. For example, a cylindrical shaped object will experience an approximately 10% reduction in the average yearly temperature because it has more surface area exposed to the darkness of space. Due to these factors, the range of temperature is utilized to capture the uncertainty in temperature estimation and will be included in the overall stochastic analysis. For the baseline deterministic scenarios, the average temperature of 219 K is assumed.

4.2 Passive Thermal Management

The most common form of thermal management for an orbiting spacecraft is passive insulation materials. These insulation materials are used to either prevent excessive heat loss from internal components or excessive heating from the environment. To compute the effectiveness of insulation materials, the heat transfer from the environment to the cryogenic propellant must be computed. There are three forms of heat

transfer: conduction, convection, and radiation [114]. Conduction is the transfer of energy in a solid medium through the collision of atomic particles, convection is the transfer of energy by the flow of a fluid, and radiation is the transfer of energy between two bodies without physical interaction or a continuous medium. In the absence of an atmosphere, heat transfer of orbiting spacecraft is governed by conduction and radiation. Radiative heat transfer is the mechanism in which the thermal heat load from the Sun and Earth is computed in the previous section and is governed by the Stefan-Boltzmann law (Equation 3), which describes the power radiated from a black body in terms of its temperature [34].

$$q = \epsilon A T^4 \tag{3}$$

Thermal conduction is governed by Fourier's law, which states that the time rate of heat transfer through a material is proportional to the negative gradient in the temperature and to the area, at right angles to that gradient, through which the heat is flowing (Equation 4), where k is the thermal conductivity of the material.

$$\vec{q} = -k \nabla T \tag{4}$$

An analytical model for the heat load through MLI was developed by NASA Marshall Space Flight Center [115]. The layer-by-layer model is a one-dimensional computation of the heat transfer and accounts for the possibility of the MLI material to have varying density, as shown in Figure 29. The model computes the total heat rate through the shield by computing the radiation between the shields, as well as solid and gas conduction through the spacer material. The equations for the three heat load modes are shown in Equations 5, 6, and 7.

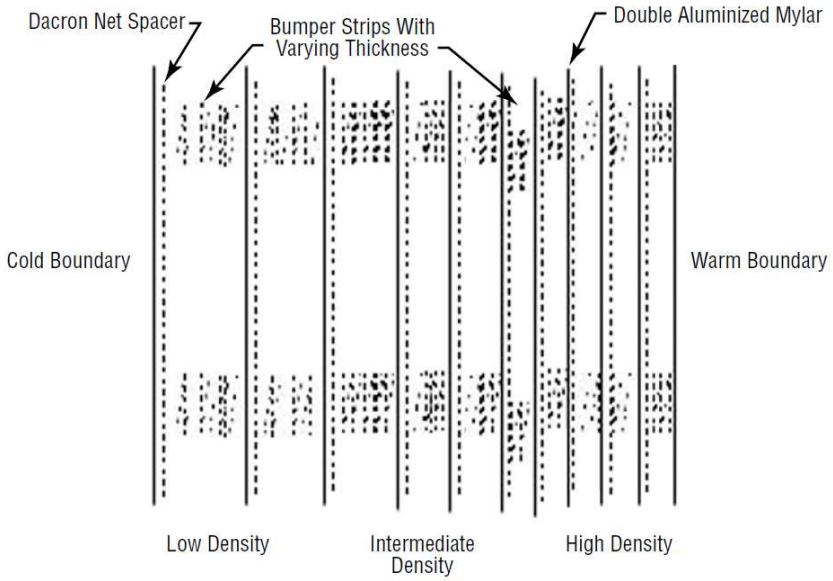

Figure 29: Representative Variable Density Multilayer Insulation Cross Section, Reproduced from [115]

$$\text{Radiation: } \frac{q}{A} = \frac{\sigma_{\mathrm{B}}(T_{\mathrm{H}}^4 - T_{\mathrm{C}}^4)}{\frac{1}{\epsilon_H} + \frac{1}{\epsilon_C} - 1} \tag{5}$$

$$\text{Solid Conduction: } \frac{q}{A} = \frac{C_2 * f * k}{dX}(T_H - T_C) \tag{6}$$

$$\text{Gas Conduction: } \frac{q}{A} = C_1 P \alpha_c (T_H - T_C) \tag{7}$$

$$C_1 = \frac{\gamma + 1}{\gamma - 1}\sqrt{0.125 R \pi M T} \tag{8}$$

For the radiation equation, σ is the Stefan-Boltzmann constant, T_H & T_C are the hot side and cold side temperatures, and ϵ_H & ϵ_C are the hot and cold side emissivity of the insulation material. For the solid conduction equation, C_2 is a material constant, f is the relative density of the spacer material compared to solid material, k is the conductivity constant of the material, and dX is the actual thickness of the spacer material between the layers. For the gas conduction equation, P is the gas pressure between the insulation layers (typically negligible in vacuum), α_c is an accommodation coefficient (typical value of 0.1), C_1 is a gas constant computed by Equation 8 in which γ is the ratio of specific heat for the gas inside the insulation

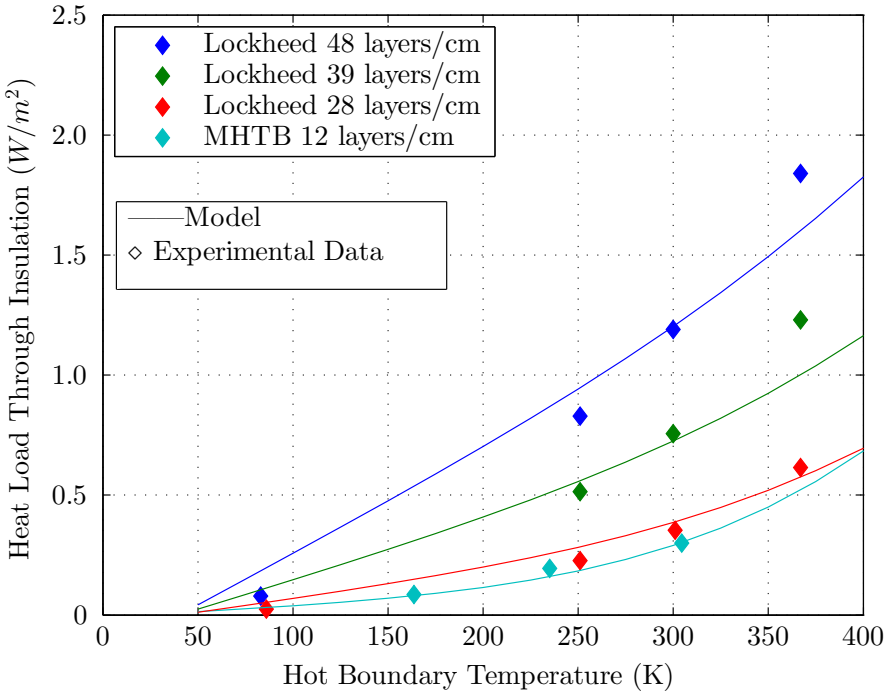

Figure 30: Comparison Between the Analytical Insulation Model to Lockheed and MHTB Experimental Data [116, 117]

layers, R is the universal gas constant, T is the average temperature of the gas, and M is the molecular weight of the gas.

The gas conduction of the insulation material assumes that there is residual gas trapped between the layers of insulation. The heat load through gas conduction is typically minimal in vacuum condition, as the pressure term in the equation is nearly zero. The analytical equation was formulated for each layer, with hot and cold temperatures for each layer as well as layer distance and emissivity of the material if it is not uniform across the layers. This creates a system of N equations with N + 1 variables, where N is the number of layers. Thus, the system of equations can be solved numerically until the heat rate in successive iteration is within a user specified convergence limit.

To validate the insulation thermal model, experimental data from Lockheed Martin's study in 1974 [116] as well as Marshall Space Flight Center's 2002 Multipurpose

Table 9: Heat Load Through Insulation Comparison between Experimental Data [116, 117] and Analytical Model

Density	T_C	T_H	Experiment (W/m^2)	Analytical (W/m^2)	% Error
Lockheed 48 layers/cm	41 K	83 K	0.079	0.184	+133%
	41 K	257 K	0.829	0.947	+14.2%
	42 K	302 K	1.19	1.20	+1.04%
	44 K	366 K	1.84	1.60	-13.0%
Lockheed 39 layers/cm	39 K	251 K	0.514	0.559	+8.78%
	41 K	300 K	0.756	0.725	-4.13%
	42 K	367 K	1.23	1.00	-18.7%
Lockheed 28 layers/cm	39 K	86 K	0.025	0.053	+112%
	41 K	251 K	0.227	0.284	+25.2%
	41 K	301 K	0.353	0.388	+10.0%
	42 K	367 K	0.615	0.574	-6.63%
MTHB 12 layers/cm	20 K	164 K	0.086	0.081	-6.33%
	20 K	235 K	0.194	0.160	-17.6%
	20 K	305 K	0.300	0.302	+0.67%

Hydrogen Test Bed (MHTB) are utilized [117]. Figure 30 shows the comparison between the analytical model and the results from both experiments and Table 9 shows the summary of the comparison. From the comparison, the model tends to over predict the heat loads through the insulation materials at low hot boundary temperature and under predicts the heat load at high hot boundary temperatures. At higher MLI density, the low hot boundary temperature error is quite large, as the model predicts more than twice the heat load compared to the experimental results. For typical hot boundary operating temperatures (between 200 and 240K as seen in Table 8), the error for the model heat leak prediction is on the order of 10 - 20%.

The primary benefit of the analytical model is that it provides the analysis for varying material properties of the MLI used for trade studies of new MLI materials without the need to generate empirical coefficients from experimental data. With the large temperature range expected for an on-orbit spacecraft, as shown in Figure 27, the performance of the MLI can vary greatly. The analytical model incorporates the temperature fluctuation with the performance estimation of the MLI. With the

Table 10: MLI Materials Property [114, 116]

	Source	Thickness (mm)	Specific Weight (kg/m^2)
Double-Aluminized Mylar	Standard Packing Corp.	0.0064	8.81e-3
Double-Aluminized Mylar	Sheldahl, Dunmore	0.0064	9.30e-3
Illusion Silk Net Spacer	John HeathCoast Co.	0.13	5.93e-3±1.38e-3
Dacron Netting Spacer	Apex Mills	0.16	6.30e-3±0.85e-3

properties of the analytical model, a stochastic analysis of the performance of MLI was developed to determine system feasibility.

$$M_{\mathrm{mli}} = \left[\gamma_{\mathrm{m}} + \frac{\gamma_{\mathrm{s}}}{t_{\mathrm{s}}}\left(\frac{1}{100\bar{N}} - t_{\mathrm{m}}\right)\right] * N * A_t \tag{9}$$

Thermal insulation mass estimation is a function of the geometry of the propellant tanks, the material properties, and installation configuration of the insulation system. From Equation 9, the mass of the MLI is a function of the specific mass of the Mylar sheets (γ_m) and the spacers (γ_s), the thickness of the Mylar sheet (t_m) and spacer (t_s), the density of the installed MLI blankets ($\bar{N}$, numbers of layer per centimeter), and the surface area of the tank (A_t) as well as the number of layers (N) installed. The material properties of the MLI blankets are based on the Lockheed Missiles & Space Company report [116], reproduced in Table 10.

4.3 Active Thermal Management

The use of thermal insulation materials is modeled like a resistor, and these can only reduce the heat rate experienced by cryogenic fluids on orbit. For permanent or very long-term storage of these cryogenic fluids, in order to eliminate or further reduce boil-off losses, active thermal management is required. Active thermal management describes systems that directly interact with the fluids, such as electrical refrigeration system or cryocoolers. Cryocoolers transfer energy from the cryogenic fluids to a working fluid through the use of heat exchangers.

Cryocoolers have a wide variety of applications. Figure 31 shows a map of the

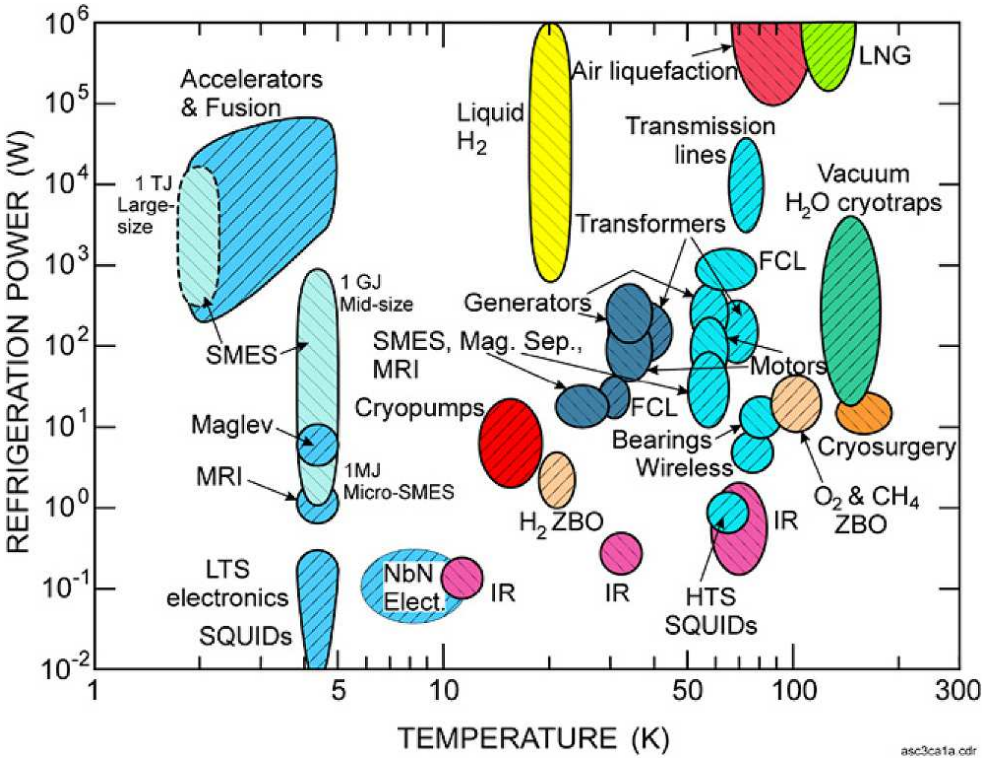

Figure 31: Map of Cryocooler Applications with Cooling Power versus Temperature, Reproduced from [51]

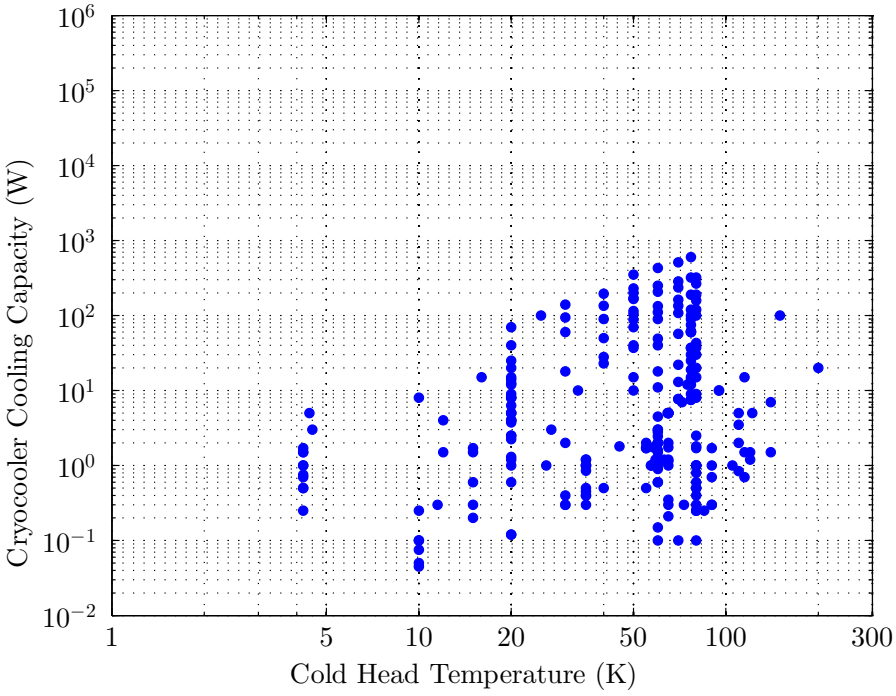

Figure 32: Performance of Cryocoolers from Appendix A

major cryocooler applications in terms of net cooling power and operating temperature required. For propellant depot applications, the propellant that requires the most cooling power is liquid hydrogen, which would require the cryocooler to operate below its boiling point temperature of 20 K with net cooling power between 1 and 1,000 kW [51]. The diverse applications of cryocoolers also mean that the design of commercial cryocoolers can be dramatically different. Almost all of the space-qualified cryocoolers developed to date have been used on small satellites or probes to cool instruments. Most of these coolers operate with a cold head temperature ranging from 4 and 120K and have cooling capability ranging from several milliwatts to tens of watts [51]. A survey of cryocoolers is compiled from a variety of sources [53, 114, 118–123] and can be found in Appendix A. These cryocoolers are shown in Figure 32 on the same scale as Figure 31. The survey includes both space qualified and ground based cryocooelers. Space qualified cryocoolers are currently used on satellites and probes to keep scientific instruments at near absolute zero temperatures. These space qualified cyrocooler have very stringent vibration and reliability requirements to ensure the lifetime of the scientific missions.

For an operating temperature of 80 K (below the boiling point of liquid oxygen), the cooling capacity of the surveyed cryocoolers ranges between 0.1 watts and 300 watts. For operating temperature of 20 K (boiling point of liquid hydrogen), the cooling capacity ranges between 0.1 watts and 70 watts. For example, the CryoMech AL-325 is a single stage Gifford-McMahon cryocooler that is capable of producing 70 watts of cooling power at 20 K [123]. The surveyed cryocoolers represents the current state-of-the-art in space qualified cryocooler technology. The current limit in cryocooler capacity is not indicative of technical limit, rather it is a due to the lack of requirements for space based cooler technology at high capacity [51, 124]. The only limitation is the performance, in terms of both electrical efficiency and system mass, for space based application.

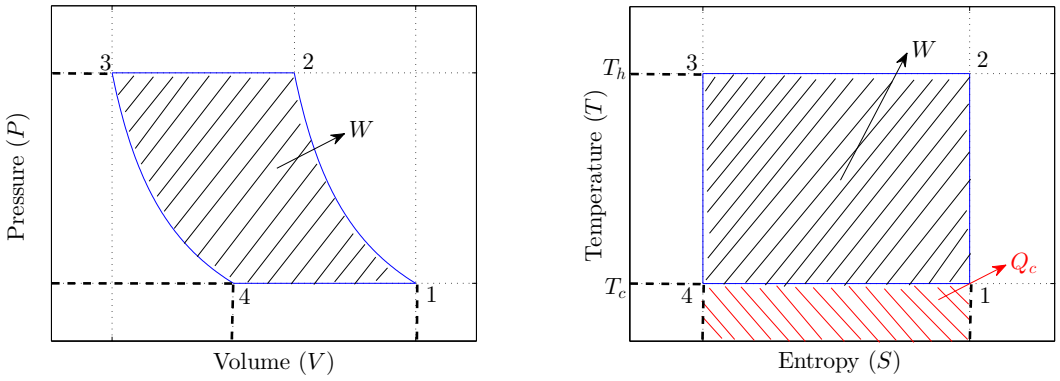

(a) P-V Diagram

(b) T-S Diagram

Figure 33: Pressure-Volume and Temperature-Entropy Diagram for a Carnot Cycle with a Condensing Working Fluid [126]

4.3.1 Cryocooler Limitations in Space

Cryocoolers can be classified as either recuperative or regenerative. Recuperative cryocoolers operate with a steady flow of fluid or gas through the system and use recuperative heat exchangers only. The working fluid is compressed at the high temperature end of the cryocooler and expansion occurs at the low temperature end where net refrigeration power is generated. Regenerative cryocoolers operate with oscillating flow and pressure and use at least one regenerative heat exchanger. Regenerative cryocoolers are analogous to AC electrical systems while recuperative coolers are analogous to DC electrical systems [125, 126].

The fundamental physics behind the operation of cryocoolers can be shown in thermodynamics cycles. Figure 33 shows the Temperature-Entropy (T-S) and the Pressure-Volume (P-V) diagrams of an ideal thermal engine in a Carnot cycle [126]. The compression and expansion of the engine produces work, which is in the center shaded area for both figures. By the second law of thermal dynamics ($\delta Q = T * \delta S$), the heat extracted from the cold reservoir (at temperature T_c) is the area under the T-S diagram (shaded in red). Thus, it can be seen that for a given thermal engine cycle, as the temperature of the cold reservoir decreases, the amount of heat extracted

decreases. In order to extract more heat at lower temperatures, the entropy of the system must increase. This is done by increasing the compression and expansion ratio of the engine, which would require larger compressor and larger volume for the working fluid. This is the primary limitation to current state-of-the-art in space based cryocooler. Because cryocoolers used on spacecraft are severely mass and volume constrained, the cooling capacity are limited.

4.3.2 Cryocooler Performance Estimation

The performance of cryocoolers is typically expressed as the coefficient of performance (COP) which is the inverse of the specific power for the cryocooler, where Q_C is the cooling capacity of the cooler and P_{in} is the electrical input power. A cooler extracts thermal heat Q_C from a cold reservoir at temperature T_C and discharges the heat to a hot reservoir at T_H at the expense of electric input power P_{in}.

$$\text{COP}_{\text{Cooler}} = \frac{Q_C}{P_{\text{in}}} \tag{10}$$

The efficiency of cryocoolers is normally quoted as a percentage of the actual cooler performance to the ideal Carnot cycle:

$$\eta = \frac{\text{COP}_{\text{Cooler}}}{\text{COP}_{\text{Carnot}}} \tag{11}$$

With the Carnot COP defined as

$$\text{COP}_{\text{Carnot}} = \frac{T_C}{T_H - T_C} \tag{12}$$

The Carnot efficiency is derived from the second law of thermodynamics and it defines a fundamental limit on the thermal efficiency of the cooling process. Using the example from the previous section (liquid hydrogen at $T_C = 20$ K and average LEO temperature $T_H = 262$ K), the theoretical limit of a cryocooler coefficient of performance operating at these temperature is only about 8%. To generate one watt

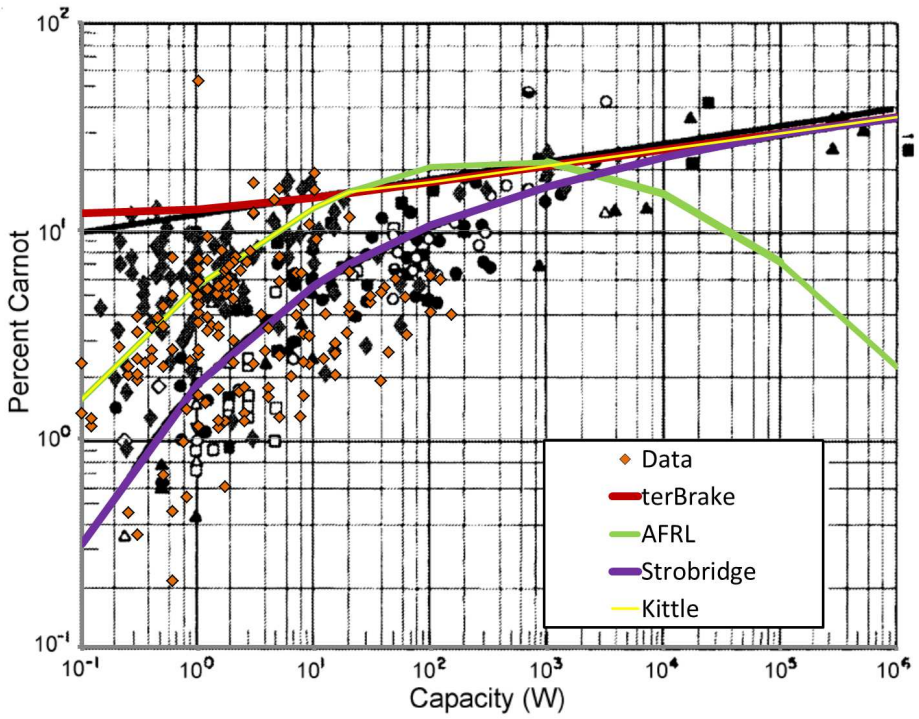

Figure 34: Efficiency of Cryocoolers from Appendix A with Estimating Relationship from Strobridge [127], ter Brake [50], and AFRL [128], Superimposed on Data Provided by Kittel [124]

of thermal cooling capacity, there must be twelve watts of electrical power. In reality, the real performance of cryocoolers is only a small fraction of the theoretical limit due to various loss mechanisms.

Kittel [124] provides a summary of performance correlations for historical cryocoolers. The survey shows three relationships to estimate the efficiency (as a percentage of Carnot), η, of cryocoolers versus the desired cooling power. The relationships are derived by Strobridge [127], ter Brake [50], and the Air Force Research Laboratory [128] (AFRL). These relationships represent the upper limit of cryocooler efficiencies at the time the curves were developed. The relationships are shown with the data from Appendix A and shown in Figure 34.

The Strobridge limit represents performance estimation using the oldest data set, while the AFRL and ter Brake include newer cryocoolers and improvements in the

efficiencies especially at the lower power range. All of the relationships discussed are purely empirically based. Therefore, the relationships are only for the range of their respective data set. The ARFL correlations is valid for cryocoolers with cooling power up to 20 Watts, while both the Strobridge and ter Brake relationships are valid for cooling power up to 10^6 watts. Kittle recommended using a combination of the AFRL correlation and the ter Brake limit. This method results in efficiency that represents the mean of the AFRL data that does not exceed the ter Brake limit, which takes full advantage data from the newer cryocoolers that have been built. This particular method [124] yields the efficiency correlation given by Equation 13. Q_C of 18.2 watts is the cross over point in which the ter Brake relationship predicts a lower efficiency than the AFRL relationship.

$$\log_{10}(\eta) = \begin{cases} -1.26281 + 0.45936(\log_{10}Q_{\mathrm{C}}) - 0.08743(\log_{10}Q_{\mathrm{C}})^2, & Q_C < 18.2 \\ -0.92237 + 0.07763(\log_{10}(1+Q_{\mathrm{C}})), & \text{otherwise} \end{cases} \tag{13}$$

4.3.3 Cryocooler Mass Estimation

The mass of the cryocooler thermal mechanical unit can be estimated using the curve fit of historical data points [129], in which the mass of the cryocooler unit is correlated with one or more of the cryocooler design variables. The cryocooler database compiled in Appendix A provides a set of data points for generating the mass estimating relationships. One of the difficulties in mass estimation of Cryocooler thermal mechanical unit is determining the proper independent variables. The data in Appendix A includes cryocoolers with a wide range of operating temperature, thermal power, and thermal cycles. Cryocoolers operating at different temperature can have drastically different designs and can lead to wide range of masses.

Figure 35 shows the mass of the cryocooler as functions of the operating temperature, the thermal cooling capacity, and the input electrical power. For all three

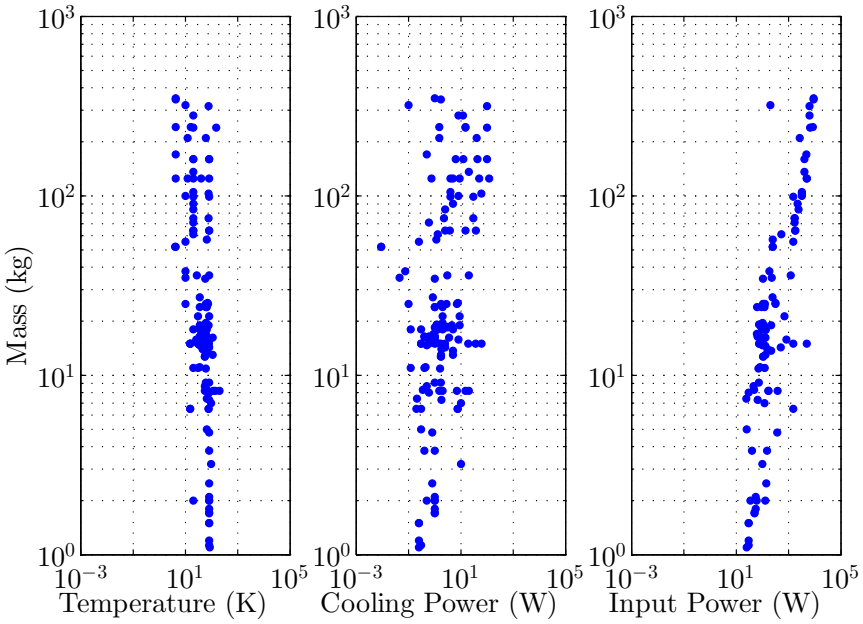

Figure 35: Cryocooler Thermal Mechanical Unit Mass as Functions of Operating Temperature, Thermal Cooling Power, and Input Electrical Power (Appendix A)

independent variables, there seem to be no direct correlation to the mass of the cryocooler system. A straight expoential curve fit results in the coefficient of correlation (R^2) of 0.057, 0.0273, and 0.1599 for each of the three independent variables respectively. The poor fit of the MER to the existing data could result in unacceptable levels of error in the estimation of system mass.

To provide the best mass estimations, separate relationships are generated for the two operating temperature of interest: 80 K for liquid oxygen and 20 K for liquid hydrogen. Figures 36(a) and 36(b) show the mass estimating relationships for the cryocooler thermal mechanical units operating at 20 K and 80 K. The resulting Mass Estimating Relationships (MERs), shown in Figure 36, have R^2 of 0.7681 and 0.9136 for Hydrogen and Oxygen, respectively. The two figures also show the dispersion of the data used to generate the MER. As the figure shows, the one standard deviation dispersion for the 80 K cryocooler mass is +75% to −45% and +43% to −31% for the 20 K cryocooler mass. These dispersions will be used to evaluate the mass estimation

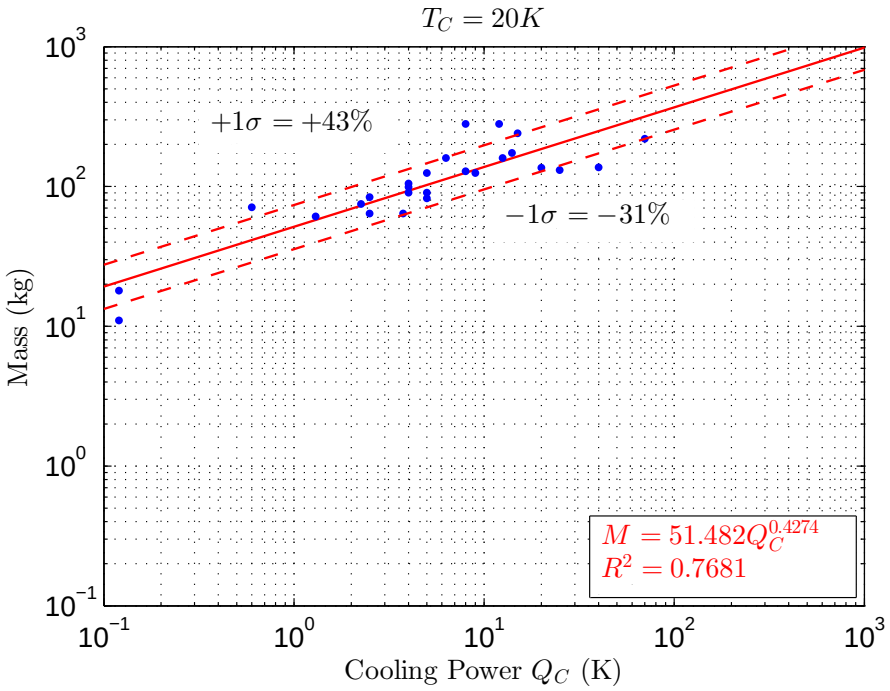

(a) Liquid Hydrogen

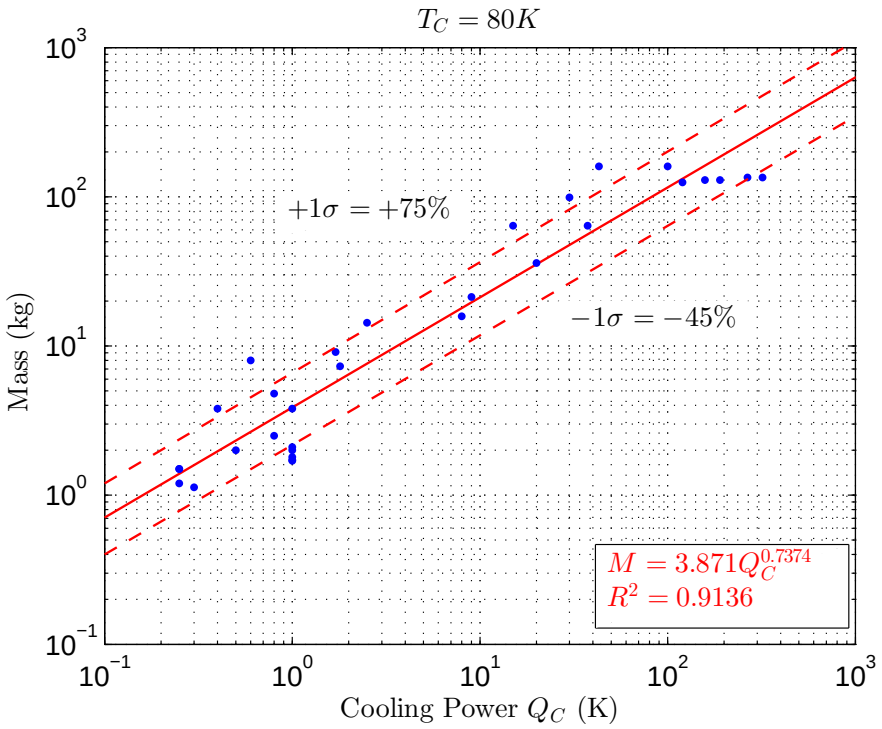

(b) Liquid Oxygen

Figure 36: Mass Estimating Relationships for Cryocooler Thermal Mechanical Units

Table 11: Cryocooler Sub System Mass Breakdown [130]

Program Subsystem Unit Mass (kg/W)				
	SHT	Rad	CPI	Misc
Multi-spectral Thermal Imager	0.046	0.087	0.003	0.025
Third Color Experiment	0.059	0.029	0.005	0.074
Cryogenic Two Phase	0.138	0.103	0.009	0.014
Cryogenic Systems Experiment	0.119	0.078	0.026	0.008
Advanced Teal Ruby Experiment	0.070	0.058	0.082	0.064
Average	0.086	0.071	0.025	0.037

uncertainties for the architecture feasibility assessment. The uncertainty analysis and the probabilistic simulation will be discussed in Section 4.6.

The developed mass estimating relationships only compute the mass of the cryocooler thermal mechanical system; it does not provide mass estimation of the compressor unit, power supply, and many of the supporting structures required to incorporate the cryocooler into a thermal system. McLean [28] provides specific weights for each of the components as functions of total power required. The total cryocooler system mass includes the thermal mechanical unit mass, the controller electronics (16% of thermal mechanics system mass [131]), the structure and heat transport (SHT) (0.097 kg/w), the radiators (Rad) (0.071 kg/w), plumbing and insulation (CPI) (0.025kg/w), and cables and other miscellaneous systems (0.032 kg/w). The nominal mass estimation utilizes the average of the five different cryocooler programs [28] shown in Table 11.

4.4 Thermal System Performance Evaluation

To evaluate the performance of the thermal management system, the evaluation criteria used is the mass loss due to boil-off as a result of the heat penetration versus the mass of thermal management systems. If there is sufficient heat penetration from the environment, phase change is induced for the cryogenic fluid, converting it from liquid to a gas, thus increasing the internal propellant tank pressure. If the pressure

Table 12: Cryogenic Fluids Thermal Properties [132]

	Boiling Point, K	Latent Heat, J/kg
H_2	20.4	452,000
O_2	90.2	213,125

approaches the design limit for the tank, the excess gas must be vented to prevent structural failure. The result of the venting process is the loss of usable propellant, called boil-off losses. The boil-off loss, the rate at which the fluid is converting into gas, can be computed using the latent heat of vaporization (H_{vap}) at the propellant's boiling point [132], shown in Table 12. Note that although the boiling point of liquid oxygen is 90 K, the majority of the cryocoolers are designed to operate at 80 K, thus all analysis was conducted with the assumption of liquid temperature of 80 K.

$$\dot{M}_{\text{loss}} = \frac{Q_{net}}{H_{\text{vap}}} \tag{14}$$

The boil-off rate, $\dot{M}_{\text{loss}}$, in kilograms per second is the ratio of the net heat absorbed by the liquid and the latent heat of vaporization of the liquid. If the desired mission can be specified, then the storage requirement (in terms of mass and time) can be known, and the overall boil-off loss can be computed for comparison. Without a specified mission, it is beneficial to represent the boil-off as a percentage of overall propellant stored for a reference time period. For the evaluations in this section, the primary figure-of-merit used for comparing different thermal system performance is percent propellant boil-off per month [115].

In addition to the heat load through the insulation described in Section 4.2, there are other heat leaks including structural (Q_s), penetration (Q_p), mixer (Q_m), and parasitic (Q_{para}) heat loads [133]. Plachta gives a brief description of the formula's origin and how it is adjusted for their particular study. The study uses the formula to compute heat loads on a small cryogenic tank in orbit (on the order of 10 m^3). All the equations are functions of the size and/or mass of the tanks or the amount of

propellant in the system, which helps scale the heat load. For conservatism, a multiplier can be applied to these heat load equations, and the impact of such multiplier can be evaluated. In this study, no multipliers were applied. The heat load formulas given by Plachta are the following:

$$Q_s(LO_2) = \frac{(M_{\text{tank}} + M_{\text{prop}})(T_H - T_C)}{1154364} \tag{15}$$

$$Q_s(LH_2) = \frac{(M_{\text{tank}} + M_{\text{prop}})(T_H - T_C)}{1200000} \tag{16}$$

$$Q_m(LO_2) = \frac{V_{\text{tank}}}{25.6} * C_2 \tag{17}$$

$$Q_m(LH_2) = \frac{V_{\text{tank}}}{16.8} * C_2 \tag{18}$$

$$Q_p = 0.0025 * (T_H - T_C)\sqrt{V_{\text{tank}}} \tag{19}$$

$$Q_{para} = 1.3636 * 10^{-6} f_{\text{eclipse}} P_{\text{in}}^{\frac{1}{3}} (T_H^2 - T_C^2) \tag{20}$$

Where M_{tank} is the mass of the propellant tank, M_{prop} is the mass of the propellant stored in the tank, and V_{tank} is the volume of the propellant tank. C_2 is the duty cycle of the mixer, where the typical value ranges between 0 and 1 to represents the precedence of time the mixer is in operation. For this study, C_2 is held constant at a value of 1 to represent conservative estimate of the heat load. f_{eclipse} is the eclipse factor for the cryocooler, i.e. the percentage of time the spacecraft is in eclipse and the cryocooler is not in operation, which is approximately 38% for LEO orbits. Notice that only the structural heat load is dependent of the propellant level in the tanks and it scales linearly with the decreasing propellant load. The majority of the heat load into the system is through the multi-layer insulation materials.

4.4.1 All-Passive Thermal System Performance

An all-passive thermal system utilizes only insulation materials that are applied to the propellant tanks. For a baseline scenario, the current state-of-the-practice materials are used to compute the resulting boil-off rates. This utilizes insulation constructed

from aluminized-mylar sheets sandwiched between silk-net spacer materials. This type of MLI is considered to be high in TRL and is used frequently for design and testing of cryogenic propellant storage techniques [115, 134]. The maturity of this technology yields higher level of confidence in its application for propellant depot concepts. This mature technology will reduce the overall development cost of the depot system due to its maturity and will be discussed in detail in Chapter 6.

Figures 37 and 38 show the percent boil-off per month for an all-passive thermal management strategy with varying layers of MLI at four levels of MLI density. Overall, as expected, the boil-off rate correlates directly to the heat load experienced by the cryogenic fluid and decreases with increasing number of MLI layers. The plots also show that as the layer density increases, the boil-off also increases, as the heat load through conduction increases. In the case of liquid oxygen, the boil-off mass decreases rapidly as the MLI layer increases up to about 100 layers. Above 100 layers, the boil-off reduction diminishes. For liquid hydrogen, the MLI effectiveness is highly dependent on the MLI layer density. To minimize the boil-off, lower density MLI is preferred.

The passive option is attractive due to the simplicity of the system. However, as the analysis shows, the use of passive thermal protection cannot completely eliminate boil-off. The effectiveness of the MLI is greatly diminished beyond 100 layers and the boil-off rates level off. The minimum boil-off obtainable for an MLI only scenario for MLI density of 12 layers per centimeter is slight above 0.5% per month for liquid hydrogen and roughly 0.25% per month for liquid oxygen. For short duration missions to the lunar surface or a near Earth object, the propellant boil-off can be manageable like during the Apollo program. However, as the mission duration increases, the boil-off loss can become a significant challenge to the overall mission and architecture feasibility. For example, a propellant depot with 200 mT of propellant at a mixture ratio of 5.5 would have roughly 2,000 kg/year hydrogen boil-off and 6,000 kg/year

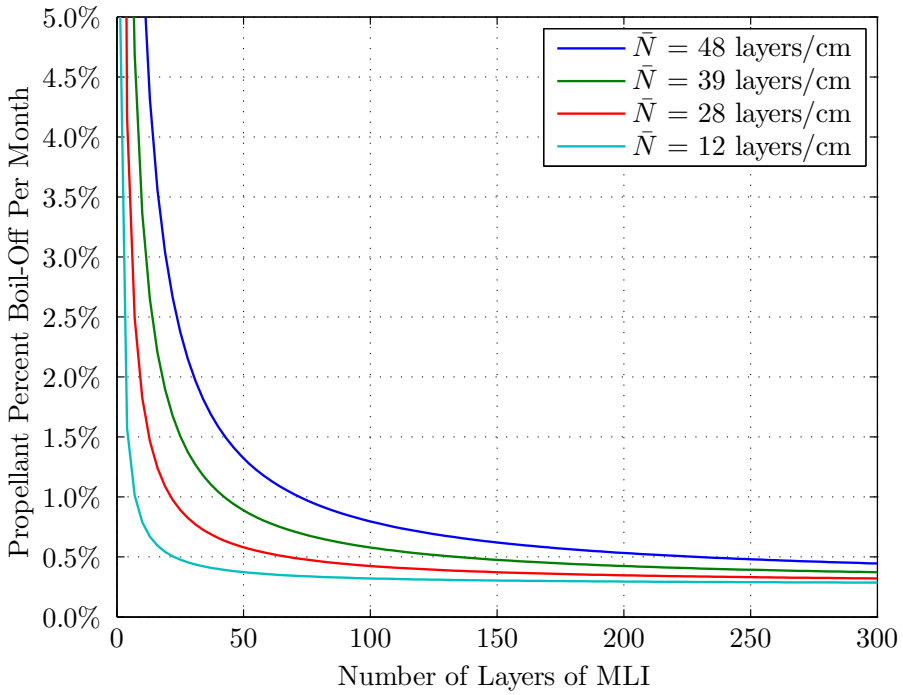

Figure 37: Percent Boil-Off Per Month as Function of # of Layers of MLI and MLI Density for 193 mT of LO_2 Storage

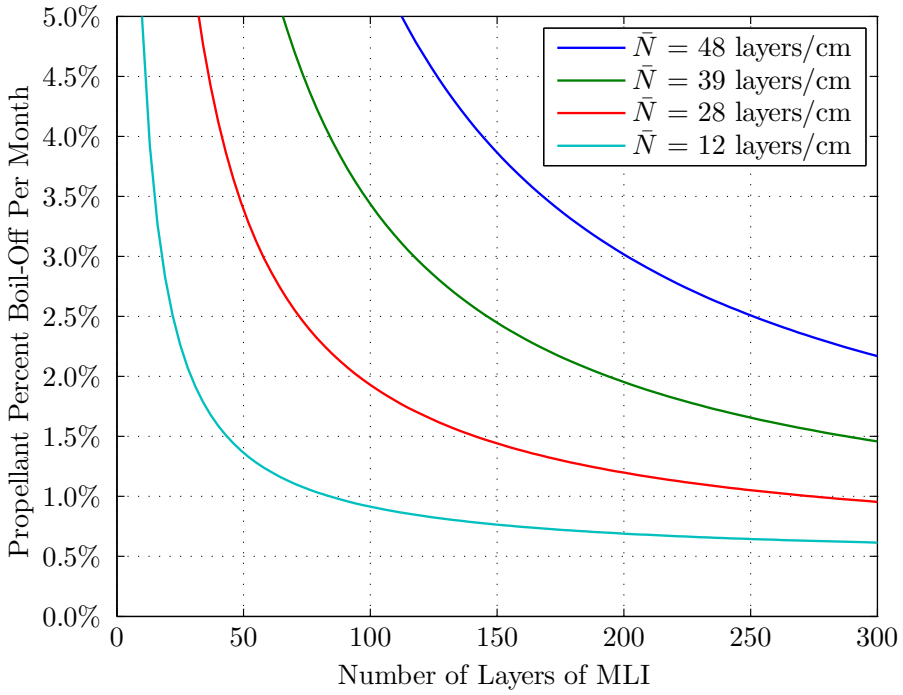

Figure 38: Percent Boil-Off Per Month as Function of # of Layers of MLI and MLI Density for 32 mT of LH_2 Storage

oxygen boil-off.

4.4.2 Integrated Passive & Active Thermal System Performance

To evaluate the joint performance of the passive insulation and active cryocoolers, the MLI density was held constant at 12 layers/cm (similar to the MHTB experiment [117]) while the number of MLI layers was varied from 1 to 100 and the cryocooler cooling capacity was varied from 0 to 100 watts. For each combination of MLI layers and cryocooler cooling power, the total heat load on the propellant was computed using the developed thermal model, and the propellant boil-off rates were computed. The results of these computations are shown in Figures 39 and 40, which plot the percent boil-off per month contours for both hydrogen and oxygen.

The figures show that for low number of MLI layers (<20 layers for Oxygen and <60 for Hydrogen), the boil-off rate remains relatively insensitive to the application of an active cryocooler. As previously discussed, the heat loads through the MLI increases exponentially with fewer layers of MLI resulting in extremely high cryocooler power requirements. The cyrocooler's cooling capacity is utilized to remove the heat load through the MLI material and ZBO is achieved when the depot's thermal balance (see Equation 1) is greater than zero. For liquid hydrogen, the 20 K cryocoolers are limited to less than 70 watts of cooling capacity as discussed in Figure 32. As Figure 40 shows, ZBO for hydrogen is achievable with a minimum of 60 layers of MLI. For liquid oxygen, ZBO is achievable with a combination of between 50 layers of MLI and cryocooler cooling power around 60 watts, which is well within the capability of current state-of-the-art coolers.

4.5 Thermal System Mass Trades

As discussed in the previous section, there are a number of combinations of passive and active thermal management that can result in the same boil-off rates for the two fluids, as demonstrated by the constant contours in Figures 39 and 40. For a

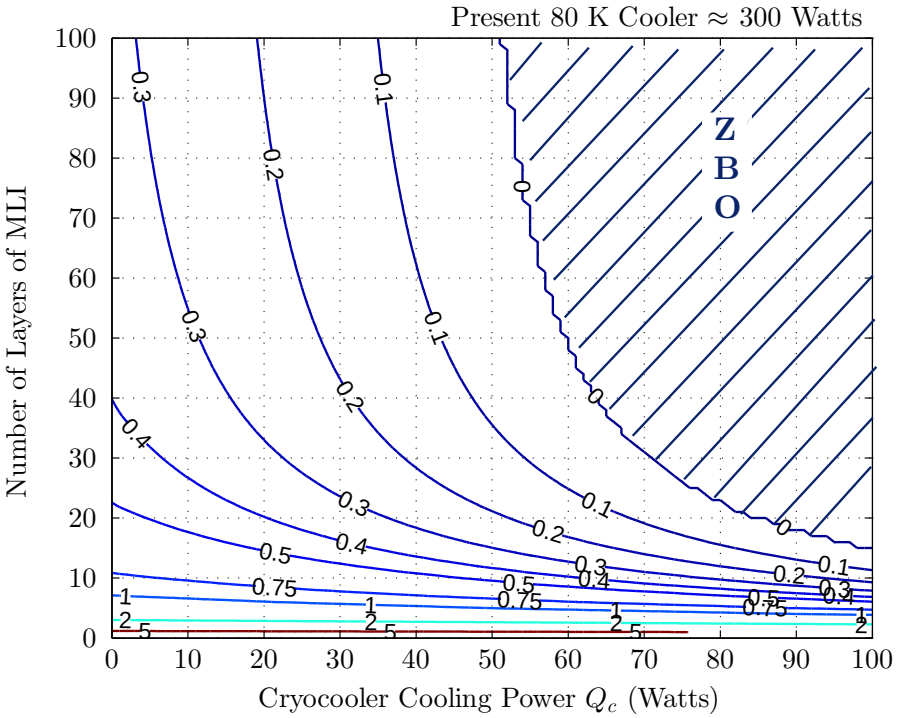

Figure 39: Constant Boil-Off Contours (%/Month) for 193mT LOx Storage in LEO with Combination Active and Passive Thermal Management, $\bar{N} = 12$ layers/cm

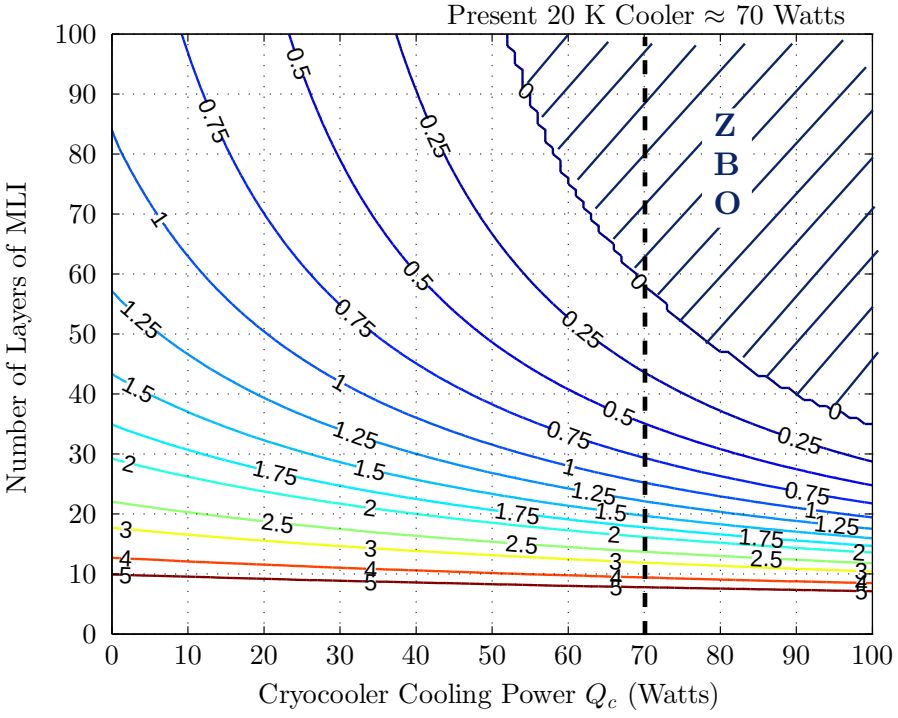

Figure 40: Constant Boil-Off Contours (%/Month) for 32mT LH2 Storage in LEO with Combination Active and Passive Thermal Management, $\bar{N} = 12$ layers/cm

given targeted boil-off rate, it is desired to determine the mass optimal combination of cryogenic thermal management system.

4.5.1 Subsystem Sizing and Mass Estimation

The primary figure of merit for evaluating the cryogenic thermal system performance is the propellant boil-off loss during the long term storage of the propellant versus the mass of the thermal management system. Section 2.3 provides a breakdown of the common elements in a propellant depot system. To estimate the mass of the various subsystems, a literature search was performed to gather historical data for the relevant systems. Mass estimating relationships were generated using the historical data, and the sizing routine was developed to estimate the mass of each component. The collected data points encompass a wide range of design conditions, requirements, and technology levels; thus, the resulting equation gives a mean approximation of the subsystem mass across this range.

The primary structure of the propellant depot system consists of the two propellant tanks (oxidizer and fuel) and the supporting structures surrounding these tanks. In addition, if the depot system is designed to have propulsion capabilities, additional structure is necessary to support the engine and carry the thrust load through the entire spacecraft. The propellant tanks are sized using historical data for launch vehicle propellant tanks. These tanks are designed specifically for the various launch and flight loads that a spacecraft experiences and is better suited than a simple pressure vessel calculation where less than 50% of the mass is computed. All of data used to generate the relevant mass estimating relationships are in Appendix B.

The mass estimating relationships for the two propellant tanks generated from the historical data is shown in Figures 41(a) and 41(b). Using an exponential curve fit on a log-log scale, the coefficient of determination (R^2) can be defined as the goodness of fit. The coefficient of determination has value between 0 and 1, where an R^2 of 1

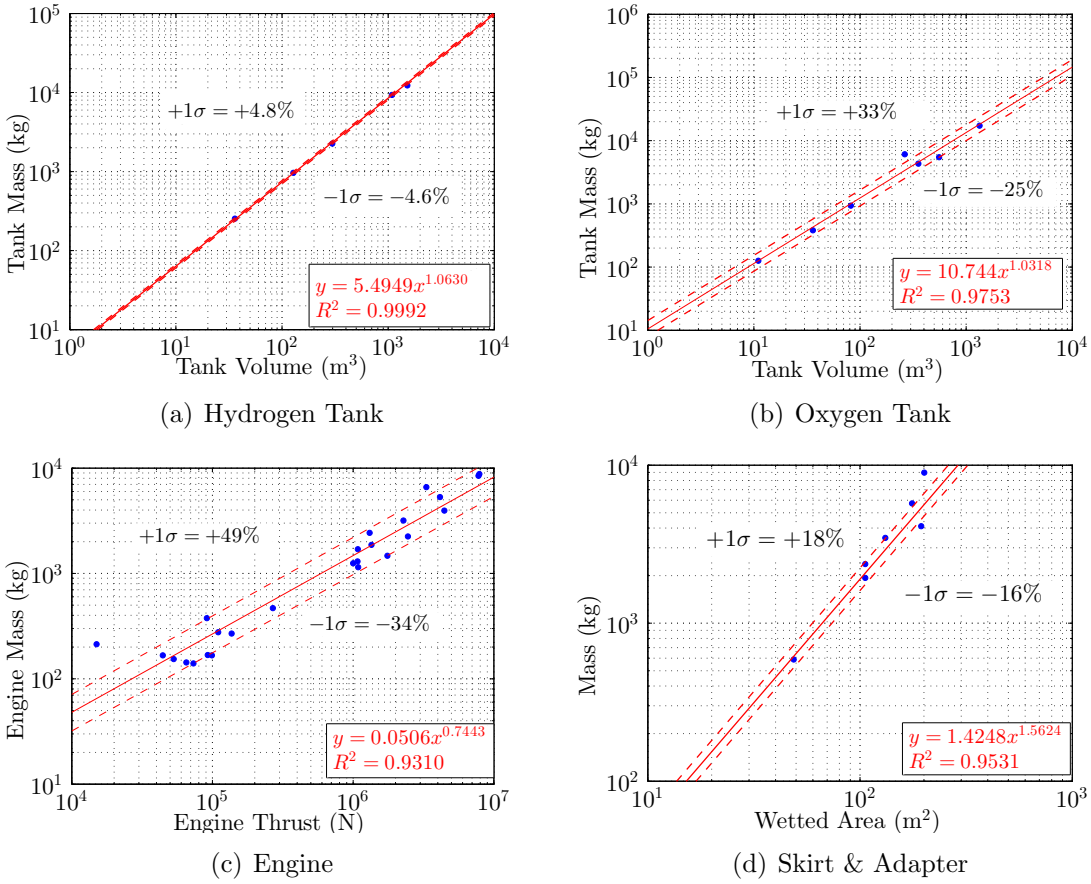

Figure 41: Propellant Depot Subsystem Mass Estimating Relationships [135]

means the estimation predicts the data perfectly and the error is zero. The hydrogen and oxygen tank curve fit results in R^2 of 0.9997 and 0.9753 respectively, indicating an excellent approximation of the data.

The propellant tanks must not only store the propellant, but also manage the propellant's transfer and usage according the mission profile. Previous chapters discussed the various options for propellant management for the purpose of propellant tankers and depots. The utilization of a propulsion system to generate acceleration for propellant transfer represents the most complex concept. The propulsion system mass sizing can be conducted using MERs generated by historical data, depending on the size and thrust requirement of the desired engine. Table B.1 shows a survey of historical launch vehicle and spacecraft engines [135]. The design thrust is a function

Table 13: Summary of Mass Estimating Relationships

LH_2 Tank:	$M = 5.4949\text{Volume}^{1.0630}$
LO_2 Tank:	$M = 10.744\text{Volume}^{1.0318}$
Intertank:	$M = 1.4248\text{Wetted Area}^{1.5624}$
Insulation:	$M = \left[\gamma_\text{m} + \frac{\gamma_\text{s}}{t_\text{s}}\left(\frac{1}{100\widetilde{N}} - t_\text{m}\right)\right] * N * A_t$
20 K Cryocooler:	$M = 51.482 Q_\text{C}^{0.4274}$
80 K Cryocooler:	$M = 3.8712 Q_\text{C}^{0.7374}$
Engine:	$M = 0.0506\text{Thrust}^{0.7443}$
Power:	$M = 132.1\text{Power(kW)}$

of the desired mission. For propellant transfer, minimal thrust is required to generate enough acceleration for the transfer activity. However, if the depot is designed to be a hybrid cryogenic propulsion stage [136], then the thrust requirement for the overall system would be much higher. The propulsion system MER is shown in Figure 41(c).

Table B.3 shows the historical data collected [135] from the Apollo program for the various intertank adapters and forward and aft skirts. These skirts and adapter are the structural supports for the propellant tanks and are necessary to integrate the system into a cohesive vehicle. The adapters are also necessary to carry part of the structural loads experienced by the depot during ascent and propellant refueling. The mass estimating relationship for the intertank and skirt is generated as a function of the device's wetted area. The MER and the coefficient of determination are shown in Figure 41(d).

The depot typically operates for long duration, solar arrays are required to generate the power required to operate the electronic systems on board. The sizing of the solar array and the mass estimation are taken from Laron [34]. The power required for the operation of the cryocooler and other on-board systems is delivered by a solar array with batteries for operation during eclipse. The solar array and battery system are similar to those used on the International Space Station and have a

specific power of 7.54 W/kg [34] or specific mass of 132.1 kg/kW, which includes the solar cell, mast, gimbals, and other supporting structures. The power distribution system, communication subsystem, instrumentation, and other subsystems are sized using mass estimating relationships generated from historical spacecraft data [135]. A summary of the mass estimating relationships developed for the mass trade analysis is shown in Table 13.

4.5.2 Mass Trades

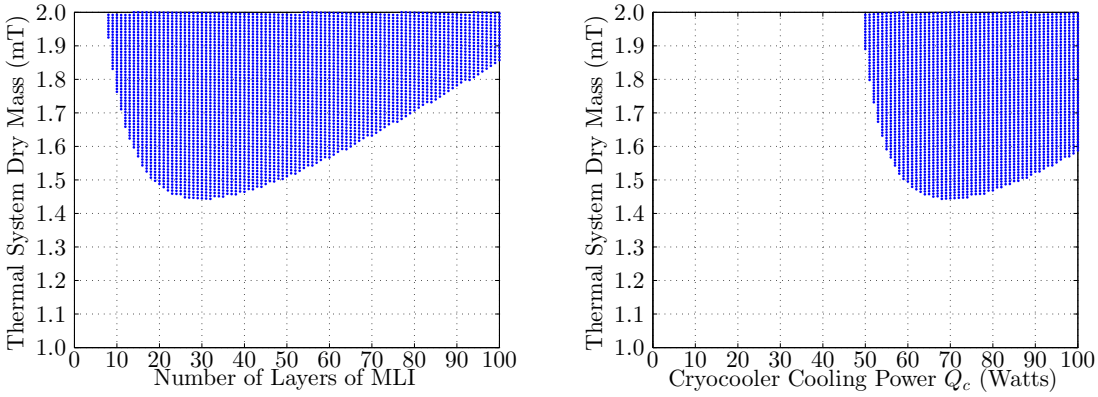

Figure 42: Liquid Oxygen Zero-Boil-Off Thermal System Mass Trade

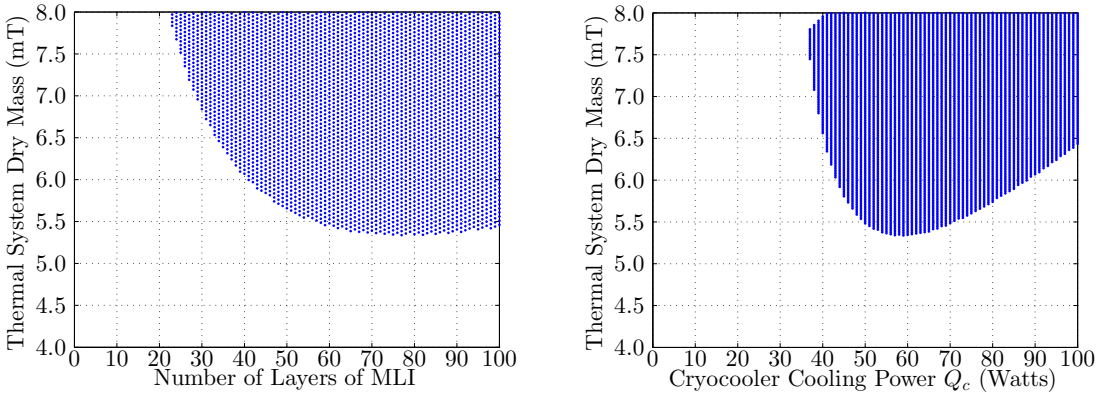

Figure 43: Liquid Hydrogen Zero-Boil-Off Thermal System Mass Trade

The most interesting and relevant scenario for mass tradeoff is the ZBO scenarios for both oxygen and hydrogen. Figures 42 and 43 show a scatter plot of the thermal system dry mass (MLI + cryocooler + power) as functions of both number of layers

of MLI and cryocooler cooling power. The figures show all the data points in the design space sweep that results in ZBO for both liquids, which are the shaded regions depicted in Figures 39 and 40. For these plots, the design space is limited to less than 100 layers of MLI and less than 100 watts of cryocooler cooling capacity.

For the liquid oxygen thermal management, the plot shows the minimal ZBO cooling power required is 50 watts but utilizing the minimal cooling power cryocooler does not result in the minimal thermal system mass. As the number of layers of MLI increases, the cryocooler cooling capacity required to achieve ZBO is reduced. However, there is a clear tradeoff between the increase in number of MLI layers and the decrease in cryocooler cooling power in terms of the overall system mass. For oxygen, the mass minimal thermal system combination is 33 layers of MLI and 68 watts of cryocooler cooling power, while the mass minimal combination for hydrogen is 80 layers of MLI and 58 watts of cooling power. The low number of MLI layers required for oxygen in the mass optimal scenario is because the cryocooler efficiency is much higher at 80 K and thus the cooler and power system mass increase is less than the mass required for higher number of MLI layers. In contrast, the mass optimal solution for hydrogen requires larger number of MLI layers because the cryocooler system mass is much higher for the operating temperature of 20 K. It is important to note that for both fluids, the mass optimal solutions fall well within the range for current state-of-the-art cryocooler capacity. Additionally, utilizing cryocoolers with cooling power lower than current state-of-the-arts can still achieve ZBO but doing so could result in significant mass penalty.

As shown in Table 8, the hot side temperature that the depot experience can vary between 210 K and 228 K with an average temperature of 219 K. The optimized thermal management in Table 14 assumes the average temperature; however, this does not capture the full range of temperature fluctuation. This leaves the possibility that the optimized ZBO scenario does not truly provide enough thermal management

Table 14: Minimal Thermal System Dry Mass for Zero Boil Off for 32 mT of Hydrogen and 192 mT of Oxygen

	MLI Layer	Q_c (watts)	MLI (kg)	Cryo (kg)	Power (kg)	Total (kg)
Hydrogen @ 20 K	80	58	1,610	1,890	1,850	5,350
Oxygen @ 80 K	33	68	274	417	761	1,450

Table 15: Cryogenic Fluid Management Scenario Description

	Oxygen		Hydrogen	
	# MLI Layers	$Q_c(watt)$	# MLI Layers	$Q_c(watt)$
A: Passive	80	0	80	0
B: Zero Boil-Off (219 K)	33	68	80	58
C: Zero-Boil-Off (228 K)	35	72	82	61

to eliminate boil-off. Performing the same thermal analysis and optimization for the higher temperature results in only a slight increase (5%) in the thermal management requirements. The mass optimal thermal requirement for ZBO for 228 K hot side temperature is 35 layers of MLI and 72 watts of cryocooler power for oxygen and 82 layer of MLI and 61 watts of cryocooler power for hydrogen.

For the purpose of providing comparison between active thermal management systems and a passive thermal management system, three cryogenic thermal management scenarios are created and summarized in Table 15. The all-passive scenario utilizes no active thermal management, but employs 80 layers of MLI for both oxygen and hydrogen. The MLI layers are limited to 80 layers due to the difficulties of manufacturing MLI. There are no documented literature that shows MLI greater than 80 layers. The two ZBO scenarios utilize the mass optimal thermal management combination for the two hot side temperatures.

For the three scenarios given in Table 15, overall system mass for each configuration is shown in Table 16. For each of the scenarios, the structure and propellant tank mass are the same while the other components have slight variation due to the changing requirement in the thermal system. All three scenarios results in propellant depot

Table 16: Propellant Depot System Dry Mass Breakdown for Different Cryogenic Fluid Management Scenarios

	Passive	ZBO (219 K)	ZBO (228 K)	
Active Thermal	0	2,300	2,500	kg
Passive Thermal	2,280	1,880	1,940	kg
Power System	970	2,620	2,780	kg
Structure	2,600	2,600	2,600	kg
Propellant Tanks	6,100	6,100	6,100	kg
Propulsion System	1,300	1,330	1,350	kg
Total	**13,250**	**16,830**	**17,270**	**kg**
Boil-Off Loss	*12,000*	*0*	*0*	*kg/yr*

dry mass less than 18 mT, which compared to the potential launch vehicle capability shown in Table 5, all but the smallest launch vehicle have enough payload capability to deliver the depot into orbit. The ZBO scenarios represent a 50% increase in system dry mass as compared to the all-passive scenario, but this increase in dry mass can provide a boil-off saving of 12 mT per year. The two ZBO scenarios differ only in the level of thermal management applied to the system and the difference between the two scenarios is only 400 kg. Thus, the modest increase in the system dry mass can provide much higher probability of achieving ZBO due to the variability of the hot side temperature. Overall, these results demonstrate that the commercial launch systems have more than enough performance capability to be utilized for hardware delivery.

The overall system level trade between the passive thermal system and active thermal system seem to favor the active thermal system for all but the shortest missions. This is illustrated in Figure 44. The depot shows the direct trade between the overall system mass for the three CFM scenario as a function of time. For storage durations less than four months, the all-passive CFM scenario yields the lowest total mass. Due to the mass loss to boil-off, the ZBO option remains the most mass efficient option for storage duration over 4 months.

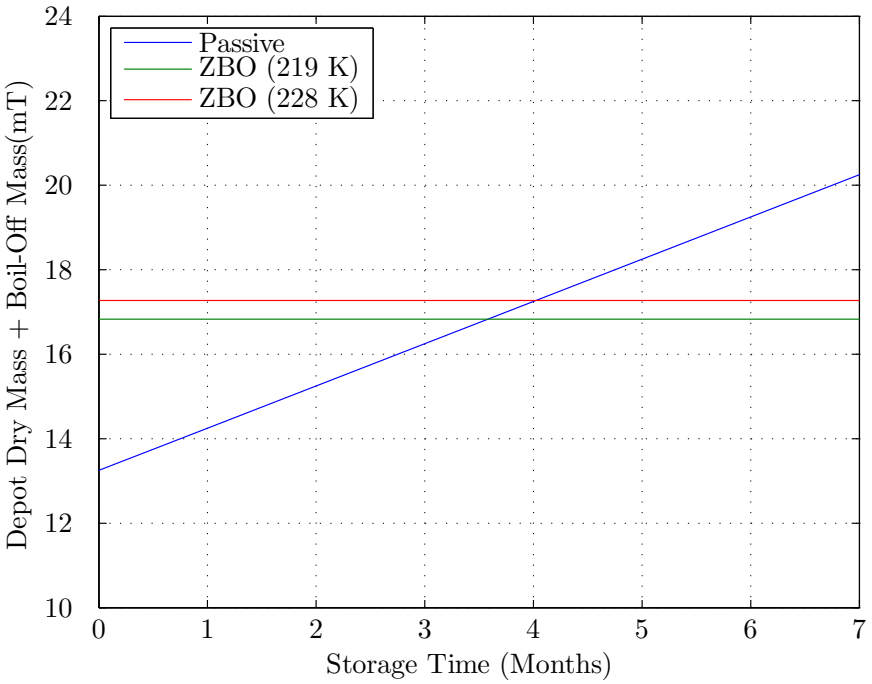

Figure 44: Propellant Depot Dry Mass Plus Boil-Off Mass as Function of Storage Time

4.6 Uncertainty Analysis and Probabilistic Simulation

The results shown so far are consistent with the majority of the literature discussion and conclusions on propellant depot presented in Chapter 2. Like most literature conclusions, the ZBO option is very attractive as it provides fairly significant mass savings in terms of propellant boil-off loss for a modest increase in overall system dry mass. However, these results, like all the results in the literature, do not account for the uncertainties in the performance and mass estimations. Traditionally, during preliminary design process such as this, design mass margins are applied to account for mass growth and uncertainty in the estimations. To improve the analysis, a probabilistic simulation is employed to quantify the effects of the uncertainty on overall performance.

The MERs generated with historical data creates mass estimations that represent the mean of the available data, resulting in model uncertainty in the estimation of

Table 17: MER Correction Factor Statistical Analysis Summary

Variable	Distribution	Parameter	
χ_{η_C}	Gamma	a = 1.769	b = 0.384
$\chi_{M_{O2Tank}}$	LogNormal	μ = -1.21E-7	σ = 0.275
$\chi_{M_{H2Tank}}$	Gamma	a = 447.5	b = 2.237E-3
$\chi_{M_{Skirts}}$	Gamma	a = 37.36	b = 0.027
$\chi_{M_{Engine}}$	LogNormal	μ = -1.45E-8	σ = 0.075
$\chi_{M_{20K}}$	Gamma	a = 8.234	b = 0.129
$\chi_{M_{80K}}$	Gamma	a = 3.655	b = 0.315
$\chi_{M_{SHT}}$	Uniform	a = 0.059	b = 0.138
$\chi_{M_{Rad}}$	Uniform	a = 0.029	b = 0.103
$\chi_{M_{CPI}}$	Uniform	a = 0.003	b = 0.082
$\chi_{M_{Misc}}$	Uniform	a = 0.008	b = 0.074
χ_{γ_m}	Uniform	a = 8.81e-3	b = 9.30e-3
χ_{γ_s}	Uniform	a = 3.90e-3	b = 7.30e-3

system performance. To model the uncertainty in the MER, the MER curve is shifted by utilizing a correction factor. The correction factor is derived from the error of the MER. The error of the MER is defined by the ratio of the residual and the actual mass of the system and the residual of the MER is the difference between the actual mass of the system and the prediction made by the equation.

$$Error = \frac{M_{\text{ActualPerformance}} - M_{\text{PredictedPerformance}}}{M_{\text{ActualPerformance}}} = \frac{Residual}{M_{\text{ActualPerformance}}} \tag{21}$$

The correction factor is defined as,

$$\chi = \frac{\text{Actual Performance}}{\text{Predicted Performance}} \tag{22}$$

To determine the value of the correction factor, a statistical analysis was conducted using the residual data for each subsystem. A probabilistic distribution is fitted to the correction factor for each of the subsystems to capture the variability of the prediction. Normal distributions would typically be used to represent this type of data [135]; however, the normal distribution has the domain of $x \in (-\inf, \inf)$ which is not ideal because the correction factor cannot be negative. Therefore, both the

LogNormal and the Gamma distributions are used to fit the data to capture the variability. For each of the subsystems, the distributions are fitted to the data, and the best fit distribution (based on the maximum log likelihood of the fit) is chosen. For limited data subsystems like the cryocooler subsystems and the MLI blanket and spacers, uniform distributions from the maximum to minimum values, based on Table 11 and Table 10, are used to capture the potential variability of the mass estimation. Table 13 shows a summary of the mass estimating relationships described in this section and Table 17 shows the statistical analysis and the resulting correction factor distributions for each of the MERs. The one standard deviation bounds for each of these correction factors can be seen in the MER plots for the individual subsystems (Figures 36 and 41).

To capture the uncertainty inherent in the mass estimation, Monte Carlo simulation is performed using the correction factors described by Equations 21 and 22 with the input distribution given by Table 17. Two scenarios were considered for this analysis: the passive thermal management shown as scenario A in Table 15 and the max temperature ZBO scenario shown as scenario C in Table 15. The average temperature scenario was not considered due to the relatively small difference between scenarios B and C.

Figure 45 shows the empirical cumulative distribution function (CDF) for the propellant depot system dry mass of a 10,000 case Monte Carlo simulation for the all-passive thermal management strategy. The figure shows that due to the uncertainty in the mass estimation, the total system dry mass can vary between 9 mT and 18.2 mT. The deterministic solution, as given by Table 16, shows a nominal system dry mass of 13.3 mT. Therefore, by using the deterministic solution, there is approximately a 50% probability that all of the uncertainties in the subsystem mass estimation are captured. In another word, there is a 50% chance that the actual system mass of the propellant depot will be greater than the deterministic solution.

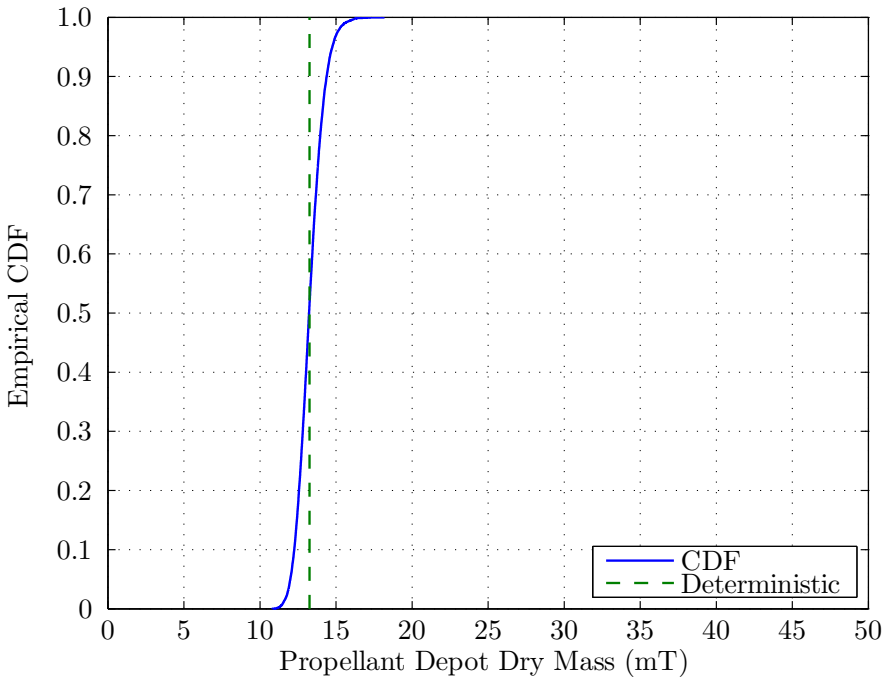

Figure 45: Empirical CDF for All Passive Propellant Depot Dry Mass (mT)

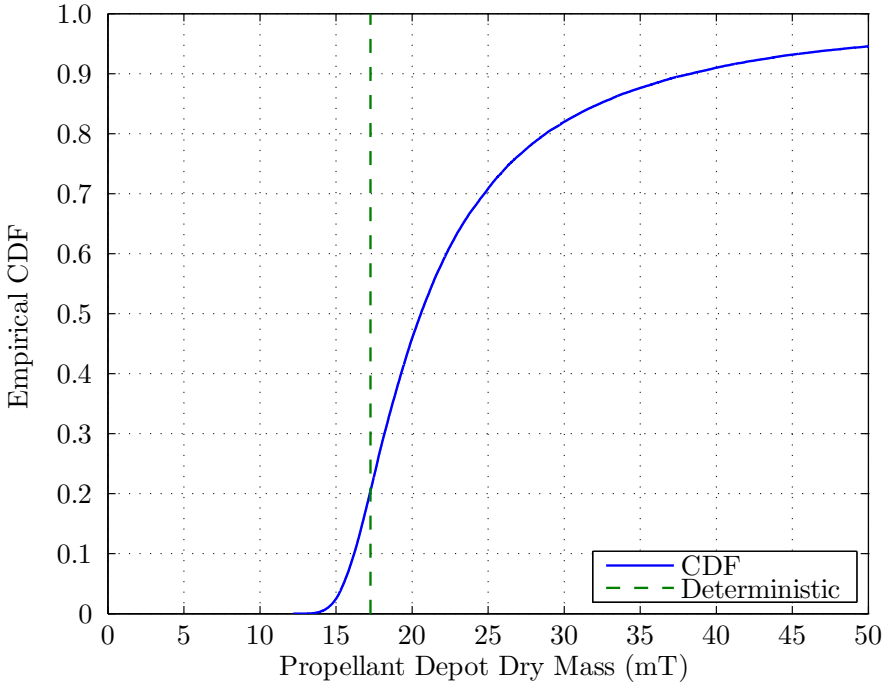

Figure 46: Empirical CDF for Zero Boil-Off Propellant Depot Dry Mass (mT)

Table 18: Nominal Payload Capability to Low Earth Orbit for Various Launch Vehicles [4, 75–77]

ULA Atlas V 551	19,000	kg
ULA Delta IV Heavy	23,600	kg
SpaceX Falcon Heavy[†]	51,000	kg
NASA Space Launch System[‡]	70,000	kg

For a system that requires high accuracies in the mass estimation, such as the case of a launch vehicle payload, this represents an unacceptable level of risk to the overall payload feasibility. If a 30% mass margin is applied to the system, as is typical in aerospace system designs in the preliminary design phase [137, 138], the depot system dry mass would increases to 17.3 mT, which increases the probability of capturing the mass uncertainty to well over 99%. Thus for the all-passive thermal management scenario, a properly applied design mass margin is sufficient in capturing the uncertainty in the mass estimation.

Figure 46 shows the empirical CDF for the propellant depot system dry mass with the mass optimal combination of passive & active thermal management that achieves ZBO for the max temperature (scenario C in Table 15). With the addition of active thermal management systems, the overall system dry mass as well as the uncertainty in the mass estimation are higher as compared to the all-passive scenario. The depot dry mass varies from 12.6 mT to over 50 mT. The deterministic solution of 17.3 mT represents on the 20th percentile of the empirical CDF, implicating 80% probability that the actual system mass would exceed the deterministic solution. Applying a 30% mass margin result in a system mass of 22.5 mT and increases the probability of capturing the mass uncertainty to roughly 55%. The dramatic increase in the variability of the depot dry mass for the ZBO scenario is primarily due to the uncertainty in the estimation of the coefficient of performance for the cryocooler. As

[†]Currently in Development, First Operational Flight Scheduled for 2015 [78]
[‡]Currently in Development, First Test Flight Scheduled for 2017 [4]

Table 19: Probability of Depot System Dry Mass of Meeting Launch Vehicle Payload Constraint

	Passive	ZBO
ULA Atlas V 551	$> 99\%$	$\approx 38\%$
ULA Delta IV Heavy	$> 99\%$	$\approx 65\%$
SpaceX Falcon Heavy[†]	$> 99\%$	$\approx 94\%$
NASA Space Launch System[‡]	$> 99\%$	$\approx 97\%$

Figure 34 shows, there is significant data dispersion for the performance estimation for cryocoolers, and this effect is compounded with the mass estimation for both cryocooler mass and the electrical power requirement for the depot. This resulted in a high uncertainty with the mass estimation of the propellant depot system mass when a cryocooler is utilized.

For both scenarios, the application of mass margin can increase the confidence of the mass estimation. However, the application of mass margin can have negative impact on the overall architecture feasibility depending on the selection of launch vehicle. For system mass estimation and the uncertainty analysis surrounding it, the feasibility assessment of the physical system depends on the ability for the designed system to be delivered to orbit on various available launch vehicles. Thus, the figure of merit in which performance feasibility is evaluated upon is the overall system dry mass of the system and the constraint imposed on the figure of merit is the payload capability of various launch vehicles. The nominal payload capabilities of the various launch vehicles are shown in Table 18. Another way to look at the problem with mass estimation uncertainty is to examine the available payload capability of the launch vehicles and determine the likelihood of the designed system fitting under the payload constraint given the uncertainty. These probabilities are shown in Table 19.

The four launch vehicles considered are more than capable of delivering the passive propellant depot into orbit, with better than 99% probability that all of the mass

[†]Currently in Development, First Operational Flight Scheduled for 2015 [78]
[‡]Currently in Development, First Test Flight Scheduled for 2017 [4]

estimation uncertainty can be captured. The high variability in the system mass due to uncertainty for the ZBO scenario results in poor performance for the two ULA vehicles. The two largest vehicles, SpaceX Falcon Heavy and NASA's initial 70 metric ton Space Launch System, the large payload capability results over 94%probability of successful delivery of the depot system to orbit regardless of the uncertainty in the system mass estimation. From a pure performance feasibility standpoint, using either the Falcon Heavy or the Space Launch System provides the highest degree of confidence that the mission will be successful. Of course there are other factors such as launch cost and vehicle reliability that must be taken into consideration when evaluating the overall architecture feasibility. These will be discussed in subsequent chapters.

4.7 Summary of Technical Feasibility Assessment

The technical performance feasibility of propellant depot was examined in this chapter. System models were developed to evaluate the performance requirements for storing cryogenic propellant on orbit. These requirements were used to size the propellant depot system to estimate the overall system mass and performance feasibility was determined by comparing the overall system mass to the potential launch vehicle performance capabilities. The results from this chapter show that the current state-of-the-art in cryocoolers are capable of providing enough thermal management to prevent the boil-off of cryogenic fluids in orbit. For mission durations shorter than four months, there is a positive mass trade of the all-passive scenario over the ZBO scenario. However, the mass of the boil-off loss becomes greater than the added system mass of the active thermal system for mission durations greater than four months.

The chosen thermal management system has direct impact on the performance feasibility of the launch vehicles. Using cryocooler technology in a propellant depot

system can drastically reduce the performance feasibility of the overall system due to the large uncertainty with the performance and mass estimation. The results of the probabilistic simulations show that for all but the largest available launch vehicles, the probability that the chosen launch vehicle is capable of handling the potential growth in the system mass due to uncertainty is very low. The all-passive scenario can be an attractive option due to the lower overall system dry mass and the decrease in the complexity of the system integration. The penalty of the all-passive depot is the propellant loss due to boil-off. Analysis of both the economic and reliability feasibility is required to determine what, if any, impact boil-off loss has on either metric to determine the optimal strategy for propellant depot based exploration architecture.

CHAPTER V

LAUNCH RELIABILITY AND PROPELLANT AGGREGATION FEASIBILITY ASSESSMENT

One of the major challenges to a propellant depot based exploration architecture is the increase in the total number of launches required as compared to a heavy-lift based architecture. Due to the increase in the required launches, some have argued that the overall mission reliability is unacceptable [14]. In order to fully understand the impact of this effect, this chapter presents an analysis of the overall reliability of the launch vehicle mission architecture, and more specifically the propellant aggregation launch requirements and feasibility assessment.

5.1 Historical Launch Reliability

One of the most critical phases of any space mission is delivering the required payload into orbit. A failure of the launch vehicle during this phase can have catastrophic consequences for the current mission and future missions. Since the Soviet Union launched Sputnik atop the R-7 Rocket on October 4, 1957, the world has seen thousands of rocket launches with payloads varying from small communication satellites to sending humans to the lunar surface. Assessing the risk, or probability, of launch failure is a critical element of architecture decision and planning. However, the process of quantifying this risk is very difficult, especially for new vehicles that have relatively few launch attempts. The thousands of worldwide rocket launches in the past 50 years provide a fairly small sample size of launch vehicles to make an accurate assessment of launch vehicle reliability. In comparison, commercial aviation has upwards of a hundred thousand flights per day around the world currently, over the

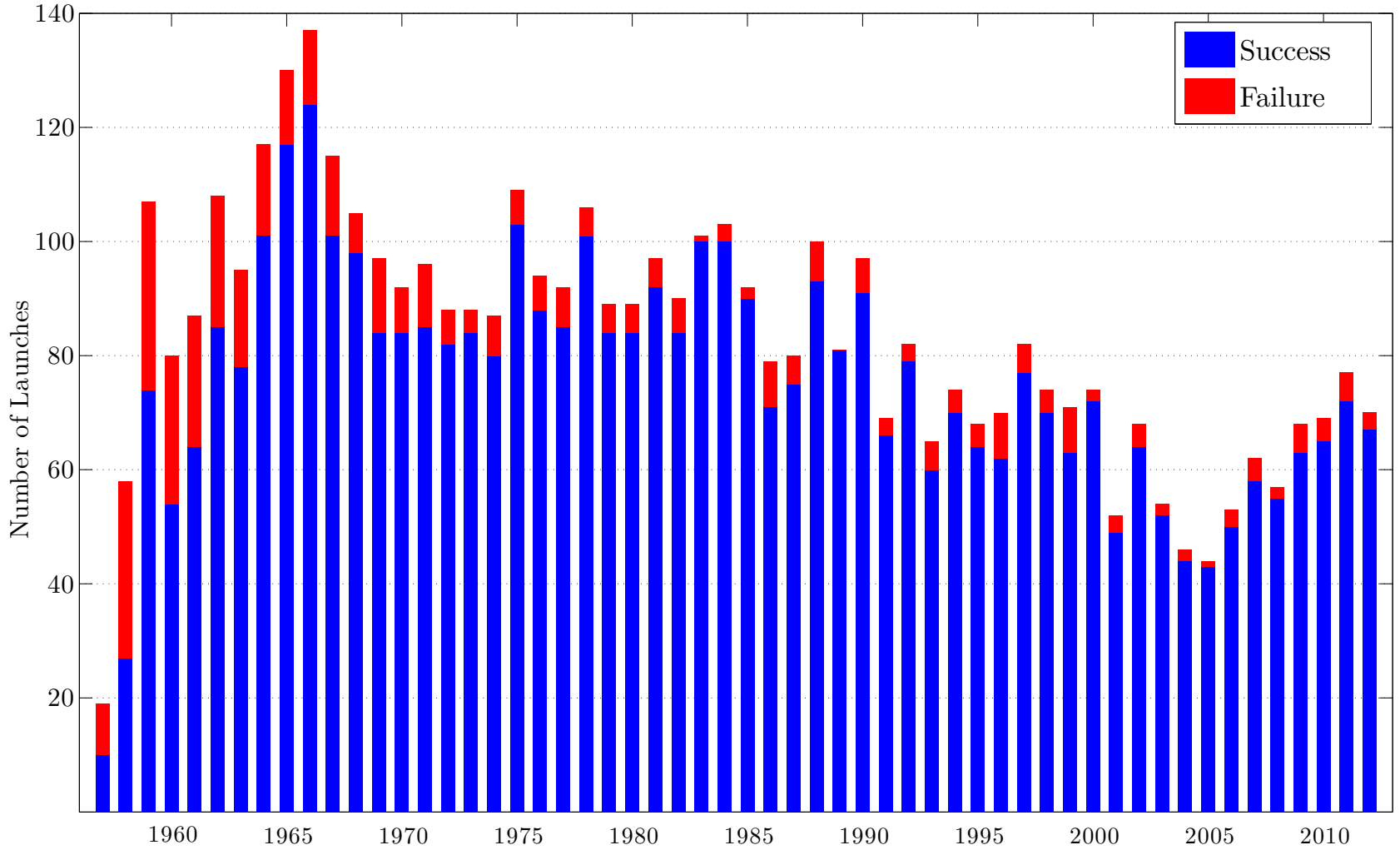

Figure 47: Summary of Global Rocket Launches from 1957 to 2012 [74, 139, 140]

course of a year or two, the data generate can give fairly high confidence in the result of frequency of failure analysis.

Figure 47 shows the summary of the majority of rocket launches from around the world between 1957 and 2012. The launch records are based on a variety of sources, most notably the *International Reference Guide to Space Launch System* by Isakowitz [74], *Space Launch Report* [139], and *NASA's Major Launch Record* [140]. The records include nearly all of the orbital flights from the United States, Russia (former Soviet Union), Japan, and European Space Agency, as well as launches from India, China, and other small countries. The data also includes the majority of the suborbital test flights in the late 1950's and early 1960's as these flights were often used as test beds for orbital launch vehicles.

The summary of global launches shows that the total number of rocket launches in the world peaked in the mid 1960's during the space race between the United States and Soviet Union. There were a large number of failures during this first decade of rocketry, and while the number of failures has diminished since then, the overall success-to-failure ratio on a yearly basis hasn't seen any dramatic change since the 1970's. Between 2003 and 2012, the worldwide rocket launches have seen an average of 3.1 failures per year with an average annual launch rate of 56.9 per year, resulting in launch reliability of approximately 0.948. In comparison, the overall reliability of launch vehicles in the 1990's and 1980's were 0.953 and 0.934 respectively.

Figure 48 shows the yearly and cumulative probability of launch success based on the global launch data collected between 1957 and 2012. In total, there are 4,654 recorded launches with 435 failures and 4,219 successes. For the purpose of the analysis in this dissertation, a launch failure includes all launches that resulted in loss of vehicle as well as any launches that result in payload delivery into incorrect orbit. The figure shows that the yearly launch success probability rose sharply between 1957 and 1970 and has fluctuated between 0.9 and 1.0 ever since with an occasional yearly

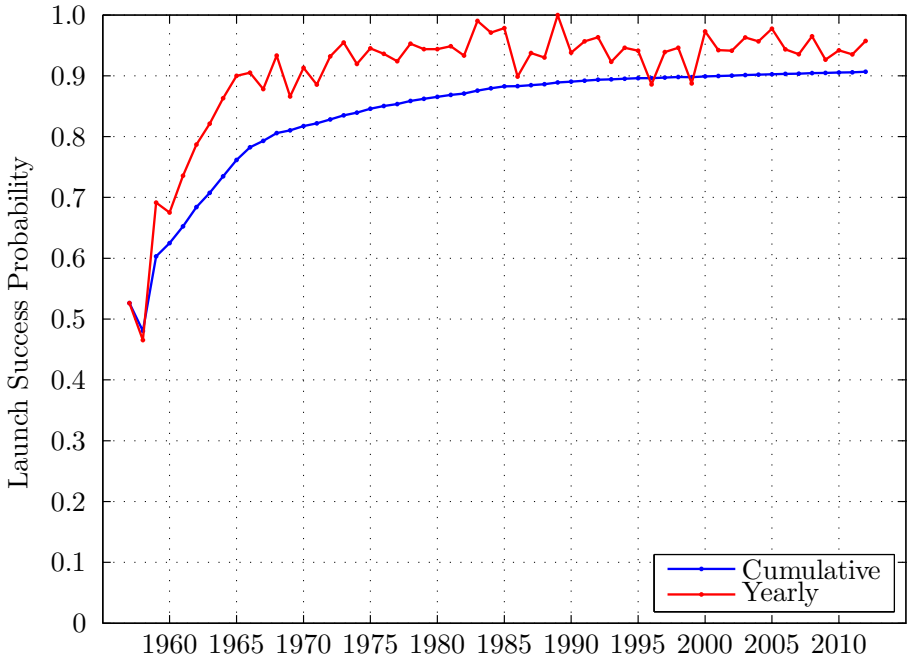

Figure 48: Global Rocket Launch Yearly and Cumulative Success Probability [74, 139, 140]

dip below 0.9 (1986, 1996, 1999). A particularly good year was 1989, as all 81 of the recorded launches were successful. Since 1970, the world experiences an average of 4.6 launch failures per year with an average launch rate of 79 per year. Cumulatively, the overall rocket launch probability of success has reached just above 0.90, and this cumulative probability has been fairly steady for the past decade.

Figure 48 shows the overall success probability of launch vehicles from a classical statistic standpoint. It would be simple to take the cumulative or the yearly success probability and apply it directly to the propellant depot architecture to determine the overall architecture reliability feasibility. For example, assuming rocket launch as independent events, the success of multiple launches is simply the product of the individual events. This is typically the method used in literature to assess the mission risk when multiple launches are involved. However, there are two deficiencies with this simple implementation of launch vehicle reliability to the propellant depot problem.

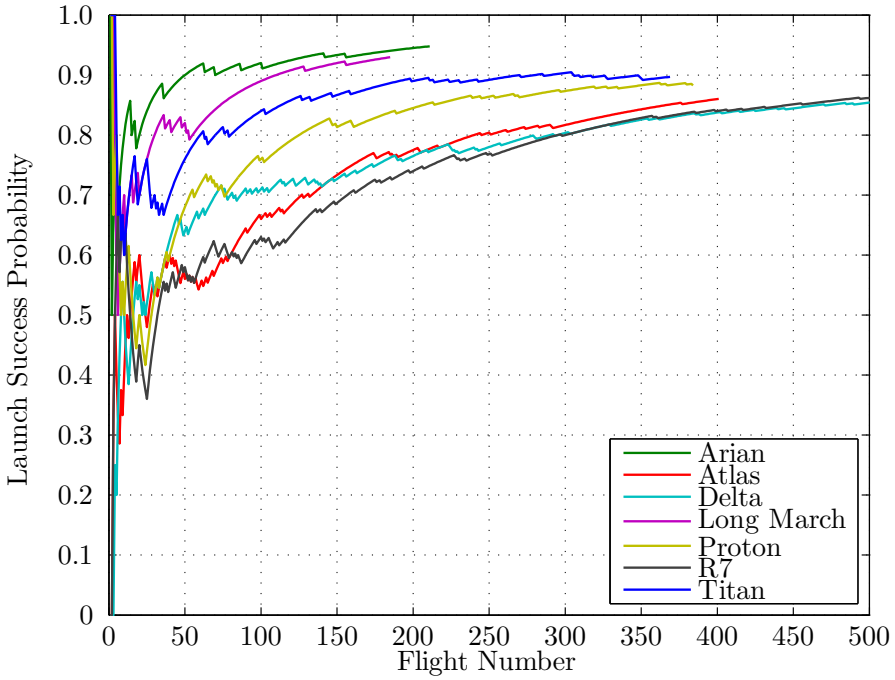

Figure 49: Individual Launch Family Historical Launch Reliability Growth Curve [74, 139, 140]

The first problem is the inability for this analysis to provide any confidence in the results. Simply put, there isn't enough data to justify the use of frequency of failure analysis with high enough confidence. Second, and more importantly, is that both the depot based architecture and the baseline heavy lift architecture have launch vehicles that have been recently developed or still in development. Although knowledge of rocket technology has improved dramatically over the past 50 years, the risk associated with a newly developed system is still relatively high and blind application of historical reliability would provide an inaccurate assessment of the overall mission success rate.

As Morse et al. [141] discussed in their paper, the historical success and failure record of launch vehicles demonstrates clear reliability growth over successive launches. This effect is shown in the cumulative worldwide launch reliability in Figure 48 as well as the individual launch vehicle reliability growth curve in Figure 49.

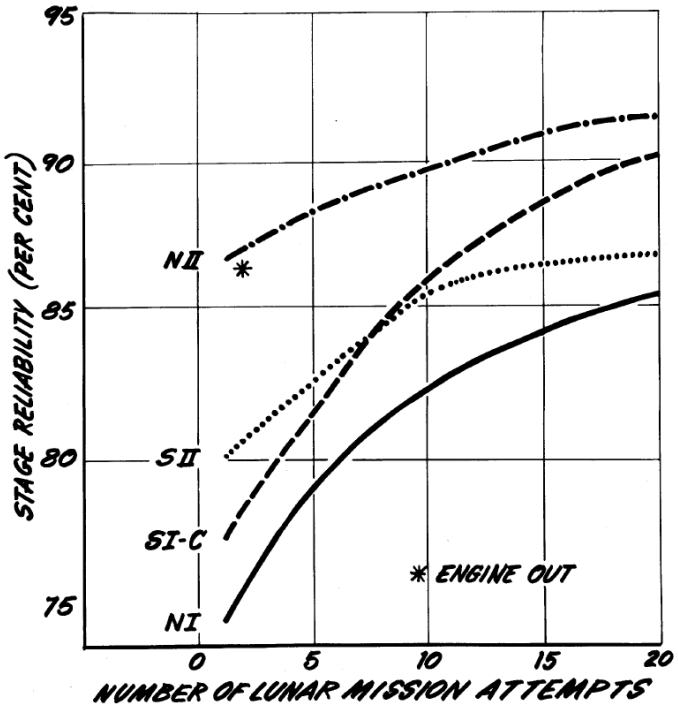

Figure 50: Reliability Growth Estimate of Various Stages of the Apollo Program, reproduced from [15]

Figure 49 shows the cumulative reliability of seven of the major launch vehicle families from around the world that has a record of over 100 launches. The figure shows the high variability of the launch success probability during the first 50 to 100 launches and the growth of the overall success probability expends beyond 200 flights in several cases. To accurately analyze the overall launch vehicle reliability, both of these issues must be addressed, and the results of which are presented in the following sections.

5.2 Launch Vehicle Infancy Reliability

One of the major concerns with assessing the risk of launch vehicle failures is the "infancy" problems with new launch vehicles. The reliability of any new launch vehicle is highly uncertain and can only be proven with a large number of demonstrated flights. Reliability growth was a major concern during the Apollo program [15] because the estimate of initial probability of success for the first few lunar missions was very low. This is demonstrated by the initial reliability assessment of the various

stages of the Saturn rocket shown in Figure 50. The initial reliability assessment of the three Saturn V stages was 0.77, 0.8, and 0.8 (assuming the SIV third stage has the same reliability as the SII stage with only one J-2 engine instead of five). This reliability equates to an initial reliability of 0.5 for the Saturn V vehicle.

For mature launches vehicles like the Delta and Atlas family, which have extensive launch records, the infancy problem has long been resolved (as shown in Figure 49). However, the design space of the propellant depot architecture includes vehicles that are currently under development and the heavy lift baseline architecture is solely dependent on the newly developed Space Launch System albeit based on Space Shuttle engine and other technologies. In order to provide a fair comparison between existing launch vehicles with newly developed vehicles with no launch record, the infancy problem must be addressed.

The infancy problem (or the infant mortality problem [141, 142]) is well known in the reliability assessment field, though the meaning is slightly different when examining launch vehicle reliability. Typically, the infancy problem refers to the increased failure rate of a product at beginning of life. For example, a new light bulb might have a higher probability of failure on its first on/off cycle than any other cycle after that. Mak [142] states that the explanation for these failures is typically defects within the manufacturing process. With launch vehicles, one can think of a family of launch vehicles as a product, and there is increased probability of failure during the first few launches of that particular family of vehicle. The cause of these failures can be attributed to a large number of causes. Unlike a light bulb, a launch vehicle is an extremely complex system with millions of parts and hundreds of subsystems that must work in unison. Thus, there are two potential levels of infant mortality problem, first at the subsystem level if any of the subsystems used are new and second at the system level if the integration method of the launch vehicle is new.

The launch vehicle infancy problem can be observed empirically from the launch

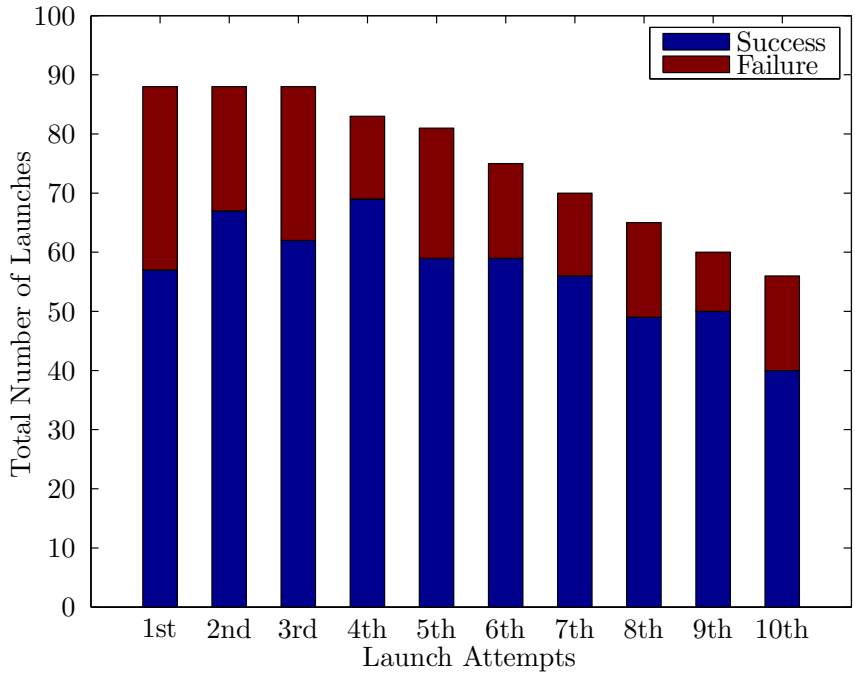

Figure 51: Summary of the First Ten Launch Attempts by 99 of the Worldwide Launch Vehicles [74, 139, 140], Appendix C

Table 20: Summary of the Results of the First Ten Launches for the Family of Launch Vehicle in Appendix C [74, 139, 140]

	Successes	Failures	Mean Failure Rate	Standard Deviation of Failure Rate
1st Launch	66	33	0.333	0.471
2nd Launch	76	23	0.232	0.422
3rd Launch	64	28	0.304	0.460
4th Launch	70	16	0.186	0.389
5th Launch	58	22	0.275	0.447
6th Launch	58	15	0.205	0.404
7th Launch	56	12	0.176	0.381
8th Launch	49	14	0.222	0.416
9th Launch	50	9	0.153	0.360
10th Launch	39	16	0.291	0.454
Total	**586**	**188**	**0.243**	**0.429**

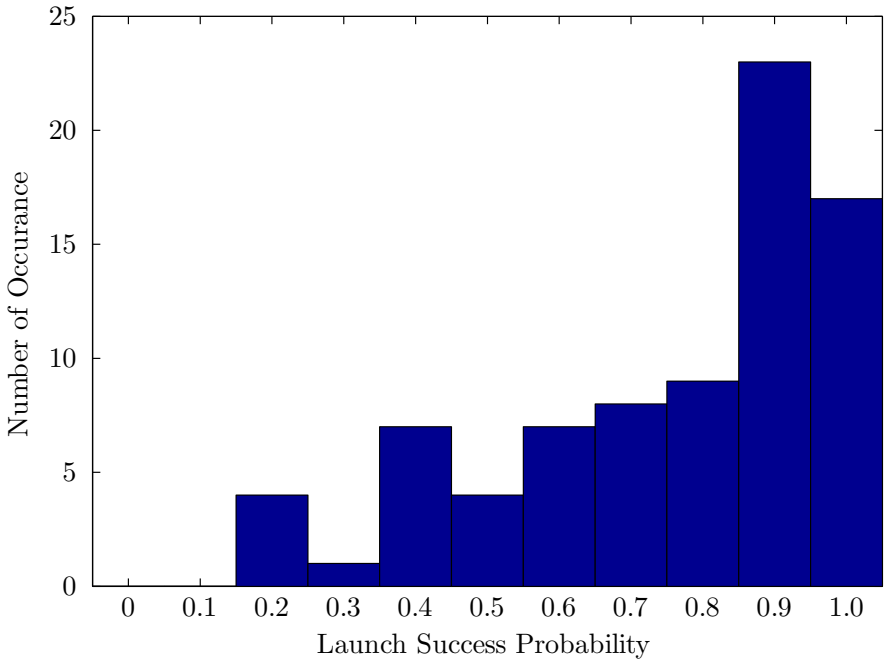

Figure 52: Histogram of the Distribution of Launch Vehicle Probability of Success through the First 10 Launches with more than 5 Launch Attempts [74, 139, 140]

vehicle database compiled for this dissertation. The 4,654 launches recorded between 1957 and 2012 can be classified into 99 launch families with at least two launches per family. The first ten launches of each of the family are recorded in Appendix C, shown in Figure 51 and summarized in Table 20. The summary shows that the mean failure rate for the first ten flights of rocket launches varies between 0.176 and 0.333. The highest of the failure rates is the first launch of each of the family, with one-third failure rate. The table shows the cumulative probability of the launch vehicles through the first 10 attempts, which provides some insight into the overall probability of success, which on average is around 75% compared to the 90% observed in Figure 48 when the launch vehicles are mature.

One way to examine the data is to examine the distribution of the failure/success rate across the 99 launch vehicles through the first 10 launches. Figure 52 shows the histogram of the probability of success for the launch vehicle data. It's important to

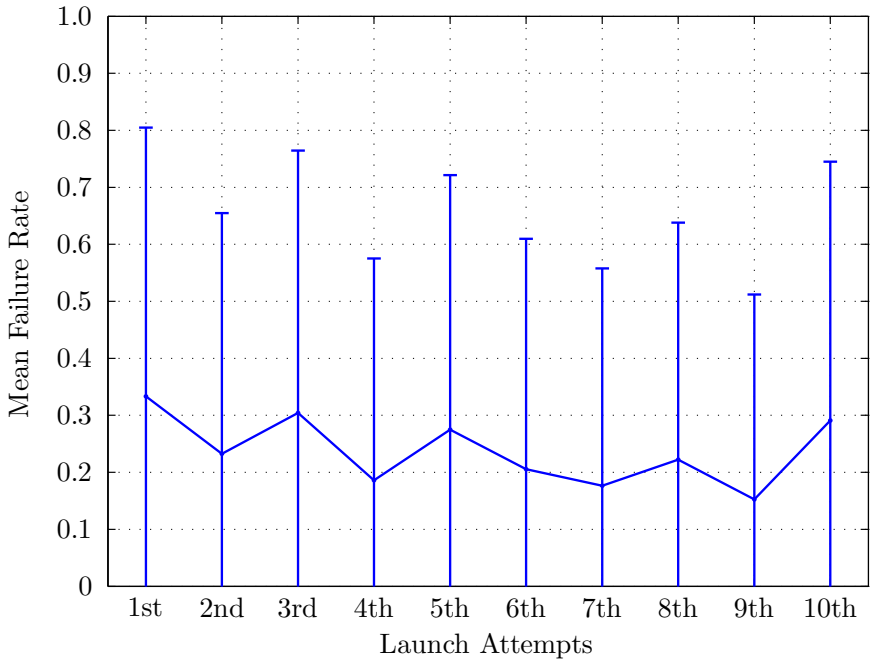

Figure 53: Mean Failure Rate Trend of the First 10 Launches for all Launch Vehicles with Error Bars Representing One Standard Deviation of the Mean Failure Rate

note that of the 99 launch vehicles examined, only 55 of them have reached the 10th launch and 19 of the launch vehicles did not reach the 5th launch before cancellation. So, the data in Figure 52 shows only the reliability of launch vehicles with at least 5 launches. Of the 80 vehicles that have at least 5 launch attempts, 17 have a perfect launch record and 9 of these vehicles were a perfect 10-for-10. The distribution of the success probability provides insight into the overall variability of the success probability in the first ten flights of a new launch vehicle. A probability distribution can be applied to the observed data to model the estimation of success probability of new launch vehicles. However the data, presented in this form, provides no information on the actual growth of the launch vehicle reliability through the first ten launches. To analyze this growth, the progression of mean failure rates from one launch to the next is examined.

Figure 53 shows the progression of the mean failure rate for the first ten flights

of all the launch vehicles with the error bars representing the one standard deviation of the mean failure rate. The mean failure rate of the launch vehicles does seem to decrease as more experience is gained by consecutive launches in the family; however the overall downward trend it fairly minimal. Table 20 also shows the standard deviation of the failure rates for each of the launch attempts. Because the sample size is fairly small, the standard deviation is quite high. The lower bound of the error bar is limited to zero because negative failure rate is not possible. The error bar shows that there is significant uncertainty involved with estimating the overall failure rate for vehicles in the first ten flights. Even though over 4000 launches have been recorded, the majority of these flights are conducted by families of launch vehicles with significant experience. There is simply not enough data of different launch vehicle families to make a good large-sample approximation of the overall failure rates. Guikema and Pate-Cornell [143] echo this sentiment in their analysis of 41 launch vehicle's launch infancy problem.

To address the hypothesis that the launch vehicle failure rate decreases with increasing launch attempts, Guikema and Pate-Cornell uses standard statistical hypothesis testing with the Smith-Satterthwite method, which is the standard two-sample z-test [144]. To make the case for increased launch vehicle reliability (or decreased failure rate) for consecutive launches, there must be 95% confidence that there is a statistical significant difference between the mean failure rates for each consecutive launches. For the testing, the null hypothesis is

$$H_o : \mu_1 - \mu_2 = 0 \tag{23}$$

indicating that there is mean of the failure rates of consecutive launches in the family is the same, or in other words, there is no statistical significance of changes in failure rates for consecutive launches in the family. The goal is to reject the null hypothesis with high confidence while accepting the alternate hypothesis,

$$H_a : \mu_1 - \mu_2 > 0 \tag{24}$$

indicating the mean failure rate decreases with consecutive launches. The standard z-test statistic is given by,

$$z = \frac{(\bar{X}_1 - \bar{X}_2)}{\sqrt{\frac{\sigma_1^2}{n_1} + \frac{\sigma_2^2}{n_2}}} \tag{25}$$

with the rejection region given by standard z table [144] for a 95% confidence as,

$$RR : z > 1.65 \tag{26}$$

Table 21 shows the resulting z-Values for each of the pairwise comparison of the consecutive launches. To reject the null hypothesis with more than 95% confidence, the z-Value must be greater than 1.65. In the nine pairwise comparisons, only the third to fourth launch satisfies the requirement to reject the null hypothesis. Examining the mean and standard deviation of failure rates, there is a sharp decrease in the failure rate from the third launch to the fourth launch in the mean failure rate and slight decrease in the standard deviation. These combined to give a fairly high level of confidence that the null hypothesis can be rejected. However, generally speaking across the first ten launches of the vehicles surveyed, there is not enough statistical significance in the data to reject the null hypothesis. In other words, from a classical statistics standpoint, the failure rates for the first ten launches in the launch vehicle family are indistinguishable from one another. Guikema and Pate-Cornell [143] came

Table 21: z-Values for Hypothesis Test of the Failure Rates for the First Ten Launches of Launch Vehicles

	1st→2nd	2nd→3rd	3rd→4th	4th→5th	5th→6th
z-Value	1.59	-1.12	1.86	-1.36	1.01
	6th→7th	7th→8th	8th→9th	9th→10th	
z-Value	0.439	-0.655	0.992	-1.80	

to similar conclusion with their work using only data from the first five launches of 41 families of launch vehicles.

The implication of this statistical test is that for a new launch vehicle system, as observed by the data, there is evidence to suggest that the overall reliability of the launch vehicle is poorer in the early launches; however, the improvement of reliability cannot be statistically demonstrated through the first ten launches. In order for the growth of the launch vehicle reliability to make a statistical significant impact, more than ten launches of any vehicle is required. Of course, as Guikema and Pate-Cornell pointed out, this interpretation of the statistical data can be problematic. The use of 95% confidence comparison with the mean of a data set that has fairly small sample size can lead to large uncertainty with the conclusion of the hypothesis test. This deficiency in the analysis of launch vehicle reliability leads to the use of Bayesian probability methods to model and analyze not only the mean and standard deviation of the infancy reliability of launch vehicles, but a complete probability distribution of the reliability. The method used for this formulation, and the results are presented in the next sections.

5.3 Bayesian Reliability Method

The driving force behind the use of Bayesian probability to discuss reliability is that the reliability metric, like the other feasibility assessment metrics discussed in this dissertation, has uncertainty associated with it. The uncertainty in the assessment of reliability means that it should not be thought of as a deterministic property but rather it must be treated as a random variable. The classical statistics analysis conducted in the previous section should not be discarded, however, but the interpretation of those results will be different with the Bayesian methods. The key difference is by using the Bayesian method, the single value of reliability is expanded to a full

probability distribution, which can provide some level of confidence with the estimation, and it allows for the distribution to be updated with new evidence that either support or detracts from the previously computed distribution.

Fundamentally, Bayesian probability derives from Bayes' theorem, which gives the relationship between two events A & B, the probability of each of the events occurring, $P(A)$ and $P(B)$, and the conditional probability of A given B and B given A, $P(A|B)$ and $P(B|A)$. The standard conditional probability is given by [144],

$$P(A|B) = \frac{P(A \cap B)}{P(B)} \tag{27}$$

$$P(B|A) = \frac{P(A \cap B)}{P(A)} \tag{28}$$

where $P(A \cap B)$ is the joint probability of both events occurring. Substituting the joint probability from the second equation into the first gives the standard form of Bayes' theorem [144],

$$P(A|B) = \frac{P(B|A) * P(A)}{P(B)} \tag{29}$$

The classical statistic interpretation of the Bayes' theorem formula is that it shows the relationship between the two conditional probabilities as fractions of the probability of the independent events. The Bayesian interpretation is based on degree of belief in a proposition before and after evidence is presented. In the above equation, $P(A)$ represents the initial belief of the event A (the prior), $P(A|B)$ represents the updated belief of event A when event B has been taken into account (the posterior), and the ratio of $P(B|A)$ and $P(B)$ represents the support event B provides for event A. Bayesian probability provides a method to update current or prior belief with new information.

In the context of launch vehicle reliability, the prior distribution in the Bayesian formulation can be thought of as the computed reliability, or estimated reliability

of the launch vehicles before any launch has been attempted. For a new launch system, this can be estimated from the infancy data shown in the previous section. The likelihood function, or the evidence used to update the prior distribution, are the actual launch records of the particular system of interest. Finally the posterior distribution, update of the infancy reliability with actual launch records, is the current best estimate of the launch vehicle's reliability going forward. The Bayesian theorem given in Equation 29 is useful to compute simple probability.

For launch reliability, where the distribution of the reliability is desired, the equation must be modified to relate probability distribution functions. The continuous random variable version of Bayes' theorem allows the computation of a probability distribution of the updated launch vehicle reliability given prior knowledge of launch reliability and actual launch records. The computation of these reliability distributions allow for Monte Carlo simulation to estimate overall reliability of architectures given various launch requirements. The equation is derived from the conditional probability of continuous random variables,

$$f_A(a|B=b) = \frac{f_{A,B}(a,b)}{f_B(b)} \tag{30}$$

$$f_B(b|A=a) = \frac{f_{A,B}(a,b)}{f_A(a)} \tag{31}$$

Combining these equations yields Bayes' theorem for continuous random variables,

$$f_A(a|B=b) = \frac{f_{A,B}(a,b)}{f_B(b)} f_A(a) \tag{32}$$

In this version, $f_A(a)$ is the probability distribution of launch vehicle reliability prior to any launch, while the posterior, $f_A(a|B=b)$, is the updated probability distribution give that the observed launch reliability is b. The likelihood function represents the probability that the observed reliability is b given that the prior distribution of launch reliability is represented by $f_A(a)$. The likelihood function can be

modeled with various density functions that best represent the process being modeled. For example, if the individual launches can be viewed as independent Bernoulli processes with success probability given by the prior distribution, the likelihood function can be modeled using the binomial distribution function [145].

Guikema and Pate-Cornell [145, 146] use beta distributions for the prior distributions because it is compliment to the binomial distribution used to model the likelihood function; this allows for the posterior distribution to be solved analytically. For all other types of prior distributions, the posterior distribution is solved numerically by integrating over the entire range of probability distribution. Guikema and Pate-Cornell [146] gives the equation for this numerical method where the likelihood function is replaced by another conditional probability statement, and the denominator represents a renormalization factor to make the resulting distribution a valid distribution.

$$f_A(a|B=b) = \frac{f_B(B=b|a)f_A(a)}{\int_x f_B(B=b|x)f_A(x)\,\mathrm{d}x} \tag{33}$$

This Bayesian updating process can be demonstrated in Figure 54. The figure assumes an initial launch reliability distribution that is modeled by a triangular distribution with the mean of 0.757. The mean of the launch reliability is taken from the summary of the first ten launches of the launch vehicle database (shown in Table 20 as mean failure rate and Figure 52 as success probability). The tree diagram shows the progression of the launch reliability distribution with each launch success or failure. The distribution in blue represents the prior distribution, while the distribution in red represents the posterior distribution.

The updated distribution has two fairly interesting characteristics. First, with each successive success or failure of the launch vehicle, the mean of the overall distribution shifts left or right accordingly. Second, from observing the cases where there are equal numbers of successes and failures, the order of success or failure is

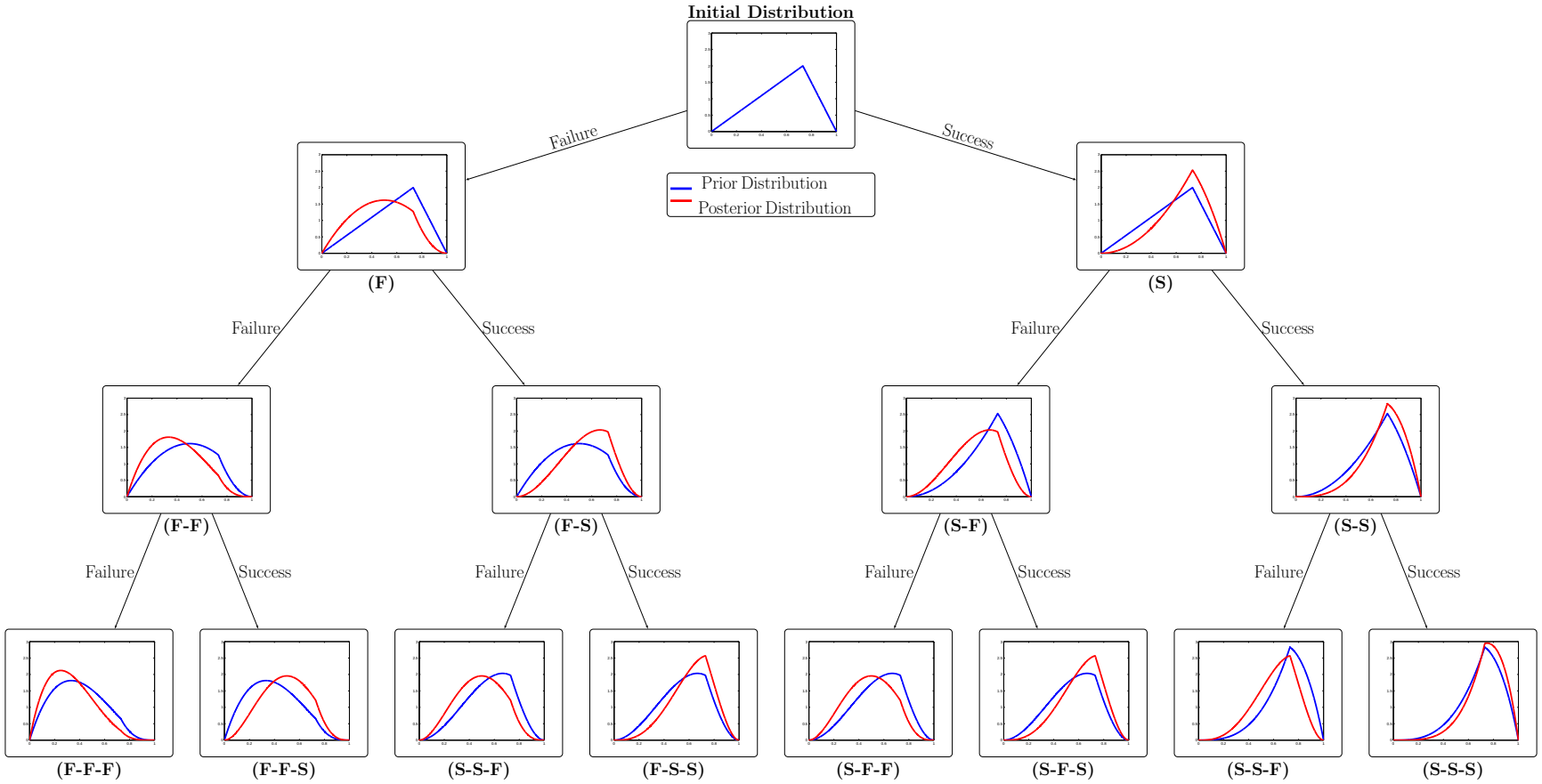

Figure 54: Bayesian Updated Launch Reliability Distribution Given Initial Triangular Distribution and Observed Success and Failure Combination for the First Three Flights, Prior Distribution in Blue, Posterior Distribution in Red

Table 22: Observed Launch Record for Launch Vehicles of Interest and Related Family, through January 31, 2014

	Vehicle		Related Family	
	Success	Failure	Success	Failure
Atlas V	48	1	305	55
Delta IV	23	1	632	81
Falcon Heavy	0	0	10	3
Space Launch System	0	0	0	0

inconsequential to the resulting posterior distribution. For example, the posterior distribution for the Fail-Fail-Success and the Success-Fail-Fail cases are identical to each other despite coming from two separate branches of the Bayesian tree. Using this technique, the observed empirical data can be used to update the launch vehicle reliability as more evidence is gathered.

For the launch vehicles of interest to the propellant depot architecture, the observed launch records for each are shown in Table 22. To estimate the future reliability of each of these vehicles, a prior distribution for the launch vehicle is needed. If no information exists to create a prior distribution, a simple uniform distribution from 0 to 1 can be used. For the Atlas and the Delta vehicles, even though these largest vehicles have fairly limited launch record, the vehicles are derived from other vehicles that have extensive launch records. Thus, prior reliability distribution can be created from analyzing the historical reliability of the other vehicles in the family. The number of trials for these launch vehicles is quite large, thus computing the Bernoulli trial probability is not possible because of the computation of large number factorials and raising the probability to the power of several hundred. Thus, for $bp > 5$ and $b(1-p) > 5$, the Bernoulli trials probability can be approximated by a normal distribution where $\mu = bp$ and $\sigma^2 = b(1-p)$ [144].

For the Falcon heavy vehicle, it utilizes three Falcon 9 cores integrated together with potential cross feeding technologies. The new development, makes the estimation of distribution difficult, but it does have heritage from the Falcon 1 and Falcon 9. For

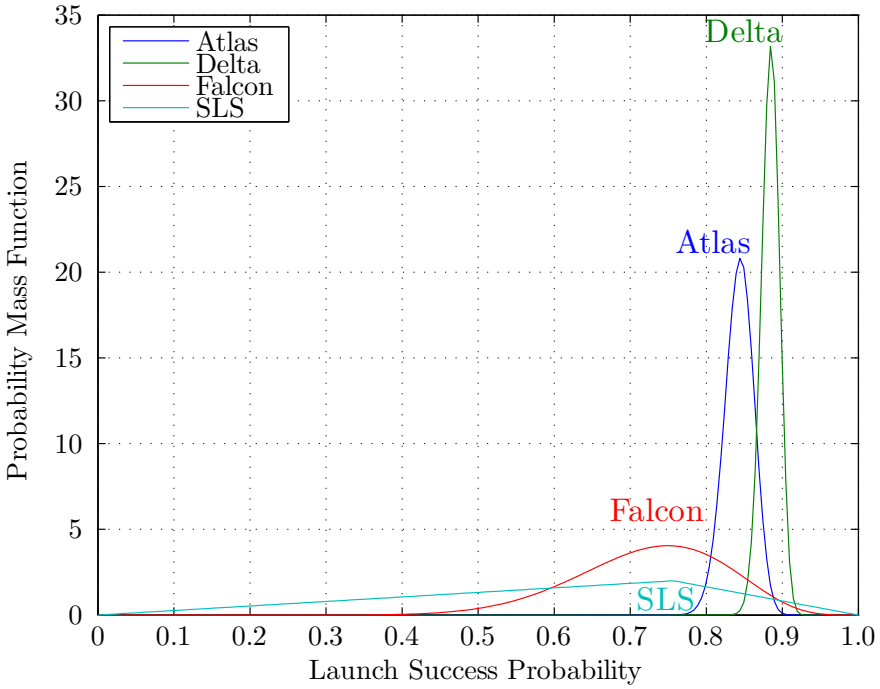

Figure 55: Prior Distribution of Launch Vehicle Reliability Based on the History of Related Launch Vehicles in the Family

the Space Launch System, even though the development is new, the vehicle utilizes many of the elements from the Space Shuttle vehicle. So some information may be gained from using the reliability of the Space Shuttle. However, the implementation and integration of these elements are very different from the Space Shuttle, thus the prior reliability estimate should be closer to that of a new vehicle.

The prior distribution for each vehicle is derived from the historical launch record of the family of launch vehicles that the new vehicles evolved from. The starting point for the launch reliability of family of launch vehicle assumes a simple uniform distribution from 0 to 1, as these vehicles were developed during the early era of rocketry and there was very little information about the reliability of rocket vehicles. The Falcon Heavy is preceded by the Falcon 1 and Falcon 9 vehicles, both of which also had a very limited launch record. Using the same uniform distribution, the Falcon vehicle's reliability can be updated using the observed data. The Space Launch

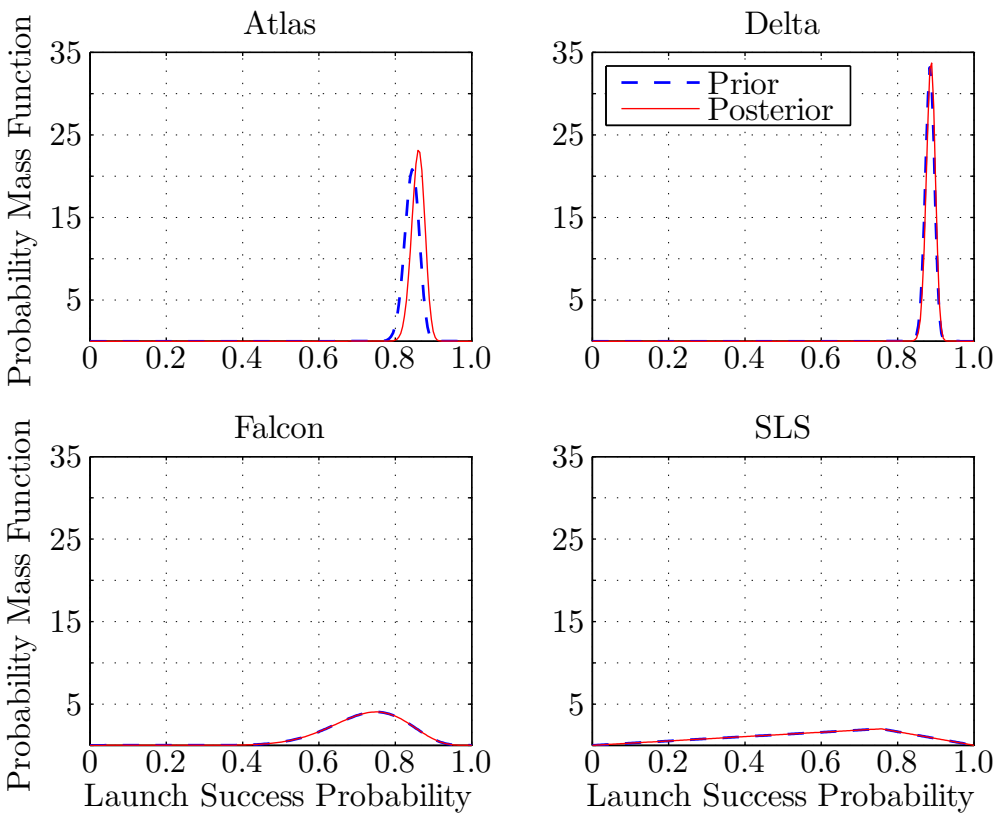

Figure 56: Posterior Distribution of Launch Vehicle Reliability Based on Observed Launch Record (Through January 31, 2014) for the Individual Launch Vehicle

System does not have the luxury of a history of family of launch vehicles; thus, the prior distribution for these vehicles is modeled using the historical infancy reliability of new launch vehicles as discussed in the previous section. Triangular distribution with mean of 0.757 is used.

Figure 55 shows the resulting prior distribution for the reliability of the Delta, Atlas, and Falcon given the reliability of the previous generation of the launch vehicles along with the triangular distribution for the SLS. The figures show that because the Delta and the Atlas come from a long line of launch vehicle family with significant launch records, the overall projection of the launch vehicle reliability is fairly stable with a very high peak. On the other hand, both the Falcon and the SLS have very little launch record to support their reliability claim, thus the projected reliability of

Table 23: Summary of the Bayesian Prior and Posterior Distribution for the Four Launch Vehicle of Interest

	Prior Distribution		Posterior Distribution	
Atlas V	Beta	$a = 305.2$ $b = 55.85$	Beta	$a = 353.4$ $b = 56.88$
Delta IV	Beta	$a = 631.0$ $b = 81.74$	Beta	$a = 654.4$ $b = 82.79$
Falcon Heavy	Beta	$a = 11.02$ $b = 4.007$	Beta	$a = 11.02$ $b = 4.007$
SLS	Triangular	$a = 0$ $b = 0.731$ $c = 1$	Triangular	$a = 0$ $b = 0.731$ $c = 1$

these vehicles are much more widespread, indicating large uncertainty in the reliability estimates for these vehicles.

Using Bayesian methods, these prior distributions are updated with the observed launch records for each of the vehicles and the results are shown in Figure 56. For the Atlas V vehicle, the recent success of launches moved the mean of the reliability distribution to the right just slightly and narrowed the spread of the distribution. The added data improved the estimate provided by the historical data. The Delta launch vehicle, which had the most extensive prior launch record, saw very little change in the reliability distribution with the additional data. For the Falcon Heavy and the SLS, because there are no data available, have no change in the reliability distribution from the prior distribution. A summary of each of these distributions is shown in Table 23.

5.4 Propellant Aggregation Launch Requirements

To determine the overall launch reliability, the number of required launches for the architecture needs to be determined. The biggest contributor of mission unreliability in propellant depot based exploration architecture is the large number of launch vehicles required for the mission. The heavy lift launch vehicle based exploration architecture presented in Chapter 2 requires the launch and on orbit rendezvous of three to four heavy lift vehicles. In comparison, the baseline depot based exploration architecture, using the Falcon Heavy to deliver all of the necessary components, requires 10 launches. As discussed in Chapter 2, if the launch vehicle success can be

viewed as independent events with some probability of success, then requiring more launches will exponentially reduce the overall success probability.

The number of launches required by a propellant depot based architecture is depended upon several factors. The variable with the most importance is of course the payload capacity for the selected launch vehicle. Chapter 4 presented a feasibility analysis on the utilization of various launch vehicles to deliver the depot hardware to orbit. The analysis showed that in order to have high confidence of successfully delivering the hardware to orbit, the largest payload capability of the available launch vehicles are preferred. However, this requirement does not apply to the delivery of the propellants that are required to fill the depot. One of the most beneficial aspects of the propellant depot based architecture is that it divides the mass required in orbit into whatever portion is most desirable for the particular mission. This provides an unparalleled amount of flexibility to the mission planning process.

The other important variables that drive the number of launches required are the overall propellant mass fraction of the tanker vehicles, the flight rate of the chosen launch vehicles, and finally the boil-off rates of the stored propellant if zero-boil-off technology is not applied and the required storage time. The overall propellant mass fraction of the tanker vehicle describes the percentage of the launch vehicle's available payload capability that can be used to deliver propellant. A portion of the payload capability must be used to account for the tanker vehicle dry mass that includes the propellant tanks, supporting structures, propellant transfer mechanisms, and other subsystems that are required for the tanker to fly autonomously and rendezvous with the propellant depot.

The actual propellant mass fraction of the tanker vehicle will be depended on the overall design and fabrication of the vehicle. Performing a detailed design of the tanker vehicle is outside the scope of this dissertation. One way to model the tanker vehicle is to examine historical systems that are similar. The launch vehicle's upper

Table 24: Launch Vehicle Upper Stage Mass Summary

	Propellant Type	Propellant Mass (kg)	Gross Mass (kg)	Propellant Mass Fraction
Fregat Soyuz	Storable	5,350	6,435	0.8314
Ariane V	Storable	9,700	10,900	0.8899
Titan II	Storable	27,000	30,000	0.9000
Titan IV	Storable	35,000	39,500	0.8861
Centaur II	LOX/LH2	16,780	18,960	0.8850
Delta II	LOX/LH2	16,820	19,300	0.8715
Centaur III	LOX/LH2	20,830	22,744	0.9158
Delta IV 4-m	LOX/LH2	20,400	24,170	0.8440
Delta IV 5-m	LOX/LH2	27,200	30,710	0.8857
Molniya 4th	LOX/RP1	5,500	7,360	0.7473
Soyuz 3rd	LOX/RP1	22,800	25,300	0.9012
Falcon 9	LOX/RP1	90,719	95,254	0.9524

stage is generally good for comparison to the tanker vehicle [5]. The upper stage's functionality, the design, and performance are all fairly similar to the tanker vehicle with the exception of the propellant transfer mechanism and the thermal management systems. If the rendezvous, docking, and propellant transfer can be conducted fairly quickly after the launch of the tanker vehicle, then the boil-off mitigation required is minimal. These exceptions can be balanced by the fact that typically upper stage vehicles have high performance propulsion system to perform the orbital maneuvers while the tanker vehicle only requires orientation and docking propulsion.

Table 24 shows a summary of upper stage vehicles with different propellant types and their respective propellant mass, gross mass, and propellant mass fraction. The majority of the propellant mass fraction lies between 0.84 and 0.95, with the Molniya 4th stage as an outlier at 0.75 because of its relatively small propellant capacity. The data suggest that better than 80% of the any launch vehicles payload capability can be utilized as propellant delivered to orbit, with the average propellant fraction of around 0.87. Thus the launch vehicle payload given by Table 18 is reduced by this fraction to account for the dry mass associated with the tanker.

Table 25: Launch Vehicle Flight Rates for Selected Launch Vehicles

Launch Vehicle	Potential Flight Rate	Demonstrated Flight Rate
Atlas V 551	5-8/year	2/year
Delta IV Heavy	5-8/year	2/year
Falcon Heavy	8-12/year	TBD
Space Launch System	0.5-2/year	TBD

The final variable that drives the number of launches required is the storage time and the vehicle launch rates. With the exception of the zero-boil-off scenario, the boil-off of the propellant will eventually require additional flights to top off the depot propellant before the mission can be performed. Additionally, the storage time also depends on the vehicle launch rates. If the vehicles can be launched in rapid succession, then the depot can be filled rather quickly to minimize the effect of propellant boil-off.

Table 25 shows the potential and demonstrated flight rates for each of the launch vehicles under consideration. The potential flight rates are from either the vehicle planning guide for the individual vehicle [75, 76, 139, 147–150] or based on the demonstrated flight rate for the vehicle's family. The demonstrated flight rates for the Delta IV Heavy and the Atlas V 551 are taken from the historical launch database developed. Note that the demonstrated launch rate for the Delta and Atlas are for the specified vehicle, the launch rate for the families of vehicles are much higher (shown as the potential flight rate). Additionally, the launch rates may be considered conservative because it represent a single work shift per day and could be increased if there is demand to justify the increase. SpaceX predicts that the Falcon Heavy can launch as much as 10-12 times per year (up to once a month) depending on the demand for the vehicle [148]. The Space Launch System's potential flight rate is taken from the budget estimate for the next 10-20 years. After first flight, the estimated cost for the SLS is roughly $1-2 Billion per launch, and thus from the budget estimate

(more detail in Chapter 6) this equates to somewhere between 2 launches per year to one launch every two years. This information can now be combined with the analysis provided in Chapter 4 to compute the propellant aggregation rates for various scenarios.

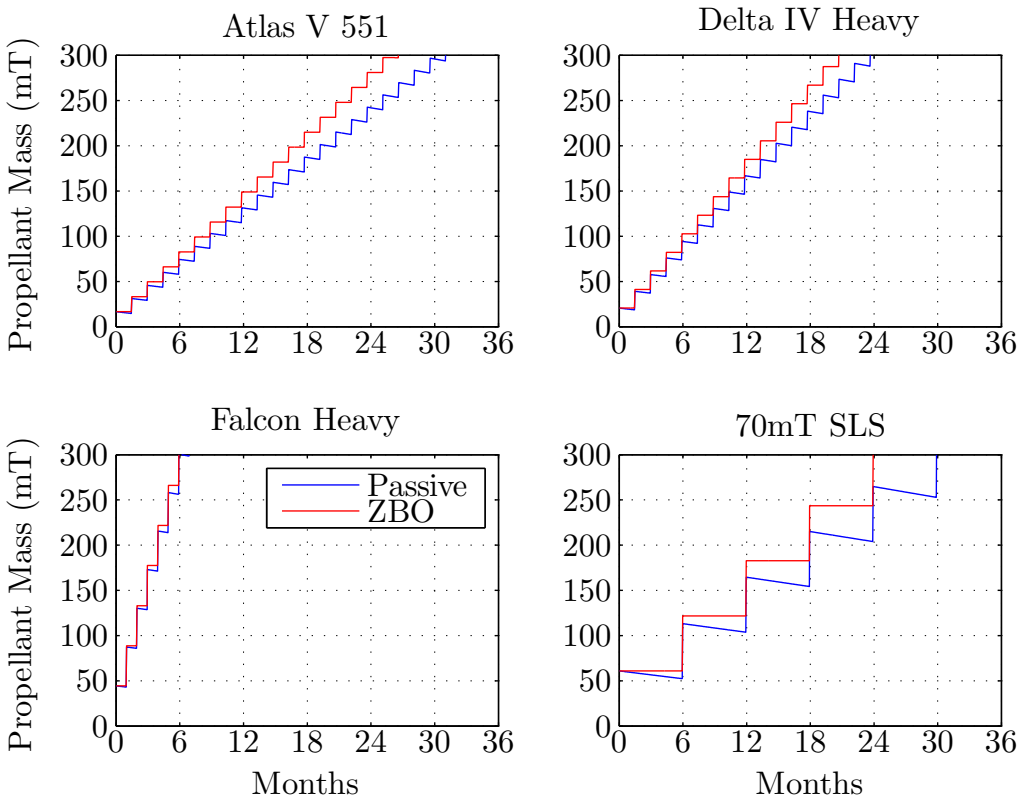

Figure 57: Propellant Aggregation as Function of Time and Cryogenic Fluid Management Strategy Using Maximum Potential Flight Rates for Each of the Launch Vehicles Under Consideration

Figure 57 shows the propellant aggregation in orbit as function of time using the maximum potential flight rate for each of the launch vehicles given in Table 25. The payload for each launch vehicle assumes a propellant mass fraction of 0.87 and tanker oxidizer-to-fuel (OF) ratio of 6 for oxygen and hydrogen. For each launch vehicle, the two cryogenic fluid management strategies discussed in Table 15 are plotted to show the effect of boil-off on the aggregation rates. The Atlas and Delta launch vehicles have very similar propellant aggregation rates due to the similarity between the two

Table 26: Breakdown of Average Propellant Aggregation Rates for Each of the Launch Vehicles and Scenarios Assuming a Tanker Oxidizer-to-Fuel Ratio of 6

		Passive	ZBO	
Atlas	LO2	268	305	kg/day
	LH2	30	52	kg/day
	OF Ratio	8.9	5.9	
Delta	LO2	338	376	kg/day
	LH2	42	64	kg/day
	OF Ratio	8.1	5.9	
Falcon	LO2	1,140	1,180	kg/day
	LH2	180	203	kg/day
	OF Ratio	6.3	5.8	
SLS	LO2	238	276	kg/day
	LH2	26	47	kg/day
	OF Ratio	9.2	5.9	

vehicles both in terms of payload capability and potential launch rates. The Falcon Heavy vehicle has the highest aggregation rate, while the 70 mT SLS has similar aggregation rate as the Delta and the Atlas despite having almost three times as much payload capacity. This suggests that the propellant aggregation rate is much more sensitive to launch rate than it is to payload capacity.

The propellant buildup rate shown in Figure 57 can be misleading, however, especially for the non-ZBO scenarios. Because the oxidizer and fuel boil-off at different rates, the total propellant aggregated in orbit may not be suitable as a figure of merit to evaluate the feasibility of the various launch vehicles. Table 26 demonstrates this by separating the total average propellant aggregation rates (in kg per day) assuming a tanker OF ratio of 6. The average propellant aggregation OF ratio is shown in the table for each of the scenarios. The ZBO cases all result in final OF ratio of approximately 6 as expected because no propellant is boiled off. However, for the non-ZBO cases, the resulting OF ratio can be completely unacceptable for the mission requirement. With the exception of the Falcon vehicle, which has the benefit of high launch rate and large payload capacity, the other vehicles all result in propellant

aggregation rates that is oxidizer rich. Thus the tanker OF ratio must be adjusted for the non-ZBO case to optimize for the resulting OF ratio. Alternatively, the architecture may utilize an additional "top off" launch that provides a last minute fuel rich tanker deliver to balance the OF ratio in the depot.

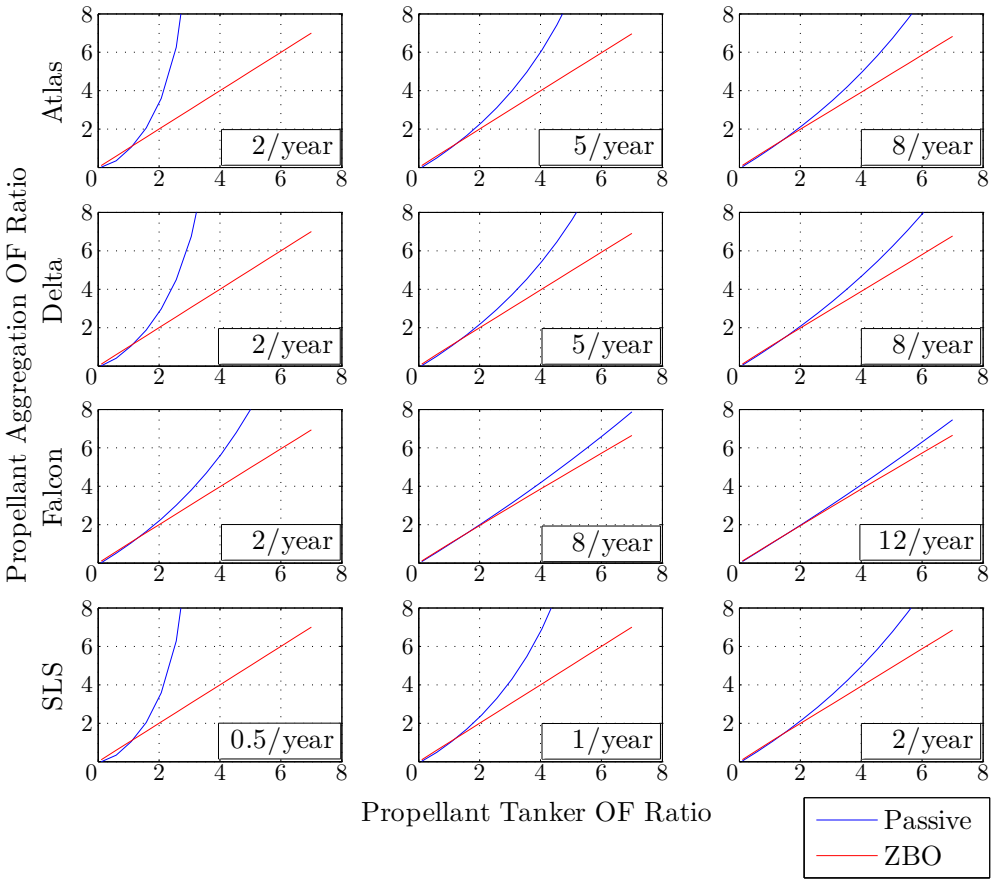

Figure 58: Resulting On-Orbit Propellant Aggregation OF Ratio as Functions of CFM Strategy, Launch Vehicle, and Propellant Tanker OF Ratio

Figure 58 shows the resulting propellant aggregation OF ratio as a function of the tanker OF ratio for all the launch vehicles with different launch rates and the two CFM strategies. The right most column in this figure is the maximum launch rate propellant aggregation shown in Figure 57. As expected, all of the ZBO cases, regardless of the other variables, results in a one-to-one correlation from the tanker

Table 27: Tanker Required Oxidizer-to-Fuel Ratio for On-Orbit Propellant Aggregation Oxidizer-to-Fuel Ratio of 6

		Passive	ZBO
Atlas	2/year	2.5	6.0
	5/year	4.0	6.0
	8/year	4.5	6.0
Delta	2/year	3.0	6.0
	5/year	4.0	6.0
	8/year	5.0	6.0
Falcon	2/year	4.0	6.0
	8/year	5.5	6.0
	12/year	5.5	6.0
SLS	0.5/year	2.0	6.0
	1/year	3.5	6.0
	2/year	4.5	6.0

OF ratio to the aggregation OF ratio. For the passive scenario, because of the different boil-off rates for the two fluids, the resulting aggregation OF ratio can be different.

The effect is most profound in the low launch rates scenarios. For the low end of the launch rate estimates (2/year for Atlas, Delta, Falcon, and 1 every 2 years for SLS), to achieve the desired OF ratio of 6, the tanker OF ratio needs to have a much lower OF ratio. For the Atlas, Delta, and SLS, to achieve an aggregation OF ratio of 6, the tanker OF ratio is between 2 and 3; and for the Falcon, the tanker OF ratio is approximately 4 to achieve aggregation OF ratio of 6. As the launch rate increases, the curve shifts towards the right and higher tanker OF ratio can be used to achieve the desired aggregation OF ratio. Table 27 shows the required tanker OF ratio for each of the scenarios to ensure the propellant aggregation OF ratio is 6. The tanker OF ratio represents another design variable that must be considered when evaluating the propellant depot based exploration architecture.

Table 28 shows the total propellant aggregation rates for each of the scenarios using the optimized tanker OF ratio shown in Table 27. For each of the scenarios, the resulting propellant aggregation OF ratio matches the architecture required OF ratio

Table 28: Total Propellant Aggregation Rates With Optimized Tanker Oxidizer-to-Fuel Ratio Ensuring Final Oxidizer-to-Fuel Ratio of 6

		Passive	ZBO	
Atlas	2/year	43	90	kg/day
	5/year	169	226	kg/day
	8/year	299	361	kg/day
Delta	2/year	63	112	kg/day
	5/year	219	279	kg/day
	8/year	380	445	kg/day
Falcon	2/year	181	241	kg/day
	8/year	870	937	kg/day
	12/year	1,320	1,390	kg/day
SLS	0.5/year	32	80	kg/day
	1/year	106	160	kg/day
	2/year	264	327	kg/day

of 6 for optimized performance of a LO2/LH2 in-space engine. As the table shows, the total propellant aggregation rates are still more sensitive to the launch rate of the launch vehicle compared to the cryogenic fluid management strategy. For example, the 70 mT SLS can increase the propellant aggregation rate from 32 kg/day to 264 kg/day by increasing the launch rate from 0.5 per year to 2 per year, but going from passive to ZBO only increases the propellant aggregation rate by 40-60 kg/day. This shows the importance of the vehicle launch rate in determining the overall propellant aggregation rates.

For a 225 mT propellant depot as required by the reference architecture to an asteroid, the number of launches required is shown in Table 29. The numbers shown in this table assumes a tanker propellant mass fraction of 0.87 and the tanker OF ratio that is optimized to provide a resulting propellant aggregation OF ratio of 6. This particular design space exploration reveals that the number of required launches for the propellant aggregation is highly sensitive to the choice of CFM strategies at low launch rates. As discussed with Table 28, by increasing the launch rate, the sensitivity to the CFM strategies can be reduced dramatically. Thus from a

Table 29: Number of Launches Required to Fill 225 mT Propellant Depot with Tanker Propellant Mass Fraction of 0.87 with Oxidizer-to-Fuel Ratio Given by Table 29

		Passive	ZBO
Atlas	2/year	29	14
	5/year	19	14
	8/year	17	14
Delta	2/year	20	11
	5/year	14	11
	8/year	13	11
Falcon	2/year	7	6
	8/year	6	6
	12/year	6	6
SLS	0.5/year	10	4
	1/year	6	4
	2/year	5	4

technology development standpoint, the option is either to invest in long term CFM technologies or to invest in the production and efficiency in the launch vehicle market. By doing so, the required number of launches can be reduced by more than 50%, thereby increasing the overall mission feasibility.

5.5 Propellant Aggregation Launch Success Probability

As the previous sections discussed, the total number of launches required to satisfy the architecture requirement is dependent on a variety of design variables. The decisions of launch vehicle selection, CFM strategy, and the maximum flight rate possible all directly impact the overall launch success probability. Computing the total launch success probability requires certain assumptions about the launch of each of the vehicles. The most straight forward method is to consider each of the launches as independent events. Doing so allows for the computation of the overall launch success as simply the probability of the individual launch, which can be obtained from Bayesian analysis, raised to the power of number of launches required.

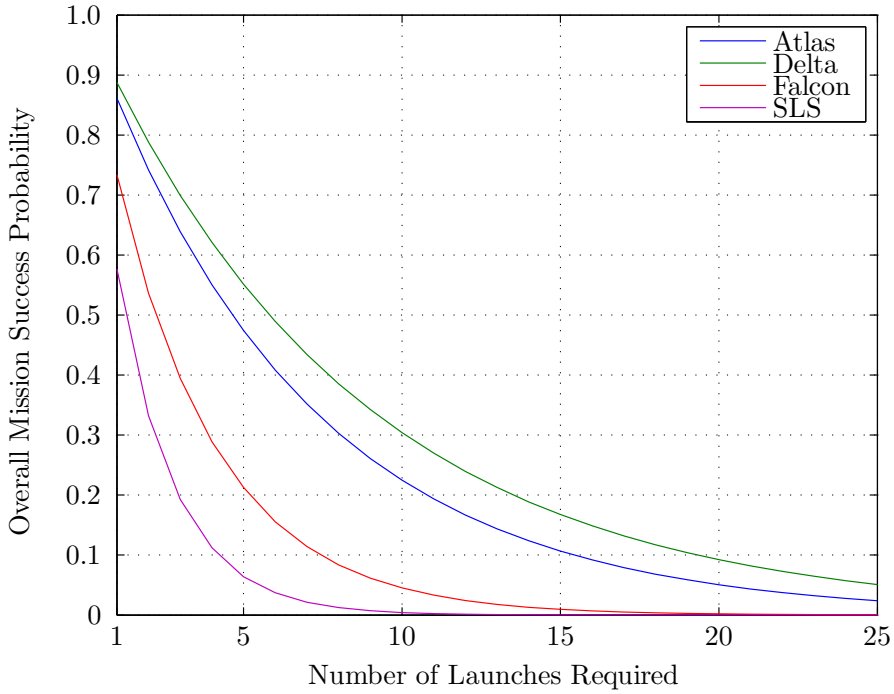

Figure 59: Mean of the Launch Success Probability as Function of Number of Launches Required with no Redundancy and Bayesian Single Launch Success Probability

As the number of launches increases, the overall launch success probability decreases at an exponential rate. This trend highlights the primary challenge to the propellant depot based exploration architecture, as discussed in Chapter 2. Typical exploration architectures require between one to four launches of heavy-lift class vehicles, resulting in an overall launch success probability between 0.9 and 0.65 (assuming an independent launch probability of 0.9). For a propellant depot based architecture, the number of launches required varies between 4 and 29 (as shown in Table 29), resulting in an overall mission success probability less than 0.65. However, the launch reliability of each of the chosen launch vehicles must be taken into consideration when evaluating the overall mission success probability.

Using Bayesian analysis, the current best estimate for the reliability of each of the four launch vehicles was presented in Section 5.3 and summarized in Table 23. Figure

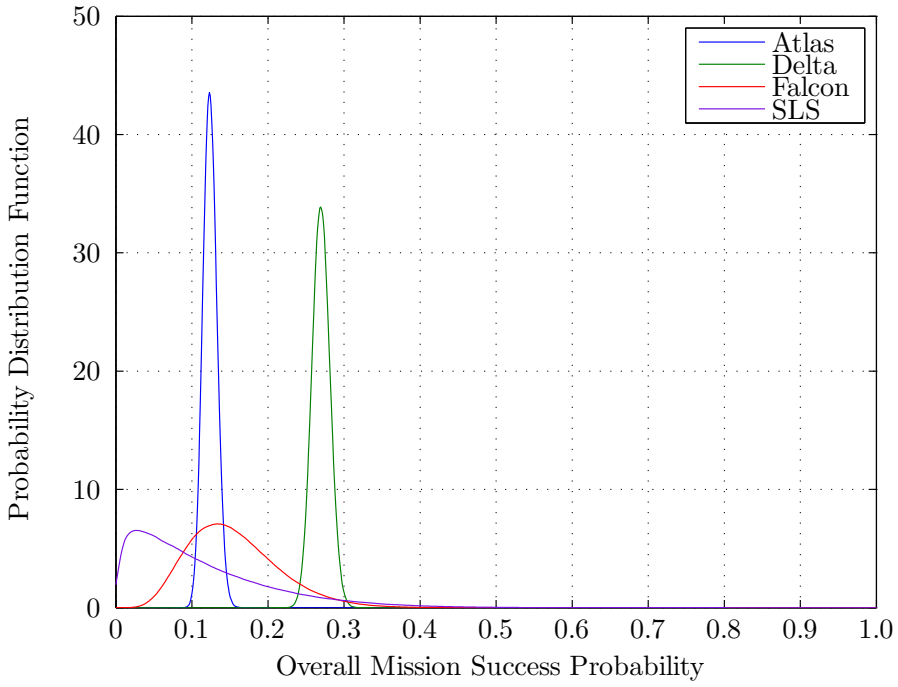

Figure 60: Probability Distribution of Propellant Aggregation Mission Success Probability in the Zero-Boil-Off Scenario with Bayesian Launch Reliability

59 shows the mean of propellant aggregation launch success probability as a function of number of launches required and the individual launch success probability given by the Bayesian analysis. Each individual launch is assigned a probability of success by sampling from the Bayesian posterior distribution and the overall mission success probability is computed with a 100,000 case Monte Carlo simulation. The mean of the overall mission success probability drops dramatically as the number of launches increases. Because the Falcon and the SLS are both relatively new launch vehicles with little launch evidence to support its reliability, these two vehicles perform rather poorly as compared to the Atlas and Delta.

Using the minimum required launch scenario from the architecture requirement analysis (assuming ZBO), the distribution of the propellant aggregation mission success probability by using each of the four launch vehicles are shown in Figure 60

Table 30: Summary of Propellant Aggregation Mission Success Probability in the Zero-Boil-Off Scenario without Launch Redundancy

Launch Vehicle	Required Flights	Mean of Mission Success Probability	Standard Deviation of Mission Success Probability
Atlas V	14	0.1238	0.0092
Delta IV	11	0.2697	0.0117
Falcon Heavy	6	0.1557	0.0591
SLS	4	0.1109	0.0897

and summarized in Table 30. It is interesting to note that despite having the lowest number of launches required, the SLS vehicle has the lowest mean probability of propellant fill-up mission success at 11%. Overall, all four vehicles provide extremely poor overall mission success probability, with very little chance of achieving success probability of over 30%. The extensive launch record of the Delta and the Atlas vehicles only serve to provide a narrower probability distribution for the overall mission success, it does not improve the probability of having numerous consecutive successful launches when each launch is treated as an independent event.

Of course, in reality the use the propellant depot based exploration architecture relaxes the constraint of requiring multiple consecutive launches to be successful by allowing the use of redundant launch vehicles. Because the propellant aggregation phase of the architecture is decoupled from the mission phase, there is no reason to require 14 successful launches out of 14 possible launches in the case of the Atlas V. The actual probability of propellant aggregation mission success should be close to 100%. It all depends on how many launch vehicles it would require to achieve the desired probability.

Typically, if the probability of each individual event is the same, the probability of having k successes in n trials can be computed easily using the formula for Bernoulli trial,

$$P(K=k) = \frac{n!}{k! * (n-k)!} * p^k * (1-p)^{n-k} \tag{34}$$

where p represents the probability of success in each of the trials. However, with the Bayesian launch analysis, each individual launch success probability is sampled from the posterior distribution given by the current launch vehicle's launch record. To compute the probability of the overall mission success where the individual event is not identically distributed, the Poisson-Binomial distribution must be used. The probability mass function for the Poisson-Binomial distribution is computed recursively by Equation 35. [144, 151, 152]

$$P(K=k) = \begin{cases} \prod_{i=1}^{n}(1-p_i) & k=0 \\ \frac{1}{k}\sum_{i=1}^{k}(-1)^{i-1}P(K=k-i)\sum_{j=1}^{n}\left(\frac{p_j}{1-p_j}\right)^i & k>0 \end{cases} \tag{35}$$

The expression computes the probability of having exactly k successes in n trials given that each of the individual events have a probability of success given by p_1, p_2, ..., p_n. In the Bernoulli trial scenario, each of these individual probabilities would be the identical. The probability of having at least k success out of n trials is computed by

$$P(K>k) = 1 - \sum_{i=0}^{k-1} P(K=i) \tag{36}$$

Taking the same launch requirement from Figure 60, the distribution of the overall mission success probability using the four launch vehicles with potential launch redundancy is shown in Figure 61. Each distribution represents a 100,000 cases Monte Carlo simulation of the aggregation mission for each of the launch vehicles and redundancy case. For each Monte Carlo case, the probability of each required launch vehicle's success is sampled from the Bayesian posterior distribution. This probability is used by Equation 35 to compute the Poisson-Binomial probability mass function, then depending on how many successful launches is required, the appropriate probability is summed to compute the overall mission success probability. The zero redundancy

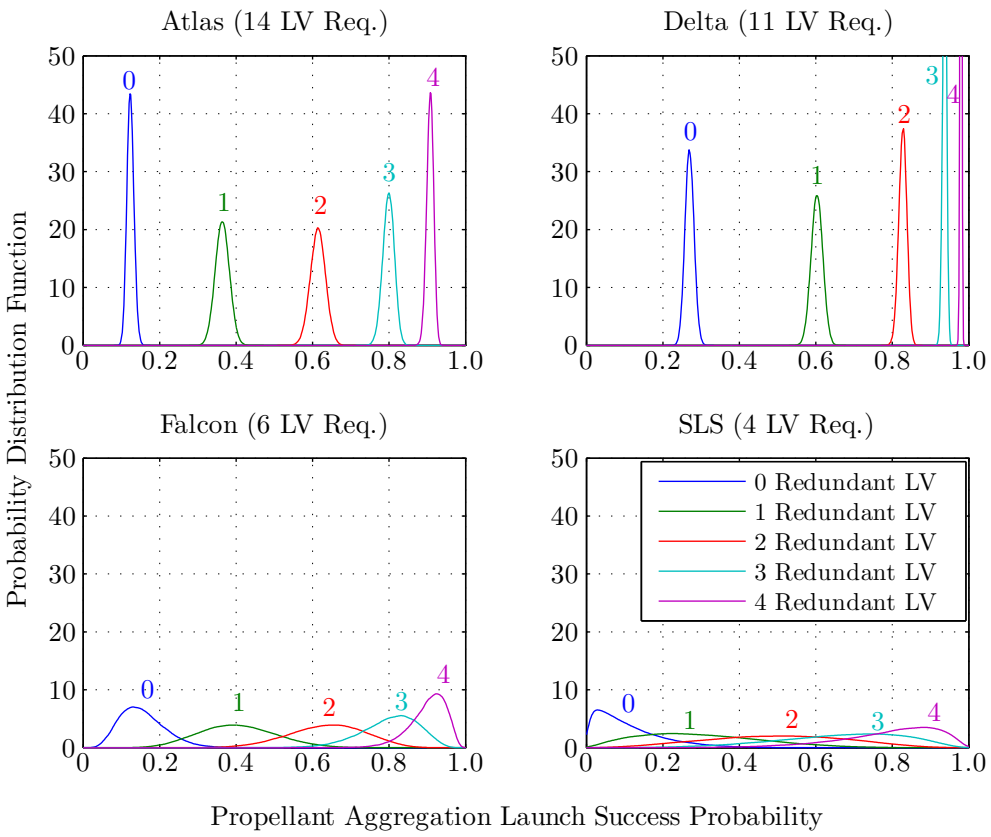

Figure 61: Probability Distribution of Propellant Aggregation Mission Success Probability in the Zero-Boil-Off Scenario with Bayesian Launch Reliability and Varying Number of Redundant Launch Vehicles Available

case for each of the launch vehicle is identical to the distribution shown in Figure 60, which is computed using the simple Bernoulli trials method, thereby validating the Poisson-Binomial method.

The distributions for all four launch vehicles clearly show a significant improvement in the overall mission success probability when redundancy is introduced. The peaks of each of distribution for all four launch vehicles shift to the right as more redundant launch vehicles are made available. The mean and standard deviation for the scenario depicted in Figure 61 is summarized in Table 31. For the Atlas, Delta, and Falcon launch vehicles, having at least four redundant launch vehicles available increases the mean of the propellant aggregation launch success probability to above 85%. The SLS is able to achieve a mean mission success probability of just over 80%

with four redundant vehicles. For the Atlas and Delta launch vehicles, the individual launch success distribution has very small standard deviation due to their extensive launch records. This results in the overall launch success with very small standard deviation as well, providing fairly high confidence in the estimation of mission success probability. On the other hand, because of their lack of launch records, the large spread of the individual launch vehicle reliability results in high uncertainty when predicting the mission success probability for the Falcon and the SLS.

Table 31: Summary of Propellant Aggregation Launch Success Probability in the Zero-Boil-Off Scenario with Bayesian Launch Reliability

Launch Vehicle	Required Flights	Redundant Flights	Mean of Mission Success Probability	Standard Deviation of Mission Success Probability
Atlas	14	0	0.0915	0.0078
		1	0.2926	0.0177
		2	0.5294	0.0216
		3	0.7280	0.0187
		4	0.8602	0.0128
Delta	11	0	0.2578	0.0116
		1	0.5867	0.0155
		2	0.8154	0.0112
		3	0.9303	0.0059
		4	0.9769	0.0025
Falcon	6	0	0.1450	0.0488
		1	0.3840	0.0852
		2	0.6146	0.0880
		3	0.7838	0.0688
		4	0.8890	0.0452
SLS	4	0	0.1172	0.0944
		1	0.3121	0.1618
		2	0.5152	0.1808
		3	0.6815	0.1627
		4	0.8031	0.1294

Expanding the design space, Figure 62 shows the mean and standard deviation of the propellant aggregation success probability given all three cryogenic fluid management scenarios, using the launch requirement from each vehicle's nominal launch rate. The figure shows the mean of the aggregation mission success probability as a function of number of redundant launch vehicles available using the solid line, and with

the dashed line representing the plus or minus one standard deviation from the mean. For both scenarios, the overall mission success probability increases as the number of redundant vehicle increases. The Atlas and Delta vehicles have very tight standard deviation bounds due to the tight bound from the individual posterior distribution.

For the Atlas, the choice of cryogenic fluid management strategy does have a large impact on the number of launches required, and thus the overall mission success changes by roughly 10% depending on the choice. The effect diminishes, however, when the number of redundant launch vehicles available is greater than six. Using the Delta launch vehicle creates an interesting scenario in that the choice of cryogenic fluid management strategy has fairly minimal impact on the mission success probability. The difference between the passive and the ZBO scenario is only three additional launches of the Delta, and Delta has the best individual launch success record which yields fairly minimal change to the overall mission success probability. Having at least four redundant Delta launches results in over 95% probability of launch success regardless of the other design options.

Using the Falcon to fill up the propellant depot provides similar launch success probability to the Atlas vehicle, even though the number of launches required is less than half that of the Atlas. The relatively new launch vehicle suffers from low confidence in the individual launch success estimate, which can be seen resulting in having fairly large standard deviation bounds for the overall launch success probability. The uncertainty of the launch success probability is reduced with increasing redundant launches available, as demonstrated by the tightening of the distribution. Similar to the Atlas, six redundant Falcon launches are needed to provide both high probability of launch success and low uncertainty in the estimate.

The SLS launch vehicle provides the worst performance for overall launch success probability. Despite having the most payload capability, the high uncertainty associated with the estimation of the SLS's reliability results in extremely high levels of

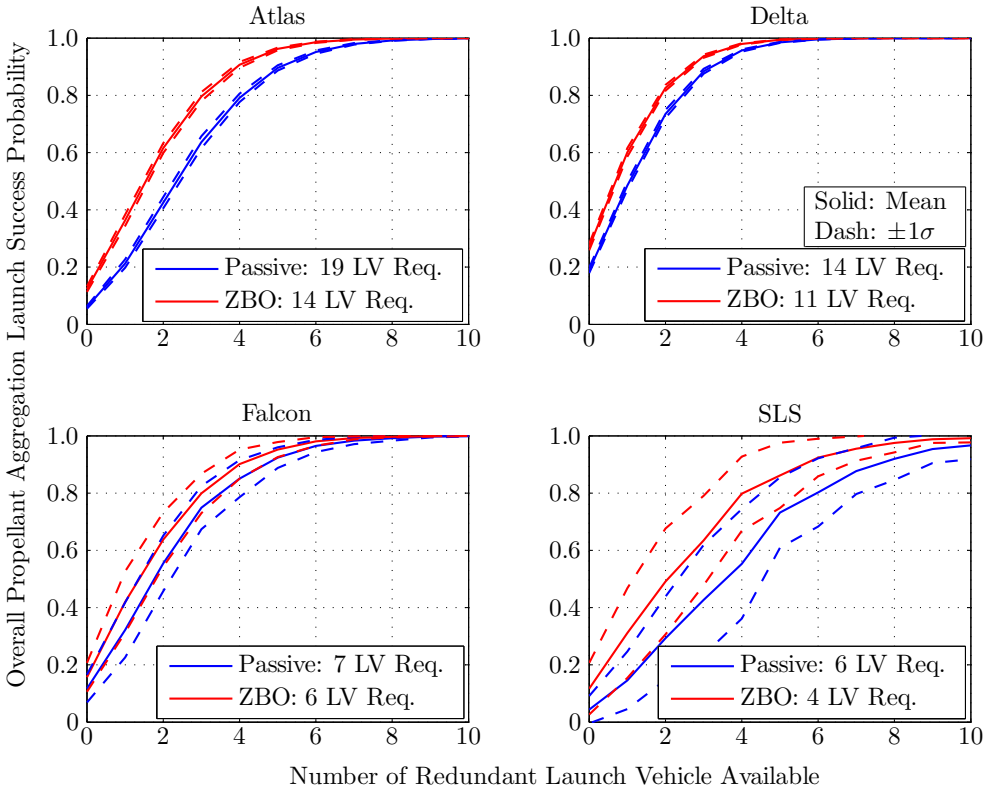

Figure 62: Probability Distribution of Propellant Aggregation Launch Success Probability in the Zero-Boil-Off Scenario with Bayesian Launch Reliability and Varying Number of Redundant Launch Vehicles Available

uncertainty in the estimation of the overall launch success probability even with large numbers of redundant vehicles. The number of required SLS launches is significantly less than the other launch options, but the launch success probability lags behind all the other options. The large spread of the distribution also shows there is large uncertainty in the estimation of the overall launch success probability, and unlike the other options, the distribution does not appear to tighten as number of redundant launches increases.

For the architecture to be completely successful, there are additional mission events that are required. Each of the propellant launches would require rendezvous and docking of the tanker vehicle to the propellant depot. Additionally, after the completion of the propellant aggregation missions, the mission hardware and crew must

be launched into orbit successfully. These elements all need to rendezvous in orbit before the mission can commence. The only difference between this chain of events and the baseline exploration architecture is the additional requirement of tanker/depot rendezvous. The mission element rendezvous and docking is near identical between the two architectures. On orbit rendezvous and docking is considered to be an extremely mature technology [153], and a catastrophic failure during this phase of the mission is unlikely due to numerous fail-safe protocols. The reliability of rendezvous and docking maneuver is beyond the scope of this thesis; however, the increase in number of rendezvous maneuver required will not decrease the overall mission reliability because of the availability of redundancy in the architecture. Similar to the launch reliability, a failure in rendezvous of the tanker and propellant depot can be mitigated with additional refueling flights.

5.6 Summary of Feasibility Assessment

The launch vehicle and mission reliability feasibility was examined in this chapter. The historical launch records for the family of launch vehicles were used to construct prior distributions of the chosen launch vehicles, and the Bayesian posterior distribution for each launch vehicle's reliability was computed using the actual launch records. For newly developed launch vehicles, the lack of launch record was mitigated by using the global launch records to estimate the overall reliability. The thermal system analysis from Chapter 4 was combined with launch schedule analysis to determine the launch requirements to meet the propellant demand of the baseline exploration architecture. The generated posterior distribution for the launch vehicle reliability was used in Monte Carlo simulation to estimate the overall launch success probability of requiring multiple launches of the same vehicle. Poisson-Bernoulli distribution was used to compute the overall launch success probability when redundant vehicles are made available.

The analysis in this chapter demonstrates the feasibility challenge to the propellant depot based architecture isn't without basis. Requiring larger number of launches to complete exploration architectures does reduce the overall launch success probability, regardless of other design options. However, the increase number of launches in propellant depot based architecture is mainly due to the need for the aggregation of propellant into orbit. These propellant aggregation launches can be decoupled from the mission critical path, which enables redundant or backup launches to be utilized. By enabling redundancy to the launch architecture, the mission reliability risk and the overall uncertainty of the launch success can be dramatically reduced. The use of currently available commercial launch vehicles, with extensive launch records to support their reliability, can greatly reduce the uncertainty of launch success probability.

Additionally, the ability to utilize multiple launch providers to supply the propellant launch may add another layer of redundancy to the overall architecture. If one of the providers suffers a failure, the propellant aggregation mission does not have to stop for the failure investigation that may take a year or two, using the Space Shuttle as an example. The mission can continue with the other launch provider with minor change to the overall mission schedule. Of course, the use of redundant launch vehicles to improve probability of overall launch success isn't without cost. The economics of the architecture is discussed in the next chapter. Additional considerations to the overall launch success probability, such as hardware launches and mix fleet launch vehicle strategy, will be discussed in the Chapter 7.

CHAPTER VI

ARCHITECTURE COST ANALYSIS AND ECONOMIC FEASIBILITY ASSESSMENT

The final area of challenge to propellant depot based exploration architectures addressed in this thesis is the economics of the architecture. The utilization of a propellant depot results in a significant increase in the number of launch vehicles required as discussed in the previous chapter, and this increase may have a dramatic impact on the overall cost of the exploration architecture. This chapter provides an analysis of the cost of developing and operating the propellant depot based architecture by examining the additional cost of the launch vehicles and the development cost of the unique hardware. The cost of the depot based architecture will be compared to the cost of the current NASA architecture, and analysis of NASA's current and projected budget will provide an overall economic constraint for the feasibility assessment metric.

6.1 Space Exploration Budget Constraints

Since the close of the Apollo program, numerous missions, architectures, and concepts of operation have been proposed for expanding the human presence beyond low-Earth orbit. However, none have successfully achieved the goal of expanding human presence beyond LEO. In the past decade, it became evident (especially following the loss of the Space Shuttle *Columbia*) that a new transportation system would be needed even to reach the ISS. During this period, NASA has developed two approaches to sustaining human spaceflight. The first of these, the *Vision for Space Exploration* [17](VSE), led to the Constellation architecture that reached its peak in launching the Ares I-X

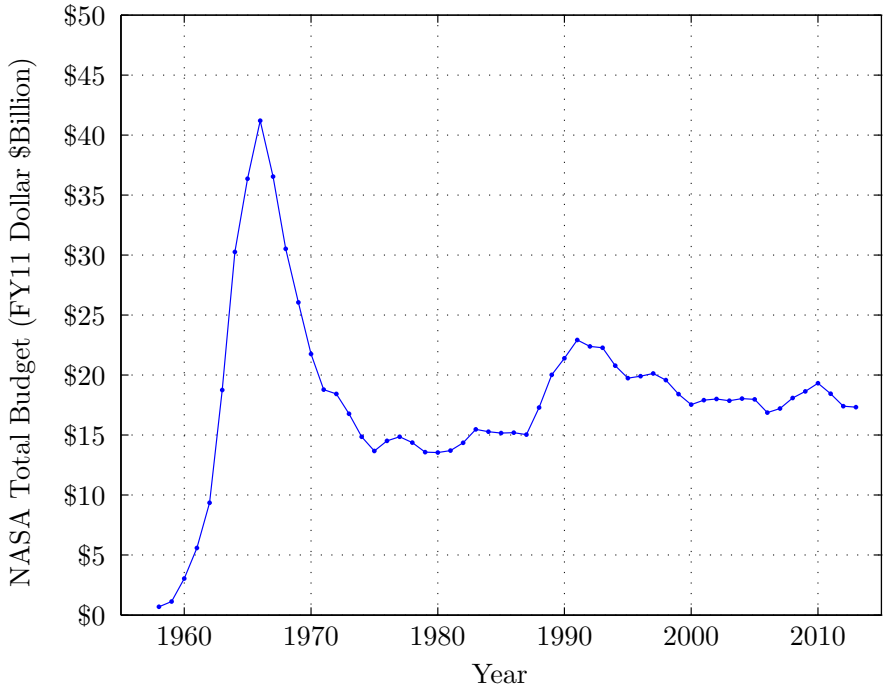

Figure 63: NASA's Budget in FY2011 Dollar from 1958 to 2013 [9]

demonstrator. The second, the 2010 *National Space Policy of the United States of America* [3], has so far yielded only a single flight test and no active mission hardware.

The drive of the the Cold War arms race in the 1960's pushed the Apollo program to success. Figure 63 plots NASA's total budget in constant FY2011 dollars. NASA's budget peaks in 1966 at over $40 billion just as the Apollo program was headed into the operations stage. After the cancellation of the Apollo program, NASA expanded its mission and vision to include more fundamental research and development in addition to human and robotic exploration. NASA's expansion came at a time in which the budget restriction became tighter. In the 1970's the budget decreased to $15 billion as NASA shifted its focus from beyond LEO exploration to the Space Shuttle program. In the late 1980's, the budget was expanded to accommodate the International Space Station program, but the budget has since fallen below $20 billion.

The 2004 Vision for Space Exploration was supposed to renew the nation's effort for beyond LEO exploration. VSE called for the retirement of the Space Shuttle

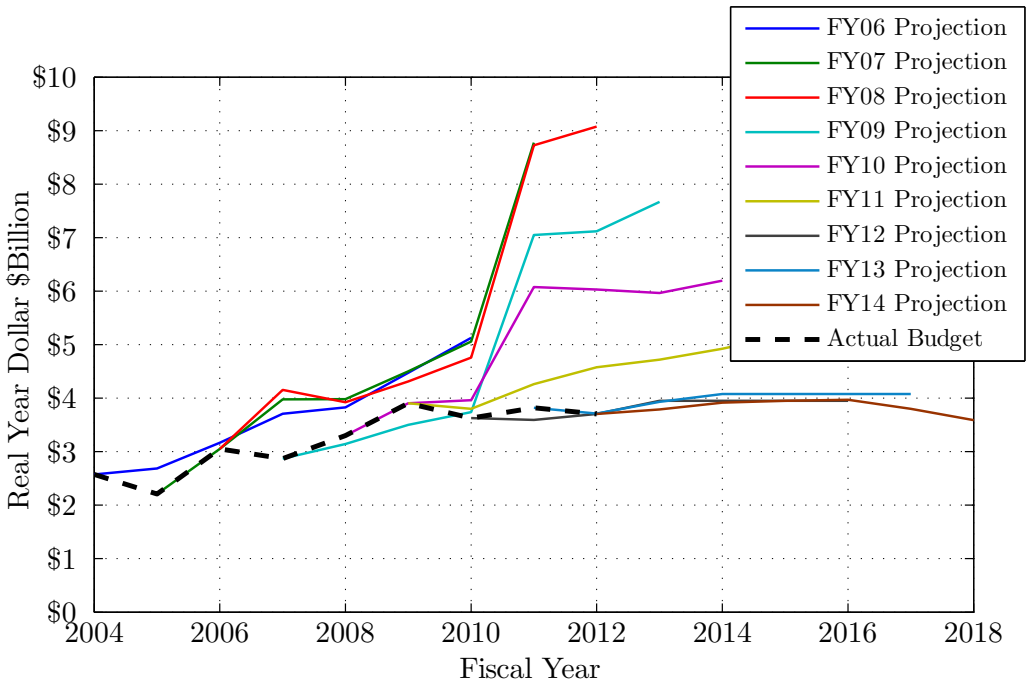

Figure 64: NASA's Exploration System Budget in Real Year Dollar from 2004 to 2012, and the Budget Projection from Each of the Fiscal Year Budget Request [7, 154]

Program to free up a portion of the NASA budget for exploration systems research and development. The FY2004 budget was the first time the Exploration System became its own budget line item. However, the retirement of the Space Shuttle was delayed multiple times, causing the NASA funding for Exploration Systems to be well under the projection of the program managers.

Figure 64 illustrates the gap between NASAs projected and actual Exploration System budget in the past decade. Each line represents the budget projection for the particular fiscal year going forward, while the dashed line shows the actual funding each year. From FY2006 until FY2013, each projected budget exceeded the actual budget often by several billion dollars. Only the FY2012, FY2013, and FY2014 projections do not anticipate significant increases in NASA funding; the others forecast an eventual yearly exploration budget of $9 billion. The failure of the Constellation program can be directly attributed to this discrepancy, as the funding for exploration

systems never reached the levels projected by NASA. The program was built on the unrealistic assumption of the budget profile, which led to significant delays development activities and ultimately to the cancellation of the entire program.

The Augustine Commission [1] provided NASA with recommendations to achieve beyond LEO exploration in the post-Constellation era. The Commission charged NASA to have realistic goals and expectations for the budget and to plan exploration activities that can be supported by realistic budget assumptions. NASA has done away with assuming significant increases in budget appropriations, especially in this new fiscally conservative time and has adapted fairly flat budget projections starting with the FY2012 budget proposal. Since becoming its own separate budget line item, the Exploration System budget peaked in 2011 at $4 billion in then-year dollars and has remain below $4 billion ever since. To evaluate a space exploration system architecture for economic feasibility, a $4 billion then-year dollar budget level is used as a constraint.

6.2 Baseline Architecture Exploration Cost

The current NASA Exploration Systems plan requires NASA to develop and build a heavy lift launch system as well as all of the unique in-space elements for all future missions. Current estimates from the Human Exploration Framework Team estimated the cost of development and first flight of all of the hardware at approximately $144 billion (FY11) over the next 20 years [4]. Table 1 (in Chapter 1) shows the breakdown of the HEFT cost by elements, and Figure 65 shows the cost breakdown by element by year. The most costly components of the current exploration architecture are the Heavy Lift Launch System (37%) and the ground operation and infrastructure that support it (12%). The crew transfer vehicle and the solar electric propulsion system are the only other systems that contribute more than 10% of the total cost of the exploration architecture. The architecture has an average annual cost of $6.85 billion

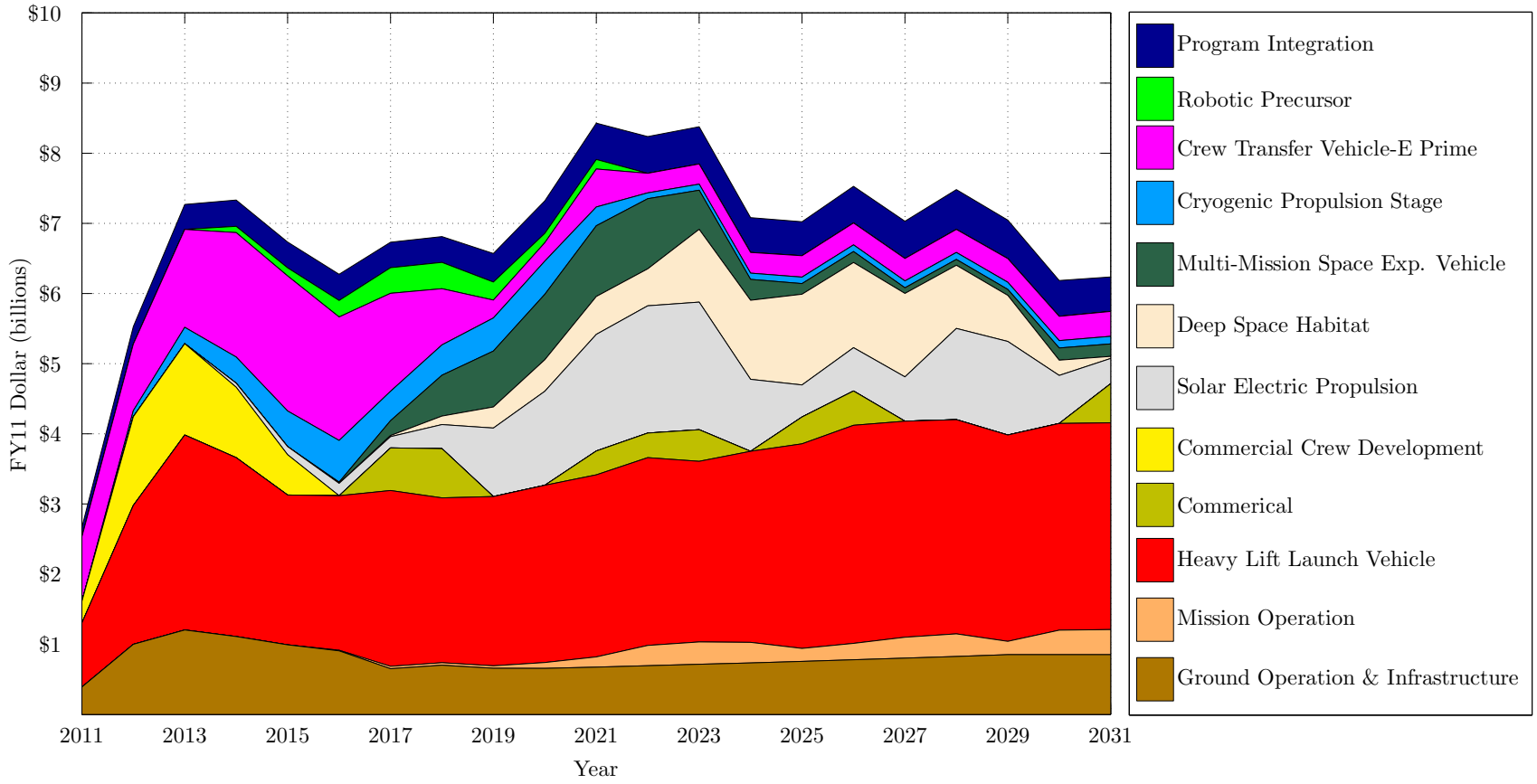

Figure 65: Human Exploration Framework Team Cost Estimate Breakdown for 2031 Manned Mission to Near Earth Asteroid [4]

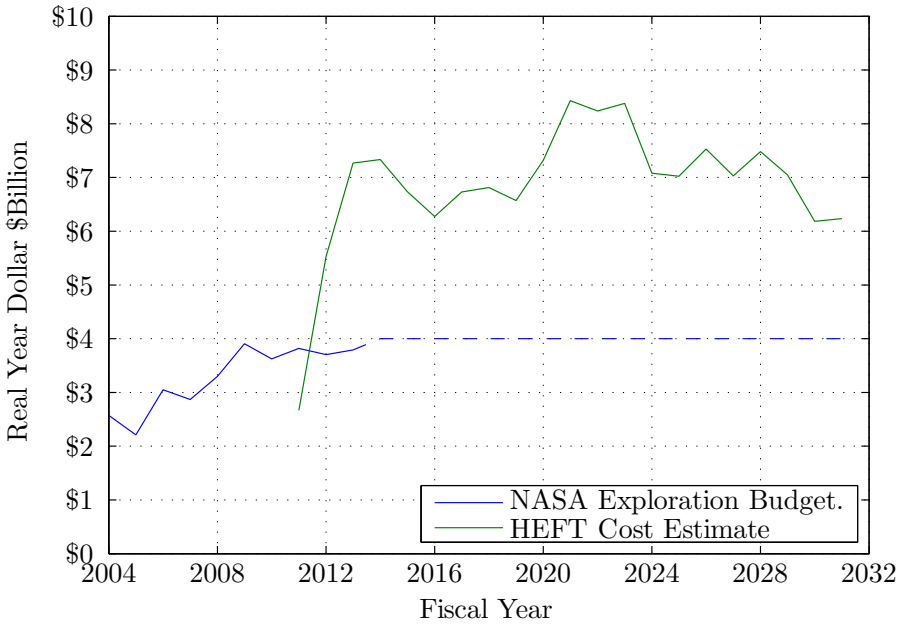

Figure 66: Human Exploration Framework Team Yearly Cost Estimate for Near Earth Asteroid Mission Compared to Actual NASA Exploration System Budget and Flat $4 billion Outyear Projection [4, 154]

(FY11 dollars), with a peak of $8.42 billion (FY11 dollars) in 2021.

Figure 66 shows the yearly cost estimate of the Human Exploration Framework team's Near Earth Asteroid mission compared to the actual exploration system budget through 2013. Plotted in dashed line is a flat $4 billion per year budget projection from 2013 to 2031. The large discrepancy between the program's expected level of expenditure and actual funding received that led to the cancellation of the Constellation program is still present. The out year projected budget for exploration systems is $4 billion per year, yet the HEFT program cost is consistently $2-4 billion more than the projected budget. The discrepancy observed in the Constellation program was identified by the Augustine commission as one of the primary issues that must be addressed in future NASA plans. However, it would appear that the recommendation did not impact subsequent policy and the current program continues to operate with an unrealistic cost profile.

In order for the current exploration program to be successful, NASA's Exploration Systems budget would have to be twice the currently projected level. The budget requirement is eerily similar to the budget requirement shown in Figure 64. Alternatively, the program can be stretched out over an additional 20 years to allow for all of the systems to be developed under current budget projection level, pushing the manned mission to Near Earth Asteroid to 2050. Both of these scenarios seem very unlikely to occur. The discrepancy between what is required and what is available is simply too large to overcome without dramatic shift in national space policy, and there is little evidence that such shift is imminent or likely.

6.3 Alternate Architecture Cost Analysis

To provide a fair comparison between the propellant depot based architecture and the NASA HEFT baseline architecture, the majority of the baseline architecture elements were utilized in the depot architecture. The primary cost difference between the baseline architecture and the depot based architecture are the launch vehicles and the development of the propellant tanker and the propellant depot.

6.3.1 Launch Vehicle Cost

A large portion of the cost of any exploration architecture is the cost of the launch vehicle. The HEFT architecture allocates nearly 38% of the total program cost to the launch vehicle. One of the primary purposes of a propellant depot based exploration architecture is to eliminate the development cost of the heavy-lift launch system and replace it with alternatives. Chapter 5 provides the analysis of the number of required launch vehicles to complete the propellant aggregation mission. The cost of these launch vehicles must be accounted for in the evaluation of the overall architecture feasibility.

Table 32 shows a summary of the cost of the price of the currently available launch vehicles in the United States. The primary difference between the commercial launch

Table 32: U.S. Launch Vehicle Launch Price Summary [75–77],HEFT

	Atlas V 551	Delta IV Heavy	Falcon Heavy*	SLS†
Price (FY11)	$290M	$300M	$81-127M	$1,600M‡
$/kg	$15.3k	$12.7k	$1.6k-$2.5k	$22.9k

"price" and the launch "cost" quoted in the HEFT cost estimate is the elimination of the development cost of the launch vehicle. When an architecture utilizes a commercial launch vehicle, the architecture pays a contracted price to deliver payload into orbit rather than spending billions of dollars to develop the necessary hardware. The total development cost ($17.4 billion) for the HEFT heavy-lift launch vehicle can buy over 1,000 Falcon 9, 430 Falcon Heavy, 183 Delta IV, or 189 Atlas V launch vehicles. The HEFT heavy lift launch vehicle is almost identical to the current Space Launch System, so the present analysis assumes the HEFT cost as the SLS cost because no data exist for the SLS development.

The assumed launch cost of the SLS shown in Table 32 is quoted in the Human Exploration Framework Team's phase I close-out report [4] as the single unit cost of the SLS hardware. The development cost of the vehicle along with the yearly ground operation and support cost will need to be amortized over the total number of launches in its lifetime. The HEFT cost estimate for the asteroid mission over 20 years shows the total development cost of the SLS to be $54 billion and ground operation and infrastructure cost of $17 billion. The HEFT development cycle requires nine total SLS launches, with six demonstration/test flights and three NEO mission operation flights, as shown in Figure 3. The total amortized cost of these nine SLS flights is $7.9 billion per flight, which would make the SLS the most expensive launch vehicle in the history of manned spaceflight. In comparison, the Space Shuttle was $1.6 billion per flight and the Saturn V was $4.7 billion per flight.

*Currently in Development, First Operational Flight Scheduled for 2015 [78]
†Currently in Development, First Test Flight Scheduled for 2017 [4]
‡Unit Cost Only, not including development, ground operation and support cost [4]

For the commercial vehicles, both the Atlas V and the Delta IV are currently operational. As with any commercial products, there is potential for price to fluctuate. However, the launch vehicle market is in relatively low demand, which keeps the price of the launch vehicles relatively high due to the high fix infrastructure cost. By increasing the demand for launch vehicles, the fix infrastructure cost can be amortized over more launches which may drive the price of the individual launch vehicles down [155]. Additionally, if an architecture has the demand for a large number of launch vehicles, it can be reasoned that a bulk order of a single family of launch vehicles can further drive the price of the individual launch vehicles down. The bulk order was used by the United States Air Force in 2013 as a method to reduce the overall cost of programs that requires a large number of launches. The cost savings for launch vehicle bulk buy is proprietary because it typically is based on individual negotiation with the launch provider. The analysis in this dissertation will utilize the nominal cost for the launch vehicle for all cost scenarios with the understanding that potential reduction to the overall cost is still possible.

The Falcon Heavy vehicle is currently in development by SpaceX. Currently, the vehicle is expected to have its first operation flight in 2015 [78]. Typically in a government program, utilizing a new launch system will require the addition of development cost to the program (as in the case of the Space Launch System). However, because the development of the vehicle is conducted by a private company, the development cost to the exploration program is minimal or none, depending on the contractual agreement between the government and the commercial company.

6.3.2 Unique Element Costs

There are only two unique elements in the alternate architecture that require a separate cost estimation: the dual use propellant depot/cryogenic propulsion stage and the propellant tanker for the propellant delivery. The expandable propellant tanker

and their propellant transfer subsystems are referred to as the tankers in the following text. To estimate the cost of the unique elements in the alternate architecture, the modeling method provided by the Handbook of Cost Engineering for Space Transportation System, or Transcost, was utilized [110]. Transcost is described as a statistical analytical model for cost estimation of space system. It utilizes historical data to generate cost estimating relationships (CER) similar to the mass estimating relationship described in Chapters 4. This costing method provides a top down approach to cost estimation, relying on the overall system level inert mass as the independent variable for cost estimation rather than detailed analysis of subsystem and component costs. This method of cost estimation is particularly useful in conceptual level of design as many of the subsystem level trade studies are incomplete. The uncertainty in the cost estimation is addressed to assess the cost risk.

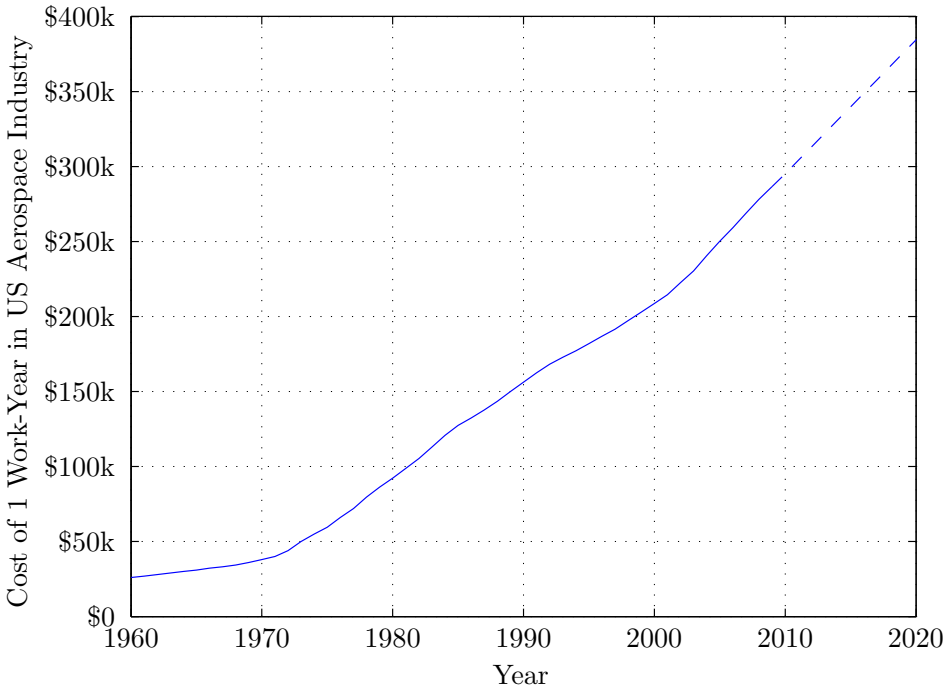

Figure 67: Cost History of 1 Work-Year in the United States Aerospace Industry [110]

The Transcost data span 40+ years of space system development and operation;

thus the CERs are generated to estimate the number of work years effort required to develop, construct, and maintain these vehicles and subsystems rather than dollars. The cost per work year is generated by estimating the total annual budget of a company or agency and dividing that by the total number of productive full time employees. The work year cost increases from year to year to adjust for inflation and increase in worker salary. The work year cost for the US between 1960 and 2009 given by the Transcost handbook [110] is shown in Figure 67 with the out year projection to 2020 as a linear extrapolation from the most recent decade of data. The linear extrapolation is given by,

$$\text{Work Year Cost} = 8933 * (Year) - 17660886 \tag{37}$$

The linear extrapolation estimates the 2011 work year cost to be $303,377. This work year cost is used to estimate the cost of all of the subsystems to provide a comparison to the FY11 cost estimate provided by the HEFT report [4].

The Transcost handbook [110] provides cost estimating relationships for several major space vehicles categories. Although none of the categories are an exact match to the two unique elements in the alternate architecture, the expendable vehicles most closely resemble the elements of interest. These expendable vehicles systems used in Transcost modeling comprises launch vehicle lower and upper stages as well as orbital transfer vehicles. The Transcost handbook normalized the cost data to constant year work-year, then provided an equation for the CER, as shown in Figure 68. The CER for the development effort for expendable vehicle is given by,

$$H_{EV} = 100 * {M_{ref}}^{0.555} * f_1 * f_2 * f_3 \tag{38}$$

where the reference mass (M_{ref}) for the expendable vehicle development cost is the dry mass of the vehicle less the engine. The factors, f_1 and f_3, are development cost correction factors to account for the degree of difficulty of the project and the

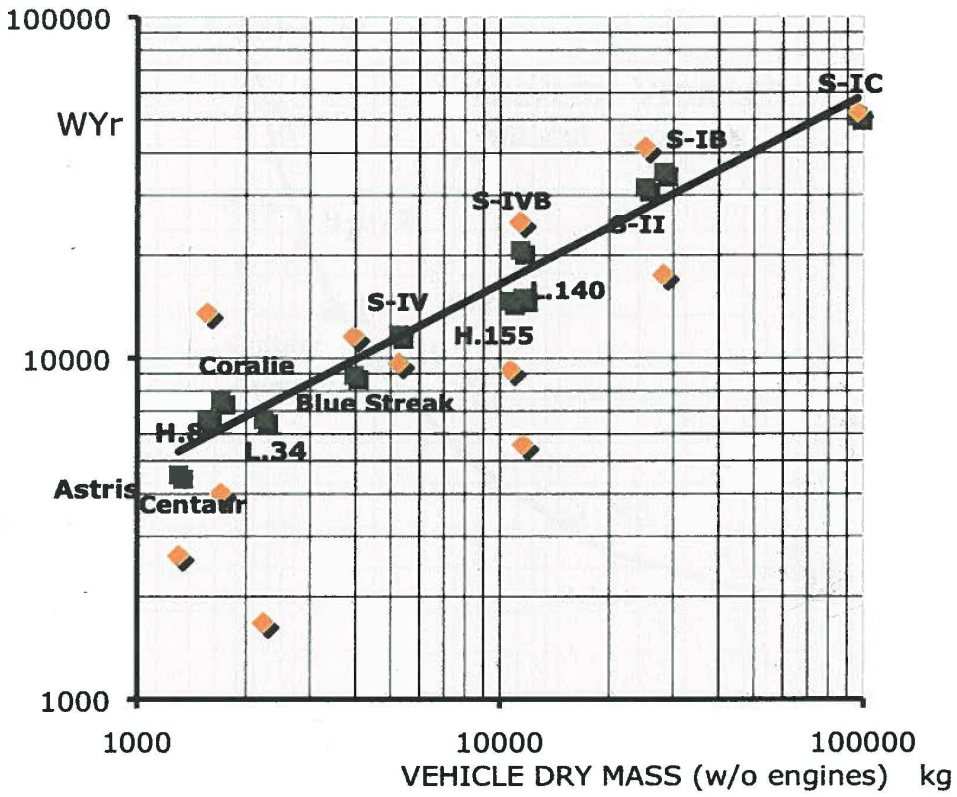

Figure 68: Transcost Cost Estimating Relationship for Expendable Stage Vehicles [110]

experience of the team, respectively, while f_2 is a technical quality factor that is delivered from technical characteristics of the individual project and varies from system to system. These factors are subjective quantities and are summarized in Table 33.

Factors f_1 and f_3 are relatively subjective in nature. At the system level, it can be difficult to quantify the system of interest into one of the categories. Each of the levels also has a range of values for the correction factors, which enhances the variability of the cost estimate. This inherent variability lends itself well to probabilistic modeling. For the propellant depot system, the technical development factors can depend highly on the level of technology it utilizes. These development cost factors can be related to the readiness levels discussed in Chapter 3 (Tables 6 and 7). Technology with low TRL and high RD3 would require high development cost factors.

Table 33: Transcost Development Cost Factors [110]

f_1	First generation system, new concept approach, involving new techniques and new technologies	1.3 - 1.4
	New design with some new technical and/or operational features	1.1 - 1.2
	Standard project, state-of-the-art (similar system already in operation)	0.9 - 1.1
	Design modification to existing systems	0.7 - 0.9
	Minor variation of existing projects	0.4 - 0.6
f_2	Specific for each system (or element type), defined by an inherent technical criterion	
f_3	New team, no relevant direct company experience	1.3 - 1.4
	Partially new project activities for the team	1.1 - 1.2
	Company / industry team with some related experience	1.0
	Team has performed development of similar projects	0.8 - 0.9
	Team has superior experience with this type of projects	0.7 - 0.8

For the three cryogenic fluid management strategies under consideration, the required technology will dictate the value of these development factors. For example, the all passive thermal management scenario utilizes essentially technologies that have a proven track record and is fairly common in the aerospace industry. Thus, the level of technology can be considered as simple modification to existing systems with new applications. The zero-boil-off propellant depot requires technologies that are new to the aerospace system, but it does not reflect a completely new generation system, only an evolutionary advancement in technology.

The technical quality factor (f_2) for the expendable stage vehicle is a function of the vehicle's net mass fraction compared to the reference net mass fraction given by historical data. The net mass fraction is defined as the dry mass plus residuals tank gas mass minus the engine mass as fraction of total useful propellant mass. Given by,

$$k_{NMF} = \frac{M_{dry} - M_{engine}}{M_{prop}} \tag{39}$$

The technical quality factor is computed as,

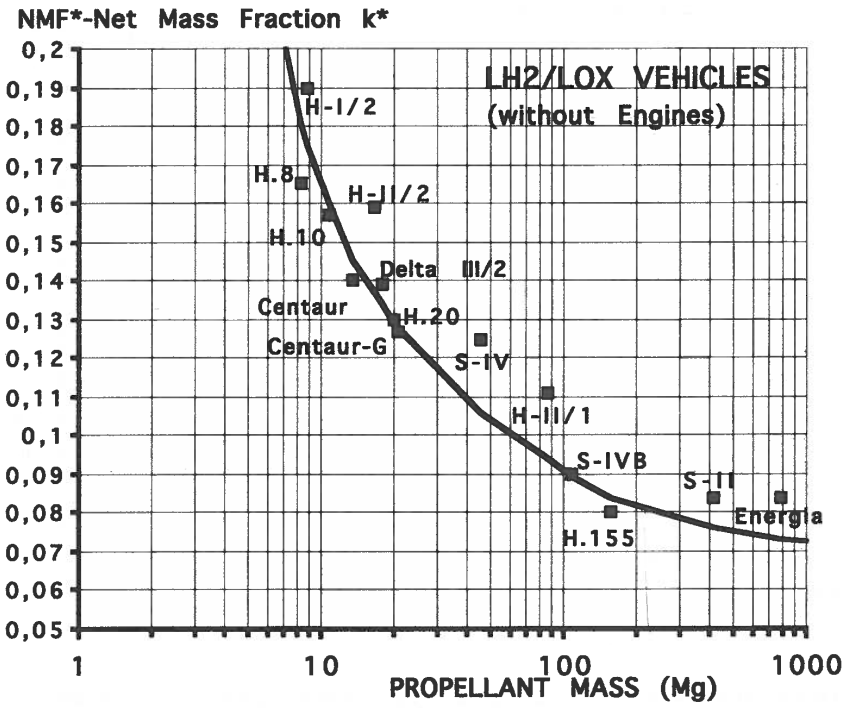

Figure 69: Reference Net Mass Fraction Curve for Technical Quality Factor (f_2) for Hydrogen/Oxygen Expendable Vehicle Development Cost Estimate [110]

$$f_2 \text{ (Expendable Vehicle)} = \frac{k_{NMF_{ref}}}{k_{NMF}} \tag{40}$$

The reference net mass fraction of hydrogen/oxygen expendable vehicle is shown in Figure 69. From the figure, a net mass fraction that is lower than the average mass fraction from historical systems would indicate more advance technologies being utilized, which would require increased cost to compensate for the advance technology. The Transcost handbook does not provide an equation for the reference curve shown in the plot. To compute the reference curve, the plot is reverse engineered to produce data points to generate the curve shown in the figure. The generated curve gives the net mass fraction as function of propellant mass (in kg).

$$k_{NMF_{ref}} = 0.4401 * \left(\frac{M_{prop}}{1000}\right)^{-0.6461} + 0.06745 \tag{41}$$

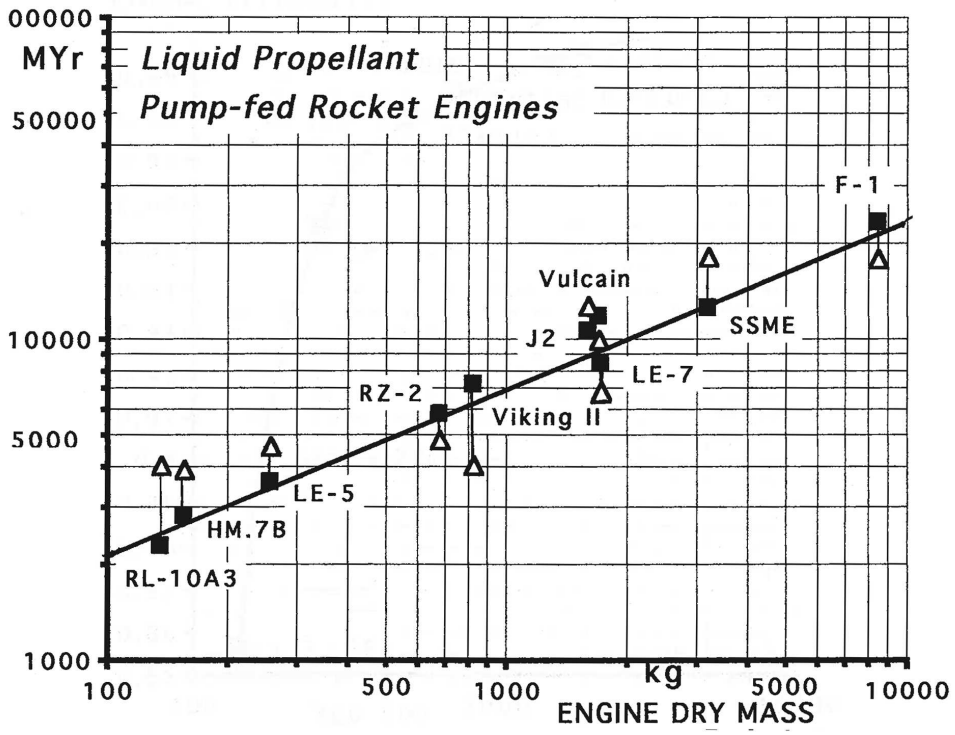

Figure 70: Transcost Cost Estimating Relationship for Liquid Propellant Rocket Engines [110]

In addition, modeling the depot as an expandable vehicle for the purpose of development cost estimation, the development of the propulsion system that is necessary for the propellant settling during tanker transfer is required. The Transcost handbook provides cost estimating relationships for rocket engines with various reference projects. Similar to the CER for the expandable vehicles, the CER for rocket engines is developed for work year effort, and the data used is shown in Figure 70. The Transcost CER for liquid propellant rocket engine is given by,

$$H_{EL} = 277 * {M_{engine}}^{0.48} * f_1 * f_2 * f_3 \tag{42}$$

$$f_2 \text{ (Engine)} = 0.026 * ln{N_Q}^2 \tag{43}$$

where the technical quality factor is a function of the desired reliability of the rocket engine, given by the number of qualification firing (N_Q) that is required. The technical

Table 34: Deterministic Development Cost Summary for Propellant Depot with Various Cryogenic Thermal Systems

	Passive	ZBO	
M_{ref}	11,950	15,750	kg
M_{prop}	225	225	mT
k_{NMF}	0.05311	0.07000	
$k_{NMF_{ref}}$	0.08075	0.08075	
f_1	0.7	1.1	
f_2	1.520	1.154	
f_3	1.0	1.0	
H_{EV}	19,493	27,107	Wk-Yr
M_{Engine}	1,300	1,350	kg
f_1	1.0	1.0	
f_2	1.0	1.0	
f_3	1.0	1.0	
Total	8,653	8,800	Wk-Yr
H_{Total}	28,146	35,907	Wk-yr
$2011	$8.54b	$10.89b	

quality factor for the liquid propulsion engine has a base value of 1.0, set at 500 test firings which represents an average value for historical engine developments [110]. Using these equations and the mass estimation from Chapter 4, the development cost for the two deterministic propellant depots (shown in Table 16) can be computed. The result of the development cost is shown in Table 34.

Using the Transcost development cost model for expendable vehicles, the nominal development cost for the passive only propellant depot is $8.54 billion and the ZBO propellant depot is $10.89 billion. The closest element to the propellant depot in the baseline architecture is the cryogenic propulsion stage, as the combined propellant depot/cryogenic propulsion stage (CPS) replaces the CPS. The current cost estimates allocates $4.813 billion for the CPS development and procurement. The development cost for the depot system is significantly more than the present NASA estimate of the CPS. However, the method in which the CPS development cost is estimated in the current report is unknown; thus one-to-one comparison cannot be made. Using only the dry mass of the CPS (12,600 kg as quoted by the HEFT report [4], less

450 kg for two RL-10 type engines) without any of the development factors, the Transcost estimate for the development of the CPS is roughly $5.61 billion without including the development of the RL-10 engines. The Transcost estimate is 17% more than the CPS cost in the HEFT report. The CPS cost in the HEFT report includes the development of a medium and a heavy class CPS as well as the theoretical first unit cost of each of the CPS variant. The development cost of the medium CPS is estimated by HEFT to be $3.2 billion, which represents a $2.41 billion discrepancy between the two cost estimates. When comparing the total cost between the baseline and the alternate architecture, the discrepancy between the cost estimation methods must be considered. The cost analysis in this dissertation is approximately 70% higher than the HEFT cost estimates; thus, the cost presented can be considered to be conservative in nature.

The unit production cost for the expendable vehicles is also derived from historical data for Transcost. The cost estimating relationship is a function of the vehicle dry mass without the engine again. It is given by,

$$F_{EV} = 1.4182 * M_{ref}^{0.6464} * f_4 \tag{44}$$

Where f_4 is a cost reduction factor relating to series production of the unit. The theoretical first unit (TFU) cost would have f_4 value of 1.0. The TFU cost for each of the propellant depot concepts is summarized in Table 35. The unit cost for the liquid propellant rocket engine is given by,

$$F_{EL} = 3.15 * M_{engine}^{0.535} * f_4 \tag{45}$$

The theoretical first unit costs for the depots are $230 million and $278 million for the passive and ZBO scenario, respectively. This combined with the development cost estimates the total propellant depot system cost to be between $8.8 billion and $11.2 billion. As a comparison, using the Transcost unit cost method, the HEFT CPS

Table 35: Deterministic Theoretical First Unit Cost Summary for Propellant Depot with Various Cryogenic Thermal Systems

	Passive	ZBO	
M_{ref}	11,950	15,920	kg
f_4	1.0	1.0	
F_{EV}	613	766	Wk-Yr
M_{Engine}	1,300	1,350	kg
f_4	1.0	1.0	
F_{EL}	146	149	Wk-Yr
Total	759	915	Wk-Yr
$2011	$230m	$278m	

unit cost is $187 million (compared to $175 million quoted in HEFT for the medium CPS), which brings the total CPS system cost to $5.8 billion.

For the propellant tankers, the development and first unit cost are summarized in Table 36. The larger tankers used on the larger launches vehicles naturally has higher development and unit cost. The total development cost for the propellant tanker is between $2-3 billion, with the theoretical first unit cost less than $156 million. The one benefit that the tanker can take advantage of is the cost reduction factor relating to the production learning curve. To complete a whole architecture, between 4 and 29 tankers are needed (as shown in Table 29) and can be manufactured in series to reduce the overall cost of each of the tanker. However, because the exact number of tankers required is probabilistic in nature, a learning curve factor is not applied to the unit cost of the tankers. This provides a relatively conservative estimate for the overall architecture cost.

6.3.3 Cost Estimation Method Comparison

Typically, to provide a fair comparison between two architectures, the architectures must use the same cost estimation methods. However, this is often not possible. For the HEFT architecture, despite providing detail costs for the majority of the elements, there is a lack of detailed design information that is required to perform cost analysis

Table 36: Deterministic Development and Theoretical First Unit Cost Summary for Propellant Tankers for Each Launch Vehicles with Propellant Mass Fraction of 0.87

	Atlas	Delta	Falcon	SLS	
Payload	19,000	23,600	51,000	70,000	kg
M_{ref}	2,470	3,068	6,630	9,100	kg
k_{NMF}	0.14943	0.14943	0.14943	0.14943	
$k_{NMF_{ref}}$	0.13930	0.12991	0.10541	0.09839	
f_1	1.0	1.0	1.0	1.0	
f_2	0.93221	0.86936	0.70544	0.65843	
f_3	1.0	1.0	1.0	1.0	
H_{EV}	7,832	8,237	10,252	11,407	Wk-Yr
\$2011	\$2.38b	\$2.50b	\$3.11b	\$3.46b	
F_{EV}	221	254	419	514	Wk-Yr
\$2011	\$67m	\$77m	\$127m	\$156m	

for each of the elements. For comparison, the Transcost method is used to estimate the cost of several common elements. The crew transfer vehicle, deep space habitat, and the multi-mission space exploration vehicles are all common elements to deliver the crew from low Earth orbit to the destination. These three elements can be used to compare the cost estimation methods used in this dissertation and those used in the HEFT report.

The three common in space elements can be separated into two Transcost categories. The Deep Space Habitat and the MMSEV are both in-space crew systems similar to the Intentional Space Station nodes and the crew transfer vehicle is a ballistic crew capsule. Transcost provides two separate cost estimating relationships for the development cost for these two space systems but combines these two system into one cost estimating relationship for unit cost analysis. These cost estimating relationships are reproduced here,

$$H_{CS} = 1113 * {M_{ref}}^{0.383} * f_1 * f_3 \tag{46}$$

$$H_{BC} = 436 * {M_{ref}}^{0.408} * f_1 * f_2 * f_3 \tag{47}$$

$$f_2 \text{ (Ballistic Capsule)} = (Crew * Days)^{0.15} \tag{48}$$

$$F_{CS/BC} = 0.16 * {M_{ref}}^{0.98} * f_4 \tag{49}$$

H_{CS} is the development cost for the crew space systems and it has no technical quality factors associated with it. H_{BC} is the development cost for the ballistic capsule and the technical quality factor for the ballistic capsule is a function of the number of crew the capsule is designed for and the number of days of active operation that the capsule is design for. $F_{CS/BC}$ is the unit cost for both of these systems. The reference mass for all three of these systems is the dry mass of the vehicle.

The development factors for the three common elements of interest are vastly different. The deep space habitat is a completely new system with new application, because the mankind has never designed a vehicle to venture beyond cis-lunar space. The MMSEV is derived from the lunar rover concepts, and though it is a new system, the ability for extensive testing here on Earth provides some experience with the manufacture of the hardware. The crew transfer vehicle represents designs that have been in use since the start of the space age.

The development and unit cost for the three common element systems are shown in Table 37. The deep space habitat's dry mass combined with the difficulty of developing a new system results in a high development cost of over $20 billion and a first unit cost of just over $1 billion. This represents a huge discrepancy compared to the $9.61 billion estimate provided by the HEFT report. Transcost method estimates the development cost for the MMSEV to be roughly $11 billion with a first unit cost of $290 million. Again this is much higher than the HEFT report estimates. The crew

Table 37: Deterministic Development and Unit Cost Summary for Deep Space Habitat, Multi-Mission Space Exploration Vehicle, and the Crew Transfer Vehicle

	DSH	MMSEV	CTV	
M_{ref}	23,600	6,700	13,500	kg
f_1	1.3	1.1	1.0	
f_2	N/A	N/A	2.066	
f_3	1.0	1.0	1.0	
H	68,432	35,750	43,623	Wk-Yr
\$2011	\$20.76b	\$10.85b	\$13.23b	
F	3,476	955	1,960	Wk-Yr
\$2011	\$1,054m	\$290m	\$595m	
HEFT Cost	*$9.61b*	*$6.32b*	*$15.15b*	

transfer vehicle's cost estimate is slightly closer to the estimate provided by HEFT. However, the HEFT estimate involves the evolutionary development of three different variant of the crew transfer vehicle, while the Transcost estimate only estimate one of these vehicles.

From this analysis, the Transcost estimates are significantly higher than the cost provided by the HEFT report. The Transcost CERs are derived from actual programs and are based on the actual costs that include unforeseen cost growth. By using the Transcost model, the depot and tanker cost are much higher than predictions made by the HEFT cost models. This extra cost margin provides conservative estimates compared to the HEFT estimates where in reality the propellant depot based architecture may have even lower cost than shown.

6.4 Total Architecture Cost Comparison

To compare the baseline architecture to the depot architecture, the cost estimates given by the HEFT report are taken at face value and the Transcost model is utilized for all unique elements. Examining the HEFT cost breakdown (Table 1), the depot based architecture replaces the heavy lift launch systems and the ground operation

and infrastructure that supports the HLLV with commercial launch vehicles, eliminates the solar electric propulsion system, and replaces the cryogenic propulsion stage with the propellant depot/cryogenic propulsion stage. Using these differences, the total architecture cost is summarized in Table 38. Note that the Atlas vehicle scenario is not included because it does not have enough payload capability to deliver the hardware necessary for the architecture. However, the vehicle can still be utilized for propellant delivery to provide redundancy to the architecture. This will be discussed in detail in Chapter 7.

Table 38: Direct Architecture Cost Comparison Using HEFT Cost at Face Value and Updating Unique Elements with Transcost Estimates for ZBO Propellant Depot Scenario

	HEFT	Delta	Falcon
Crew Transfer Vehicle		$15,153	
Deep Space Habitat		$9,617	
Program Integration		$9,187	
Multi-Mission Space Exploration Vesicle		$6,315	
Commercial Crew Development		$4,453	
Commercial		$3,883	
Mission Operation		$3,175	
Robotic Precursor		$1,703	
Launch Vehicle & Ground Operation	$70,722	$7,227	$5,145
In-Space Cryogenic Propulsion	$4,813	$11,170	$11,170
Solar Electric Propulsion	$14,875	N/A	N/A
Total	**$143,896**	**$71,883**	**$69,801**

The common elements between the HEFT and depot architectures account for $53.5 billion, or 37% of the entire HEFT cost estimate. Using the cost estimates from Transcost, the zero-boil-off scenario architecture's total costs are $71.9 billion and $69.8 billion for utilizing the Delta and the Falcon vehicles respectively. In Table 38, the development and first unit cost for the propellant depot is categorized as the in-space cryogenic propulsion and the total number of commercial flights required along with the development and unit cost for the propellant tankers are both categorized in the launch vehicle line. Both of the propellant depot architecture scenarios are

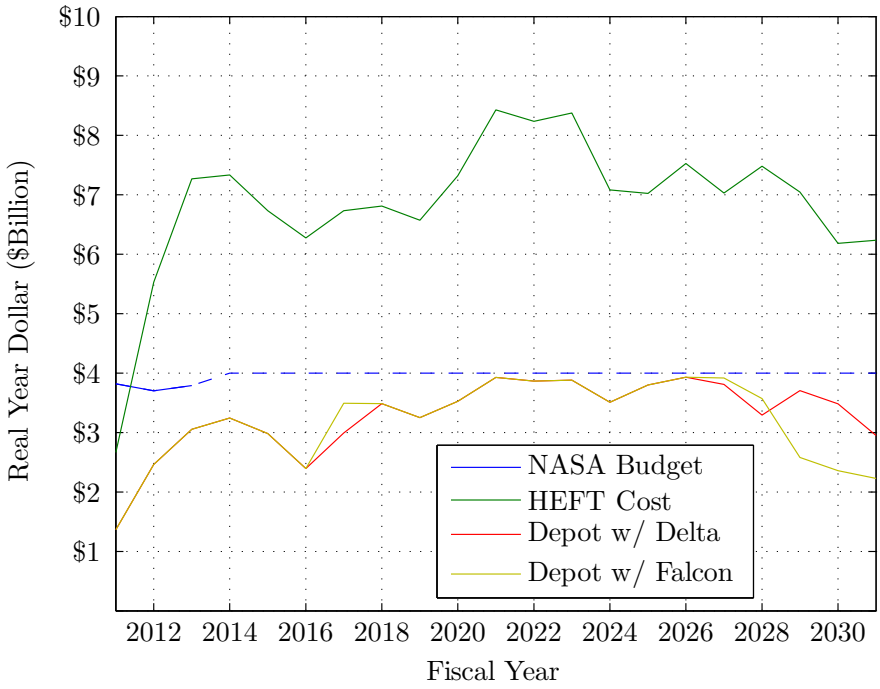

Figure 71: Yearly Cost for Depot Architecture with HEFT Baseline Cost for Common Elements Compared to $4 Billion NASA Outyear Budget Projection

nearly half the cost for the baseline HEFT architecture.

Figure 71 shows the yearly cost for the two depot based exploration architectures compared with the HEFT baseline cost and the NASA projected budget. The yearly cost for the two depot based architectures assumes an 8-year development cycle for the propellant depot/cryogenic propulsion system between 2018 and 2026, and 2 year development cycle for the propellant tanker from 2027 and 2028. The propellant depot is launched into orbit in 2028, with refueling missions occurring in 2029 and 2030, and final hardware and crew launch in 2031. Overall, the depot based architecture is beneath the $4 billion per year budget projection for the duration of the development cycle for the manned mission to NEA.

For the projected years (2011 to 2031), the total estimated budget is $83.3 billion, which means the two depot architectures result in a budget surplus of $11.4 billion (Delta) and $13.5 billion (Falcon). As a point of comparison, the current HEFT

cost estimate results in a budget deficit of $60.6 billion over the same time period. Using the $4 billion per year budget projection and evenly distributing the cost of the architecture over each fiscal year, the HEFT architecture will have enough total budget for completion in the year 2047. Alternatively, with the budget surplus, the two depot based architectures can shorten the development cycle and complete the NEA mission 3 or 4 years earlier than the current deadline.

6.5 Impact of CER Uncertainty in Architecture Cost

Table 39: CER Correction Factor Statistical Analysis Summary

Variable	Distribution	Parameter	
$\chi_{H_{EV}}$	Gamma	a = 45.455	b = 0.02178
$\chi_{H_{EL}}$	Gamma	a = 62.968	b = 0.01532
$\chi_{H_{CS}}$	Gamma	a = 104.15	b = 0.009658
$\chi_{H_{BC}}$	Gamma	a = 86.098	b = 0.01168
$\chi_{F_{EV}}$	Gamma	a = 144.50	b = 0.006963
$\chi_{F_{EL}}$	Gamma	a = 44.842	b = 0.02442
$\chi_{F_{CS/BC}}$	Gamma	a = 118.36	b = 0.008408

Similar to the mass estimating relationships in Chapter 4, the historical data derived cost estimating relationship has uncertainties associated with the cost estimation. As such, these uncertainties are analyzed for the economic feasibility assessment. The MER correction factor (Equation 22) can similarly be used on the Transcost CER to capture the variability of the overall data. The statistical distribution for the CER correction factors are shown in Table 39. Once again, gamma distributions are used for each of the CER correction factors to have domain of $x \in (0, \text{inf})$.

Using the CER correction factor distributions, Monte Carlo simulation can be performed to evaluate the impact of the CER uncertainty on the overall variability of the cost estimates. Figure 72, shows the empirical cumulative distribution function for the development plus first unit cost for the ZBO propellant depot system. The deterministic solution only captures approximately 60% of the potential variability in

the cost estimation. A 30% margin applied to the ZBO depot cost estimation brings the total cost of the depot to $14.5 billion, which provides over 95% confidence in capturing the total uncertainty in the cost estimation. As discussed in the previous section, the estimate exploration system budget surplus in the propellant depot architecture is in excess of $14 billion. Thus, the application of the cost margin to increase the confidence of capturing the uncertainty should not cause the architecture to exceed the projected budget over the course of the program.

The previous sections discussed the architecture costs utilizing the deterministic mass estimates for the unique elements to the propellant architecture. However, as shown in Chapter 4, there exists uncertainty in the mass estimations of these elements. The CERs are a function of these mass estimations, thus the uncertainty of the MERs is analyzed in tandem with the cost estimation. Figure 73 shows the empirical cumulative distribution function for the development and first unit cost for the ZBO propellant depot in the presence of MER uncertainty only. The mass used for this cost estimation is the same 100,000 case Monte Carlo simulation shown in Figure 46. Comparing Figure 73 and Figure 72, there is significant reduction in the overall variability in the development and first unit cost for the propellant depot. The uncertainty in the mass estimation does contribute to the overall variability of the overall cost, but, as seen from the figure, the effect is relatively minimal.

Taking the HEFT common elements at face value and only modifying the cost estimates for the unique elements (Table 38), the empirical cumulative distribution function for the architecture's total cost is shown in Figure 74. The figure shows the architecture cost for utilizing the Delta and the Falcon vehicles. The cost variability for the propellant depot for these two options are the same, the difference in the CDF comes from the variability in the propellant tanker development and unit cost. The Falcon architecture's deterministic solution captures more of the variability in the

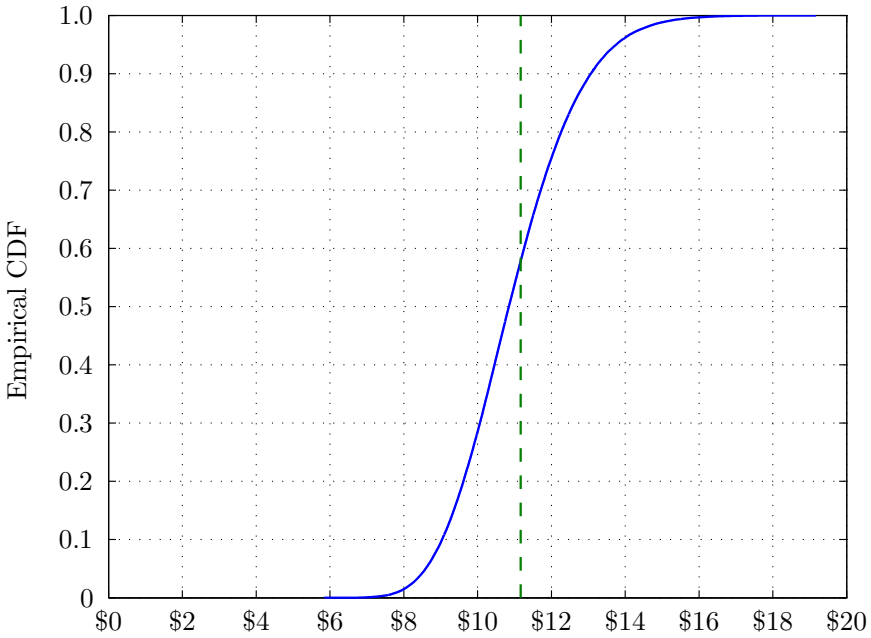

Figure 72: 100,000 Case Monte Carlo Simulation for Zero-Boil-Off Propellant Depot Development and First Unit Cost ($billion) Estimate with CER Uncertainty Only

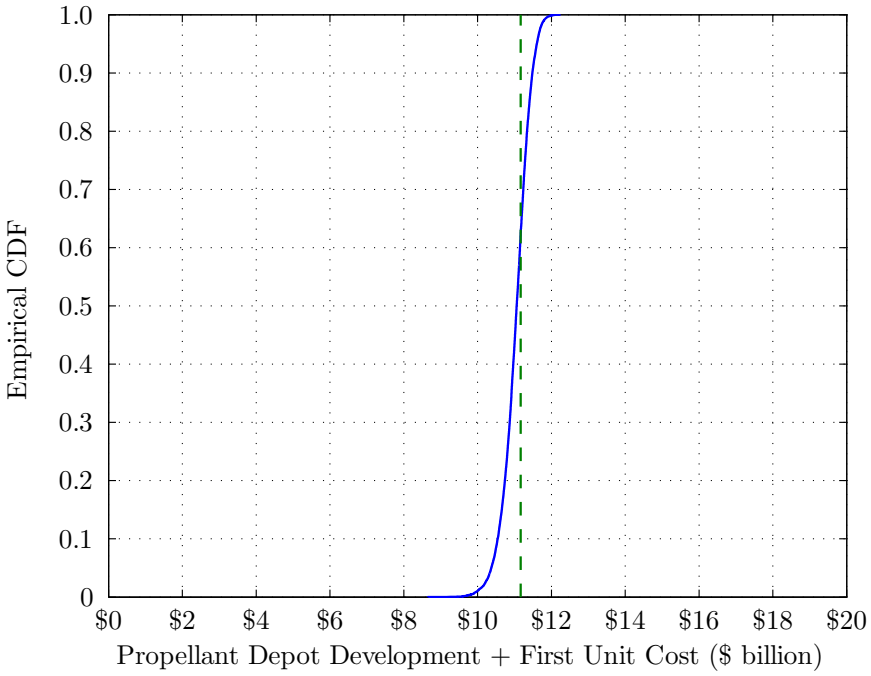

Figure 73: 100,000 Case Monte Carlo Simulation for Zero-Boil-Off Propellant Depot Development and First Unit Cost ($billion) Estimate with MER Uncertainty Only

total architecture cost compared to the Delta architecture because the Falcon architecture requires less launches of the propellant tankers, thus reducing the variability of the total architecture cost.

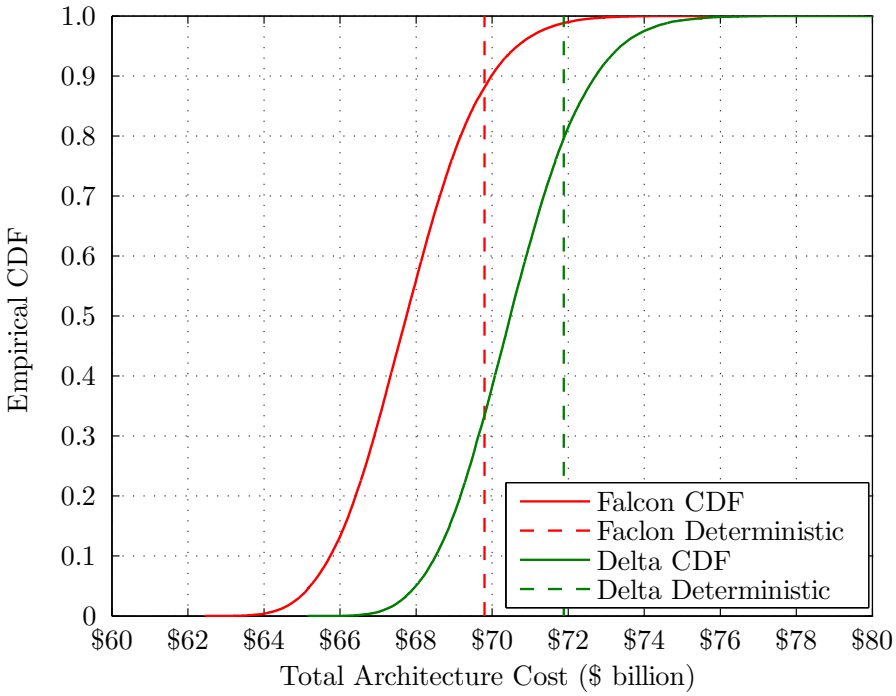

Figure 74: 100,000 Case Monte Carlo Simulation for Zero-Boil-Off Propellant Depot Based Exploration Architecture Total Cost ($billion) with CER Uncertainty

6.6 Cost of Mission Reliability

Section 5.5 provided the analysis of the overall propellant mission success probability given the various launch vehicles and design space options. The analysis showed that without redundancy in the launch vehicles, the overall mission success probability is less than 10%. To increase the mission success probability, the propellant depot based exploration architecture requires the use of launch redundancy. The majority of the required launches in the propellant depot based exploration architecture is delivering propellant into orbit, thus the failure of one or more of these launches does not impact the critical mission hardware. Of course any failure would require replacement flights

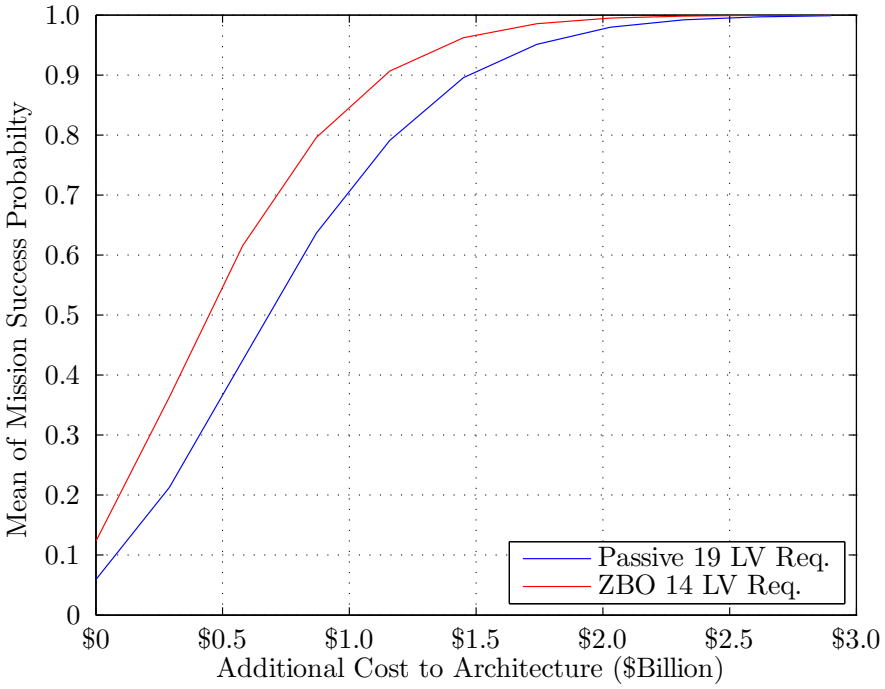

Figure 75: Mean of Propellant Aggregation Mission Success Probability as Function of Additional Cost to Architecture for Utilizing the Atlas V 551 Launch Vehicle

to deliver the required propellant into orbit. The ability to use replacement flights in the event of single launch failure results in higher mission success probability as shown in Section 5.5.

The number of additional launch vehicles required to increase the overall mission success probability translates directly to the increase cost to the overall architecture. To ensure high probability of mission success, the architecture must plan to utilize the replacement flights and thus budget the cost associated with purchasing the additional vehicles. As an example, Figure 75 shows the propellant aggregation mission success probability as a function of additional cost compared to the no redundancy scenario. To ensure a mission success probability of over 90%, the architecture will need an additional $1.5 billion allocated to launch vehicle cost if the architecture utilizes Atlas V exclusively for propellant delivery. If the budget can be increased by $2 billion, the

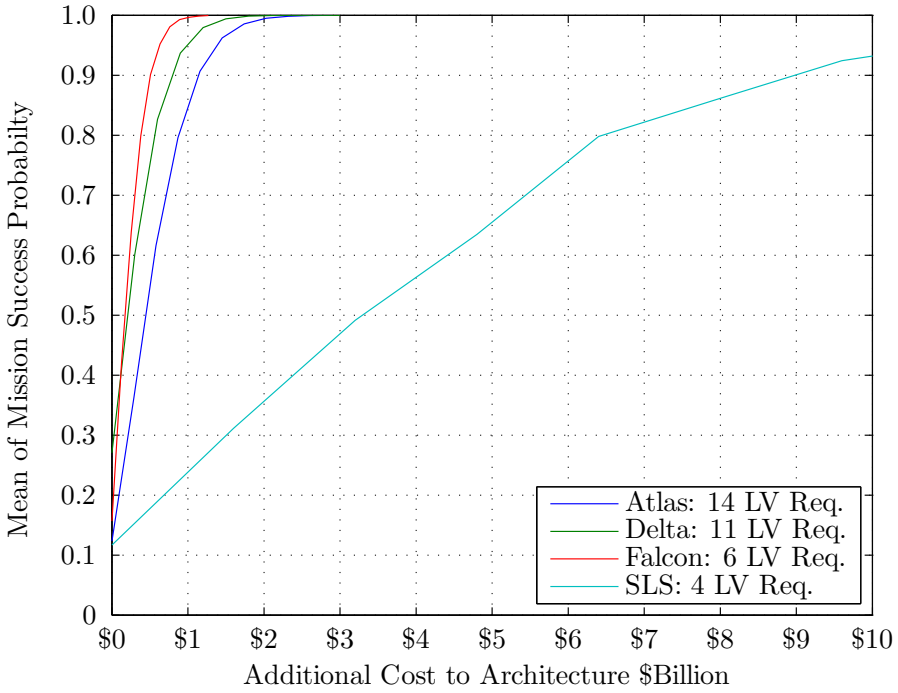

Figure 76: Mean of Propellant Aggregation Mission Success Probability as Function of Additional Cost to Architecture for Zero-Boil-Off Cryogenic Fluid Management

propellant aggregation mission success probability can be increased to 98%. Beyond $2 billion of additional budget, the mission success probability reaches a diminishing return, as the probability asymptotically approaches 100%.

The cost of the individual launch vehicle can have dramatic impact on the cost of increase mission success probability. Figure 76 shows the mean of the mission success probability as function of increase cost to architecture for all four of the launch vehicles under consideration. As the plot clearly shows, despite requiring the least number of launches, the SLS provides the worse mission success probability as a function of additional cost to architecture. This is due to both the extremely high cost of the SLS launch vehicle and the low reliability of a newly developed system. In comparison, even though the Falcon Heavy is a new vehicle, its low price per launch results in the best performance compared to the other two commercial launch

vehicles. It's interesting to note that at a price of $1.6 billion per launch (same as the Space Shuttle), which is already a conservative estimate by neglecting the ground operation cost, the cost of a single additional SLS launch can buy enough launch redundancy for the other three vehicles to achieve mission success probability better than 90%. Additionally, not included in this analysis is the potential downtime that an SLS would have to endure in the event of an accident, resulting in a review board similar to the Space Shuttle accident review.

6.7 Summary of Economic Feasibility Assessment

The cost of the propellant depot based exploration architecture was discussed in this chapter. The recent history of NASA's exploration system budget was examined to determine the level of funding that can be used as an appropriate assumption for the economic constraint. Based on the data, flat funding of $4 billion per year was found to be a reasonable constraint for the analysis. Examination the HEFT architecture revealed the program would be $60 billion over budget during the program's current schedule. To achieve the same goal with the same cost, the program would require an additional 15 years to have enough budget to complete the architecture as it currently exists.

Using cost estimating relationships provided by Transcost, the unique elements of the propellant depot architecture were analyzed to produce both development and flight unit cost. The analysis showed the total development and unit cost for the propellant depot system is just over than $11 billion. If the uncertainty in the cost estimation and mass estimation are included, the cost can range between $6 billion to $20 billion, while the $11 billion nominal cost represents the 60th percentile of the cost estimation. By taking the common elements in the HEFT report cost at face value, the total propellant depot architecture can range from $60 billion to $80 billion. The depot architecture's total cost produces a budget surplus of between

$3 billion to $23 billion over the same time period as the HEFT architecture. This represents a significant improvement in the economic feasibility as compared to the current baseline architecture. Of course the various options outlined in the previous chapters will impact the total cost of the architecture. The next chapter will discuss the overall feasibility of the integrated architecture.

CHAPTER VII

INTEGRATED ARCHITECTURE FEASIBILITY ASSESSMENT

Chapters 4, 5, and 6 provided feasibility assessments of the individual areas outlined at the end of Chapter 3. The overall feasibility of the architecture is presented in this chapter by combining the three areas and evaluating the various exploration options and examining the probability of meeting all of the constraints imposed with the highest probability and least sensitivity.

7.1 Stochastic Feasibility Assessment

The goal of this dissertation is to expand on typical deterministic feasibility assessments and uncertainty analysis to determine the probability of meeting the technical, economic, and launch success constraints. The satisfaction of constraints is not a simple Boolean function, rather each design option results in distribution functions that have a probability of satisfying the constraints. The goal of the design space exploration will be to maximize the probability of satisfying all of the constraints concurrently. Further, it is desired that the design choices lead to low sensitivity of the probability of constraint satisfaction.

To evaluate the overall architecture feasibility, all of the uncertainties variables are incorporated into the Monte Carlo simulation. The mass estimation uncertainty is compared to the cost estimation for the propellant depot development and unit cost. The number of launches required is impacted by the propellant tanker capacity, the launch vehicle launch rates, as well as the choice of cryogenic fluid management techniques. The total mission cost has the highest variability because it aggregates

the uncertainties in the mass estimation as well as the required number of launch vehicles. The Monte Carlo simulation generates probability distributions for each of the evaluation metrics and for each of the configurations of interest. Table 40 shows the summary of the Monte Carlo simulation variables for the overall architecture feasibility assessment.

Table 40: Architecture Feasibility Monte Carlo Simulation Variable Summary

Variable	Distribution	Parameter	
Mass Uncertainty Correction Factors			
Cryocooler COP	Gamma	$a = 1.769$	$b = 0.384$
Oxidizer Tank	LogNormal	μ = -1.21E-7	$\sigma = 0.275$
Hydrogen Tank	Gamma	$a = 447.5$	b = 2.24E-3
Intertank & Skirt	Gamma	$a = 37.36$	$b = 0.027$
Engine Correction	LogNormal	μ = -1.45E-8	$\sigma = 0.075$
20 K Cryocooler	Gamma	$a = 8.234$	$b = 0.129$
80 K Cryocooler	Gamma	$a = 3.655$	$b = 0.315$
Structure & Heat Transport	Uniform	$a = 0.059$	$b = 0.138$
Radiator	Uniform	$a = 0.029$	$b = 0.103$
Plumbing & Insulation	Uniform	$a = 0.003$	$b = 0.082$
Miscellaneous System	Uniform	$a = 0.008$	$b = 0.074$
MLI Mylar Sheet Specific Mass	Uniform	a = 8.81E-3	b = 9.30E-3
MLI Spacer Specific Mass	Uniform	a = 3.90E-3	b = 7.30E-3
Launch Vehicle Reliability			
Atlas V	Beta	$a = 353.4$	$b = 56.88$
Delta IV	Beta	$a = 654.4$	$b = 82.79$
Falcon Heavy	Beta	$a = 11.02$	$b = 4.007$
Space Launch System	Triangular	$a = 0$ $b = 0.731$	$c = 1$
System Cost Uncertainty Correction Factors			
Expendable Vehicle DDTE	Gamma	$a = 45.4$	$b = 0.0218$
Rocket Engine DDTE	Gamma	$a = 63.0$	$b = 0.0153$
Crew System DDTE	Gamma	$a = 104$	$b = 0.00966$
Ballistic Capsule DDTE	Gamma	$a = 86.1$	$b = 0.0117$
Expendable Vehicle Unit Cost	Gamma	$a = 145$	$b = 0.00696$
Rocket Engine Unit Cost	Gamma	$a = 44.8$	$b = 0.0244$
Crew System/Capsule Unit Cost	Gamma	$a = 118$	$b = 0.00841$

7.1.1 Launch Success Feasibility versus Economic Feasibility

The first pairwise comparison is between the overall launch success probability and the overall architecture cost probability. This comparison was briefly discussed in Section 6.6 by examining the cost of the increase reliability to the propellant aggregation mission with redundant propellant tanker flights. The cost used for comparisons in Section 6.6 uses the deterministic launch cost for the vehicle and does not incorporate the cost of the tanker vehicles.

Figure 77 shows the joint probability density function for the ZBO Falcon Heavy based propellant depot architecture with no redundant launch vehicles available for the propellant aggregation mission. Figure 78 shows the same joint probability for six redundant launch vehicles. Figure 77 shows the majority of the solutions have lower launch success probability while the deterministic cost is around the center of the distribution. Comparison between the two figures shows the benefit of the addition of redundant flights. The overall launch success probability increases dramatically, but the overall architecture cost increase is fairly minimal. The architecture cost increase with the addition of redundant vehicles is highly dependent on the cost of the launch vehicles. The Delta Heavy ZBO depot scenario can provide insight into the effects of higher launch vehicle prices on the overall increase in architecture cost.

Figures 79 and 80 show the joint probability distribution for total launch success probability and total architecture cost for the Delta Heavy based ZBO propellant depot architecture with no redundancy and six redundant vehicles respectively. The Delta based architecture requires more than twice the number of propellant launches as compared to the Falcon based architecture. However, as discussed in Chapter 5, the extensive launch record for the Delta results in increased reliability for the individual launch success rates. This results in a total launch success probability distribution with significantly less dispersion. The Delta vehicle's launch cost is twice that of theFalcon Heavy. As a result, the addition of redundant launch vehicles results

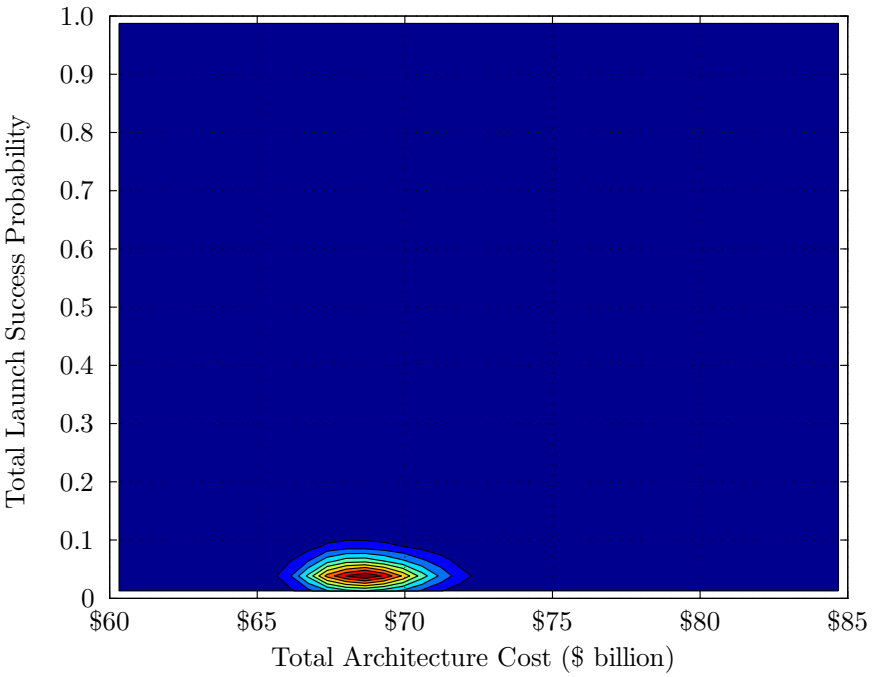

Figure 77: Joint Probability Density of Total Launch Success and Total Architecture Cost for Zero-Boil-Off Falcon Heavy Based Propellant Depot Architecture with No Backup Flight Available

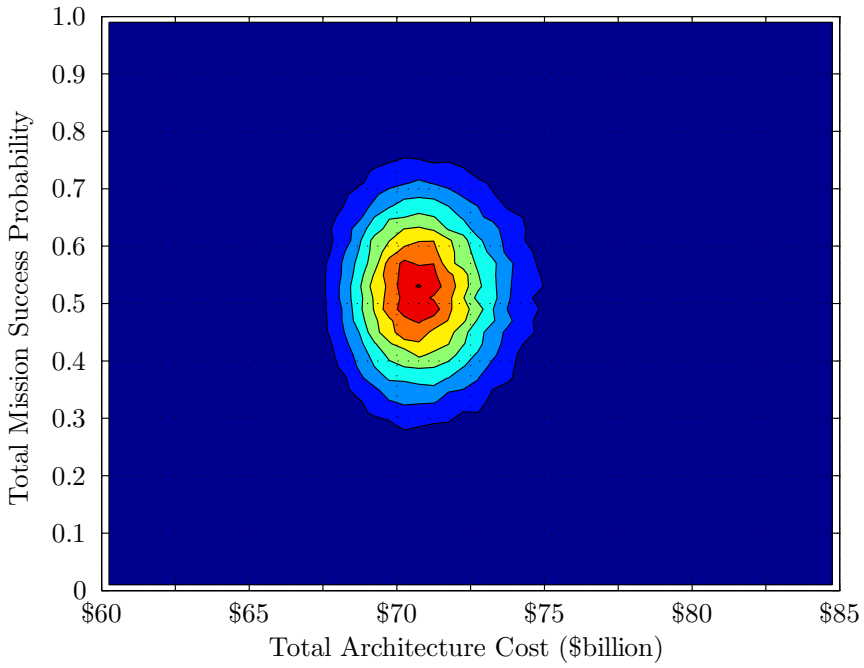

Figure 78: Joint Probability Density of Total Launch Success and Total Architecture Cost for Zero-Boil-Off Falcon Heavy Based Propellant Depot Architecture with Six Backup Flights Available

in a difference of $170 million in the overall architecture cost per redundant vehicle utilized.

By utilizing the Delta to deliver all of the necessary components, the overall mission probability can reach over 70% due to the high reliability of the Delta vehicle. The probabilistic simulation shows the architecture cost for the six redundant launch vehicle scenarios ranging from $70 to $78 billion, which is only $3 to $8 billion (4 to 10 percent) more than the Falcon scenario. The increase in launch success probability is extremely favorable, especially considering the minimal cost increase. Recall discussions from Chapter 6, the project budget for the duration of the architecture is roughly $84 billion. These depot based exploration architectures are still well under the budget constraints.

Figure 81 shows the joint probability distribution of mission launch success and total architecture cost for both cryogenic fluid management strategy (Table 15) and various backup flight scenarios. The figures in each row represents the joint probability density for the same CFM strategy with varying number of backup flights available, while the each column represents the same number of backup flights available across the different CFM strategies. The simulation for the non-ZBO options uses a uniform distribution to estimate the number of propellant flights required, which is a function of the vehicle's flight rates. The maximum/minimum number of propellant flights required is shown in Table 29.

For the Falcon Heavy based depot architecture, the total mission probability is relatively insensitive to the choice of CFM strategy. The Falcon Heavy's large payload capability results in almost no change to the number of launch vehicles required when CFM strategy and flight rate is changed (either 6 or 7 propellant launches required). The overall architecture cost does increase slightly due to the technology required for the cryocoolers. Additionally the dispersion of the cost estimates increases as well due to higher uncertainties in estimating the cost of the advanced technology.

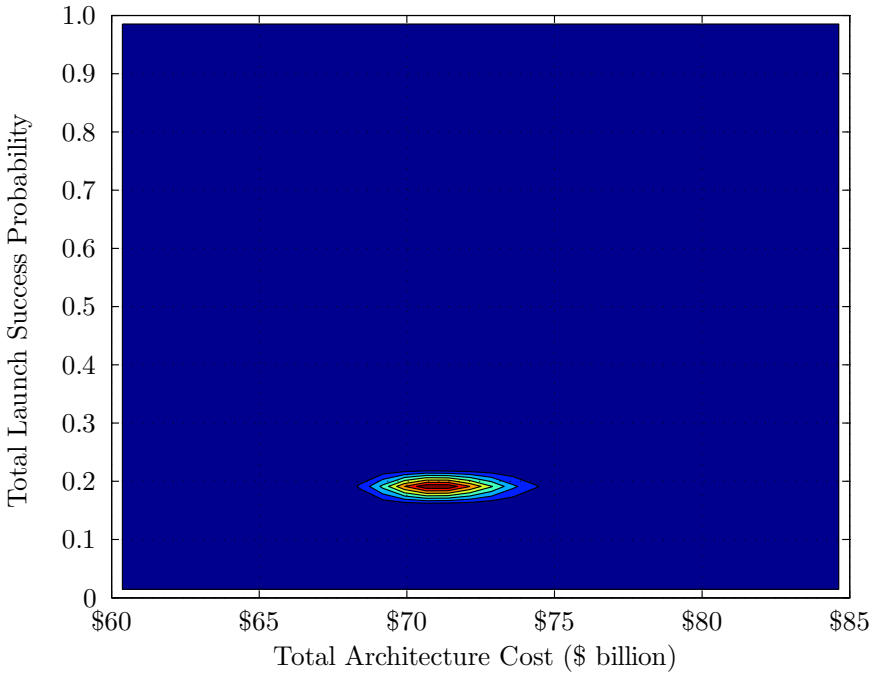

Figure 79: Joint Probability Density of Mission Launch Success and Total Architecture Cost for Zero-Boil-Off Delta IV Based Propellant Depot Architecture with No Backup Flight Available

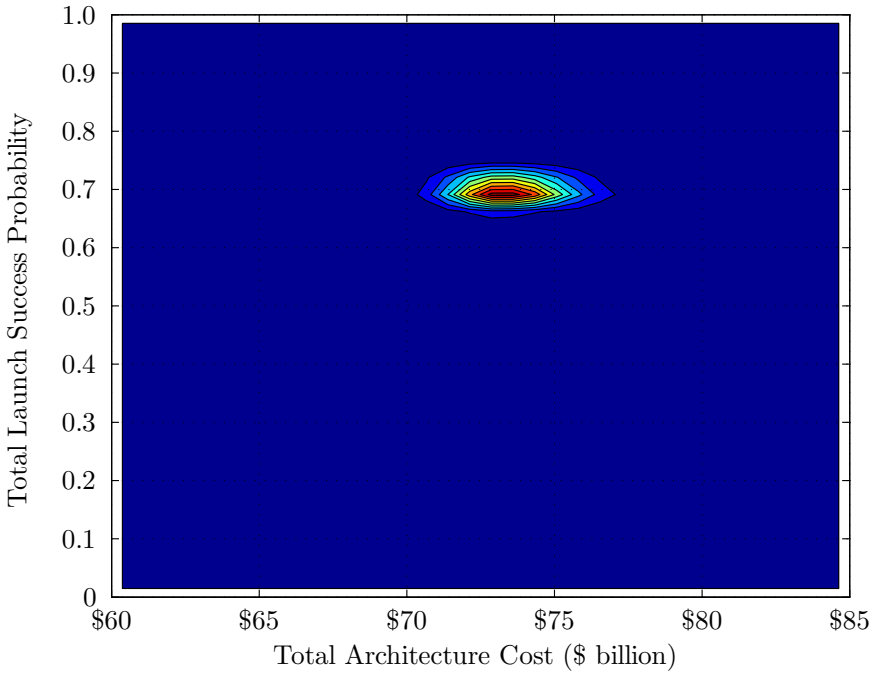

Figure 80: Joint Probability Density of Mission Launch Success and Total Architecture Cost for Zero-Boil-Off Delta IV Based Propellant Depot Architecture with Six Backup Flights Available

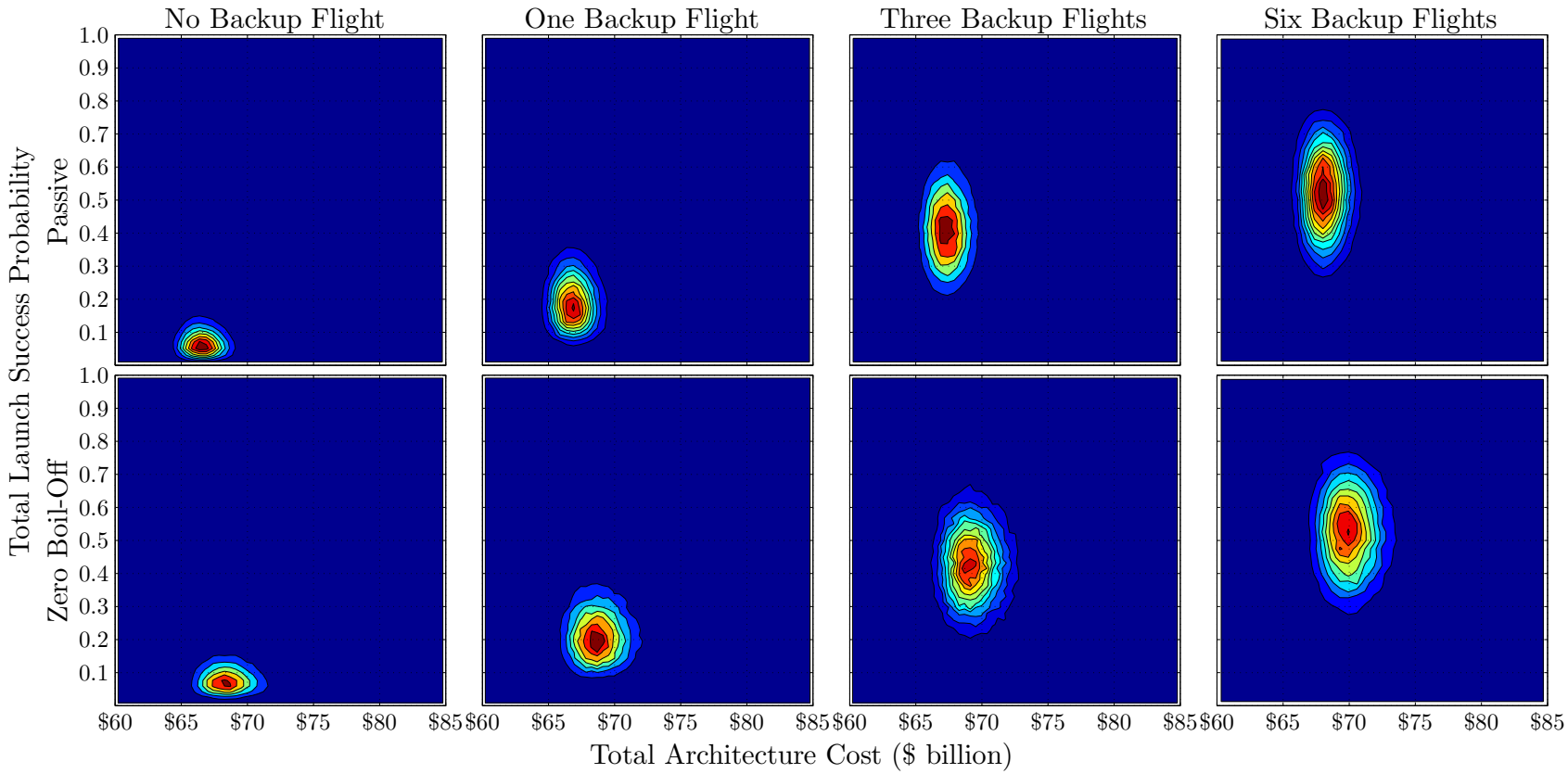

Figure 81: Joint Probability Density of Mission Launch Success and Total Architecture Cost for Falcon Heavy Based Propellant Depot Architecture with Various Cryogenic Fluid Management Strategy and Backup Flight Scenario

As previously discussed, increasing the number of available backup flights increases the overall launch success probability rapidly. With three backup Falcon flights, the overall launch success probability can reach as high as 60%, which is 20% higher than the baseline HEFT architecture (assuming four required flights of the SLS resulting in HEFT architecture reliability of 0.391). With six backup flights available, the overall launch success can be as high as 80%. The cost increase from the backup flights is fairly minimal compared to the overall architecture. The mean of the total architecture cost for the no backup flight scenario is roughly $66 to $68 billion depending on the CFM strategy. To include six backup flights, the mean of the total architecture cost increases by an average of $2-3 billion, or 3-5% of the total architecture cost. It is important to note that for all scenarios, the probabilistic simulation show that the Falcon Heavy based exploration architecture poses no risk of exceeding the expected budget constraint of $84 billion.

Figure 82 shows the same joint probability density function for the Delta IV Heavy based propellant depot architecture. Generally speaking the same trend is observed for both the Falcon and the Delta based architecture for both total launch success probability and total architecture cost. The primary difference between the two architectures is the dispersion of the data is significantly less for the Delta based architecture. Because the Delta vehicle has an extensive launch record to support its reliability, there is significantly less uncertainty with the individual launch success probability (as shown in Figure 56). This results in tighter upper and lower bounds for the total launch success probability regardless of the number of launches required.

Due to the lower payload capability (as compared to the Falcon heavy), the choice of CFM strategy does have a small impact on both the overall launch success probability and total architecture cost. The number of propellant launches required varies anywhere between 11 to 20, and this wide range (as function of both CFM strategy and launch rates) results in the sloped probability distribution seen in the all passive

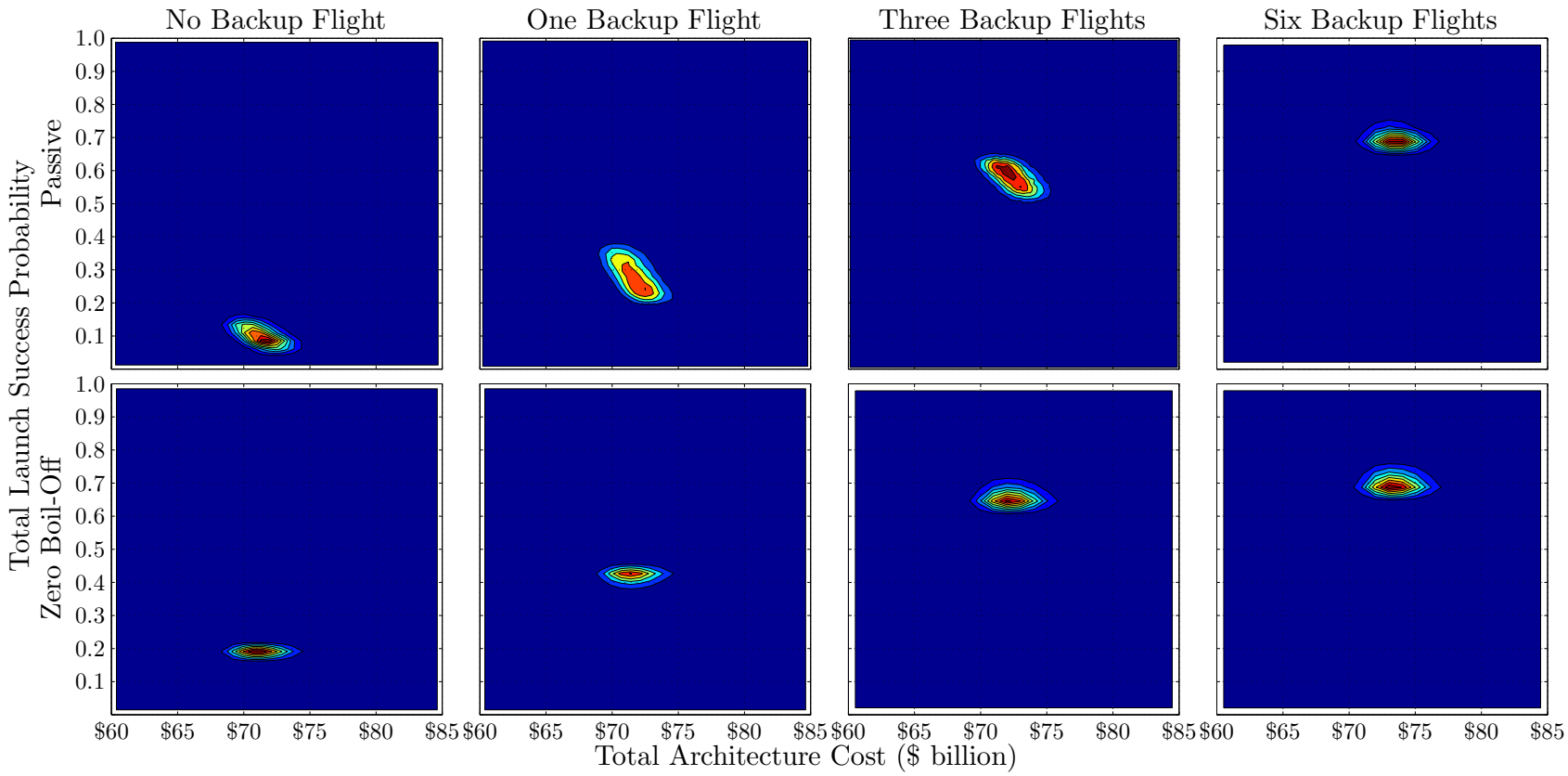

Figure 82: Joint Probability Density of Mission Launch Success and Total Architecture Cost for Delta IV Heavy Based Propellant Depot Architecture with Various Cryogenic Fluid Management Strategy and Backup Flight Scenario

scenario. The distribution for the all passive CFM with up to three backup flights available indicate decreasing overall launch success probability with increasing architecture cost. This is counter-intuitive as typically increasing cost should increase the launch success probability. However, the cost for each of these scenarios is dictated mostly by the launch requirements, and thus more launches required higher architecture cost while simultaneously decreasing the overall launch success probability. The effect is eliminated with increasing number of backup flights, as the architecture becomes less sensitive to the number of launches required. The same can be said regarding the scenarios which utilizes cryocoolers as the range of number of launches required is reduced.

The overall launch success probability is slightly higher for the Delta based architecture compared to the Falcon based architecture. With six backup flights available, the overall launch success probability is centered on 70% for the Delta based architecture with very little variation, compared to the Falcon architecture, which has launch success probability that ranges from 30% to 70%. Due to the higher launch cost for the Delta vehicle, the overall architecture cost is slightly higher as compared to Falcon architecture. However, none of the scenarios considered show any risk of exceeding the projected $84 billion budget constraint.

It's important to note that the benefit of backup flights to the architecture reaches diminishing returns beyond six flights. Beyond six backup flights for both architecture scenarios, the propellant aggregation mission reaches well over 99% probability of success. With this many backup flights available, the contribution of the mission unreliability from the propellant aggregation mission is insignificant, and the overall launch success probability is dominated by the probability of hardware launch and assembly success. The overall launch success probability is limited by the space hardware launches that are necessary. If the hardware launches redundancy is enabled, then the launch success probability can be increased even further. This will be

investigated further in this chapter.

7.1.2 Performance Feasibility versus Economic Feasibility

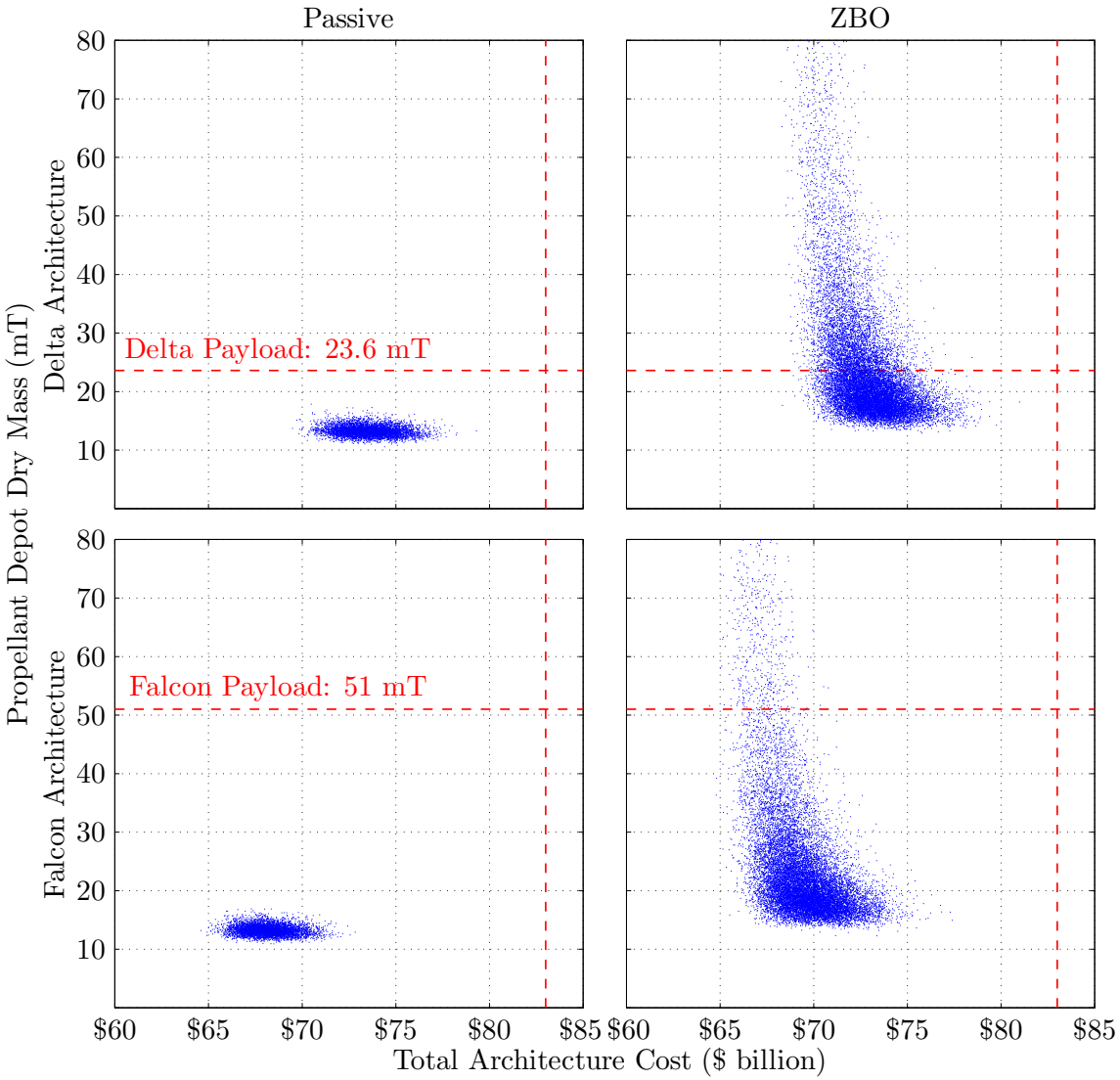

Figure 83: Scatter Plot of Propellant Depot Dry Mass and Total Architecture Cost of Delta IV Heavy and Falcon Heavy Based Propellant Depot Architecture with Various Cryogenic Fluid Management Strategies and Six Backup Flights

Figure 83 shows scatter plots from the probabilistic simulation. The propellant depot dry mass is used as a measure of performance feasibility as it is sized to provide enough propellant to perform the mission and the launch vehicle payload capability

are used as constraints. The figures show the total architecture cost spread for the six backup flight scenario as it is the most likely cost scenario (given the maximum probability of launch success). Note that the propellant depot dry mass probabilistic simulation is independent of the redundant flight scenario. The plot also shows the constraint lines for both the propellant depot dry mass and the total architecture cost.

As discussed previously, both of the scenarios fall under the budget constraint defined in Chapter 6. The passive scenario simulations all fall under the launch vehicle payload constraint for both the Delta and the Falcon architecture. For the ZBO scenarios, the constraint violation becomes a significant issue for the Delta architecture. Over 30% of the simulations violate the Delta payload constraint, while 5% of the simulations violate the Falcon payload constraint. This result shows that in order to enable ZBO propellant depot in the exploration architecture, a larger payload launch vehicle than the Delta is required to have higher confidence in the performance feasibility. Despite the increase in constraint violation, the Falcon architecture has 95% of the cases in the feasible space. Looking back at Figure 81, the inclusion of the ZBO cryocooler makes relatively little impact on the overall launch success probability and total architecture cost for the Falcon Heavy based architecture. Because of the Falcon Heavy's high payload capacity and low launch cost, the benefits the ZBO cryocoolers is greatly diminished.

7.2 Total Architecture Feasibility Summary

To summarize the total architecture feasibility assessment, Monte Carlo simulations for each of the different CFM strategies and backup flight scenarios are performed. The constraints for each of the feasibility evaluation metric are defined. The economic feasibility constraint is the total budget estimate of $83.3 billion, which was derived in Chapter 6. The performance feasibility constraints are the payload capacity of

the launch vehicle for the particular scenario (23.6 mT for Delta and 51 mT for Falcon). The propellant tanker is sized for the particular launch vehicle and the mission hardware is distributed across multiple launches. Thus the primary performance assessment required is to determine if the launch vehicle has enough payload capacity to deliver the depot in a single launch. The reliability feasibility constraint was derived from the baseline architecture. The baseline HEFT architecture requires four launches of the newly developed Space Launch System, this equates to a baseline launch success probability of 39% assuming no redundancy for the hardware launches. Thus, for direct comparison, the alternate architecture launch success probability must exceed the baseline launch success probability. If the alternate architecture mission probability is greater than the baseline, it means that the propellant aggregation portion of the architecture does not negatively impact the overall architecture in terms of safety and reliability.

Table 41 shows the summary of the feasibility assessment for the both Delta IV and Falcon Heavy based propellant depot exploration architectures. The table tabulates the mean and standard deviation of each of the feasibility metrics as well as the probability of constraint satisfaction in the presence of uncertainty. The color coding (Red, Yellow, and Green) represents three levels of risk that the particular architecture poses to violation of the particular constraint. These levels of risk are based on both the probability of meeting the constraint and the standard deviation of the probability distribution. Green represents low risk area, where the probability of constraint satisfaction is greater than 90% with low variability; red represents high risk area, where the probability of constraint satisfaction is less than 65%; and yellow represents medium risk area in which the probability of satisfying the constraint may be high but there is insignificant variability in the data.

The feasibility of the Falcon Heavy based architecture is moderate. The performance feasibility for the Falcon heavy based architecture is insensitive to the cryogenic

Table 41: Summary of Total Architecture Feasibility for Propellant Depot Exploration Architecture

			Performance Feasibility			Reliability Feasibility			Economic Feasibility		
		Backups	μ	σ	% Satisfy	μ	σ	% Satisfy	μ	σ	% Satisfy
		Constraints:	*M_{Depot} < 23.6 mT*			*P_{Launch} > 0.391*			*Cost < $83.3 billion*		
Falcon Heavy Architecture	Passive	0	13.3 mT	0.84 mT	**100%**	0.073	0.0352	**0%**	$66.6b	$1.12b	**100%**
		1	13.3 mT	0.84 mT	**100%**	0.196	0.0706	**1%**	$66.9b	$1.12b	**100%**
		3	13.3 mT	0.84 mT	**100%**	0.413	0.1008	**58%**	$67.4b	$1.12b	**100%**
		6	13.3 mT	0.84 mT	**100%**	0.523	0.1125	**87%**	$68.2b	$1.12b	**100%**
		9	13.3 mT	0.84 mT	**100%**	0.538	0.1150	**89%**	$68.9b	$1.13b	**100%**
		12	13.3 mT	0.84 mT	**100%**	0.538	0.1150	**89%**	$69.7b	$1.14b	**100%**
	ZBO	0	26.8 mT	45.3 mT	**95%**	0.084	0.0372	**0%**	$67.8b	$1.65b	**100%**
		1	26.8 mT	45.3 mT	**95%**	0.217	0.0715	**2%**	$68.1b	$1.65b	**100%**
		3	26.8 mT	45.3 mT	**95%**	0.431	0.1011	**64%**	$68.6b	$1.66b	**99%**
		6	26.8 mT	45.3 mT	**95%**	0.527	0.1137	**88%**	$69.4b	$1.66b	**99%**
		9	26.8 mT	45.3 mT	**95%**	0.537	0.1153	**89%**	$70.1b	$1.67b	**99%**
		12	26.8 mT	45.3 mT	**95%**	0.538	0.1150	**89%**	$70.9b	$1.67b	**99%**
		Constraints:	*M_{Depot} < 51 mT*			*P_{Launch} > 0.391*			*Cost < $83.3 billion*		
Delta IV Architecture	Passive	0	13.3 mT	0.84 mT	**100%**	0.101	0.0254	**0%**	$71.3b	$1.34b	**100%**
		1	13.3 mT	0.84 mT	**100%**	0.282	0.0476	**22%**	$71.7b	$1.33b	**100%**
		3	13.3 mT	0.84 mT	**100%**	0.580	0.0362	**100%**	$72.5b	$1.34b	**100%**
		6	13.3 mT	0.84 mT	**100%**	0.692	0.0162	**100%**	$73.6b	$1.34b	**100%**
		9	13.3 mT	0.84 mT	**100%**	0.700	0.0158	**100%**	$74.7b	$1.35b	**100%**
		12	13.3 mT	0.84 mT	**100%**	0.700	0.0159	**100%**	$75.9b	$1.34b	**100%**
	ZBO	0	26.8 mT	45.3 mT	**66%**	0.189	0.0092	**0%**	$67.6b	$1.93b	**100%**
		1	26.8 mT	45.3 mT	**66%**	0.422	0.0142	**98%**	$70.9b	$1.64b	**100%**
		3	26.8 mT	45.3 mT	**66%**	0.655	0.0153	**100%**	$71.7b	$1.63b	**100%**
		6	26.8 mT	45.3 mT	**66%**	0.698	0.0158	**100%**	$72.8b	$1.63b	**100%**
		9	26.8 mT	45.3 mT	**66%**	0.700	0.0159	**100%**	$73.9b	$1.64b	**99%**
		12	26.8 mT	45.3 mT	**66%**	0.700	0.0159	**100%**	$75.1b	$1.65b	**99%**

fluid management strategy. For both passive and ZBO strategies, the probability of satisfying the performance constraint of the Falcon heavy payload is greater than 95%. However, the standard deviation of the dry mass Monte Carlo simulation is extremely high for the ZBO scenario, signifying very high levels of uncertainty with the mass estimation. Thus, the ZBO scenario increases the risk to the overall feasibility of the architecture.

The launch reliability feasibility of the Falcon Heavy based architecture poses moderate to high risk to the overall feasibility of the architecture. From the Monte Carlo simulation, it is clear that the Falcon Heavy based architecture is simply not feasible without the use of significant number of redundant flights with the currently established launch reliability. For the scenarios with no redundant flights, the overall launch success probability is less than 10% for both CFM scenarios. The probability increases as the number of redundant flights increases (as shown in Chapter 5), but it never exceeds 54%. As discussed in the previous sections, the benefit of increasing number of redundant flights eventually reaches diminishing returns above six flights. With six redundant flights available, the mean launch success probability is just above 50% with standard deviation of 11%. The probability that the launch success probability is greater than the baseline probability is 88 - 87%. Thus, the overall mission has a high probability of being more reliable than the current baseline architecture, but the risk to the overall architecture feasibility still exists as the nominal probability is relatively low. The launch of the mission hardware, which in this analysis does not have redundancy, becomes the major limiting factor for overall launch success probability.

The economic feasibility is greater than 99% for all of the design options under consideration. As discussed in the previous sections, taking the common elements cost from the HEFT report and estimating the cost of the unique elements with Transcost, the propellant depot based architecture poses nearly no risk of exceeding

the estimated exploration system budget estimate of $4 billion per year. Even with the cost estimation uncertainty, the Monte Carlo simulation shows the probability of constraint satisfaction of over 99% for all of the depot design scenarios considered. Additionally, the standard deviation of the architecture cost is less than $2 billion for all scenarios considered, so the dispersion of the architecture cost is minimal. For both of these reasons, the economic feasibility for the Falcon Heavy based propellant depot exploration architecture is high.

For the Delta IV architecture, the primary difference between the constraints for the two architectures are the reduction of the performance feasibility constraint to match the Delta IV Heavy payload. Overall, the feasibility of Delta based architecture is similar to the Falcon based architecture. The performance feasibility assessment reveals increased risk to the performance feasibility for the ZBO scenario. The probability of the vehicle's payload capability to capture the uncertainties in the performance estimation is only 66% and poses higher risk to the overall architecture feasibility as compared to the Falcon architecture. The simulation shows little to no risk of exceeding the cost constraint, and though the overall cost is slightly higher than the Falcon based architecture, the dispersion of the cost estimation remains relatively low and the probability of constraint satisfaction remains high.

The reliability feasibility assessment for the Delta architecture shows improvement as compare to the Falcon architecture. Despite the fact that the Delta architecture typically requires more launch vehicles due to its lower payload capability, the overall launch success probability is better than the Falcon architecture. The extensive launch record for the Delta launch vehicle results in high reliability and high confidence in the launch vehicle's performance (Figure 56). This results in improvement to the overall launch success probability as compared the Falcon based architecture. The reliability feasibility is still dependent on the use of redundancy in the propellant aggregation phase, as the overall launch success probability remains less than 20%

without redundancy. The launch success probability exceeds the baseline HEFT architecture with high confidence with only 2-3 redundant launch vehicles in the Delta architecture, as compared to 5 - 6 in the Falcon architecture. Coincidentally, the cost for 2 - 3 Delta IV Heavy is nearly identical to the estimate cost for 5 -6 Falcon Heavys.

Table 42 shows the architecture feasibility summary for the two launch vehicles options with space hardware redundant flights. The performance feasibility remains unchanged from the previous discussions, while the launch success probability and the architecture cost are updated. For the launch success probability, the potential for hardware launches to have redundancy results in significant increase in the overall launch success probability. For both the Delta and Falcon scenarios, with six or more redundant flights, the overall launch success probability is greater than 95%. If the baseline HEFT architecture's SLS has the high reliability of a Delta vehicle, the four launches required will result in a launch success probability of 70%. Using this as new constraint, the overall risk of the propellant depot architecture reliability feasibility would still require at least six redundant launches to ensure high probability of meeting the constraint. The economic feasibility remains unchanged for both scenarios. With the inclusion of hardware launch redundancy, the total architecture cost increases by $1 to $6 billion depending on the scenario, but the probability of satisfying the constraint is still over 97% for all of the scenarios considered.

From an architecture decision making standpoint, the Delta based architecture seems to be the better option because of the increase in reliability feasibility with little to no impact to the other two feasibility metrics. However, with the high projected launch rate of the Falcon Heavy, its reliability may be significantly improved by the time the exploration architecture begins. It is interesting to note that the total architecture cost for the Delta based architecture is relatively insensitive to the choice of CFM strategy. The reduction in launch cost in the ZBO scenario is completely

Table 42: Summary of Total Architecture Feasibility for Propellant Depot Exploration Architecture with Hardware Redundancy

			Performance Feasibility			Reliability Feasibility			Economic Feasibility		
		Backups	μ	σ	% Satisfy	μ	σ	% Satisfy	μ	σ	% Satisfy
		Constraints:	*M_{Depot} < 51 mT*			*P_{Launch} > 0.700*			*Cost < $83.3 billion*		
Falcon Heavy Architecture	Passive	0	13.3 mT	0.84 mT	**100%**	0.073	0.0352	**0%**	$66.6b	$1.12b	**100%**
		1	13.3 mT	0.84 mT	**100%**	0.236	0.0820	**40%**	$68.7b	$1.12b	**100%**
		3	13.3 mT	0.84 mT	**100%**	0.632	0.1039	**78%**	$67.4b	$1.12b	**100%**
		6	13.3 mT	0.84 mT	**100%**	0.935	0.0370	**97%**	$70.8b	$1.12b	**100%**
		9	13.3 mT	0.84 mT	**100%**	0.993	0.0063	**100%**	$72.8b	$1.13b	**100%**
		12	13.3 mT	0.84 mT	**100%**	0.999	0.0006	**100%**	$74.8b	$1.14b	**100%**
	ZBO	0	26.8 mT	45.3 mT	**95%**	0.084	0.0372	**0%**	$67.8b	$1.65b	**100%**
		1	26.8 mT	45.3 mT	**95%**	0.262	0.0816	**0%**	$68.5b	$1.66b	**100%**
		3	26.8 mT	45.3 mT	**95%**	0.666	0.0948	**63%**	$69.9b	$1.65b	**100%**
		6	26.8 mT	45.3 mT	**95%**	0.947	0.0302	**95%**	$72.1b	$1.65b	**100%**
		9	26.8 mT	45.3 mT	**95%**	0.995	0.0044	**100%**	$74.2b	$1.66b	**99%**
		12	26.8 mT	45.3 mT	**95%**	0.999	0.0001	**100%**	$76.3b	$1.67b	**99%**
		Constraints:	*M_{Depot} < 23.6 mT*			*P_{Launch} > 0.700*			*Cost < $83.3 billion*		
Delta IV Architecture	Passive	0	13.3 mT	0.84 mT	**100%**	0.101	0.0254	**0%**	$71.3b	$1.34b	**100%**
		1	13.3 mT	0.84 mT	**100%**	0.316	0.0558	**11%**	$72.0b	$1.32b	**100%**
		3	13.3 mT	0.84 mT	**100%**	0.757	0.0536	**100%**	$73.3b	$1.29b	**100%**
		6	13.3 mT	0.84 mT	**100%**	0.979	0.0090	**100%**	$75.3b	$1.25b	**100%**
		9	13.3 mT	0.84 mT	**100%**	0.999	0.0001	**100%**	$77.3b	$1.21b	**99%**
		12	13.3 mT	0.84 mT	**100%**	0.999	0.0001	**100%**	$79.3b	$1.16b	**99%**
	ZBO	0	26.8 mT	45.3 mT	**66%**	0.189	0.0092	**0%**	$70.5b	$1.63b	**100%**
		1	26.8 mT	45.3 mT	**66%**	0.485	0.0150	**100%**	$71.3b	$1.64b	**100%**
		3	26.8 mT	45.3 mT	**65%**	0.885	0.0081	**100%**	$72.9b	$1.63b	**99%**
		6	26.8 mT	45.3 mT	**66%**	0.995	0.0006	**100%**	$75.2b	$1.63b	**99%**
		9	26.8 mT	45.3 mT	**66%**	0.999	0.0001	**100%**	$77.5b	$1.64b	**98%**
		12	26.8 mT	45.3 mT	**66%**	0.999	0.0001	**100%**	$79.8b	$1.64b	**97%**

offset by the higher development cost associated with propellant depot technologies. With the availability of redundant vehicles, the architecture does not suffer from reduced reliability with the increase in propellant flights as a result of boil-off, and the performance feasibility increases dramatically as the depot dry mass is reduced without the high cryocooler power requirement.

The overall benefit for utilizing the Falcon vehicle is a slight reduction in the overall architecture cost due to lower launch cost. However, as discussed in Chapter 6, the propellant aggregation mission phase only accounts for less than 20% of the total architecture cost. So the potential savings provided by the Falcon vehicle does not have as much appreciable impact on the overall architecture feasibility as the Delta vehicle's improved reliability. If the Delta IV's launch price can be reduced by 30-40%, then the Delta architecture's total cost will be fairly indistinguishable from the Falcon architecture. On the other hand, if the Falcon Heavy's reliability can be demonstrated improved to the level of the Delta IV, then the Falcon architecture can provide the same cost saving without sacrificing launch reliability. As mentioned in Chapter 6, there is potential for launch price reduction by negotiating bulk purchase price with the launch provider, further improving the economic feasibility for both architectures.

CHAPTER VIII

DISSERTATION SUMMARY AND CONCLUSIONS

This final chapter of the dissertation draws conclusions regarding the overall feasibility of propellant depot based exploration architecture. A review of the research goals is provided and discussion of the fulfillment of each goal is presented. The chapter also summarizes the results from each of the individual feasibility assessments as well as the integrated assessment of architecture feasibility.

8.1 Research Goals

The primary goal of the research presented in this dissertation is to investigate the feasibility of exploration architectures that utilizes on orbit propellant depot and propellant transfer as a mean to eliminate the need for heavy lift class launch vehicles. The research question presented in Chapter 1 requires the feasibility of the architecture be evaluated objectively without bias. The research accomplishes four distinct goals in response to the research question as defined in Section 1.2: system modeling, constraint definition, and uncertainty analysis.

System models are developed to evaluate the design options for feasibility assessment. Chapter 4 presented the propellant depot thermal and mass models that provide the basis for performance feasibility assessment. The thermal model is used to evaluate the various cryogenic fluid management strategies in the design space. The different strategies result in different levels of propellant boil-offs that dictates the launch vehicle requirements. The propellant load is derived from the mission requirements provided by the baseline architecture and the propellant depot system mass is computed using mass estimating relationships derived from historical data.

The mass estimation models are used to evaluate the impact of cryogenic fluid management strategies on the overall system mass.

Launch vehicle reliability models are developed using Bayesian probability analysis of the launch records for the launch vehicles of interest. Launch records for the vehicles as well as the vehicle's relating family is combined to form posterior probability distribution for the launch vehicle's reliability. The posterior reliability distribution is used to estimate the overall mission success probability with the use of Monte Carlo simulation and Poisson binomial distributions. The propellant aggregation mission success probability compounded with the hardware launch success probability yields the total architecture mission success probability, which is used as the evaluation metric for reliability feasibility assessment.

Architecture cost models are developed using historical cost data from the Transcost model. The cost estimating relationships are used to investigate the impact of various design options on the overall cost for the unique elements of the propellant depot architecture. The cost of the common elements from the baseline architecture was taken at face value, and the overall architecture cost is used as the evaluation metric for economic feasibility assessment.

These metrics are evaluated with the architecture constraints to determine feasibility. The performance feasibility constraint is derived from the launch vehicle payload capacity. To meet performance feasibility, the launch vehicle of choice must be able to deliver all of the necessary hardware into orbit with high probability. The reliability feasibility constraint is derived from the baseline architecture launch requirement. Using the Bayesian model developed to estimate launch reliability, the baseline architecture's newly developed heavy lift launch vehicle's reliability can be estimated with global historical launch records. The overall baseline architecture mission success probability can be then computed using the resulting posterior reliability distribution. Finally, the analysis of NASA's Exploration Systems budget in

the past decade provided a basis for the economic feasibility constraint. The budget expectation for the duration of the baseline architecture is used as the constraint for evaluation.

Sensitivity of each of the system metrics to the available design options is investigated using probabilistic methods. The probabilistic method also enabled the analysis of uncertainties in the evaluation of system metrics. Monte Carlo simulations are utilized to capture the uncertainties and to investigate the impact of uncertainties on the feasibility assessment in each of the areas. This analysis provides an unique insight into the assessment of feasibility, as it provides the levels of risk associated with the feasibility claim.

8.2 Conclusions

The stochastic feasibility assessment of a propellant depot space exploration architecture shows that the utilization of propellant depot has greater than 90% probability of meeting payload, reliability, and cost feasibility with the use of redundant launch vehicles. The challenge to feasibility of propellant depot based architecture (Section 2.7) provided the basis for the feasibility areas of interest. The analysis in this dissertation shows these challenges to the propellant depot based architecture can be mitigated. The challenges to the a propellant depot architecture produced three research questions that were addressed systematically in this dissertation.

The first research questions set forth in Section 2.7 addresses the major technical challenge of propellant depot based architecture. The analysis shows the boil-off of cryogenic propellant can become a burden to overall mission mass required for mission duration longer than six months if active cryocoolers are not utilized. The current state-of-the-art cryocoolers are capable of providing cooling capacity to achieve ZBO of the cryogenic propellants. For both passive and ZBO thermal management, the probability of meeting the performance metric is greater than 95% if the larger Falcon

Heavy vehicle is utilized to deliver the depot. The uncertainty in the performance estimation of cryocoolers, primarily from the estimation of the coefficient of performance, increases the overall risk to the performance feasibility. The infusion of additional technologies have the potential to reduce the propellant boil-off without the increase in the overall system mass, but it bring additional technical risk to the architecture.

The second research question addresses the launch reliability of the propellant depot architecture. The mission reliability feasibility analysis agrees with the challenge that the increase in the number of required launches decreases overall mission reliability. However, the analysis also shows that the utilization of redundant or backup flights can significantly mitigate this effect. Because the depot architecture can use commercial launch vehicles, it can utilize multiple providers with multiple vehicles for redundancy. The majority of the increase in required flights in the depot architecture consists of the aggregation of propellant in orbit. Propellant in orbit can be considered as a common commodity, and the loss of the vehicle delivering propellant into orbit is not detrimental to the overall mission success. Also, the utilization of a propellant depot removes the aggregation of propellant from the mission critical path. The launch reliability is further enhanced in the depot based architecture with the ability to utilize highly reliable launch vehicles with extensive launch records rather than newly developed vehicles with high risk of failure due to the reliability infancy problem.

The final research question addresses the economic implication of the propellant depot based architecture. The economic feasibility analysis shows that regardless of design options, the depot based architecture is less than half of the cost of the baseline architecture and has nearly no risk of exceeding the defined budget constraint of $4 billion per year. The claim that a propellant depot based architecture is more costly due to the increase in the number of flights is not true. One of the great benefits

of the depot architecture is the ability to utilize existing launch vehicles and infrastructure. The development cost of new launch vehicles and new infrastructure can often dominate the overall architecture cost, as in the case of the baseline architecture where more than 50% of the total architecture cost is devoted to the HLLV and its ground operations.

The integrated architecture feasibility analysis shows the lower technology option, without the need of advanced cryocoolers, provides the highest probability of satisfying all three feasibility constraints. Despite the increase in launch vehicles required as a result of propellant boil off replenishment, the mission reliability and economic feasibility both remain relatively high for the scenarios without high-power cryocoolers. The critics' challenge that the advanced technology is required in order for depot based architecture to be feasible is not an accurate reflection of the analysis shown.

The design decision of the choice of launch vehicle tends to lean toward the vehicle with the highest reliability because of the high sensitivity of overall mission success probability. The economic feasibility is not affected at all by the choices of the two launch vehicles that can be utilized as the sole launch provider in the depot based architecture. The performance feasibility is not an issue if the high power cryocooler option is removed from the design space. If the economic constraint becomes more stringent, the launch vehicle choice may become a feasibility challenge as there would be a trade-off between high reliability and low cost. In this scenario, there could potentially be compromise solution, where the low-cost, low-reliability launch vehicle can be utilize from the non-mission critical flights that can utilize redundancy to improve the overall reliability, and the high cost-high reliability launch vehicle can be utilized to launch mission critical hardware. This combination of launch vehicles also provide an added layer of redundancy as the failure of a single vehicle will not impact the schedule of the other vehicle.

The mixed fleet vehicle concept can be extended even further with the inclusion

of other vehicles that have been eliminated for various reasons. For example, the Atlas V vehicle was eliminated from consideration because it does not have enough performance capability to deliver the necessary mission hardware. However, the high reliability of the Atlas is still desired in the overall architecture. Thus, utilizing the Atlas wherever its limited performance allows can bring an extra level of robustness to the architecture that the single provider scenario cannot reach. Going beyond the Atlas, if additional launch vehicles from international partners, such as Europe's Ariane or Russia's Proton, can be utilized to deliver propellant or hardware, the international cooperation can further strengthen the feasibility of the overall architecture.

To further the discussion, propellant depot architecture may make propellant delivery a commodity to be desired in orbit. This can drive the capitalistic innovation for fully reusable launch vehicles that should be economical to operate and maintain. These innovations may lead to increased access to space and open the door for limitless economic growth in the space exploration industry. The potential economic benefit of a propellant depot based architecture alone is motivation enough to warrant further consideration of the architecture.

8.3 Contributions and Future Work

The primary research goal for the research is to provide an objective evaluation of the feasibility of the propellant depot architecture of interest. To accomplish the goals, the research utilizes stochastic methods to evaluate the performance metrics. This method is different than feasibility assessments in literature, as reviewed in Chapter 3. The treatment of system metric as probabilistic variables allows for both the evaluation of feasibility, when compared to a set of predefined constraints, as well as the confidence of the feasibility assessment. The inclusion of uncertainty analysis in the assessment of feasibility provide information on the levels of risks associated with the various design options that can be difficult to quantify objectively

with deterministic methods. The stochastic assessment method described in this dissertation can be applied to any concept of operation to objectively evaluate its feasibility.

The application of the stochastic methods in this dissertation is limited to the areas of feasibility identified specifically for the propellant depot based exploration architecture. These feasibility areas may not be applicable or appropriate to every concept of operation of interest, thus additional stochastic methods to evaluate other areas of feasibility can be developed. Additionally, there are areas of feasibility that can be difficult to quantify with system metrics such as political or legal feasibility. These areas of feasibility would require additional work to develop the proper evaluation metric as well as appropriate constraints for feasibility evaluation.

For the propellant depot exploration architecture, the feasibility assessment can be expanded. The cryogenic fluid management technology considered for this dissertation is limited to the utilization of multi-layer insulation and cryocoolers. The primary objective was to investigate the impact on architecture performance feasibility when utilizing current state-of-the-art technologies. The addition of more advanced technologies in the cryogenic fluid management design space may provide increased performance feasibility for all mission durations. The technical risks associated with using advanced technology in the design space, however, must be quantified as part of the performance feasibility assessment. Additionally, analysis of the lifetime of both passive and active thermal management systems will be required to determine the re-usability of the propellant depots.

As briefly discussed in Chapter 5, the global launch vehicle market is growing rapidly with the introduction of various commercial launch vehicles. Any these launch vehicles may be utilized to deliver propellant into orbit if there is high demand of propellant as an in-space commodity. The utilization of a mixed fleet of launch vehicles

has three potential benefits. First, it improves the ability for an exploration architecture to utilize redundancy to improve the overall launch success probability. If one of the launch providers suffers a failure, the other launch providers can continue to supply the necessary propellant to orbit during the failure review and re-certification of the failed launch vehicle. Second, it may increase the on-orbit propellant aggregation rates as each of the launch vehicle can deliver on its own schedule. Finally, the mixed fleet option creates natural competition between the launch providers, which may reduce the cost of propellant aggregation. The utilization of a mixed fleet of launch vehicles is likely to improve on the overall feasibility of propellant depot architecture.

Finally, the feasibility analysis shown in this dissertation compared the depot architecture to the HEFT architecture directly. The comparison showed a cost savings of more than $50 billion over the course of the program, which results only in a single manned mission to an asteroid. The goal of human space exploration is to establish a permanent human presence on the Moon or Mars. To achieve this goal would require many manned missions to these destinations. The most relevant extension of the work in this thesis is to perform stochastic feasibility assessment of an entire exploration campaign. The full benefit of the utilization of propellant depots and reusable elements in orbit will can be only be realized when multiple missions are involved. The full architecture feasibility analyses need to be expanded to investigate the recurring cost and reliability of sending flagship class manned missions to beyond low-Earth orbit and determine the overall feasibility and the extensibility of propellant depot architectures.

APPENDIX A

SURVEY OF CRYOCOOLERS

Table A.1: Cryocooler Database Compiled from NRL Memorandum Report 5490 [53].

Manufacturer	**Model**	**Temp** (K)	**Input Power** (Watts)	**Cooling Capacity** (Watts)	**Mass** (kg)
A.D. Little	RR	60	2670	40	210
A.D. Little	RR	12	2670	1.5	210
Air Products	CS 308	4.2	9000	1.7	344
Air Products	CS 208L	20	6300	12	280
Air Products	CS 208R	20	6300	8	280
Air Products	CS 204SL	20	3200	8	100
Air Products	CS 204	20	3200	4	105
Air Products	CS 202	20	1700	2.25	75
Air Products	CS 201	20	1700	0.6	71
Air Products	CS 108	77	6300	100	316
Air Products	CS 104	77	3200	60	103
Air Products	CS 102	77	1700	30	75
Air Products	CS 308L	1.2	9000	1	350
Air Products	CS 304	4.2	4800	0.5	170
Air Products	CS 302	4.2	2.5	0.25	127
AiResearch		20	2200	20	90.3
AiResearch	Ai 851310	80	500	2.5	14.3
AiResearch	IR TECH	20	4000	20	136
Aisin	Aisin	20	6600	15	240
Aisin	Aisin	100	6600	150	240
Cryogenic Consultants	R400	4.2	5000	0.75	125
Cryogenic Consultants	R700	4.2	8500	1.5	242
Cryomech	GB07	16	8500	15	242
Cryomech	GB04	12	5000	4	125
Cryomech	GB04	20	5000	9	125
Cryomech	GB03	20	5000	5	125
Cryomech	AL05	40	5000	50	125
Cryomech	AL05	80	5000	120	125
Cryomech	AL03	30	700	2	21.3
Cryomech	AL03	80	700	9	21.3

Continued on next page

Table A.1 – *Continued from previous page*

Manufacturer	**Model**	**Temp** (K)	**Input Power** (Watts)	**Cooling Capacity** (Watts)	**Mass** (kg)
Cryomech	AL01	80	1200	20	36
Cryomech	AL01	27	1200	3	36
Cryosystem	21	10	1500	0.25	55.5
CTI-Cryogenics	CTI 21	4.5	1500	3	6.5
CTI-Cryogenics	CTI 21	77	1500	15	6.5
CTI-Cryogenics	CTI 22	77	1500	7.5	6.5
CTI-Cryogenics	CTI 22	15	1500	0.3	6.5
CTI-Cryogenics	CTI 350	15	1500	1.5	15
CTI-Cryogenics	CTI 350	77	1500	19	15
CTI-Cryogenics	Cti 1020	15	5000	0.6	15
CTI-Cryogenics	Cti 1020	77	5000	37	15
CTI-Cryogenics	CTI 1050	15	5000	1.7	15
CTI-Cryogenics	CTI 1050	77	5000	62	15
CTI-Cryogenics	CTI CM2	80	50	1	1.72
CTI-Cryogenics	CTI CM4	80	60	1	2
CTI-Cryogenics	CTI CM5	80	30	0.3	1.13
CTI-Cryogenics	CTI SP77A	80	140	0.8	2.5
CTI-Cryogenics	CTI VM1	80	370	0.8	4.8
CTI-Cryogenics	CTI 120	80	830	8	15.8
CTI-Cryogenics	CTI 120	26	830	1	15.8
Galileo Corp	Galileo	80	30	0.25	15
Hitachi	II	4.5		30	165
Hitachi	III	4.5		5	45
JPL	GAR-MII	4	129	1	2
L'Air Liquide	RCF 30-4	20	1500	4	99
L'Air Liquide	RCF 30-4	80	1500	30	99
Leybold Heraeus	RG580/RW3	20	1800	3.75	64
Leybold Heraeus	RG580/RW3	80	1800	37.5	64
Leybold Heraeus	RG580/RW6	20	4000	6.3	160
Leybold Heraeus	RG580/RW6	80	4000	100	160
Leybold Heraeus	RG1040	20	4000	12.5	160
Leybold Heraeus	RG1040	80	4000	43	160
Leybold Heraeus	RG210/RW3	20	1800	2.5	64
Leybold Heraeus	RG210/RW3	80	1800	15	64
Magnavox	MX 7040	80	30	0.25	1.2
Magnavox	MX 7045	85	25	0.25	1.1
Magnavox	MX 7043	80	55	1	2.1
Magnavox	HD1033C	80	50	1	1.7
MMR	K7001	77		0.75	1
MMR	RK01	90		3	0.2

Continued on next page

Table A.1 – *Continued from previous page*

Manufacturer	**Model**	**Temp** (K)	**Input Power** (Watts)	**Cooling Capacity** (Watts)	**Mass** (kg)
Osaka Oxygen	Cryomini D	20	2400	2.5	84
Oxford University		80	35	0.5	2
Philips Lab	JHV/APL	10	30	1.5	7.2
Philips Lab	JHV/APL	90	30	0.3	7.2
Philips USFA	UA 7044	80	55	1	1.8
Philips USFA	UA 7039	80	30	0.25	1.5
Ricor Ltd	K 413G	80	40	0.4	3.8
Ricor Ltd	K 505	80	30	0.25	1.35
Ricor Ltd	K 405	80	150	1	3.8

Table A.2: Cryocooler Database Compiled from Spacecraft Thermal Handbook Vol. II [114].

Manufacturer	**Model**	**Temp** (K)	**Input Power** (Watts)	**Cooling Capacity** (Watts)	**Mass** (kg)
Astrium	4K	4	250	0.009	52
Astrium	10K	10	228	0.045	35
Astrium	20K	20	133	0.12	18
JPL	Planck	18	530	1.3	61
BATC	30K	30	75	0.3	15
BATC	SB 235	40	132	0.5	16.2
BATC	SB 235	110	132	3.5	16.2
BATC	335	35	80	0.4	16.4
BATC	335	60	80	0.6	16.4
Raytheon	PSC	60	88	3	18.6
Raytheon	PSC	35	88	1.2	18.6
NGST	45K	45	155	1.8	14
NGST		55	106	1.7	12.7
NGST		57	105	1	34.5
BATC	HIRDLS	57	66	1	16.4
RSC	35K PSC	35	114	1.2	19
RSC	35K PSC	60	114	4.5	19
NGST	6020	65	101	5	18
LM	MPT	65	25	0.3	5
Creare	HST	72	315	7	25
NGST	MPT	80	30	0.6	8
Astrium	50-80K	80	66	1.85	7.3
NGS	HEC-CE	95	120	10	7
HNGST	nextgen CE	55	170	2	8.2
HNGST	nextgen CE	140	170	7	8.2

Continued on next page

Table A.2 – *Continued from previous page*

Manufacturer	**Model**	**Temp** (K)	**Input Power** (Watts)	**Cooling Capacity** (Watts)	**Mass** (kg)
Raytheon	RSP2	58	131	1.75	13
Raytheon	RSP2	110	131	5	13
NGST	HEC ABI	60	170	1.5	8.2
NGST	HEC ABI	200	170	20	8.2
NGST	MPT	120	40	1.2	8.1
Ball	SB160	60	71	1.6	10.9
Ball	SB335	35	81	0.45	11.1
Northrop	HEC	95	100	10	3.2
Northrop	6020 MTI	60	101	2	19.56

Table A.3: Cryocooler Database Compiled from D.S. Glaister, Cryocooler 10 [118].

Manufacturer	**Model**	**Temp** (K)	**Input Power** (Watts)	**Cooling Capacity** (Watts)	**Mass** (kg)
Ball		35	80	0.4	16.4
Ball		60	80	0.6	16.4
Ball		30	75	0.3	15
Ball		60	61	0.9	17
Ball		65	248	1.15	57
Ball		122	248	5	57
Ball		10	115	0.1	25
Creare		65	215	5	13.7
Creare		35	105	1	15
Creare		77	315	7.7	25.3
Creare		65	120	1	24
JPL		10	200	0.1	320
JPL		20	400	1.2	320
LMMS		60	130	2	14.6
LMMS		35	99	0.5	14.7
LMMS		59	133	1.2	17.9
LMMS		60	104	1.45	15
LMMS		77	215	9	19
MMS		60	73	1	9.1
MMS		80	73	1.7	9.1
MMS		20	122	0.12	11
MMS		30	122	0.4	11
MMS		10	186	0.075	38
MMS		4.2	250	0.009	52
Raytheon		65	104	1.75	25
Raytheon		60	125	2.8	25

Continued on next page

Table A.3 – *Continued from previous page*

Manufacturer	**Model**	**Temp** (K)	**Input Power** (Watts)	**Cooling Capacity** (Watts)	**Mass** (kg)
Raytheon		65	74	1.2	19.2
Raytheon		35	93	1	24
Raytheon		60	63	3	24
TRW		65	48.5	0.35	8.3
TRW		115	38.2	1.5	8.2
TRW		65	24.4	0.21	7.4
TRW		35	107	0.3	18
TRW		60	101	2	18
TRW		57	67	1	16.4
TRW		35	245	0.85	27.2
TRW		55	106	1.75	12.7
TRW		55	46	0.5	8.7

Table A.4: Cryocooler Database Compiled from various Conference Papers [119–122].

Manufacturer	**Model**	**Temp** (K)	**Input Power** (Watts)	**Cooling Capacity** (Watts)	**Mass** (kg)
Ball	SB235E	35	255	2.64	14.4
Ball	SB235E	85	255	10.4	14.4
Ball	SB235	35	150	1	10.5
Ball	SB235	85	150	2	10.5
Ball	SB230	35	55	0.6	9.5
Space Dynamics Lab	GIFTS	55	174	1.5	8.8
Space Dynamics Lab	GIFTS	140	174	8	8.8
Air Liquide	LPTC	50	160	2.3	5.5
Northrop	NGST	77		1.1	0.782
Northrop	NGST	150		4	0.782
Sunpower	CPT60-A2	60	100.2	2.1	5

Table A.5: Cryocooler Database From CryoMech Database [123]

Manufacturer	**Model**	**Temp** (K)	**Input Power** (Watts)	**Cooling Capacity** (Watts)	**Mass** (kg)
CryoMech	AL10	77	1300	14	63.2
CryoMech	AL10	50	1300	10	63.2
CryoMech	AL10	60	1300	11	63.2
CryoMech	AL10	70	1300	13	63.2
CryoMech	AL25	77	1250	25	65.5

Continued on next page

Table A.5 – *Continued from previous page*

Manufacturer	**Model**	**Temp** (K)	**Input Power** (Watts)	**Cooling Capacity** (Watts)	**Mass** (kg)
CryoMech	AL25	50	1250	15	65.5
CryoMech	AL25	60	1250	18	65.5
CryoMech	AL25	70	1250	22	65.5
CryoMech	AL60	77	2000	60	68.2
CryoMech	AL60	50	2000	40	68.2
CryoMech	AL60	60	2000	49	68.2
CryoMech	AL60	70	2000	57	68.2
CryoMech	AL63	50	3200	37	82.4
CryoMech	AL63	20	3200	5	82.4
CryoMech	AL63	30	3200	18	82.4
CryoMech	AL63	40	3200	28	82.4
CryoMech	AL125	77	3900	120	91.1
CryoMech	AL125	50	3900	70	91.1
CryoMech	AL125	60	3900	90	91.1
CryoMech	AL125	70	3900	108	91.1
CryoMech	AL200	77	5100	190	129.6
CryoMech	AL200	50	5100	104	129.6
CryoMech	AL200	60	5100	133	129.6
CryoMech	AL200	70	5100	162	129.6
CryoMech	AL200	80	5100	190	129.6
CryoMech	AL200	50	5100	88	129.6
CryoMech	AL200	60	5100	111	129.6
CryoMech	AL200	70	5100	135	129.6
CryoMech	AL200	80	5100	158	129.6
CryoMech	AL230	50	5500	115	131
CryoMech	AL230	20	5500	25	131
CryoMech	AL230	30	5500	60	131
CryoMech	AL230	40	5500	90	131
CryoMech	AL300	77	7500	320	134.8
CryoMech	AL300	50	7500	200	134.8
CryoMech	AL300	60	7500	250	134.8
CryoMech	AL300	70	7500	285	134.8
CryoMech	AL300	80	7500	320	134.8
CryoMech	AL300	50	7500	166	134.8
CryoMech	AL300	60	7500	208	134.8
CryoMech	AL300	70	7500	237	134.8
CryoMech	AL300	80	7500	266	134.8
CryoMech	AL325	25	11200	100	219.5
CryoMech	AL325	20	11200	70	219.5
CryoMech	AL325	30	11200	140	219.5

Continued on next page

Table A.5 – *Continued from previous page*

Manufacturer	**Model**	**Temp** (K)	**Input Power** (Watts)	**Cooling Capacity** (Watts)	**Mass** (kg)
CryoMech	AL325	40	11200	195	219.5
CryoMech	AL325	50	11200	230	219.5
CryoMech	AL330	50	7500	170	137.1
CryoMech	AL330	20	7500	40	137.1
CryoMech	AL330	30	7500	94	137.1
CryoMech	AL330	40	7500	135	137.1
CryoMech	AL600	77	7500	600	139.7
CryoMech	AL600	50	7500	350	139.7
CryoMech	AL600	60	7500	430	139.7
CryoMech	AL600	70	7500	510	139.7
CryoMech	PT10	77	1300	12	68.1
CryoMech	PT30	77	1900	37	69.9
CryoMech	PT60	77	3300	60	79.6
CryoMech	PT63	40	4000	23	85.7
CryoMech	PT90	77	5000	90	122.4
CryoMech	PT403	4.2	3000	0.25	91.2
CryoMech	PT405	4.2	4900	0.5	128.7
CryoMech	PT407	4.2	7000	0.7	130.7
CryoMech	PT410	4.2	8400	1	186.2
CryoMech	PT415	4.2	10700	1.5	256.5
CryoMech	PT803	20	3400	4	90.2
CryoMech	PT805	20	4900	8	128.7
CryoMech	PT810	20	8000	14	173.9

APPENDIX B

HISTORICAL AEROSPACE SYSTEM MASS DATA

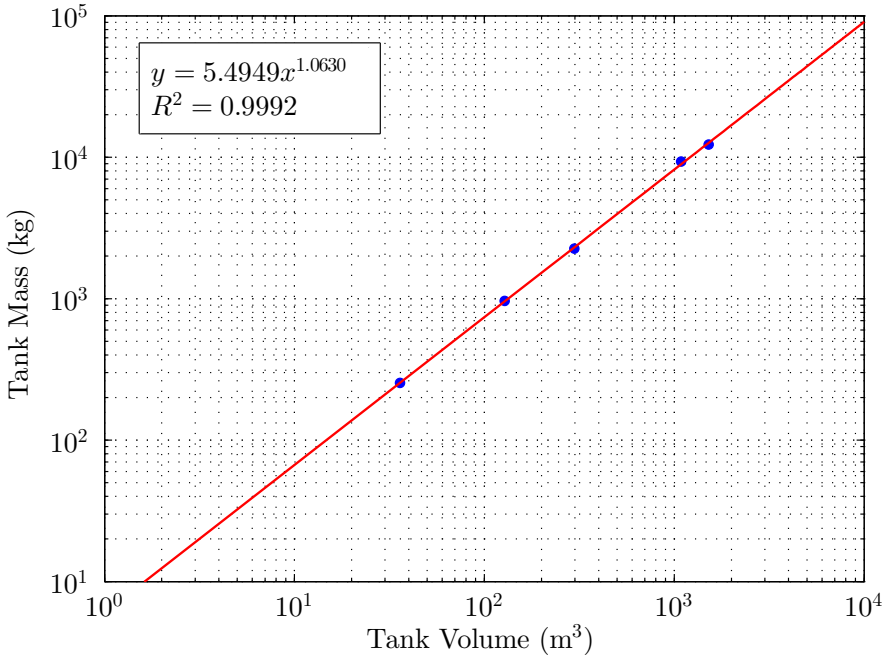

Figure B.1: Liquid Hydrogen Tank and Spacecraft Liquid Propellant Engine Mass Estimating Relationship [135]

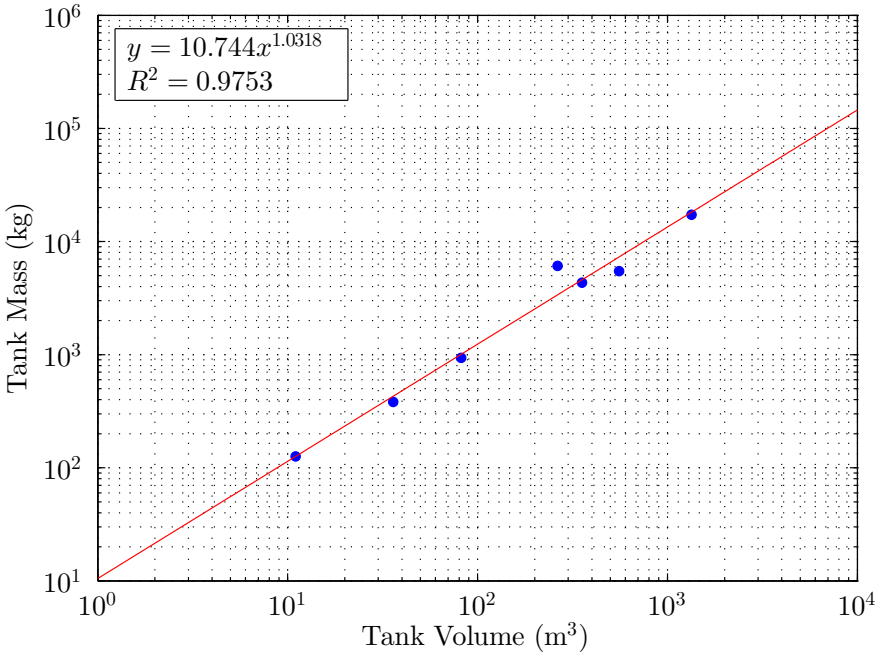

Figure B.2: Liquid Oxygen Tank Mass Estimating Relationship [135]

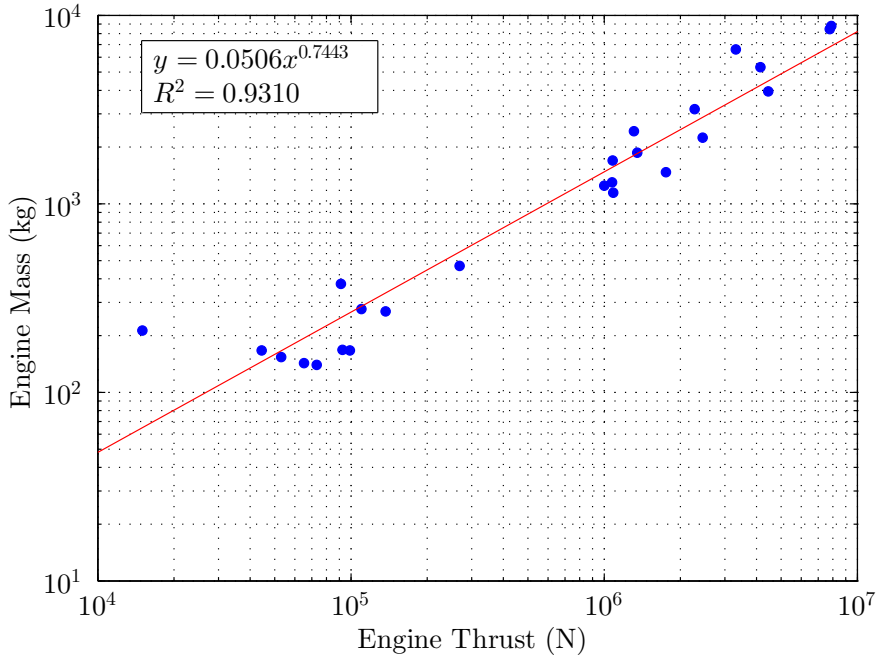

Figure B.3: Launch Vehicle and Spacecraft Liquid Propellant Engine Mass Estimating Relationship [135]

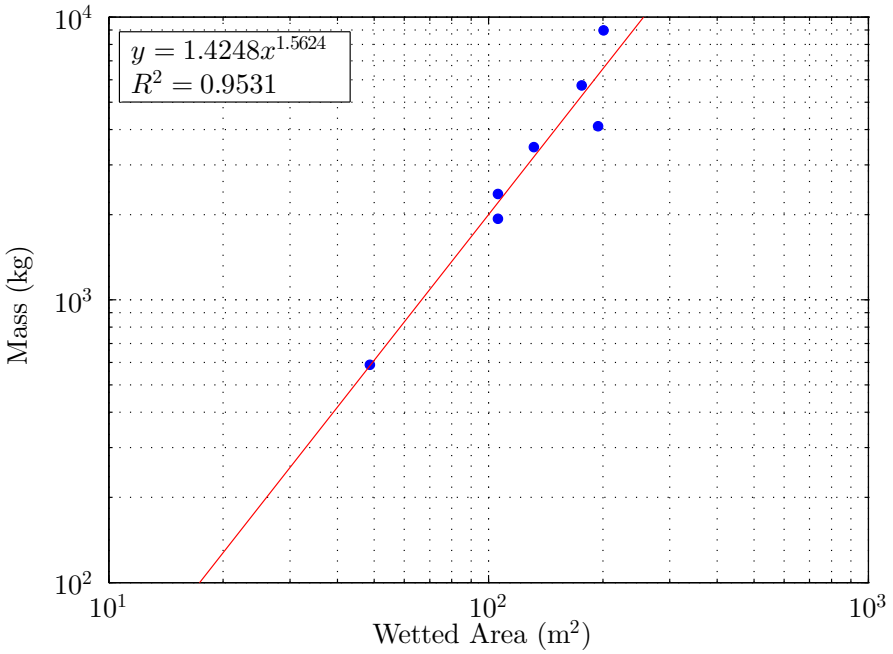

Figure B.4: Propellant Tank Inter-tank and Skirt Mass Estimating Relationship [135]

Table B.1: Engine Mass as Function of Designed Thrust [135]

	Thrust [kN]	Mass [kg]		Thrust [kN]	Mass [kg]
LEM Ascent	15.0	213	LE-7	1,080	1,700
LEM Descent	44.4	167	RS-27	1,085	1,146
RS-72	53	154	J-2X	1,310	2,427
RL10A-5	65.2	143	Vulcain 2	1,350	1,869
RL10A3-3A	73.26	140	NK-43	1,754	1,473
Apollo SM	91.0	376	SSME	2,278	3,177
RL10A-4	93.5	168	Titan LR-87	2,450	2,244
RL10A-4-2	99.1	167	RS-68	3,312	6,597
RL10B-2	110	277	RD-180	4,142	5,307
LE-5B	137.0	269	RS-76	4,448	3,955
MA-5	268.6	469	F-1	7,775	8,444
J-2	1,000	1,249	RD-170	7,890	8,776
Vulcain	1,075	1,300			

Table B.2: Propellant Tank Historical Mass Data

	LH_2 Tank		LO_2 Tank	
	Volume [m^3]	Mass [kg]	Volume [m^3]	Mass [kg]
Centaur	36	254	11	126
S-IV	128	964	36	382
S-IVB	298	2,262	82	937
S-I			264	6,100
S-II	1,088	9,312	355	4,332
Shuttle	1,519	12,287	556	5,478
SIC			1,338	17,232

Table B.3: Intertank & Skirt MER as Function of Wetted Area

	Area [m^2]	Mass [kg]
SIC Aft Skirt	194.2	4,112
SIC Intertank	220.7	5,975
SIC Forward Skirt	105.9	2,368
SIC-SII Stage	175.8	5,725
SII Forward Skirt	105.9	1,935
SII-SIVB Stage	131.6	3,468
SIVB Forward Skirt	48.69	558.8

APPENDIX C

RESULT OF THE FIRST TEN LAUNCHES OF 99 LAUNCH VEHICLE FAMILY

The data compiled in this Appendix comes from a variety of sources. Most notably the *International Reference Guide to Space Launch System* by Isakowitz [74], *Space Launch Report* [139], and *NASA's Major Launch Record* [140]. Additional information was gather from a variety of internet sources, all of which are freely available to the public. Launch data has been compiled into a Launch Vehicle History Database spreadsheet which is continuously updated with new launch data. The database spreadsheet can be requested by contacting the author at Patrick.Chai[at]gatech.edu .

Table C.1: Result of the First 5 Launches of 99 Families of Launch Vehicles from Around the World [74, 139, 140]

			1st Launch		2nd Launch		3rd Launch		4th Launch		5th Launch	
Country	**Family**	**Vehicle**	Date	Result	Date	Result	Date	Result	Date	Result	Date	Result
China	Long March	Feng Bao	08/10/72	**Success**	09/18/73	**Failure**	07/12/74	**Failure**	07/26/75	**Success**	12/16/75	**Success**
		LM CZ-1	04/24/70	**Success**	03/03/71	**Success**						
		LM CZ-2	11/05/74	**Failure**	11/26/75	**Success**	12/07/76	**Success**	01/26/78	**Success**	09/09/82	**Success**
		LM CZ-3	01/29/84	**Success**	04/08/84	**Success**	02/01/86	**Success**	03/07/88	**Success**	12/22/88	**Success**
		LM CZ-4	09/07/88	**Success**	09/03/90	**Success**	05/10/99	**Success**	10/14/99	**Success**	09/01/00	**Success**
Europe	Ariane	Ariane 1	12/24/79	**Success**	05/23/80	**Failure**	06/19/87	**Success**	12/20/81	**Success**	09/09/82	**Failure**
		Ariane 2	05/31/86	**Failure**	11/21/87	**Success**	05/17/88	**Success**	10/28/88	**Success**	01/27/89	**Success**
		Ariane 3	08/04/84	**Success**	11/10/84	**Success**	02/08/85	**Success**	05/08/85	**Success**	09/12/86	**Failure**
		Ariane 4	06/15/88	**Success**	12/11/88	**Success**	03/06/89	**Success**	06/05/89	**Success**	08/08/89	**Success**
		Ariane 5	06/04/96	**Failure**	10/30/97	**Failure**	10/21/98	**Success**	12/10/99	**Success**	03/21/00	**Success**
	Diamant	A	11/26/65	**Success**	02/17/66	**Success**	02/08/67	**Failure**	02/15/67	**Success**		
		B	03/10/70	**Success**	12/12/70	**Success**	04/15/71	**Success**	12/06/71	**Failure**	05/21/72	**Failure**
		BP4	02/06/75	**Success**	05/17/75	**Success**	09/27/75	**Success**				
	Vega	Vega	02/13/12	**Success**	05/07/13	**Success**						
India	Satellite Launch Vehicle	SLV	08/10/79	**Failure**	07/18/80	**Success**	05/31/81	**Failure**	04/17/83	**Success**		
		ASLV	03/24/87	**Failure**	07/13/88	**Failure**	05/20/92	**Failure**	05/04/94	**Success**		
		PSLV	09/20/93	**Failure**	10/15/94	**Success**	03/21/96	**Success**	09/29/97	**Failure**	05/26/99	**Success**
		GSLV	04/18/01	**Failure**	05/08/03	**Success**	09/20/04	**Success**	07/10/06	**Failure**	09/02/07	**Failure**
Isreal	Shavit	Shavit	09/19/88	**Success**	04/03/90	**Success**	09/15/94	**Failure**	04/05/95	**Success**	01/22/98	**Failure**
Japan	M-Vehicle	L-4S	09/26/66	**Failure**	12/20/66	**Failure**	04/13/67	**Failure**	09/22/69	**Failure**	02/11/70	**Success**
		M-3	09/16/74	**Success**	02/24/75	**Success**	02/04/76	**Failure**	02/19/77	**Success**	02/04/78	**Success**
		M-4	09/25/70	**Failure**	02/16/71	**Success**	09/28/71	**Success**	08/19/72	**Success**		
		M-V	02/12/97	**Success**	07/03/98	**Success**	02/10/00	**Failure**	05/09/03	**Success**	07/10/05	**Success**
	H-Vehicle	N-1	09/09/75	**Success**	02/29/76	**Success**	02/23/77	**Success**	02/16/78	**Success**	02/06/79	**Success**
		N-2	02/11/81	**Success**	08/10/81	**Success**	04/04/83	**Success**	08/05/83	**Success**	01/23/84	**Success**
		H-1	08/13/86	**Success**	08/27/87	**Success**	04/19/88	**Success**	09/16/88	**Success**	09/09/89	**Success**
		H-2	08/29/01	**Success**	04/04/02	**Success**	09/10/02	**Success**	12/14/02	**Success**	03/28/03	**Success**
England	Black Arrow		06/28/69	**Failure**	03/04/70	**Success**	09/02/70	**Failure**	10/28/71	**Success**		
S. Korea	Naro	Naro-1	08/25/09	**Failure**	06/10/10	**Failure**	01/30/13	**Success**				
N. Korea	Unha	Unha	09/19/88	**Failure**	04/03/90	**Failure**	09/15/94	**Success**				
Brazil	VLS	VLS	12/01/85	**Failure**	05/18/89	**Success**	12/02/97	**Failure**	12/11/99	**Failure**	08/22/03	**Failure**

Continued on next page

Table C.1 – *Continued from previous page*

			1st Launch		2nd Launch		3rd Launch		4th Launch		5th Launch	
Country	**Family**	**Vehicle**	Date	Result	Date	Result	Date	Result	Date	Result	Date	Result
Russia / Soviet Union	Energia	Energia	05/15/87	**Success**	11/15/88	**Success**						
	Kosmos	C-1	01/01/64	**Success**	01/01/65	**Success**	02/02/65	**Success**	03/03/65	**Success**	04/04/65	**Success**
	Proton	8K82	07/16/65	**Success**	11/02/65	**Success**	03/24/66	**Failure**	07/06/66	**Success**		
		8K82K	03/10/67	**Success**	04/08/67	**Failure**	09/27/67	**Failure**	11/22/67	**Failure**	03/02/68	**Success**
	R-7	Semyorka	03/15/57	**Failure**	07/12/57	**Failure**	08/21/57	**Success**	09/07/57	**Success**	01/26/58	**Failure**
		Polyot	10/04/57	**Success**	11/03/57	**Success**	04/27/58	**Failure**	05/15/58	**Success**	11/01/63	**Success**
		Luna	09/23/58	**Failure**	10/11/58	**Failure**	12/04/58	**Failure**	01/02/59	**Failure**	06/18/59	**Failure**
		Vostok	05/15/60	**Success**	07/28/60	**Failure**	08/19/60	**Success**	12/01/60	**Success**	12/22/60	**Failure**
		Molniya	10/10/60	**Failure**	10/14/60	**Failure**	04/04/61	**Failure**	02/12/61	**Success**	08/25/62	**Failure**
		Voskhod	11/16/63	**Success**	05/18/64	**Success**	07/01/64	**Success**	09/13/64	**Success**	10/06/64	**Success**
		Soyuz	12/17/65	**Success**	07/20/66	**Success**	11/28/66	**Success**	12/14/66	**Failure**	02/07/67	**Success**
	Zenit	Zenit-2	10/22/85	**Success**	12/28/85	**Success**	07/30/86	**Success**	10/22/86	**Success**	02/14/87	**Success**
		Zenit-3	03/28/99	**Success**	10/10/99	**Success**	03/12/00	**Failure**	07/29/00	**Success**	10/21/00	**Success**
United States	Atlas	LV-3	12/18/58	**Success**	09/09/59	**Failure**	11/26/59	**Failure**	02/26/60	**Failure**	05/24/60	**Success**
		SLV-3	08/14/64	**Success**	09/23/64	**Success**	10/08/64	**Success**	12/04/64	**Success**	01/23/65	**Success**
		A	06/11/57	**Failure**	09/25/57	**Failure**	12/17/57	**Success**	01/10/58	**Success**	02/07/58	**Failure**
		B	07/19/58	**Failure**	08/02/58	**Success**	08/29/58	**Success**	09/14/58	**Success**	09/18/58	**Failure**
		C	12/24/58	**Success**	01/27/59	**Success**	02/20/59	**Failure**	03/19/59	**Failure**	07/21/59	**Success**
		D	04/04/59	**Failure**	05/19/59	**Failure**	06/06/59	**Failure**	07/29/59	**Success**	08/11/59	**Success**
		F	04/06/68	**Success**	07/11/68	**Success**	03/17/69	**Success**	08/06/71	**Success**	10/02/72	**Success**
		E	12/08/80	**Failure**	12/18/81	**Failure**	12/20/82	**Success**	03/28/83	**Success**	07/14/83	**Success**
		H	02/09/83	**Success**	06/13/83	**Success**	02/05/84	**Success**	02/09/86	**Success**	03/15/87	**Success**
		G	06/09/84	**Failure**	03/22/85	**Success**	06/29/85	**Success**	09/28/85	**Success**	12/04/86	**Success**
		I	07/25/90	**Success**	04/18/91	**Failure**	03/13/92	**Success**	08/22/92	**Failure**	03/25/93	**Failure**
		II	12/07/91	**Success**	02/10/92	**Success**	06/09/92	**Success**	07/02/92	**Success**	07/19/93	**Success**
		V	08/21/02	**Success**	05/14/03	**Success**	07/17/03	**Success**	12/17/04	**Success**	03/11/05	**Success**
	Athena	Athena	08/15/95	**Failure**	08/23/97	**Success**	01/07/98	**Success**	01/27/99	**Success**	04/27/99	**Failure**
	Titan	I	02/06/59	**Success**	02/25/59	**Success**	04/03/59	**Success**	05/04/59	**Success**	08/14/59	**Failure**
		II	03/16/62	**Success**	06/07/62	**Success**	07/11/62	**Success**	07/25/62	**Success**	09/12/62	**Success**
		III	09/01/64	**Failure**	12/10/64	**Success**	02/11/65	**Success**	05/06/65	**Success**	06/18/65	**Success**
		34D	06/20/83	**Success**	01/31/84	**Success**	04/14/84	**Success**	06/25/84	**Success**	12/04/84	**Success**
		IV	06/14/89	**Success**	06/08/90	**Success**	11/13/90	**Success**	03/08/91	**Success**	11/08/91	**Success**

Continued on next page

Table C.1 – *Continued from previous page*

			1st Launch		2nd Launch		3rd Launch		4th Launch		5th Launch	
Country	**Family**	**Vehicle**	Date	Result	Date	Result	Date	Result	Date	Result	Date	Result
United States	Delta / Thor	DM-18	01/26/57	**Failure**	04/20/57	**Failure**	08/30/57	**Failure**	09/20/57	**Success**	10/03/57	**Failure**
		Able	04/24/58	**Failure**	07/10/58	**Success**	07/23/58	**Success**	08/17/58	**Failure**	10/11/58	**Failure**
		Agena	02/28/59	**Failure**	04/13/59	**Success**	06/03/59	**Failure**	06/25/59	**Failure**	08/13/59	**Success**
		Ablestar	04/13/30	**Success**	06/22/60	**Success**	08/18/60	**Failure**	10/04/60	**Success**	11/30/60	**Failure**
		Burner	05/20/65	**Success**	09/10/65	**Success**	01/08/66	**Failure**	03/31/66	**Success**	09/16/66	**Success**
		Delta	05/13/60	**Failure**	08/12/60	**Success**	11/23/60	**Success**	03/25/61	**Success**	07/21/61	**Success**
		A	10/02/62	**Success**	10/27/62	**Success**						
		B	12/13/62	**Success**	02/13/63	**Success**	04/02/63	**Success**	05/07/63	**Success**	06/19/63	**Success**
		C	10/03/64	**Success**	12/21/64	**Success**	01/22/65	**Success**	02/03/65	**Success**	05/29/65	**Success**
		D	08/19/64	**Success**	04/06/65	**Success**						
		E	11/06/65	**Success**	12/16/65	**Success**	02/28/66	**Success**	07/01/66	**Success**	08/17/66	**Success**
		G/J	12/14/66	**Success**	09/07/67	**Success**	07/04/08	**Success**				
		N	08/16/68	**Success**	12/15/68	**Success**	02/26/69	**Success**	06/29/69	**Success**	08/09/69	**Success**
		M	09/18/68	**Failure**	12/18/68	**Success**	02/05/69	**Success**	03/21/69	**Success**	07/26/69	**Failure**
		L	08/27/69	**Failure**	01/31/72	**Success**						
		0100	07/23/71	**Success**	10/15/72	**Success**	12/10/72	**Success**	07/16/73	**Failure**	11/06/73	**Success**
		1000	09/22/72	**Success**	11/10/72	**Success**	04/20/73	**Success**	06/10/73	**Success**	10/26/73	**Success**
		2000	01/18/74	**Failure**	04/13/74	**Success**	05/17/74	**Success**	10/10/74	**Success**	11/*15/74	**Success**
		3000	12/12/75	**Success**	03/26/76	**Success**	09/13/77	**Failure**	05/11/78	**Success**	12/15/78	**Success**
		4/5000	08/27/89	**Success**	11/18/89	**Success**	06/12/90	**Success**				
		II	02/14/89	**Success**	06/10/89	**Success**	08/18/89	**Success**	10/21/89	**Success**	12/11/89	**Success**
		III	08/27/98	**Failure**	05/05/99	**Failure**	08/23/00	**Failure**				
		IV	11/20/02	**Success**	03/11/03	**Success**	08/29/03	**Success**	12/21/04	**Failure**	05/24/06	**Success**
	Shuttle	STS	04/12/81	**Success**	11/12/81	**Success**	03/22/82	**Success**	06/27/82	**Success**	11/11/82	**Success**
	US Historical	Juno	12/06/58	**Failure**	03/03/59	**Success**	07/16/59	**Failure**	08/15/59	**Failure**	10/13/59	**Success**
		Jupiter-C	02/01/58	**Success**	03/05/58	**Failure**	03/26/58	**Success**	07/26/58	**Success**	08/24/58	**Failure**
		Mercury	12/16/60	**Success**	01/31/61	**Success**	03/24/61	**Success**	05/05/61	**Success**	07/21/61	**Success**
		Saturn I	10/27/61	**Success**	04/25/62	**Success**	11/16/62	**Success**	03/28/63	**Success**	01/29/64	**Success**
		Saturn V	11/09/67	**Success**	04/04/68	**Failure**	12/21/68	**Success**	03/03/69	**Success**	05/18/69	**Success**
		SCOUT	07/01/60	**Success**	10/04/60	**Success**	12/14/60	**Failure**	02/16/61	**Success**	06/30/61	**Failure**
	Falcon	Falcon 1	03/24/06	**Failure**	03/21/07	**Failure**	08/03/08	**Failure**	09/28/08	**Success**	07/14/09	**Success**
		Falcon 9	06/04/10	**Success**	12/08/10	**Success**	05/22/12	**Success**	10/08/12	**Success**	03/01/13	**Success**

Continued on next page

Table C.1 – *Continued from previous page*

			1st Launch		2nd Launch		3rd Launch		4th Launch		5th Launch	
Country	**Family**	**Vehicle**	Date	Result	Date	Result	Date	Result	Date	Result	Date	Result
	Orbital Sciences	Pegasus	04/05/90	**Success**	07/17/91	**Failure**	02/09/93	**Success**	04/25/93	**Success**	05/19/94	**Failure**
		Minotaur	01/27/00	**Success**	05/28/00	**Success**	07/19/00	**Success**	12/04/01	**Success**	03/16/02	**Success**
		Taurus	03/13/94	**Success**	02/10/98	**Success**	10/03/98	**Success**	12/20/99	**Success**	03/12/00	**Success**
		Antares	04/21/13	**Success**	09/18/13	**Success**						

Table C.2: Result of the Launches 6-10 of 99 Families of Launch Vehicles from Around the World [74, 139, 140]

			6th Launch		7th Launch		8th Launch		9th Launch		10th Launch	
Country	**Family**	**Vehicle**	Date	Result	Date	Result	Date	Result	Date	Result	Date	Result
China	Long March	Feng Bao	08/30/76	**Success**	11/10/76	**Failure**	09/14/77	**Success**	04/16/78	**Success**	07/27/79	**Failure**
		LM CZ-1										
		LM CZ-2	08/19/83	**Success**	09/12/84	**Success**	09/18/85	**Success**	10/06/86	**Success**	08/05/87	**Success**
		LM CZ-3	02/04/90	**Success**	04/07/90	**Success**	12/28/91	**Failure**	02/08/94	**Success**	07/21/94	**Success**
		LM CZ-4	03/15/02	**Success**	05/15/02	**Success**	10/21/03	**Success**	09/08/04	**Success**	11/06/04	**Success**
Europe	Ariane	Ariane 1	06/16/83	**Success**	10/19/83	**Success**	03/05/84	**Success**	03/23/84	**Success**	07/02/85	**Success**
		Ariane 2	04/02/89	**Success**								
		Ariane 3	03/28/86	**Success**	09/16/87	**Success**	03/11/88	**Success**	07/21/88	**Success**	09/08/88	**Success**
		Ariane 4	10/27/89	**Success**	01/22/90	**Success**	02/22/90	**Failure**	07/24/90	**Success**	10/12/90	**Success**
		Ariane 5	09/14/00	**Success**	11/16/00	**Success**	12/20/00	**Success**	03/08/01	**Success**	07/12/01	**Failure**
	Diamant	A										
		B										
		BP4										
	Vega	Vega										
India	Satellite Launch Vehicle	SLV										
		ASLV										
		PSLV	10/22/01	**Success**	09/12/02	**Success**	10/17/03	**Success**	05/05/05	**Success**	01/10/07	**Success**
		GSLV	04/15/10	**Failure**	12/25/10	**Failure**						
Isreal	Shavit	Shavit	05/28/02	**Success**	09/06/04	**Failure**	06/11/07	**Success**	06/22/10	**Success**		
Japan	M-Vehicle	L-4S										
		M-3	09/16/78	**Success**	02/21/79	**Success**	02/17/80	**Success**	02/21/81	**Success**	02/20/83	**Success**
		M-4										
		M-V	02/21/06	**Success**	09/22/06	**Success**						
	H-Vehicle	N-1	02/22/80	**Success**	09/03/82	**Success**						
		N-2	08/02/84	**Success**	02/12/86	**Success**	02/19/87	**Success**				
		H-1	02/07/90	**Success**	08/28/90	**Success**	08/25/91	**Success**	02/11/92	**Success**		
		H-2	11/29/03	**Failure**	02/26/05	**Success**	01/24/06	**Success**	02/18/06	**Success**	09/11/06	**Success**
England	Black Arrow											
S. Korea	Naro	Naro-1										
N. Korea	Unha	Unha										
Brazil	VLS	VLS										

Continued on next page

Table C.2 – *Continued from previous page*

			6th Launch		7th Launch		8th Launch		9th Launch		10th Launch	
Country	**Family**	**Vehicle**	Date	Result	Date	Result	Date	Result	Date	Result	Date	Result
Russia / Soviet Union	Energia	Energia										
	Kosmos	C-1	05/05/65	**Success**	06/06/54	**Success**	01/01/66	**Failure**	01/01/67	**Success**	02/02/67	**Success**
	Proton	8K82										
		8K82K	04/22/68	**Failure**	09/14/68	**Success**	11/10/68	**Success**	11/16/68	**Success**	01/20/69	**Failure**
	R-7	Semyorka	03/29/58	**Success**	04/04/58	**Success**	05/24/58	**Failure**	07/10/58	**Failure**	12/24/58	**Failure**
		Polyot	04/12/64	**Success**								
		Luna	09/12/59	**Success**	10/04/59	**Success**	04/15/60	**Failure**	04/16/60	**Failure**		
		Vostok	03/09/61	**Success**	03/25/61	**Success**	04/12/61	**Success**	08/06/61	**Success**	12/11/61	**Failure**
		Molniya	09/01/62	**Failure**	09/12/62	**Failure**	10/24/62	**Failure**	11/01/62	**Success**	10/04/62	**Failure**
		Voskhod	10/12/64	**Success**	02/22/65	**Success**	03/07/65	**Success**	03/18/65	**Success**	04/17/65	**Success**
		Soyuz	04/23/67	**Success**	10/27/67	**Success**	10/30/67	**Success**	04/14/68	**Success**	04/15/68	**Success**
	Zenit	Zenit-2	03/18/87	**Success**	05/13/87	**Success**	08/01/87	**Success**	08/28/87	**Success**	05/15/88	**Success**
		Zenit-3	03/19/01	**Success**	05/09/01	**Success**	06/16/02	**Success**	06/10/03	**Success**	08/08/03	**Success**
United States	Atlas	LV-3	07/29/60	**Failure**	09/25/60	**Success**	10/11/60	**Failure**	12/15/60	**Failure**	01/31/61	**Success**
		SLV-3	03/12/64	**Success**	04/03/65	**Success**	04/28/65	**Success**	05/27/65	**Success**	06/25/65	**Success**
		A	02/20/58	**Failure**	04/05/58	**Failure**	06/03/58	**Success**				
		B	11/18/58	**Success**	11/29/58	**Success**	12/18/58	**Success**	01/16/59	**Failure**	02/04/59	**Success**
		C	08/24/59	**Success**								
		D	09/09/59	**Failure**	09/09/59	**Success**	09/17/59	**Failure**	10/06/59	**Success**	10/10/59	**Success**
		F	07/13/74	**Success**	04/12/75	**Failure**	04/30/76	**Success**	06/23/77	**Success**	12/08/77	**Success**
		E	11/17/83	**Success**	06/13/84	**Success**	09/08/84	**Success**	12/12/84	**Success**	03/12/85	**Success**
		H										
		G	03/26/87	**Success**	09/25/89	**Success**						
		I	09/03/93	**Success**	04/13/94	**Success**	06/24/94	**Success**	05/23/95	**Success**	04/30/96	**Success**
		II	11/28/93	**Success**	12/15/93	**Success**	08/03/94	**Success**	10/06/94	**Success**	11/29/94	**Success**
		V	08/12/05	**Success**	01/19/06	**Success**	04/20/06	**Success**	03/09/07	**Success**	06/15/07	**Failure**
	Athena	Athena	09/24/99	**Success**	09/30/01	**Success**						
	Titan	I	12/12/59	**Failure**	02/02/60	**Success**	02/05/60	**Failure**	02/24/60	**Success**	03/08/60	**Failure**
		II	10/12/62	**Success**	10/26/62	**Success**	12/06/62	**Failure**	12/19/62	**Success**	10/10/63	**Failure**
		III	10/15/65	**Failure**	12/21/65	**Failure**	06/16/66	**Success**	07/29/66	**Success**	08/26/66	**Failure**
		34D	12/22/84	**Success**	08/28/85	**Failure**	04/18/86	**Failure**	10/26/87	**Success**	09/02/88	**Success**
		IV	11/28/92	**Success**	08/02/93	**Failure**	02/07/94	**Success**	05/03/94	**Success**	08/27/94	**Success**

Continued on next page

Table C.2 – *Continued from previous page*

			6th Launch		7th Launch		8th Launch		9th Launch		10th Launch	
Country	**Family**	**Vehicle**	Date	Result	Date	Result	Date	Result	Date	Result	Date	Result
United States	Delta / Thor	DM-18	10/11/57	**Success**	10/24/57	**Success**	12/19/57	**Success**	01/28/58	**Failure**	02/28/58	**Failure**
		Able	11/08/58	**Failure**	01/23/59	**Failure**	02/28/59	**Success**	03/21/59	**Success**	04/08/59	**Success**
		Agena	08/19/59	**Success**	11/07/59	**Success**	11/20/59	**Failure**	02/04/60	**Failure**	02/19/60	**Failure**
		Ablestar	02/22/61	**Success**	06/26/61	**Success**	11/15/61	**Success**	01/24/62	**Failure**	05/10/62	**Failure**
		Burner	02/08/67	**Success**	06/26/67	**Success**	08/23/67	**Success**	10/11/67	**Success**	05/23/68	**Success**
		Delta	08/16/61	**Success**	02/08/62	**Success**	03/07/62	**Success**	04/26/62	**Success**	06/19/62	**Success**
		A										
		B	07/26/63	**Success**	11/26/63	**Success**	12/21/63	**Success**	01/21/64	**Success**	03/19/64	**Failure**
		C	07/01/65	**Success**	08/25/65	**Failure**	02/03/66	**Success**	05/25/66	**Success**	03/08/67	**Success**
		D										
		E	10/02/66	**Success**	10/26/66	**Success**	01/11/67	**Success**	01/26/67	**Success**	03/22/67	**Success**
		G/J										
		N	09/29/71	**Success**	10/21/71	**Failure**	03/11/72	**Success**				
		M	11/22/74	**Success**	01/04/70	**Success**	03/20/70	**Success**	04/22/70	**Success**	07/23/70	**Success**
		L										
		0100										
		1000	12/16/73	**Success**	04/09/75	**Success**	06/21/75	**Success**				
		2000	11/22/74	**Success**	12/18/74	**Success**	01/22/75	**Success**	02/06/75	**Success**	03/07/75	**Success**
		3000	12/06/79	**Success**	02/14/80	**Success**	09/09/80	**Success**	11/15/80	**Success**	05/22/81	**Success**
		4/5000										
		II	01/24/90	**Success**	02/14/90	**Success**	03/26/90	**Success**	04/13/90	**Success**	06/01/90	**Success**
		III										
		IV	06/28/06	**Success**	11/04/06	**Success**	11/11/07	**Success**	01/18/09	**Success**	06/27/09	**Success**
	Shuttle	STS	04/04/83	**Success**	06/18/83	**Success**	08/30/83	**Success**	11/28/83	**Success**	02/03/84	**Success**
	US Historical	Juno	03/23/60	**Failure**	11/03/60	**Success**	02/25/61	**Failure**	04/27/61	**Success**	05/24/61	**Failure**
		Jupiter-C	10/23/58	**Failure**								
		Mercury										
		Saturn I	05/28/64	**Success**	09/18/64	**Success**	02/16/65	**Success**	05/25/65	**Success**	07/30/65	**Success**
		Saturn V	07/16/69	**Success**	11/14/69	**Success**	04/11/70	**Success**	01/31/71	**Success**	07/26/71	**Success**
		SCOUT	08/25/61	**Failure**	10/16/61	**Success**	03/01/62	**Success**	03/29/62	**Success**	04/26/62	**Failure**
	Falcon	Falcon 1										
		Falcon 9	09/20/13	**Success**								

Continued on next page

Table C.2 – *Continued from previous page*

			6th Launch		7th Launch		8th Launch		9th Launch		10th Launch	
Country	**Family**	**Vehicle**	Date	Result	Date	Result	Date	Result	Date	Result	Date	Result
	Orbital Sciences	Pegasus	06/27/94	**Failure**	08/03/94	**Success**	04/03/95	**Success**	06/22/95	**Failure**	03/09/96	**Success**
		Minotaur	10/15/02	**Success**	12/11/02	**Success**	04/11/05	**Success**	09/23/05	**Success**	04/15/06	**Success**
		Taurus	09/21/01	**Failure**	05/20/04	**Success**	02/24/09	**Failure**	03/04/01	**Failure**		
		Antares										

REFERENCES

[1] Review of US Human Spaceflight Plans Committee, Augustine, N., et al., "Seeking a Human Spaceflight Porgram Worthy of a Great Nation," National Aeronautics and Space Administration, October 22, 2009, Office of Science and Technology Policy.

[2] Connolly, J. F., "Constellation Program Overview," National Aeronautics and Space Administration, October 2, 2006, Constellation Program Office.

[3] Obama, B., "National Space Policy of the United States of America," June 28, 2010, Office of the President of the United States, Washington, DC: The White House.

[4] Olson, J., "Human Exploration Framework Team Phase I Closeout," National Aeronautics and Space Administration, September 2, 2010.

[5] Wilhite, A., Arney, D., Jones, C., and Chai, P., "Evolved Human Space Exploration Architecture Using Commercial Launch/Propellant Depots," *IAC-12,D3,2,3,x15379*, 63rd International Astronautical Congress, Naples, Italy, International Astronautical Federation, October 2012.

[6] "Manned Lunar Landing: Program Mode Comparison," National Aeronautics and Space Administration, July 30, 1962, Office of Manned Space Flight, NASA-TM-X-66764.

[7] Stanley, D. O., Cook, S., Connolly, J., Hamaker, J., Ivins, M., Peterson, W., Geffre, J., Cirillo, B., McClesky, C., Hanley, J., et al., "NASA's Exploration System Architecture Study," Technical Memorandum 2005-214062, National Aeronautics and Space Administration, November 2005.

[8] Mars Architecture Steering Group and Drake, B. G., "Human Exploration of Mars Design Reference Architecture 5.0," Special Publication 2009-566, National Aeronautics and Space Administration, July 2009.

[9] Rogers, S., "NASA Budgets: U.S. Spending on Space Travel since 1958 UPDATED," The Guardian: `http://www.guardian.co.uk/news/datablog/2010/feb/01/nasa-budgets-us-spending-space-travel`, February 1, 2010, accessed October 1, 2012.

[10] Arney, D. C., Wilhite, A. W., Chai, P. R., and Jones, C. A., "A Space Exploration Strategy that Promotes International and Commercial Participation," *Acta Astronautica*, Vol. 94, January 2014, pp. 104–115.

[11] Chai, P. R. and Wilhite, A., "Design Considerations for Orbital Propellant Depot," *GLEX-2012,05,1,7,x12325*, 2012 Global Space Exploration Conference, Washington D.C., International Astronautical Federation, May 2012.

[12] Chandler, F., Bienhoff, D., Cronick, J., and Grayson, G., "Propellant Depot for Earth Orbit and Lunar Exploration," *AIAA 2007-6081*, AIAA SPACE 2007 Conference & Exposition, Long Beach, California, American Institute of Aeronautics and Astronautics, September 2007.

[13] Chato, D., "Experimentation for the Maturation of Deep Space Cryogenic Refueling Technologies," Technical Paper 2008-214929, National Aeronautics and Space Administration, 2008.

[14] Griffin, M. D. and Pace, S., "Propellant Depot Instead of Heavy Lift?" SpaceNews: `http://www.spacenews.com/article/propellant-depots-instead-heavy-lift`, November 2, 2011, accessed January 1, 2013.

[15] "Manned Lunar Landing: Operation Analysis and Mode Comparison," National Aeronautics and Space Administration, June 1, 1962, NASA-TM-X-74752.

[16] Mars Architecture Steering Group and Drake, B. G., "Reference Mission 3.0: Addendum to the Human Exploration of Mars: The Reference Mission of the NASA Mars Exploration Study Team," Special Publication 6107-ADD, National Aeronautics and Space Administration, June 1998.

[17] O'Keefe, S., "The Vision for Space Exploration," February 2004, National Aeronautics and Space Administration.

[18] Arney, D. and Wilhite, A., "Orbital Propellant Depots Enabling Lunar AArchitecture Without Hevey-Lift Launch Vehicles," *Journal of Spacecraft and Rockets*, Vol. 47, No. 2, 2010, pp. 353–360.

[19] Dipprey, N. F. and Rotenberger, S. J., "Orbital Express Propellant Resupply Servicing," *AIAA 2003-4898*, AIAA/ASME/SAE/ASEE Joint Propulsion Conference and Exhibit, Huntsville, Alabama, American Institute of Aeronautics and Astronautics, July 2003.

[20] Cadu, E., Corban, R., and Stevenson, S., "Cryogenic Propellant Management Architecture to Support the Space Exploration Initiative," *AIAA 1990-3713*, 1990.

[21] Howell, J. T., Mankins, J. C., and Fikes, J. C., "In-Space Cryogenic Propellant Depot Stepping Stone," *IAC-05-D3.2.01*, 56th International Astronautical Congress, Fukuoka, Japan, International Astronautical Federation, October 2005.

[22] Fikes, J., Howell, J. T., and Henley, M., "In-Space Cryogenic Propellant Depot (ISCPD) Architecture Definition and Systems Studies," *IAC-06-D3.3.08*, 57th International Astronautical Congress, Valencia, Spain, International Astronautical Federation, October 2006.

[23] Goff, J. A., Kutter, B. F., Zegler, F., Bienhoff, D., Chandler, F., and Marchetta, J., "Realistic Near-Term Propllant Depots: Implementation of a Critical Spacefaring Capability," *AIAA 2009-6756*, AIAA SPACE 2009 Conference & Exposition, Pasadena, California, American Institute of Aeronautics and Astronautics, September 2009.

[24] Mulder, T. A., "Orbital Express Autonomous Rendezvous and Capture Flight Operations," *AIAA 2008-6768*, AIAA/AAS Astrodynamics Specialist Conference & Exhibit, Honolulu, Hawaii, Ameri, August 2008.

[25] Young, J. J., *A Value Proposition for Lunar AArchitecture Utilizing On-Orbit Propellant Refueling*, Ph.d. thesis, Georgia Institute of Technology, May 2009.

[26] Axdhal, E., Chai, P., Gaebler, J., Grimes, M., Long, M., Lugo, R., Rowland, R., and Wilhite, A., "Reusable Lunar Transportation Architecture Utilizing Orbital Propellant Depots," *AIAA-2009-6711*, AIAA SPACE 2009 Conference and Exposition, Pasadena, California, American Institute of Aeronautics and Astronautics, Sept 2009.

[27] Kutter, B. F., Zegler, F., O'Neil, G., and Pitchford, B., "A Practial, Affordable Cryogenic Propellant Depot Based on ULA's Flight Experience," *AIAA 2008-7644*, AIAA SPACE 2008 Conference & Exposition, San Diego, California, American Institute of Aeronautics and Astronautics, September 2008.

[28] McLean, C., Pitchford, B., Mustafi, S., Wollen, M., Walls, L., and Schmidt, J., "Simple, Robust Cryogenic Propellant Depot for near Term Applications," *IEEEAC Paper # 1044*, 2011 IEEE Aerospace Conference, Big Sky, Montana, Institute of Electrical and Electronics Engineers, March 2011.

[29] Zegler, F. and Kutter, B. F., "Evolving to a Depot-Based Trasnportation Architecture," *AIAA 2010-8638*, AIAA SPACE 2010 Conference & Exposition, Anaheim, California, American Institute of Aeronautics and Astronautics, 2010.

[30] Chai, P. R. and Wilhite, A., "Cryogenic Thermal Management of Orbital Propellant Depots," *IAC11-D.1.2.3*, 62nd Internaional Astronautical Congress, Cape Town, South Africa, International Astronautical Federation, October 2011.

[31] Gravlee, M., Kutter, B., Wollen, M., Rhys, N., and Walls, L., "CRYOTE (Cryogenic Orbital Testbed) Concept," *AIAA 2009-6440*, AIAA SPACE 2009 Conference and Exposition, Pasadena, California, American Institute of Aeronautics and Astronaustics, September 2009.

[32] Moser, D. J., "Prospects for Composite LOX Tankage," *AIAA 93-2249*, AIAA/SAE/ASME/ASEE 29th Joint Propulsion Conference and Exhibit, Monterey, California, American Institute of Aeronautics and Astronautics, June 1993.

[33] Mallick, K., Cronin, J., Arzberger, S., Tupper, M., Grimes-Ledesma, L., Lewis, J., Paul, C., and Walsh, J., "Ultralight Linearless Composite Tank for In-Space Applications," *AIAA 2004-5801*, Space 2004 Conference and Exhibit, San Diego, California, American Institute of Aeronautics and Astronautics, September 2004.

[34] Larson, W. J. and Wertz, J. R., editors, *Space Mission Analysis and Design*, Space Technology Series, Microcosm Press and Kluwer Academic Publishers, El Segundo, California, 3rd ed., 2004.

[35] Humble, R. D., Henry, G. N., and Larson, W., *Space Propulsion Analysis and Design*, Space Technology Series, McGraw-Hill, 1st ed., 1995.

[36] Emme, E. M., "Historical Perspectives on Apollo," *AIAA 67-839*, AIAA 4th Annual Meeting and Technical Display, Anaheim, California, American Institute of Aeronautics and Astronautics, October 1967.

[37] Low, G. M., "Apollo Spacefcraft," *AIAA 69-1095*, AIAA 6th Annual Meeting and Technical Display, Anaheim, California, American Institute of Aeronautics and Astronautics, October 1969.

[38] Hyle, C., Foggatt, C., Weber, B., Gerbracht, R., and Diamant, L., "Abort Planning for Apollo Missions," *AIAA 70-94*, AIAA 8th Aerospace Sciences Meeting, New York, New York, American Institute of Aeronautics and Astronautics, January 1970.

[39] Braun, R. D., "Investment in Our Future: Exploring Space Through Innovation and Technology," Presentation at TEDxNASA, Newport News, Virginia, November 20, 2010.

[40] Martin, J. J., "Cryogenic Testing of a Foam-Multilayer Insulation Concept in a Simulated Preluanch Environment," *AIAA 92-3182*, AIAA/SAE/ASME/ASEE 28th Joint Propulsion Conference and Exhibit, Nashville, Tennessee, American Institute of Aeronautics and Astronautics, July 1992.

[41] Gruszczynski, M., Throp, V., Heim, W., and Swanson, N., "Design, Development, and Test of the Atlas Liquid Hydrogen Propellant Tank Foam Insulation System," *AIAA 91-1438*, AIAA 24th Thermophysics Conference, Honolulu, Hawaii, American Institute of Aeronautics and Astronautics, June 1991.

[42] Stark, J., Leonhard, K., and Bennett, F., "Cryogenic Thermal Control Technology Summaries," Contractor Report 134747, National Aeronautics and Space Administration, San Diego, California, December 1974.

[43] Knoll, R. H., Stochl, R. J., and Sanabria, R., "A Review of Candidate Multilayer Insulation Systems for Potential Use on Wet-Launched LH2 TanTank for Space Exploration Initiative Lunar Missions," Technical Memorandum 104493, National Aeronautics and Space Adminstration, Cleveland, Ohio, June 1991.

[44] Mather, J., "The James Webb Space Telescope and Future IR Space Telescopes," *AIAA 2004-5985*, AIAA SPACE 2004 Conference and Exhibit, San Diego, California, American Institute of Aeronautics and Astronautics, September 2004.

[45] Dew, M., Lin, J., Kutter, B., Madlangbayan, A., Willey, C., Allwein, K., and Pitchford, B., "Design and Development of an In-Space Deployable Sun Shield for Atlas Centaur," *AIAA 2008-7764*, AIAA SPACE 2008 Conference & Exposition, San Deigo, California, American Institute of Aeronautics and Astronautics, September 2008.

[46] Back, J., Schuettpelz, B., Ewing, A., and Laue, G., "James Webb Space Telescope Sunshield Membrane Assembly," *AIAA 2009-2156*, 50th AIAA/ASME/ASCE/AHS/ASC Structures, Structural Dynamics, and Materials Conference, Palm Spring, California, American Institute of Aeronautics and Astronautics, May 2009.

[47] Feller, J., Plachta, D., Millis, G., and McLean, C., "Demostration of a Cryogenic Boil-Off Reduction System Employing an Actively Cooled Thermal Radiation Shield," *Cryocoolers*, Vol. 16, 2008, pp. 601–609.

[48] Haruyama, T., Kasami, K., Matsubara, Y., Nishitani, T., Maruno, Y., Giboni, K., and Aprile, E., "High-Power Pulse Tube Cryocooler for Liquid Xenon Particle Detectors," *Cryocoolers*, Vol. 13, 2005, pp. 689–694.

[49] Radebaugh, R., "Pulse Tube Cryocooler for Cooling Infrared Sensors," *Proceedings of SPIE, The Internaional Society for Optical Engineering, Infrared Technolgoy and Applications XXVI*, Vol. 4130, 2000, pp. 363–379.

[50] ter Brake, H. and Wiegerinck, G., "Low-Power Cryocooler Survey," *Cryogenics*, Vol. 42, 2002, pp. 705–718.

[51] Radebaugh, R., "Cryocoolers: the State of the Art and Recent Developments," *Journal of Physics: Condensed Matter*, Vol. 21, No. 16, 2009, pp. 9.

[52] Daunt, J. and Goree, W., "Miniature Cryogenic Refrigerators," Tech. Rep. Contracts Nonr-263(70) and N00014-67-C-0393, Office of Naval Research, 1969.

[53] Smith, J., Robinson, J. G., and Iwasa, Y., "Survey of the State-of-the-Art of Minature Cryocoolers for Superconducting Devices," NRL Memorandum Report 5490, Naval Research Laboratory, Washington, DC, 1984.

[54] Bruning, J., Torrison, R., Radebaugh, R., and Nisenoff, M., "Survey of Cryocoolers for Electronic Applications (C-SEA)," *Cryocoolers*, Vol. 10, 1999, pp. 829–835.

[55] Chato, D., "Cryogenic Technology Development for Exploration Missions," *AIAA 2007-953*, 45th AIAA Aerospace Sciences Meeting and Exhibit, Reno, Nevada, American Institute of Aeronautics and Astronautics, January 2007.

[56] Griffin, J., "Background and Program Approach for the Development of Orbital Fluid Resupply Tankers," *AIAA 86-1601*, AIAA/ASME/SAE/ASEE 22nd Joint Propulsion Conference, Huntsville, Alabama, American Institute of Aeronautics and Astronautics, June 1986.

[57] Chato, D., "Technologies for Refueling Spacecraft On-Orbit," *AIAA 2000-5107*, AIAA SPACE 2000 Conference and Exposition, Long Beach, California, American Institute of Aeronautics and Astronautics, September 2000.

[58] Baize, L., Vanhove, M., Flagel, P., and Novelli, A., "The ATV 'Jules Verne' Supplies the ISS," *AIAA 2008-3537*, SpaceOps 2008 Conference, Heidelberg, Germany, American Institute of Aeronautics and Astronautics, May 2008.

[59] Boretz, J., "Orbital Refueling Techniques," *Journal of Spacecraft and Rockets*, Vol. 7, 1970, pp. 513–522.

[60] Bonometti, J., Sorensen, K., Jensen, R., Dankanich, J., and Frame, K., "Free Re-Boost Electrodynamic Tether on the International Space Station," *AIAA 2005-4545*, 41st AIAA/ASME/SAE/ASEE Joint Propulsion Conference and Exhibit, Tucson, Arizona, American Institute of Aeronautics and Astronautics, July 2005.

[61] Martin, J. and Holt, J., "Magnetically Actuated Propellant Orientation Experiment, ContControl Fluid Motion with Magnetic Field in Low-Gravity Environment," Technical Memorandum 210129, National Aeronautics and Space Administration.

[62] Marchetta, J., "Simulation of LOX Reorientation Using Magnetic Positive Positioning," *Microgravity Science and Technology Journal*, Vol. 18, 2006, pp. 31–39.

[63] Marchetta, J. and Hochstein, J., "Simulation and Prediction of Magnetic Propellant Reorientation in Reduced Gravity," *Journal of Propulsion and Power*, Vol. 20, No. 5, 2004, pp. 927–935.

[64] Schmidt, G., Carrigan, R., Hahs, J., Vaughan, D., and Foust, D., "No-Vent Fill Pressurization Test Using a Cryogen Simulant," *AIAA 92-3062*, AIAA/SAE/ASME/ASEE 28th Joint Propulsion Conference and Exhibit, Nashville, Tennessee, American Institute of Aeronautics and Astronautics, July 1992.

[65] Chato, D. J., "Thermodynamic Modeling of the No-Vent Fill Methodology for Transferring Cryogen in Low Gravity," *AIAA 88-3403*, AIAA/ASME/SAE/ASEE 24th Joint Propulsion Conference, Boston, Massachusetts, American Institute of Aeronautics and Astronautics, July 1988.

[66] Chato, D. J., "Ground Testing for the No-Vent Fill of Cryogenic Tanks: Results of Tests of a 71 Cubic Foot Tank," *AIAA 93-1967*, AIAA/SAE/ASME/ASEE 29th Joint Propulsion Conference and Exhibit, Monterey, California, American Institute of Aeronautics and Astronautics, June 1993.

[67] Blatt, M., Merino, G., and Symons, E., "Capillary Device Refilling," *AIAA 80-1095*, AIAA/SAE/ASME 16th Joint Propulsion Conference, Hartford, Connecticut, American Institute of Aeronautics and Astronautics, June 1980.

[68] Chato, D. J. and Kudlac, M., "Screnn Channel Liquid Acquisition Device for Cryogenic Propellants," *AIAA 2002-3983*, 38th AIAA/ASME/SAE/ASEE Joint Propulsion Conference and Exhibit, Indianapolis, Indiana, American Institute of Aeronautics and Astronautics, July 2002.

[69] Kudlac, M. T. and Jurns, J. M., "Screen Channel Liquid Acquisition Devices for Liquid Oxygen," *AIAA 2006-5054*, 42nd AIAA/ASME/SAE/ASEE Joint Propulsion Conference and Exhibit, Sacramento, California, American Institute of Aeronautics and Astronautics, July 2006.

[70] Doux, C. J. and Justak, J. F., "Liquid Oxygen Test Results for an Optical Mass Gauge Sensor," *AIAA 2009-5393*, 45th AIAA/ASME/SAE/ASEE Joint Propulsion Conference and Exhibit, Denver, Colorado, American Institute of Aeronautics and Astronautics, August 2009.

[71] Sullenberger, R. M., Munoz, W. M., Lyon, M. P., Vogel, K., Yalin, A. P., Korman, V., and Polzin, K. A., "Optical Mass Gauging System for Measuring Liquid Levels in a Reduced-Gravity Environment," *Journal of Spacecraft and Rockets*, Vol. 48, No. 3, May-June 2011, pp. 528–533.

[72] Green, S. T., Walter, D. B., Dodge, F. T., Deffenbaugh, D. M., Siebenaler, S. P., and VanDresar, N. T., "Ground Testing of a Compression Mass Gauge," *AIAA 2004-4154*, 40th AIAA/ASME/SAE/ASEE Joint Propulsion Conference and Exhibit, Fort Lauderdale, Florida, American Institute of Aeronautics and Astronautics, July 2004.

[73] Zimmerli, G. A., Asipauskas, M., Wagner, J. D., and Follo, J. C., "Propellant Quantity Gauging Using the Radio Frequency Mass Gauge," *AIAA 2011-1320*, 49th AIAA Aerospace Sciences Meeting including the New Horizon Forum and Aerospace Exposition, Orlando, Florida, American Institute of Aeronautics and Astronautics, January 2011.

[74] Isakowitz, S. J., Hopkins, J. B., and Hopkins, J. P., *International Reference Guide to Space Launch Systems*, American Institute of Aeronautics and Astronautics, Reston, Virginia, 4th ed., 2004.

[75] Space Exploration Technologies Corporation, "Falcon 9 Launch Vehicle Payload User's Guide," SpaceX, `http://www.spacex.com/falcon9.php`, 2009, Accessed: January 1, 2013.

[76] United Launch Alliance, "Delta IV Payload Planners Guide," `http://www.ulalaunch.com/site/pages/Products_DeltaIV.shtml`, 2007, Accessed: January 1, 2013.

[77] United Launch Alliance, "Atlas V Launch Services User's Guide," `http://www.ulalaunch.com/site/pages/Products_AtlasV.shtml`, 2010, Accessed: January 1, 2013.

[78] Lindsey, C., "SpaceX Awarded 2 EELV-Class Mission from USAF," NewSpaceWach, `http://newspacewatch.com/articles/spacex-awarded-2-eelv-class-missions-from-the-usaf.html`, December 5, 2012, Accessed: May 14, 2013.

[79] Associated Administrator for Commercial Space Transportation, "Commercial Space Transportation: Quarterly Launch Report (2002 First Quarter)," United States Department of Transportation, Federal Aviation Administration, `http://www.faa.gov/about/office_org/headquarters_offices/ast/media/quarter0201.pdf`, 2002, Accessed: May 1, 2013.

[80] "Feasibility", *Merriam-Webster's Dictionary and Thesaurus*, Merriam-Webster, Inc., May 2007.

[81] Vanderplaats, G. N., *Numerical Optimization Techniques for Engineering Design*, Vanderplaats Research & Development, Inc., Colorado Springs, CO, 4th ed., 2005.

[82] National Aeronautics and Space Administration, "NASA System Engineering Handbook," Special Publication 2007-6105, National Aeronautics and Space Administration, Washington D.C., December 2007.

[83] Arney, D. A., *Rule-Based Graph Theory to Enable Exploration of the Space Sytem Architecture Design Space*, Ph.d. thesis, Georgia Institute of Technology, 2012.

[84] Blanchard, B. S. and Fabrycky, W. J., *Systems Engineering and Analysis*, Prentice Hall International Series in Industrial and Systems Engineering, Prentice-Hall, Inc., 3rd ed., 1998.

[85] Heaton, A. F. and Longuski, J. M., "Feasibility of a Galileo-Style Tour of the Uranian Satellites," *Journal of Spacecraft and Rockets*, Vol. 40, No. 4, July - August 2003, pp. 591–596.

[86] Parlos, A. G. and Metzger, J. D., "Feasibility Study of a Contained Pulsed Nuclear Propulsion Engine," *Journal of Propulsion and Power*, Vol. 10, No. 2, March - April 1994, pp. 269–278.

[87] Loftus, H., Montanino, L., and Bryndle, R., "Powder Rocket Feasibility Evaluation," *AIAA 72-1162*, AIAA/SAE 8th Joint Propulsion Specialist Conference, November 1972.

[88] Hawke, R., Brooks, A., Fowler, C., and Peterson, D., "Electromagnetic Railgun Launchers: Direct Launch Feasibility," *AIAA Journal*, Vol. 20, No. 7, 1981, pp. 978–985.

[89] Takayanagi, H., Suzuki, T., and Fujita, K., "Feasibility Assessment of Nonstop Mars Sample Return System," *AIAA 2010-624*, 48th AIAA Aerospace Sciences Meeting Including the New Horizons Forum and Aerospace Exposition, January 2010.

[90] Brophy, J. R., Gershman, R., Landau, D., Polk, J., Porter, C., Yeomans, D., Allen, C., willie Williams, and Asphaug, E., "Asteroid Return Mission Feasibility Study," *AIAA 2011-5665*, 47th AIAA/ASME/SAE/ASEE Joint Propulsion Conference & Exhibit, July 2011.

[91] Deckert, W. H. and Hickey, D. H., "Summary and Analysis of Feasibility-Study Designs of V/STOL Transport Aircraft," *Journal of Aircraft*, Vol. 7, No. 1, Januray - February 1970, pp. 66–72.

[92] Hammond, W. E., *Space Transportation: A systems Approach to Analysis and Design*, AIAA Education Series, American Institute of Aeronautics and Astronautics, 1999.

[93] Mankin, J. C., "Technology Rediness Levels," April 1995, White Paper, Advanced Concepts Office, Office of Space Access and Technology, National Aeronautics and Space Administration.

[94] Mankin, J. C., "Research & Development Degree of Difficulty," March 1998, White Paper, Advanced Concepts Office, Office of Space Access and Technology, National Aeronautics and Space Administration.

[95] John, "Technology Readiness and Risk AAssessment: A New Approach," *Acta Astronautica*, Vol. 65, March 2009, pp. 1208–1215.

[96] Phillips, J. J., *Return on Investment*, Gulf Publishing, 1997.

[97] Alipour, M., Dorodi, H., and Pishgahi, S., "Feasibility Study of e-Insurance Services in Iranian Insurance Companies (Asia Insurance Co)," *International Journal of Business and Social Science*, Vol. 2, No. 10, 2011, pp. 277–281.

[98] Burch, J. G., "Adaptation of Information Systems Building Blocks to Design Forces," *Journal of Management Information Systems*, Vol. 3, No. 1, 1986, pp. 96–104.

[99] Overton, R., *Feasibility Studies Made Simple*, Martin Management Services, 2000.

[100] Dieter, G. E., *Engineering Design: A Materials and Processing Approach*, McGraw-Hill Higher Education Series, McGraw Hill, Inc, 3rd ed., 2000.

[101] Meshkat, L. and Shapiro, A., "Probabilistic Risk Assessment for Concurrent, Conceptual Design of Space Missions," *AIAA 2005-6765*, 2005.

[102] Matsumura, T., Haftka, R., and Kim, N. H., "Conservativeness in Failure Probability Estimate: Redesign Risk vs Performance," *AIAA 2013-1818*, 2013.

[103] Roy, C. J. and Oberkampf, W. L., "A Complete Framework for Verification, Validation, and Uncertainty Quantification in Scientific Computing," *AIAA 2010-124*, 48th AIAA Aerospace Sciences Meeting Including the New Horizons Forum and Aerospace Exposition, Januray 2010.

[104] Oberkampf, W. L., Helton, J. C., and Sentz, K., "Mathematical Representation of Uncertainty," *AIAA 2001-1645*, Non-Deterministic Approaches Forum, American Institute of Aeronautics and Astronautics, April 2001.

[105] Agarwal, H., Renaud, J. E., Preston, E. L., and Padmanabhan, D., "Uncertainty Quantification using Evidence Theory in Multidisciplinary Design Optimization," *Reliability Engineering and System Safety*, Vol. 85, 2004, pp. 281–294.

[106] Thunnissen, D. P., *Propagating and Mitigating Uncertainty in the Design of Complex Multidisciplinary Systems*, Ph.d. thesis, California Institute of Technology, Pasadena, California, 2005.

[107] Rubinstein, R., *Simulation and the Monte Carlo Methods*, Wiley Series in Probability and Mathematical Statistics, John Wiley and Sons, 1981.

[108] Mathias, D., Go, S., Gee, K., and Lawrence, S., "Simulation assisted risk assessment applied to launch vehicle conceptual design," *Reliability and Maintainability Symposium, 2008. RAMS 2008. Annual*, Jan 2008, pp. 74–79.

[109] Maggio, G., Hark, F., and Sen, D., "Physics Based Risk Assessment of Launch Vehicles," *Probabilistic Safety Assessment and Management*, edited by C. Spitzer, U. Schmocker, and V. Dang, Springer London, 2004, pp. 2199–2205.

[110] Koelle, D. E., *Handbook of Cost Engineering for Space Transportation System*, No. Report No. TCS-TR-190, TCS-TransCostSystems, 3rd ed., 2010.

[111] Bate, R. R., Mueller, D. D., and White, J. E., *Fundamentals of Astrodynamics*, Dover Publications, 1971.

[112] Gilmore, D. G. and Bello, M., editors, *Satellite Thermal Control Handbook*, The Aerospace Corporation Press, El Segundo, California, 1994.

[113] Griffin, M. D. and French, J. R., *Space Vehicle Design*, AIAA Education Series, American Institute of Aeronautics and Astronautics, 2nd ed., 2004.

[114] Donabedian, M. and Gilmore, D., *Spacecraft Thermal Control Handbook*, Vol. 2, AIAA (American Institute of Aeronautics & Astronautics), Reston, Virginia, 2003.

[115] Hastings, L., Hedayat, A., and Brown, T., "Analytical Modeling and Test Correlation of Variable Density Multilayer Insulation for Cryogenic Storage," Technical Memorandum 2004-213175, National Aeronautics and Space Administration, May 2004.

[116] Keller, C., Cunnington, G., and Glassford, A., "Thermal Performance of Multilayer Insulations," Contractor Report 134477, National Aeronautics and Space Administration, April 1974, Lockheed Missiles & Space Company.

[117] Hedayat, A., Brown, T., Hastings, L., and Martin, J., "Variable Density Multilayer Insluation for Cryogenic Storage," *AIAA 00-36922*, 2000.

[118] Glaister, D., Donabedian, M., Curran, D., and Davis, T., "An Overview of the Performance and Maturity of Long Life Cryocoolers for Space Applications," *Cryocoolers*, Vol. 10, 2002, pp. 1–19.

[119] Gully, W., Glaister, D., Hendershott, P., Kotsubo, V., Lock, J., Marquardt, E., Garcia-Perciante, A., Callen, J., Shaing, K., Hegna, C., et al., "Ball Aerospace Next Generation Two-Stage 35K coolers: the SB235 and SB235E," *Cryocoolers*, Vol. 14, 2007, pp. 49–55.

[120] Trollier, T. et al., "Design of a Large Heat Lift 40 K to 80 K Pulse Tube Cryocooler for Space Applications," *Cryocoolers*, Vol. 14, 2007, pp. 75–82.

[121] Petach, M., Waterman, M., Tward, E., and Bailey, P., "Pulse Tube Microcooler for Space Application," *Cryocoolers*, Vol. 14, 2007, pp. 89–93.

[122] Wilson, K., Fralick, C., Gedeon, D., Yoshida, M., and Kawahara, S., "Sunpower's CPT60 Pulse Tube Cryocooler," *Cryocoolers*, Vol. 14, 2007, pp. 123–132.

[123] CryoMech, "Cryorefrigerators," `http://www.cryomech.com/products/cryorefrigerators/`, 2014, Accessed: July 1, 2014.

[124] Kittel, P., "Cryocooler Performance Estimator," *Cryocoolers*, Vol. 14, 2006, pp. 563–572, Proceedings of the 14th International Cryocooler Conference, Annapolis, Maryland. June 14-16, 2006.

[125] Radebaugh, R., "Development of the Pulse Tube Refrigerator as an Efficient and Reliable Cryocooler," *Proc. Institute of Refrigeration (London)*, 2000.

[126] Walker, G., *Cryocoolers*, Springer, New York, New York, 1983.

[127] Stronbridge, T., "Cryogenic Refrigerators - An Updated Survey," Technical Note 655, National Bureau of Standards, 1974.

[128] Davis, T. and Abhyankar, N., "Long Life Cryocoolers for Space Applications, A Database Update," *Cryocoolers*, Vol. 13, 2005, pp. 599–608.

[129] Dylewski, T. J., "Criteria for Selecting Curves for Fitting to Data," *AIAA Journal*, Vol. 8, No. 8, August 1970, pp. 1411–1415.

[130] Glaister, D. and Curran, D., "Spacecraft Cryocooler System Integration Trades and Optimization," *Cryocoolers*, Vol. 9, 2001, pp. 873–884.

[131] Ladner, D., "Performance and Mass vs. Operating Temperature for Pulse Tube and Stirling Cryocoolers," *Cryocoolers*, Vol. 16, 2011, pp. 633–644.

[132] Salerno, L. and Kittel, P., "Cryogeinc and the Human Exploration of Mars," *Cryogenics*, Vol. 39, 1999, pp. 381–388.

[133] Plachta, D. W., Christie, R., Jurns, J., and Kittel, P., "Passive ZBO storage of liquid hydrogen and liquid oxygen applied to space science mission concepts," *Cryogenics*, Vol. 46, 2006, pp. 89–97, doi:10.1016.

[134] Doherty, M. P., Meyer, M. L., Motil, S. M., and carol A. Ginty, "Cryogenic Propellant Stroage Transfer (CPST) Technology Maturation: Establishing a Foundataion for Technology Demonstration Mission (TDM)," *AIAA 2013-5458*, AIAA SPACE 2013 Confernece and Exposition, San Diego, CA, American Institute of Aeronautics and Astronautics, September 2013.

[135] Chai, P. R. and Wilhite, A. W., "Quantifying the Effects of Model Uncertainty on Design Mass Margin in Advanced Earth-to-Orbit Launch Vehicles," *AIAA 2010-8631*, AIAA Space 2010 Conference and Exposition, Anaheim, California, American Institute of Aeronautics and Astronautics, 2010.

[136] Wilhite, A., Arney, D., and Chai, P., "Permenant Manned Outpost with Commerical Launch and Propellant Depot," *AIAA 2012-5112*, AIAA SPACE 2012 Conference & Exposition, Pasadena, California, American Institute of Aeronautics and Astronautics, September 2012.

[137] "Mass Properties Control for Space Systems," Dec. 2006, AIAA S-120-2006.

[138] "AIAA Recommended Practice for Mass Properties Control for Satellites, Missiles, and Launch Vehicles," Aug. 2000, AIAA R-020A-1999e.

[139] Kyle, E., "Space Launch Report," `http://www.spacelaunchreport.com/`, 2013, Accessed: July 1, 2013.

[140] National Aeronautics and Space Administration, "NASA Major Launch Record," http://history.nasa.gov/pocketstats/sect%20B/MLR.pdf, Accessed: July 1, 2013.

[141] Morse, E., Fragola, J., and Putney, B., "Modeling Launch Vehicle Reliability Growth as Defect Elimination," *AIAA 2010-8836*, AIAA SPACE 2010 Conference and Exposition, Anaheim, California, 2010.

[142] Mak, T., "Infant Mortality - The Lesser Known Reliability Issue," *13th IEEE International On-Line Testing Symposium*, 2007.

[143] Guikema, S. D. and Pate-Cornell, M. E., "Probatility of Infancy Problems for Space Launch Vehicles," *Reliability Engineering and System Safety*, Vol. 87, 2005, pp. 303–314.

[144] Devore, J. L., *Probability and Statistics for Engineering and the Sciences*, CENGAGE Learning, Brooks/Cole, Boston, MA, 8th ed., 2001.

[145] Guikema, S. D. and Pate-Cornell, M. E., "Bayesian Analysis of Launch Vehicle Reliability," *AIAA 2003-1175*, 2003, 41th Aerospace Sciences Meeting and Exhibit, Reno Nevada.

[146] Guikema, S. D. and Pate-Cornell, M. E., "Bayesian Analysis of Launch Vehicle Success Rate," *Journal of Spacecraft and Rockets*, Vol. 41, No. 1, 2004, pp. 93–102.

[147] United Launch Alliance, "ULA Launch Manifest, 12 Month Projection," http://www.ulalaunch.com/site/pages/News_Manifest.shtml, 2012, Accessed: October 20, 2012.

[148] Space Exploration Technologies Corporation, "Falcon 9 Launch Manifest," http://www.spacex.com/launch_manifest.php, 2012, Accessed: October 1, 2012.

[149] Bergin, C., "Preliminary NASA Plan shows Evolved SLS Vehicle is 21 Years Away," http://www.nasaspaceflight.com/2011/07/preliminary-nasa-evolved-sls-vehicle-21-years-away/, July 27, 2011, Accessed: April 23, 2012.

[150] "Space Launch System (SLS) Advanced Booster Engineering Demonstration and/or Risk Reduction," NASA Solicitation and Proposal Integrated Review and Evaluation System, Feb. 2011, Solicitation: NNM12ZPS001N.

[151] Shah, B., "On the Distribution of the Sum of Independent Interger Valued Random Variables," *American Statistics*, Vol. 27, No. 3, June 1973, pp. 123–124.

[152] Chen, S. X. and Liu, J. S., "Statistical Applications of the Poisson-Binomial and Conditional Bernoulli Distributions," *Statistica Sinica*, Vol. 7, 1997, pp. 875–892.

[153] Polites, M., "As Assessment of the Technology of Automated Rendezvous and Capture in Space," NASA/TP 1998-208528, National Aeronautics and Space Administration, 1998.

[154] National Aeronautics and Space Administration, "Budget Documents, Strategic Plans and Performance Reports," `http://www.nasa.gov/news/budget`, Accessed: January 31, 2014.

[155] Kutter, B. F., "Commercial Launch Services: an Enabler for Launch Vehicle Evolution and Cost Reduction," United Launch Alliance Publications: `http://www.ulalaunch.com/site/docs/publications/CommercialLaunchServicesanEnabler20067271.pdf`, 2006, Accessed: October 1, 2013.